How cellular ATP/ADP ratios and reactive oxygen species affect AMPK signalling

Elizabeth Clare Hinchy

Dissertation submitted for the degree of

Doctor of Philosophy

September 2017

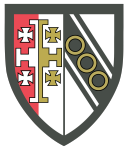

Selwyn College
Cambridge

Abstract

How cellular ATP/ADP ratios and reactive oxygen species affect AMPK signalling

Elizabeth Clare Hinchy

Mitochondria are key generators of cellular ATP, vital to complex life. Historically, mitochondrial generation of reactive oxygen species (ROS) was considered to be an unregulated process, produced by dysfunctional mitochondria. More recently, mitochondrial ROS generated by complex I, particularly by the process of reverse electron transfer (RET), has emerged as a potentially biologically relevant signal that is tightly-regulated and dependent on mitochondrial status. ROS production by RET is reported to play a role in the innate immune response and lifespan extension in fruit flies. One way in which mitochondrial ROS may behave as a signal is by altering the activity of AMP-activated protein kinase (AMPK), a key metabolic sensor and regulator of cell metabolism, which is activated when cellular ATP levels decrease during energy demand. Mitochondria can signal to AMPK via the magnitude of the cellular ATP/AMP and ATP/ADP ratios, which alter in response to mitochondrial function. Our view is mitochondria may also signal to AMPK via ROS. Important studies have helped to clarify the role of exogenous or cytosolic ROS in AMPK regulation. However, the effects of mitochondrial ROS on AMPK activity, specifically that generated by complex I, remain unclear and is the main focus of this thesis. I characterized the effects of exogenous H_2O_2 on cellular AMPK activity, ATP/ADP ratios and cellular redox state in a cell model. I then compounded this with selective mitochondria generated ROS by the mitochondria-targeted redox-cycler, MitoParaquat (MPQ). AMPK activity appeared to correlate with decreasing cell ATP/ADP ratios, indicating that both sources of ROS primarily activate AMPK in an AMP/ADP-dependent mechanism. In parallel, I developed an approach for analyzing the redox state of candidate proteins, an important step in determining if a protein is directly regulated by ROS. I also initiated development of a cell model for studying the downstream effects of mitochondrial ROS production by RET, by expressing alternative respiratory enzymes in a mammalian cell line.

Declaration

This dissertation was written in partial fulfillment of the requirements for the degree of Doctor of Philosophy. With the exception of any collaborations that are mentioned throughout the text, this dissertation describes my own work carried out under the supervision of Dr. Michael P. Murphy from October 2013 until September 2017. Any information that is derived from other sources is referenced accordingly.

Elizabeth Clare Hinchy

September 2017

Acknowledgements

Firstly, I thank my supervisor, Dr. Mike Murphy, for the opportunity of carrying out my PhD research in his lab. The constant guidance and support has been invaluable and the last four years have been one of the most challenging but rewarding endeavors. I have learned a huge amount and I'm extremely grateful for the experiences.

I have been lucky to be a part of a supportive lab and I thank Tracy, Angela, Tom, Sabine and Seb for ensuring the smooth running of the lab over the last four years, allowing us all to dedicate our time to our projects. The whole lab and others in the department have been a source of technical knowledge, guidance and help. I'm grateful to Tom, Andy and Anja for helping with important experiments when times were extremely busy and to Hiran, Ellen, Lee, Andy, Angela, Tracy, AJ, Edward and Mark for general experimental advice and guidance. Thank you to Mike, Hiran and Angela for reading this thesis and offering constructive comments.

It was a great experience to work closely with Lucie in the pursuit of a common aim and I'm grateful to her and Helena for their immense hard work and patience over the course of our collaboration.

I'm thankful for my introduction to science at University College Cork, for all those who taught me, guided me and who instilled in me a love of learning, and for my Amgen friends, who shared my interests.

I thank my Cambridge friends and Richard for their constant kindness, love, support and all the happy memories, and for serving perspective and wine in equal measures. Finally, I thank my family for their continuing support and understanding, especially my parents for always making my education a priority, for their generosity, their sacrifices and for teaching me the value of hard work and perseverance.

Abbreviations

All abbreviations, unless listed, are as described in the “Instructions to Authors” of the Biochemical Journal (http://www.biochemj.org).

ΔP	proton motive force
ΔpH	pH gradient
Δψ	membrane potential
α-KD	α subunit kinase domain
ACC	acetyl-coA carboxylase
ADaM	allosteric drug and metabolite binding pocket
ADP	adenosine-5’diphosphate
AID	autoinhibitory domain
AMP	adenosine-5’monophosphate
AMPK	AMP-activated protein kinase
ANT	adenine nucleotide translocase
AOX	alternative oxidase
ATP	adenosine-5’triphosphate
BCA	bcinchoninic acid assay
BSA	bovine serum albumim
CAC	citric acid cycle
CAMKKB	Ca^{2+}/calmodulin-activated protein kinase kinase B
CBM	carbohydrate-binding module
CBS	cystathionine-β-synthase domain
ChREBP	carbohydrate-responsive element-binding protein
CoA-SH	coenzyme A
CPT 1	carnitine/palmitoyl-transferase 1
Cyt c	cytochrome c
DMEM	Dulbecco's Modified Eagle’s Medium
DMSO	dimethyl sulfoxide
DTT	dithiothreitol
e^-	electron
E_h	reduction potential
ETC	electron transport chain
$FADH_2$	flavin adenine dinucleotide (reduced)
FBS	foetal bovine serum
FBP	fructose-1,6-bisphosphate
FMN	flavin mononucleotide
FOXO	forkhead box O
FRT	flp recombination target
GAPDH	glyceraldehyde 3-phosphate dehydrogenase
GLUT	glucose transporter
GMP	guanosine-5’-monophosphate
Gpx	glutathione peroxidase

GR	glutathione reductase
Grx	glutaredoxin
GS	glycogen synthase
GSH	glutathione (reduced)
GST	glutathione-S-transferase
GTP	guanosine-5'-triphosphate
HEK	human embryonic kidney
HIF-1α	hypoxia-inducible factor-1α
HMGR	HMG-CoA reductase
ICDH	isocitrate dehydrogenase
IMM	inner mitochondrial membrane
IMS	intermembrane space
KEAP1	kelch-like ECH-associated protein 1
LKB1	liver kinase B1
MAVS	mitochondrial antiviral signalling
MnSOD	manganese superoxide dismutase
MPTP	mitochondrial permeability transition pore
MQ H_2O	Milli-Q H_2O
mTORC	mammalian target of rapamycin complex
mtDNA	mitochondrial DNA
NDI1	single subunit yeast NADH dehydrogenase
NEM	N-ethylmaleimide
NES	nuclear export sequence
$NO^{\bullet}$	nitric oxide
NRF	nuclear respiratory factor
OCR	oxygen consumption rate
OMM	outer mitochondrial membrane
OXPHOS	oxidative phosphorylation
PAGE	polyacrylamide gel electrophoresis
PBS	phosphate buffered saline
PCA	perchloric acid
PEP	phosphoenolpyruvate
PGC1a	peroxisome proliferator-activated receptor gamma coactivator 1-α
Pi	phosphate
PFK	phosphofructokinase
PK	pyruvate kinase
PP	protein phosphatase
PPi	pyrophosphate
Pr	protein
Prx	peroxiredoxin
PTM	post-translational modification
PVDF	polyvinylidene difluoride
RE	restriction enzyme

RET	reverse electron transfer
ROS	reactive oxygen species
rpm	revolutions per minute
RT	room temperature
RX	electrophile
SDH	succinate dehydrogenase
SDS	sodium dodecyl sulfate
SOD	superoxide dismutase
SREBP1c	sterol regulatory element-binding protein 1c
ST-loop	serine/threonine rich loop
T2D	type 2 diabetes
TA	tris-acetate buffer
TBS	tris buffered saline
TCEP	tris (2-carboxyethyl)phosphine hydrochloride
Tet	tetracycline
TH	transhydrogenase
TIM	translocase of the inner membrane
TOM	translocase of the outer membrane
Trx	thioredoxin
TrxR/TR	thioredoxin reductase
Tx100	triton X-100
Q	ubiquinone
QH_2	ubiquinol
VDAC	voltage-dependent anion channel

Table of contents

Preface

Chapter 1: Introduction

Chapter 1

Introduction

1.1 General introduction

Mitochondria are subcellular organelles found in nearly all eukaryotic cells and are the site of ATP production by oxidative phosphorylation (OXPHOS) as well as many other functions. Mitochondria are considered to have evolved over 2 billion years ago when an oxygen-utilising α-proteobacteria formed a symbiotic relationship with and was engulfed by an archaeal or early eukaryotic cell (Gray, 2012, Lane and Martin, 2010). Over time, many of the genes of the engulfed, oxygen-utilising cell transferred into the genome of the host cell, resulting in a non-autonomous, sub-cellular, oxygen-metabolising organelle providing an efficient source of energy to the host cell. The engulfed organelle maintained some of its own genes and so retained some ability, via gene expression, to adapt and maintain its proton motive force (ΔP), crucial for survival. It is thought the advantageous bioenergetics of the relationship between the endosymbiont and the host cell enabled the host cell genome to increase vastly in complexity and thus flexibility, and that this advancement facilitated the evolution of complex life as we know it (Lane and Martin, 2010). Thus, for the vast majority of eukaryotic cells, survival is dependent on fully functioning mitochondria that can respond rapidly to changes in the environment to provide a stable energy supply in response to changing energy demands.

Mitochondria can acutely respond to short-term energy demand by increasing or decreasing ATP synthesis by OXPHOS, dependent on the magnitude of the ΔP (Brown, 1992, Murphy and Brand, 1987, Chance and Williams, 1956, Mitchell, 1961). However, the level of mitochondrial ATP production in cells is also dependent on electron supply to the mitochondrial respiratory complexes (required for generation of the ΔP) and the quantity of mitochondria in the cell. Adapting these variables to the energy demand requires communication between the mitochondria and the other cell sub-compartments. For example, substrate availability for the citric acid cycle (CAC) and fatty acid oxidation, which occur in the mitochondria and provide electrons to the respiratory complexes, is initially

controlled by hormone effects on storage tissues, e.g. adipose tissue or liver. Then once taken up by the target cell, the supply of the substrate to mitochondria is further controlled by many processes in the cytosol. Furthermore, mitochondrial biogenesis (i.e. the growth and division of pre-existing mitochondria) requires increased transcription of mitochondrial genes encoded by mitochondrial DNA and also those encoded by the nucleus (Lane and Martin, 2010). To facilitate communication between mitochondria and the rest of the cell, eukaryotic cells have evolved energy-sensing systems that can rewire whole cellular metabolism to maintain a stable energy supply with varying energy demand. AMP-activated protein kinase (AMPK) plays a key role in energy sensing and is considered to be one of the cell's master regulators of energy metabolism (Carling et al., 2011, Hardie et al., 2012, Garcia and Shaw, 2017, Hardie et al., 2016). AMPK senses energy demand as an increase in cellular AMP and ADP relative to ATP and then adapts a broad range of cellular processes to promote ATP production and inhibit ATP expenditure. AMPK can regulate mitochondrial ATP production in the short-term by increasing electron supply for OXPHOS (e.g. by promoting fatty acid oxidation and cellular glucose uptake), and AMPK can also bring about long-term adaptation by affecting transcription factors controlling mitochondrial gene expression from both mitochondrial and nuclear genomes.

Communication between mitochondria and AMPK is vital to sustain complex life. Mitochondria are key producers of cellular ATP so can signal to AMPK, which senses and responds to changes in the adenine nucleotide pool. Mitochondria are also important producers of reactive oxygen species (ROS), which, if generated in excess, can overwhelm the many antioxidant defences within the mitochondrial matrix and lead to oxidative damage and eventual cell death (Smith et al., 2012). However, there is a growing view that the production of ROS from mitochondria can act as a redox signal to the rest of the cell. ROS produced particularly by reverse electron transport (RET) is now suggested by us and several other labs to be a potential signal during periods of metabolic adaptation, as RET is tightly regulated and responsive to mitochondrial status (Chouchani et al., 2014, Mills et

al., 2016, Scialo et al., 2016, Chouchani et al., 2016). As ROS, such as H_2O_2, can modify protein function by oxidising cysteine thiols, ROS has been investigated as an alternative regulator of AMPK activity, perhaps signaling to AMPK to upregulate antioxidant defense systems in the cell (Zaha et al., 2016, Jager et al., 2007, Qi and Young, 2015, Kim et al., 2011, Greer et al., 2007). While several important papers have helped to clarify the role of exogenously-generated or cytosolic ROS in AMPK activity (Zmijewski et al., 2010, Auciello et al., 2014, Shao et al., 2014), less clear is the role of mitochondrial ROS (Emerling et al., 2009, Mungai et al., 2011, Hart et al., 2015), particularly that produced by RET, in the regulation of AMPK.

In the next sections I outline the general principles of mitochondrial energy metabolism, mitochondrial ROS production and redox signalling, before focusing on AMPK - a vital link between mitochondria and the rest of the cell.

1.2 Structure and functions of mitochondria

1.2.1 Mitochondrial architecture and dynamics

Evidence of the endosymbiotic theory is apparent in the architecture of the mitochondrion. Mitochondria are composed of two phospholipid bilayers: the outer and inner membranes, which have distinct components and functions. The outer mitochondrial membrane (OMM) shows similarity to other eukaryotic cell membranes, while the inner mitochondrial membrane (IMM) shares characteristics with a bacterial cell membrane, such as the presence of cardiolipin (Cavalier-Smith, 2006). The OMM contacts the cytosol, is permeable to small molecules (< 5 kDa) and contains channels and transport proteins (e.g. translocase of the outer membrane (TOM)) to facilitate the inward transfer of proteins synthesised outside the mitochondria (Mannella, 1992, Wiedemann and Pfanner, 2017). The OMM has many other functions, including roles in cell death, mitochondrial fission and fusion, mitophagy, inflammation and other cell processes (Friedman and Nunnari, 2014, Arnoult et al., 2011). The IMM is more protein-dense than the OMM, being the site of the respiratory complexes I – IV and the F_OF_1-ATP synthase, (which are mainly responsible for ATP production by oxidative phosphorylation) as well as carrier and transport proteins for metabolites or externally synthesised proteins (e.g. translocases of the inner membrane (TIMs)) (Wiedemann and Pfanner, 2017). The IMM is highly folded into sub-structures called cristae, which greatly increases the surface area of the IMM and maximises the area available for oxidative phosphorylation.

The OMM and IMM are separated by an inter-membrane space (IMS), a distinct compartment in which lies Cytochrome c (Cyt c), which is involved in electron transfer along the respiratory chain but is also released from the IMS into the cytoplasm along with other proteins during apoptosis. The IMS also contains other proteins, e.g. Cu/Zn superoxide dismutase (SOD), which is responsible for detoxification of superoxide, a potentially harmful by-product of oxygen metabolism (Herrmann and Riemer, 2010).

The IMM surrounds a protein-rich mitochondrial matrix in which lie projections of some of the respiratory complexes and F_OF_1-ATP synthase, as well as many other enzymes responsible for metabolic and redox-reactions (e.g. enzymes of the CAC, amino acid and fatty acid metabolism and ROS metabolism). The matrix is also the site of many copies of the simplified mitochondrial genome (and gene transcription and translation machinery), which shares characteristics with the bacterial genome and is further evidence of the endosymbiotic origin of mitochondria (Lane and Martin, 2010). The mammalian mitochondrial DNA (MtDNA) is a circular, double-stranded 16,569 bp genome (Gustafsson et al., 2016). It encodes 37 genes: 22 for transfer RNAs, 2 for ribosomal RNAs and 13 for polypeptides. All the 13 polypeptides encoded by mammalian MtDNA are components of respiratory chain complexes (I, III and IV) or F_OF_1-ATP synthase, while complex II is entirely encoded by nuclear DNA. The other respiratory complexes and F_OF_1-ATP synthase also contain subunits encoded by the nuclear genome and all other proteins in the mitochondria are entirely encoded by the nuclear genome.

Mitochondria used to be depicted in textbooks as individual rod-shaped structures **(Figure 1.1)**. However, it is now clear that mitochondria are present as a dynamic, fused and elongated network (Lee and Yoon, 2016). Mitochondria exist in a constant state of fission and fusion that facilitates changes in morphology and serves as a quality control mechanism for identifying dysfunctional mitochondria and targeting them for degradation by mitophagy. The volume and network of mitochondria in the cell can also vary rapidly depending on the function and metabolic demands of the cell (Jornayvaz and Shulman, 2010, Zong et al., 2002, Civitarese et al., 2007).

A

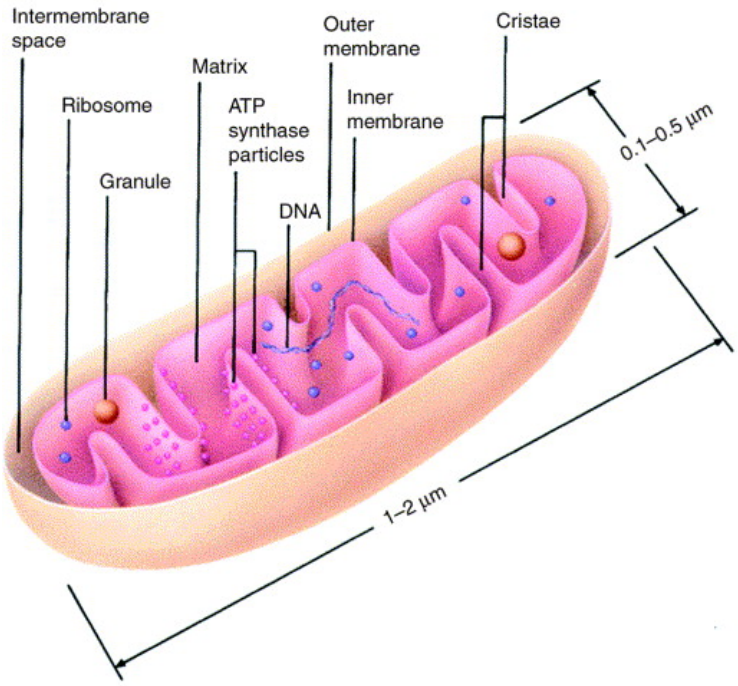

B

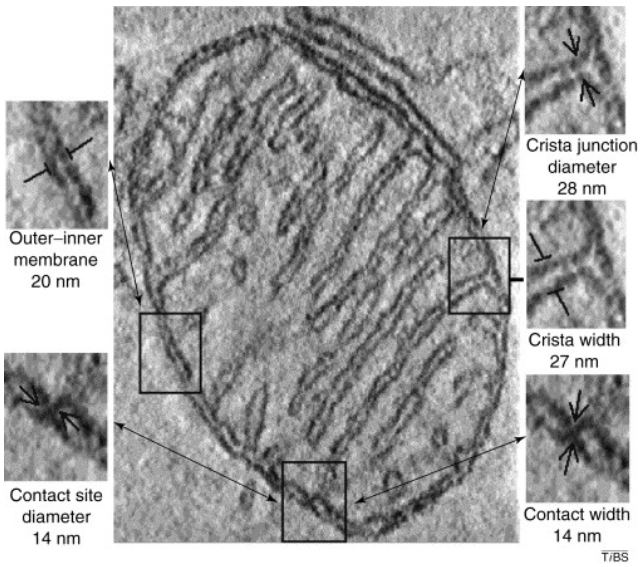

Figure 1.1: Mitochondrial morphology. (A) *Cartoon image of the mitochondrion (Lodish and Darnell, 1995).* ***(B)*** *Electron micrograph of the mitochondrion (Frey and Mannella, 2000).*

1.2.2 Oxidative phosphorylation

Oxidative phosphorylation (OXPHOS) is an energy-transducing process in which ATP is formed during aerobic respiration by the phosphorylation of ADP by F_OF_1-ATP synthase. Energy for this ATP synthesis is provided by an electrochemical proton potential gradient known as the proton motive force (ΔP) that is generated across the IMM, first outlined by Mitchell in his chemiosmotic hypothesis (Mitchell, 1961). The ΔP is composed of a pH gradient (ΔpH) (more basic in the matrix) and membrane potential (ΔΨ) (more negative in the matrix). When glucose, amino acids and fatty acids are oxidised, electrons are first passed to the electron carriers NADH or $FADH_2$ and then passed along respiratory complexes that make up the electron transport chain (ETC), each with increasing reduction potential (E_h) (i.e. more oxidising) (Sazanov, 2015). In addition, ubiquinone (Q) in the IMM and Cyt C in the IMS also act as electron carriers. Finally, electrons are passed to the terminal electron acceptor, O_2, which is reduced to H_2O at complex IV. This electron transport is an exergonic process and provides energy to complexes I, III and IV to pump protons from the matrix to the IMS against the electrochemical proton gradient, establishing the ΔP. The ΔP then drives H^+ back down the gradient into the matrix via F_OF_1-ATP synthase, which uses the energy to phosphorylate ADP to form ATP (Watt et al., 2010). In this way substrate oxidation is coupled to ATP synthesis by electron transfer to O_2 and the ΔP.

Aerobic respiration involves several interconnecting metabolic pathways that converge on electron donation to the ETC and thus enables ATP synthesis by OXPHOS. Glycolysis in an oxygen-independent process that occurs in the cytosol, during which 1 molecule of glucose is converted (in a series of 10 enzyme reactions) into 2 molecules of pyruvate, with a net production of 2 X ATP and 2 X NADH molecules (Rich and Marechal, 2010). The NADH, an electron carrier, is shuttled into the mitochondria by the malate-aspartate shuttle where it is oxidised by complex I and contributes electrons to the ETC. In addition, some NADH in the cytosol is passed to the Q pool by the action of glycerophosphate dehydrogenase.

The pyruvate (X 2) is transported into the mitochondrial matrix where it is decarboxylated by pyruvate dehydrogenase, forming 1 molecule of acetyl-coA and releasing 1 molecule of NADH (per pyruvate) to be oxidised by complex I. The acetyl-coA sourced from glycolysis contributes to a larger pool of acetyl-coA (from the oxidation of amino acids and fatty acids) and enters the CAC, an 8-enzyme series of reactions that results in amino acid precursors, co-factors (CoA-SH), electron carriers (NADH, $FADH_2$ and QH_2) and energy equivalents (GTP or ATP) as well as CO_2 and H_2O by-products (Akram, 2014). Each molecule of acetyl-coA is oxidised to 3 X NADH, 1 X $FADH_2$, 1 X GTP (or ATP) and 2 X CO_2. NADH and $FADH_2$ products from the CAC cycle (and also directly from fatty acid oxidation) donate electrons to the ETC via complex I and II, respectively. The succinate intermediate of the CAC cycle also contributes electrons to the ETC via complex II. While glycolysis produces 2 X ATP (net) directly from 1 molecule of glucose, aerobic respiration theoretically produces a further ~ 36 X ATP from 1 molecule of glucose: 2 X ATP from the CAC and ~ 34 X ATP from OXPHOS (with electron donations from 10 X $NADH_2$ and 4 X $FADH_2$ (including 2 X $FADH_2$ from 2 X succinate oxidation). Thus, aerobic respiration of glucose is more energy efficient than glycolysis alone (Rich and Marechal, 2010). Fatty acids (FAs) are energy-rich compounds and their oxidation produces about twice the energy compared with carbohydrates (39 KJ g^{-1} for palmitate compared with 15 KJ g^{-1} for glucose. During fatty acid oxidation, every 2-carbon unit released from acyl-CoA generates 1 X $FADH_2$ and 1 X NADH. Every acetyl-CoA molecule then yields 3 X NADH, 1 X $FADH_2$ and 1 X GTP in the CAC cycle, resulting in a total yield of ~ 130 X ATP for the degradation of the 16-carbon FA palmitate (Rohrig and Schulze, 2016). Thus, fatty acid oxidation is more energy efficient than glucose oxidation. Below I outline in greater detail the individual contributions of the respiratory complexes and F_OF_1-ATP synthase to the OXPHOS process.

NADH is oxidised at the flavin mononucleotide (FMN) site of complex I (NADH:Q oxidoreductase), releasing 2 electrons, which are transferred along a series of Fe-S clusters (with increasing reduction potential (E_h)) in complex I, and then onto Q to

form QH_2 (Sazanov, 2015, Hirst and Roessler, 2016) Electron transfer is coupled to H^+ pumping by complex I across the IMM, contributing to the ΔP. Electrons also enter the ETC via complex II (succinate:Q oxidoreductase). Succinate is oxidised to fumarate by the succinate dehydrogenase activity of complex II. This results in reduction of the complex II co-factor FAD to $FADH_2$. $FADH_2$ is then re-oxidised to FAD as electrons are transferred from $FADH_2$ along a series of Fe-S clusters to Q, which becomes reduced (QH_2). $FADH_2$ is also produced as a by-product of acetyl-coA oxidation in the CAC cycle and also during fatty acid oxidation, and can directly contribute electrons to Q via complex II. No protons are pumped during this electron transfer through complex II. Electrons from QH_2 are then donated to complex III (cytochrome bc_1 complex) at the Q_0 site. In a reaction known as the Q cycle, 1 electron from QH_2 is transferred onto an Fe-S cluster on complex III and the second electron to a b-haem group. 2 X H^+s are transferred into the IMS. The Fe-S domain then rotates and the electron is transferred to Cyt c in the IMS. The other electron is transferred to a second b-haem group of a higher E_h on complex III. Q then binds at a second Q-binding site, Q_i and becomes re-reduced to QH_2 (by the haem electrons) in a 2-step process that requires 2 cycles of QH_2 oxidation at Q_0. Thus, 1 X QH_2 molecule is oxidised and 2 X Cyt c molecules are reduced coupled to the pumping of 4 X H^+ and 2 X charges across the IMM. Cyt c then transfers electrons to complex IV (cytochrome c oxidase). O_2 is reduced to 2 X H_2O molecules using 4 X e^- from Cyt c and 4 X H^+ from the matrix. During this process, a further 4 X charges and 2 X H^+ are transported from the matrix to the IMS. In summary, during respiration, charges and protons are transferred from the mitochondrial matrix to the IMS, generating the ΔP: 10 from NADH, 6 from succinate **(Figure 1.2)**.

F_OF_1-ATP synthase then uses the H^+ gradient established across the IMM by the ETC to synthesise ATP from ADP and Pi **(Figure 1.2)**. ADP and Pi bind the β subunit of F_OF_1-ATP synthase, which can cycle between different conformational states that either favour the binding of ADP and Pi, or the phosphorylation of ADP and release of ATP (Watt et al., 2010). As H^+s re-enter the matrix through F_OF_1-

ATP synthase, the 8-subunit c-ring rotates. The c-ring is attached to an asymmetric stalk that also rotates and causes conformational change in the β subunit that favours phosphorylation of ADP to form ATP. ATP is then released and exported to the cytosol to for energy requiring processes. The Pi for phosphorylation is imported into the matrix via the phosphate carrier and ATP is exported from the matrix in exchange for ADP by the adenine nucleotide translocase (ANT).

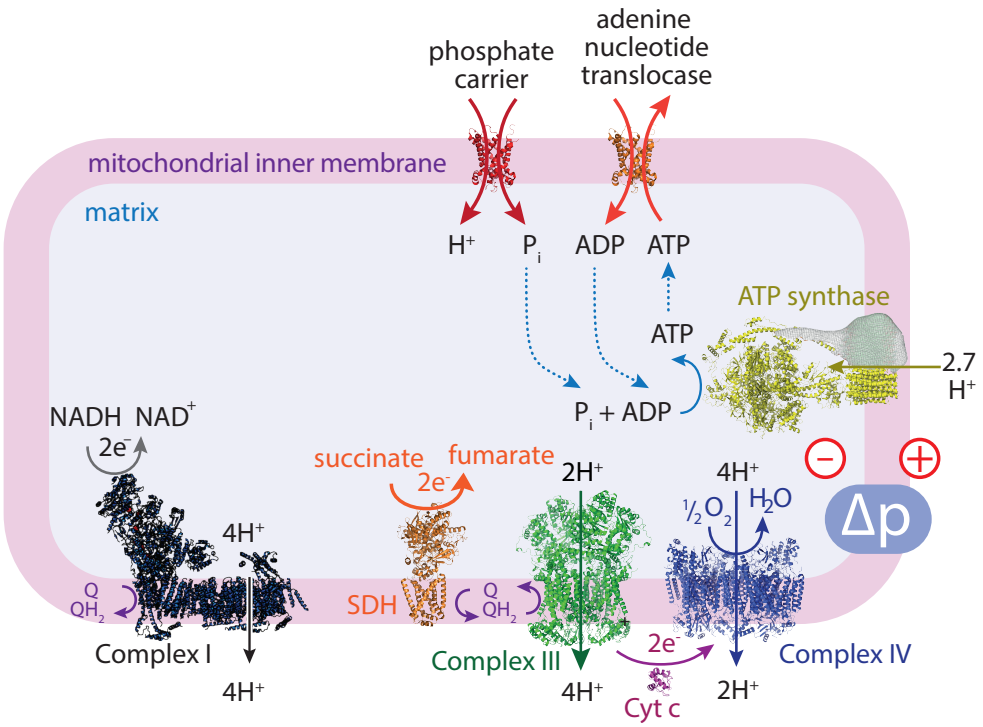

Figure 1.2: The electron transport chain and process of oxidative phosphorylation in mammalian mitochondria. *Electrons are donated to complex I or complex II of the ETC from electron carriers NADH or $FADH_2$, respectively. Electrons are passed along the respiratory complexes, aided by ubiquinone (Q) in the IMM and cytochrome c (Cyt C) in the IMS, each with increasing reduction potential (E_h) (i.e. more oxidising). Finally, electrons are passed to the terminal electron acceptor, O_2, which is reduced to H_2O at complex IV. The electron transport is an exergonic process and provides energy to complexes I, III and IV to pump protons and charges from the matrix to the IMS against the electrochemical proton gradient, establishing the ΔP. The ΔP then drives H^+ back down the gradient into the matrix via F_OF_1-ATP synthase, which uses the energy to phosphorylate ADP to form ATP. 2.7 protons are required by the F-ATPase to make each ATP molecule (Watt et al., 2010).*

1.2.3 Other functions of mitochondria

Mitochondria are involved in many processes other than carbohydrate, fatty acid and amino acid metabolism and ATP synthesis (Duchen and Szabadkai, 2010, Murphy, 2009, Wallace et al., 2010, Smith et al., 2011, Smith et al., 2012). Below I outline other functions of mitochondria that are closely integrated into the workings of the cell.

Mitochondria are involved in many other biosynthetic processes, such as the assembly of iron-sulfur (Fe–S) clusters and haem biosynthesis (Paul and Lill, 2015, Ye and Rouault, 2010). Fe–S clusters are small, highly conserved, inorganic protein co-factors present in the mitochondria, cytosol and nucleus. They enable a range of functions in proteins, including electron transfer in redox reactions (e.g. in respiratory complexes) and catalytic activity in chemical reactions (e.g. aconitase and SDH in the CAC cycle). Fe–S proteins play a role in ATP synthesis, amino acid and co-factor biosynthesis, tRNA modification, and are necessary for genome stability. All Fe–S protein biogenesis is initiated by the mitochondrial iron-sulfur cluster (ISC) assembly machinery (Paul and Lill, 2015). Iron-containing heme groups are also synthesised in (and exported from) mitochondria and are found in cytochromes, haemoglobin and myoglobin. Thus, heme groups play a vital role in ATP production, oxygen transport and muscle function (Ye and Rouault, 2010).

Mitochondria play a role in calcium storage and signalling. Mitochondria are intimately associated with the endoplasmic reticulum (Murley and Nunnari, 2016) which assists in determining the fission of the organelle, and also the movement of calcium from the endoplasmic reticulum to the cytosol and from there into the mitochondrial matrix as a way of modulating mitochondrial ATP production (Mammucari et al., 2011, Brand and Murphy, 1987).

Mitochondria exert control over cell death and survival. Mitochondria play a central role in programmed cell death by apoptosis. The mitochondrial pathway of

apoptosis involves the release of factors such as Cyt c from the IMS as a critical step in committing the cell to activating the apoptotic cell death programme (Tait and Green, 2010). As well as programmed cell death, the central role of mitochondria in ATP production means that damage to the organelle, such as loss of ΔP (depolarization), will lead to necrotic cell death, due to the lack of ATP preventing the cell from sustaining ion gradients. During necrotic cell death the induction of the mitochondrial permeability transition pore (MPTP) is a major player, committing the cell to a rapid death (Halestrap, 2005, Rasola and Bernardi, 2011). Mitochondria have quality control mechanisms in place to maintain a polarized ΔP and thus sufficient cell ATP/ADP ratios to avoid necrotic cell death. As previously described, mitochondria have a dynamic morphology brought about by continuous processes of fission and fusion of the mitochondria (Lee and Yoon, 2016). Polarized mitochondria can undergo fusion, creating continuous, reticulated networks. This is thought to maximize OXPHOS potential and potentiation of functional mtDNA to a greater network of mitochondria. Fusion processes are ΔP-dependent and in depolarized mitochondria (insufficient ΔP to make ATP or enable active transport), fusion is inhibited. With fusion inhibited, increased mitochondrial fission occurs, which isolates dysfunctional mitochondria from the greater network. Fission results in the division of a mitochondrion into daughter organelles. There is often great heterogeneity in the daughter organelles, due to differential segregation of multiple copies of mtDNA during fission, some which may have developed mutations in genes that contribute to mitochondrial dysfunction. Those daughter organelles with depolarized ΔP can be targeted for destruction by mitophagy, whereas daughter organelles with polarized mitochondria can recommence normal fusion and fission cycling and re-join the population of functional mitochondria in the cell.

1.3 Mitochondrial ROS production

Our understanding of how mitochondria impact on the rest of the cell has expanded considerably over the past few years. In addition to their metabolic roles,

mitochondria are now emerging as hubs for a range of signalling processes. One way in which this may occur is through the generation of ROS that emanates from the organelle as a redox signal. Mitochondria are a major source of ROS within the cell (Murphy, 2009, Arnoult et al., 2011, Tormos et al., 2011). These ROS come from the respiratory chain, primarily in the form of superoxide that then goes on to form hydrogen peroxide (H_2O_2) (Murphy, 2009). These ROS can overwhelm the multitude of antioxidant defences within the mitochondrial matrix and thereby cause extensive oxidative damage to mitochondria that contributes to a wide range of pathologies (Smith et al., 2012). More interesting is the growing view that the production of ROS from mitochondria can act as a redox signal to the rest of the cell, suggesting that the production of ROS by mitochondria may be a way in which the mitochondria "talks" to the rest of the cell, coordinating the function of the mitochondria with that of the cell (Murphy, 2009, Arnoult et al., 2011, Tormos and Chandel, 2010, Holmstrom and Finkel, 2014). Below I outline the main sources of ROS production in mitochondria, the mechanisms of production and also degradation. Later, I outline the involvement of mitochondrial ROS in cellular redox signalling.

1.3.1 Sources of mitochondrial ROS production

The superoxide anion ($O_2^{\cdot -}$) (produced from the one electron reduction of O_2) is the proximal ROS liberated by the respiratory chain, mainly from the reduced FMN of complex I (Pryde and Hirst, 2011, Murphy, 2009, Chouchani et al., 2016) (releasing superoxide towards the matrix) and from the Q cycle of complex III (releasing superoxide into both the matrix and the IMS). The production of superoxide by complex III occurs in response to inhibition at the internal Q-binding site by inhibitors such as antimycin A, which is unlikely to be physiological (Murphy, 2009). However, there are a number of reports that complex III may be a source of superoxide as a signal during hypoxia (Bell and Chandel, 2007, Chandel et al., 1998), but the mechanistic details of how this occurs are obscure. Other enzymes can also interact with the Q pool and lead to superoxide production by complex I, e.g. electron transfer flavoprotein (ETC), which is reduced during fatty acid

oxidation and transfers electrons to the Q pool (Murphy, 2009).

Superoxide can be also generated within the matrix from other sources, e.g. dehydrogenases and the adrenodoxin reductase/adrenodoxin/cytochrome P_{450} system that receives electrons from the NADPH pool (Murphy, 2009). However, in many situations ROS production from these complexes is in response to damage leading to a back up of electrons that spill out as superoxide (Murphy, 2009). As a potential redox signal, it is likely that the ROS generation would be more regulated (Holmstrom and Finkel, 2014). Superoxide generation from complex I can be regulated (Murphy, 2009), particularly through the process of RET and may be the best understood potential source of redox signalling from mitochondria (Chouchani et al., 2016).

There are other locations within mitochondria, such as the IMS that can also produce superoxide, which may be important in redox signalling, e.g. α-glycerophosphate dehydrogenase at the outer surface of the IMM can produce superoxide (Murphy, 2009). However, redox signals generated from the matrix may most directly enable the organelle to feed back to the rest of the cell about its metabolic status (Chouchani et al., 2016).

1.3.2 Superoxide production by complex I

Complex I is one of the main sites of superoxide production in mitochondria, which can be produced during either forward or reverse electron transfer (Murphy, 2009) **(Figure 1.3)**. Superoxide production during forward electron transfer can occur when there is a highly reduced matrix NADH/NAD^+ ratio. NADH donates electrons to the ETC via complex I. An FMN co-factor on complex I accepts the electrons and passes them through a chain of seven Fe-S centres to the Q-binding site. When the FMN is fully reduced (dependent on a reduced NADH/NAD^+ pool), superoxide is generated from the reaction between O_2 and reduced FMN. Inhibition of complex I with rotenone increases superoxide production by this mechanism, as rotenone binds the Q-binding site on complex I and leads to a back up of electrons onto FMN, causing it to become hyper-reduced. Physiologically, superoxide could

be produced by this mechanism due to damage to or mutation of the respiratory chain, ischaemia, loss of Cyt c or low ATP demand, which would increase the matrix NADH/NAD^+ ratio.

Superoxide can also be generated from complex I by reverse electron transfer (RET) (Murphy, 2009, Chouchani et al., 2016). RET requires a highly reduced Q pool and a high ΔP, which forces electrons back from the Q pool onto complex I, reducing the FMN. The reduced FMN can then either donate electrons to NAD^+ to form NADH or to O_2 to form superoxide. The Q pool can be reduced by electron donation by succinate, α-glycerophosphate, fatty acid oxidation or by co-expressing the alternative respiratory enzyme, NDI1 (a single subunit NADH dehydrogenase) (Murphy, 2009, Chouchani et al., 2016, Mills et al., 2016, Scialo et al., 2016). A high ΔP can be achieved if the Q pool is reduced enough to donate electrons to complex III and IV as well as to the FMN of complex I, and is enhanced by low rates of ATP synthesis. Superoxide production by RET is inhibited by rotenone, indicating that electrons enter into complex I through the Q-binding site(s) (Murphy, 2009, Chouchani et al., 2016).

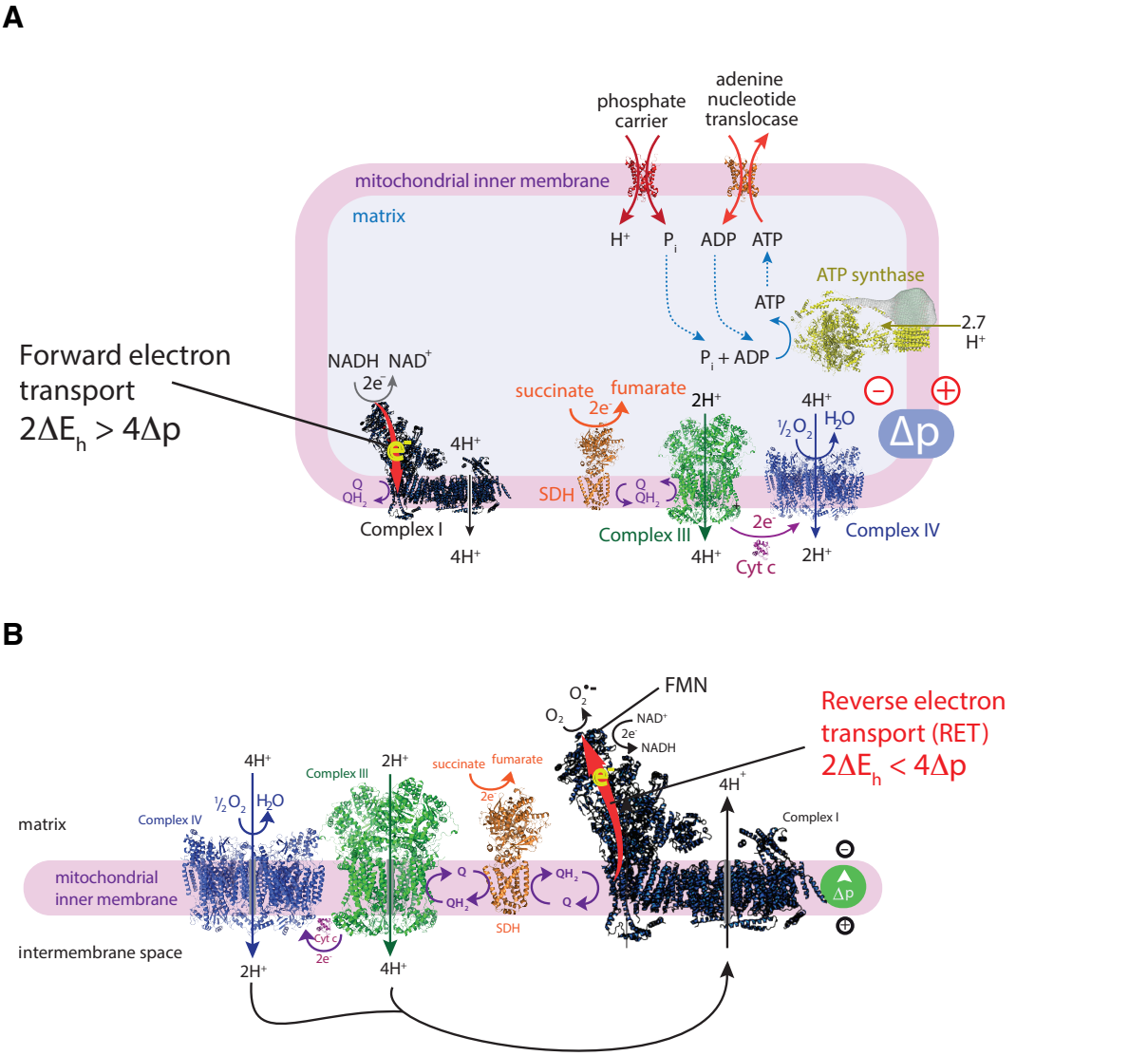

Figure 1.3. Forward and reverse electron transport by complex I. (A) *In forward electron transfer, NADH donates two electrons to complex I, which transfer along a series of Fe-S clusters to reduce Q to QH_2. When the NADH/NAD^+ ratio is high, or electron transfer to the rest of the ETC is inhibited, electrons can back up and hyper-reduce the FMN, leading to superoxide generation by reduction of O_2. The redox energy difference from the transfer of electrons between NADH/NAD^+ and Q/QH_2 (ΔE_h) drives the pumping of four protons across the IMM to maintain the protonmotive force (ΔP) that drives ATP synthesis. For forward electron transfer, the ΔE_h needs to be greater than the energy required to pump the protons against the ΔP: $2\Delta E_h > 4\Delta P$.* ***(B)*** *The direction of electron transport can be reversed if the ΔP is high and/or the Q pool is very reduced so that $4\Delta P > 2\Delta E_h$. Then, electrons can flow backward through complex I and onto the FMN from where they can reduce NAD^+ to NADH or O_2 to superoxide. The red arrow in complex I indicates the direction of electron transfer. Cyt c, cytochrome c; SDH, succinate dehydrogenase. (Chouchani et al., 2016).*

1.3.3 Mitochondrial superoxide and hydrogen peroxide metabolism

Superoxide produced in the matrix is itself not highly reactive and cannot permeate membranes. However, nitric oxide ($NO^{\bullet}$) can diffuse into mitochondria and react with superoxide to generate peroxynitrite ($ONOO^{-}$), which is highly reactive and damaging. Superoxide can also directly inactivate some Fe-S centers in proteins, such as aconitase (Murphy, 2012). Superoxide is generally dismutated rapidly to H_2O_2, spontaneously or enzymatically by the high concentration of MnSOD (Murphy, 2009). H_2O_2 in the presence of ferrous or cuprous ions can generate the very reactive hydroxyl radical ($OH^{\bullet}$) (Murphy, 2012). The hydroxyl radical and peroxynitrite can cause oxidative damage to mitochondrial proteins, DNA and lipids. The IMM contains a high proportion of unsaturated fatty acids, which are susceptible to lipid peroxidation. This can make the IMM more permeable to protons, which can uncouple OXPHOS and disrupt the activity of membrane proteins. Lipid peroxidation can also generate reactive species, such as 4-hydroxynonenal, which can also damage mitochondrial proteins and DNA. To prevent oxidative damage to DNA, lipids and protein, H_2O_2 can be scavenged by a number of matrix non-protein and protein thiols with specialised functions, including the peroxiredoxin/thioredoxin and mitochondrial glutathione systems **(Figure 1.4)** (Murphy, 2012, Cox et al., 2009), explained in greater detail below.

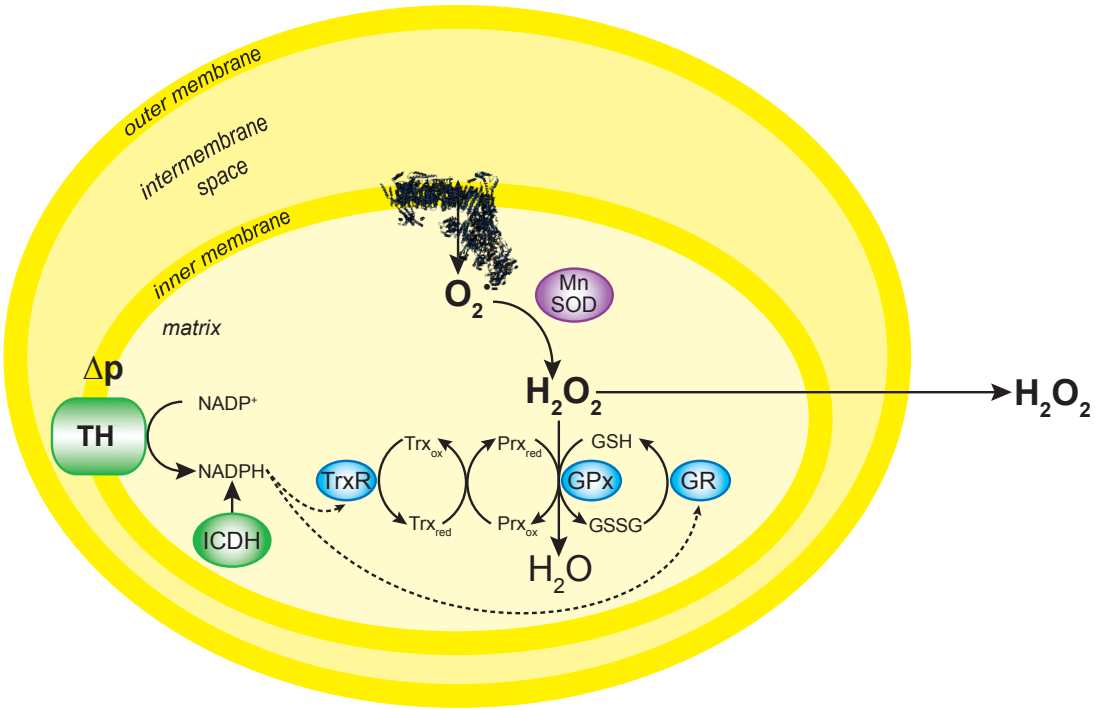

Figure 1.4 A simplified schematic of mitochondrial superoxide and H_2O_2 metabolism. *Superoxide produced to the matrix is dismutated to H_2O_2 by manganese superoxide dismutase (MnSOD). H_2O_2 is metabolised to H_2O by the action of peroxidases, including peroxiredoxin (Prx) and glutathione peroxidase (Gpx). Prx is recharged by thioredoxin (Trx). Levels of reduced Trx are controlled by thioredoxin reductase (TrxR), which in turn is regulated by the NADPH/$NADP^+$ pool and its determinants. Gpx uses glutathione (GSH) to reduce oxidised Prx, which is recycled by glutathione reductase (GR). H_2O_2 is also membrane permeable (Vissers et al., 2018).*

1.3.3.1 The peroxiredoxin/thioredoxin system

Peroxiredoxins (Prx) are a family of thiol peroxidases that help to maintain the redox balance of the cell by reducing H_2O_2 to H_2O and are re-charged by thioredoxin (Trx) (Chae et al., 1994, Cox et al., 2009, Murphy, 2012). Different Prx isoforms are located in different subcellular compartments: Prx 1, 2, and 6 in the cytosol; Prx 3 and 5 in the mitochondrial matrix (Prx 5 is also present in peroxisomes); Prx 4 is secreted. Active Prx monomers form reversible, inter-protein disulfide bridges when oxidised, which results in Prx homodimerisation and temporary inactivation. Typically, two cysteine Prxs contain an active thiol that reacts rapidly with H_2O_2 to generate a sulfenic acid (-SOH). This sulfenic acid then

reacts with an adjacent thiol on another Prx to form a dimer with an inter-protein disulfide. The modification is readily reversible by interaction with Trx, which reduces the disulfide to a dithiol form (-SH). Extended oxidation can cause thiol modifications that do not lead to Prx dimerisation: sulfinic acid ($–SO_2H$), which is slowly reversible by sulfiredoxin, and sulfonic acid ($–SO_3H$)), which is not reversible. Trxs (Trx 2 in the mitochondrial matrix, Trx 1 in the cytosol) reduce disulfide bonds on proteins, including those in Prxs. An active thiol in Trx acts as a nucleophile, attacking the target disulfide bond and forming an intermediate disulfide bridge with the substrate protein. This is then reduced by the attack of the second Trx thiol, resulting in a dithiol on the substrate protein. Trx is then recycled from a disulfide form to a dithiol form by thioredoxin reductase (TR), which uses NADPH as a reducing modality (Murphy, 2012) **(Figure 1.5)**.

1.3.3.2 The mitochondrial glutathione system

Glutathione (GSH) is synthesized in the cytosol and then transported into mitochondria. Inside mitochondria, the GSH pool is primarily (95%–99%) reduced, with a small amount of oxidised glutathione disulfide (GSSG). The GSH pool is maintained and reduced by glutathione reductase (GR), which uses NADPH as a reducing power **(Figure 1.6)**. GSH degrades peroxides using glutathione peroxidase (Gpx), of which two forms exist in the matrix: soluble Gpx 1 mainly degrades H_2O_2 and Gpx 4 is adsorbed to the matrix surface of the IMM, where it degrades phospholipid hydroperoxides to alcohols, protecting against lipid peroxidation. Glutathione-S-transferases (GSTs) use GSH to detoxify electrophiles including xenobiotics and products of oxidative damage, such as epoxides and alkyl hydroperoxides. Glutaredoxins (Grx) catalyze the deglutathionylation of proteins, which can occur when protein thiols are oxidised and react with GSH. Grx 2 exists in mitochondria and Grx 1 in the cytosol (Murphy, 2012).

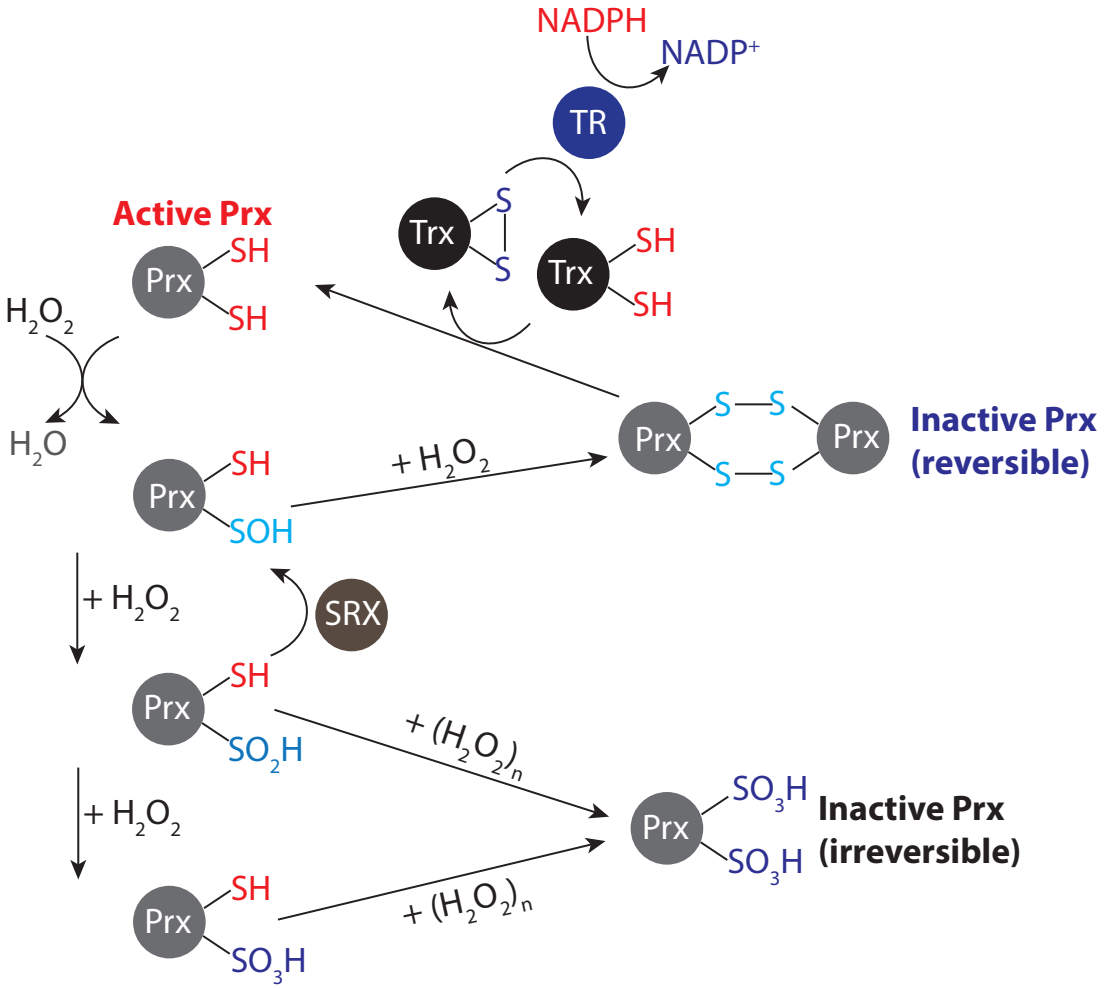

Figure 1.5 The peroxiredoxin/thioredoxin system. *Peroxiredoxins (Prxs) reduce H_2O_2 to H_2O, forming sulfenic acids (-SOH), which lead to the formation of inter-molecular homodimers linked by disulfide bridges. Hyperoxidation can lead to sulfinic acid (-SO_2H) or sulfonic acid (-SO_3H) modifications, which are slowly reversible (by sulfiredoxin (SRX)), or irreversible, respectively. Hyperoxidised Prxs are inactive and indicative of oxidative damage. Prx dimers are recycled by thioredoxins (Trx), which in turn are regulated by thioredoxin reductase (TR) and NADPH.*

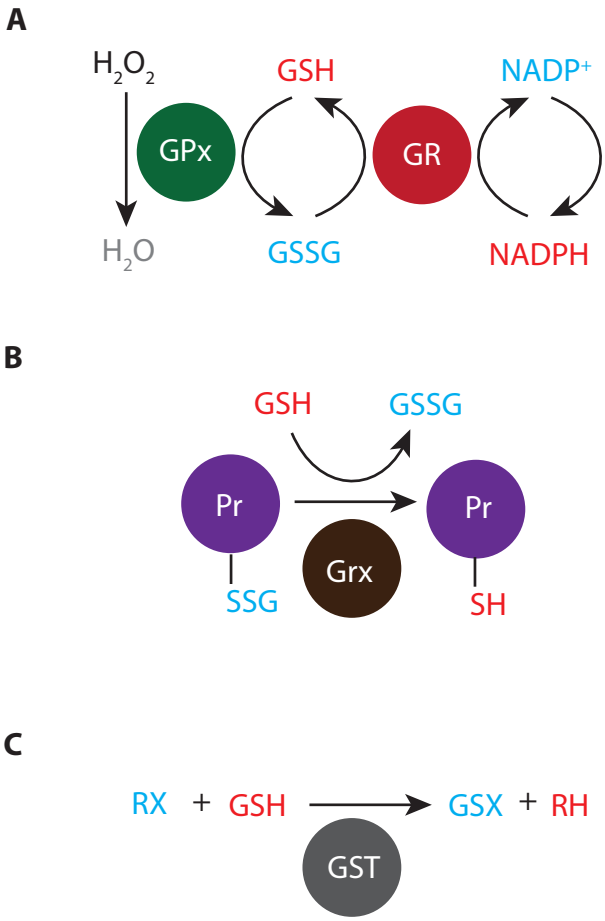

Figure 1.6 The mitochondrial glutathione system. (A) *Glutathione peroxidase (Gpx) metabolises H_2O_2 to H_2O, using reduced glutathione (GSH). Oxidised glutathione (GSSG) is recycled back to GSH by glutathione reductase (GR).* ***(B)*** *GSH exchanges with protein (Pr) thiols, catalysed by glutaredoxin (Grx).* ***(C)*** *GSH reacts with electrophiles (RX), catalyzed by glutathione-S-transferase (GST).*

1.4 Mitochondrial Redox Signalling

Mitochondrial redox signalling may be an essential facet of the health and fate of the cell. Situations in which mitochondrial ROS signalling seems to be particularly important are in the activation of cells such as macrophages during inflammation (Mills et al., 2016, Green et al., 2011) and also when mitochondria act as signalling hubs in the response to viral infections (Buskiewicz et al., 2016). However, there are considerable uncertainties about the mechanisms and significance of mitochondrial redox signalling, some key points of which I discuss below.

1.4.1 How mitochondrial ROS can behave as a redox signal

For mitochondrial H_2O_2 to be a redox signal it is important that it be responsive to mitochondrial status (Holmstrom and Finkel, 2014, Finkel, 2012, Janssen-Heininger et al., 2008). One way in which this can occur is in the alteration to the generation of superoxide at complex I in response to changes in the ΔP and the redox state of the Q pool (Murphy, 2009, Chouchani et al., 2016). RET is exquisitely sensitive to these factors, both of which are central components of mitochondrial function and which vary in direct response to mitochondrial activity and do not require artificial intervention. For example, ROS production by RET might be enhanced when mitochondria are inactive and over-supplied with electrons and minimised when mitochondria are active (Murphy, 2009, Chouchani et al., 2016). Therefore, the current view of our and other labs is that RET at complex I may be a major physiological source of superoxide within the mitochondrial matrix.

In addition to modulation by the factors that affect ΔP and Q redox state, RET could be affected by other changes to complex I, for example by post translational modifications (PTMs) such as phosphorylation (Covian and Balaban, 2012). This is only a theoretical possibility at this stage. The rate of RET by complex I is also affected by the proportion of complex I that is in the active or the deactive state. For example, during ischaemia, complex I adopts the deactive state (Gorenkova et al., 2013, Drose et al., 2016) but whether such transitions are used to regulate RET

is not known. Finally, complex I can exist as an isolated complex, or as a supercomplex with other respiratory chain complexes (Moreno-Loshuertos and Enriquez, 2016). The physiological role, if any, of supercomplex formation is not clear at present (Blaza et al., 2014). However, as changes in the extent of complex I incorporation into supercomplexes correlates with changes in mitochondrial ROS formation it may be that these processes are interrelated (Lopez-Fabuel et al., 2016, Moreno-Loshuertos and Enriquez, 2016). Therefore, RET at complex I is determined by factors that alter the ΔP and the Q redox state, with the possibility that PTMs, conformation changes or incorporation into supercomplexes may also affect RET.

The process of RET has been found to be biologically relevant in several scenarios. Pathologically, after blood flow is restored to ischaemic tissue (e.g. after heart attacks and strokes) superoxide production by RET has been found to contribute to tissue damage known as ischaemia reperfusion injury. The rapid oxidation of the succinate that accumulates during ischaemia favours reduction of the Q pool. The reduced Q pool favours proton pumping by complexes III and IV, helping maintain a large ΔP upon reperfusion and the degradation of adenine nucleotides during ischaemia limits ADP availability upon reperfusion that would otherwise diminish ΔP by stimulating mitochondrial ATP synthesis (Chouchani et al., 2016). The result is a burst of superoxide by RET through complex I when oxygenated blood flow is restored. RET has also been reported to contribute to the metabolic adaptation of immune cells during inflammation (Mills et al., 2016), the immune response to viral infection (Buskiewicz et al., 2016) and lifespan extension in fruit flies (Scialo et al., 2016).

1.4.2 Regulation of mitochondrial ROS

Once formed within the mitochondrial matrix, the H_2O_2 level can then be regulated by its degradation or rate of release. Superoxide produced in the matrix is dismutated to membrane-permeable H_2O_2 by the high concentration of MnSOD (Murphy, 2009). Although superoxide is a negatively charged molecule that will not

readily diffuse through membranes, it is possible that some superoxide that escapes MnSOD may also act independently as a signalling molecule within the matrix, by acting on the Fe-S centre in aconitase, for example (Gardner, 2002, Hurd et al., 2012). There are effects of MnSOD level of expression on cell fate that are poorly understood (Hart et al., 2015), perhaps suggesting that the balance between superoxide and H_2O_2 level may modulate signalling pathways.

Most studies indicate that the Prx 3 is the major peroxidase in mitochondria (Cox et al., 2009, Winterbourn and Hampton, 2008). Thus, regulating the activity of Prx 3 may be a key way of modulating H_2O_2 levels within mitochondria. The activity of Prx is modulated by the ratio of its active to reversibly inactive form, due to disulfide bond formation (Cox et al., 2009, Cox et al., 2008). Extended oxidation can also cause less readily reversible thiol modifications that do not lead to dimerisation. Prx can be oxidised to a sulfinic acid form that can be slowly reactivated by sulfiredoxin (Noh et al., 2009) or a sulfonic acid form that is not reversed. These alterations may alter the flux of H_2O_2 from the mitochondria. There is also the possibility that Prx activity may be altered by PTMs, or by the formation of higher order structures of Prx (Barranco-Medina et al., 2009), but the details of these are not clear yet. Finally, the activity of Prx and other peroxidases in mitochondria is determined by the redox state of the mitochondrial nicotinamide adenine dinucleotide phosphate (NADPH) pool. The NADPH pool itself can respond to a number of factors: the activity of ΔP-dependent transhydrogenase (TH), isocitrate dehydrogenase (ICDH) and malic enzyme which maintain NADPH, and the redox state of the GSH and Trx systems which are reduced by NAPDH (Murphy, 2012, Murphy, 2015, Nickel et al., 2015). Thus, several factors potentially regulate the steady state level of H_2O_2 in mitochondria.

1.4.3 Transfer of mitochondrial redox signals from mitochondria to the cytosol

The concept of mitochondrial redox signalling as a mode of communication to other cell compartments is based on the assumption that H_2O_2 produced in the

mitochondria can also diffuse to the cytosol. In the cytosol, H_2O_2 could alter enzyme activity either directly through reversible oxidation of cysteine thiols, or indirectly by facilitating redox-relay interactions with other redox-sensitive proteins (Prxs, Trxs etc.) (Herrmann and Riemer, 2012, Sobotta et al., 2015). For H_2O_2 itself to act as a redox signal it has to leave the mitochondria and enter the cytosol. It is known that isolated mitochondria can produce a flux of H_2O_2 from both the IMS and the matrix (Murphy, 2009) and this indicates that H_2O_2 itself can leave the mitochondrion and pass to the cytosol. However, the evidence for this occurring in whole cells is less clear. The passage of H_2O_2 through the plasma membrane, for example in response to its generation outside the cell by NADPH oxidases, is mediated by aquaporins (Bienert et al., 2007, Miller et al., 2010). There have been reports of aquaporin 8 in the IMM (Calamita et al., 2005, Marchissio et al., 2012), however these have been disputed (Yang et al., 2006) and no aquaporins are found in data bases of mitochondrial proteins, such as MitoCarta2. The very large ratio of the surface area of the IMM to the matrix volume may enable the rapid diffusion of H_2O_2 through the IMM phospholipid bilayer in the absence of aquaporins (Yang et al., 2006). In the IMS the H_2O_2 should then be able to diffuse out of that compartment by movement through porins in the OMM. However, due to the multitude of antioxidant defence systems in the matrix, the level of ROS production required to overwhelm these systems and pass to the cytosol may be high.

The above scenario indicates how H_2O_2 itself could move from the matrix to the rest of the cell. It is also possible that the H_2O_2 in the mitochondrial matrix can alter mitochondrial metabolism, perhaps by altering the activity of metal-centre proteins (Winterbourn, 2013), and thus lead to the generation of another signal that can pass on to the rest of the cell, for example by generating an electrophile.

1.4.4 The role of cysteine thiols in redox signalling

The way in which H_2O_2 acts as a signal requires that it affect the activity or location of a protein in some way (Collins et al., 2012, Gough and Cotter, 2011, Holmstrom

and Finkel, 2014). This is usually thought to happen by the redox modification of a target cysteine residue. Cysteine residues in proteins contain reactive thiol groups, whose redox state is a critical mediator of protein function. Under normal physiological conditions, the majority of exposed thiol groups are maintained in a reduced state (Leichert and Jakob, 2004, Menger et al., 2015). However, fluctuations in cellular redox state can lead to a range of oxidative thiol modifications, including the formation of disulfide bonds, *S*-sulfenylation, *S*-nitrosation, *S*-acetylation or *S*-glutathionylation (Paulsen and Carroll, 2013). These oxidative modifications can affect the activity, binding interactions, lifetime or localisation of a protein (Holmstrom and Finkel, 2014). Importantly, the majority of these post-translational redox modifications are reversible, therefore they are capable of functioning as a signalling mechanism, as well as in the response of the cell to oxidative stress (Collins et al., 2012). Thiol groups can become irreversibly oxidised under conditions of oxidative stress, often leading to degradation of the affected proteins. Compared to other amino acids, cysteines are under-represented in proteins due to their high reactivity and either tend to be extremely highly, or very poorly, conserved (Marino and Gladyshev, 2010). However, not all cysteines are equally susceptible to oxidative modification. For instance, solvent-exposed cysteines are more likely to be redox-sensitive than cysteines buried within the protein structure (Murphy, 2012). Since multiple redox-reactive cysteine residues with different susceptibilities to oxidation can be present within a protein, many redox states are possible for a single protein. Thus, it is important to be able to identify and quantify the changes in these protein thiols under various biological conditions.

Cysteine thiol oxidation can be caused by the direct reaction of H_2O_2 with the target, and can be reversible, (e.g. reversible inactivation of tyrosine phosphatases through oxidation of an active site cysteine thiol (Meng et al., 2002)) or irreversible (e.g. thiol akylation of Kelch-like ECH-associated protein 1 (KEAP 1), inducing nuclear translocation of nuclear factor erythroid 2-related factor 2 (NRF 2) (Kobayashi and Yamamoto, 2006)). However, an alternative mechanism has also

been described in some cases such that it is not H_2O_2 itself that acts as a direct signal but that it is picked up by a disulfide relay such that this then passes on the redox signal to the target protein (Sobotta et al., 2015, Azevedo et al., 2003, Herrmann and Riemer, 2012) **(Figure 1.7)**.

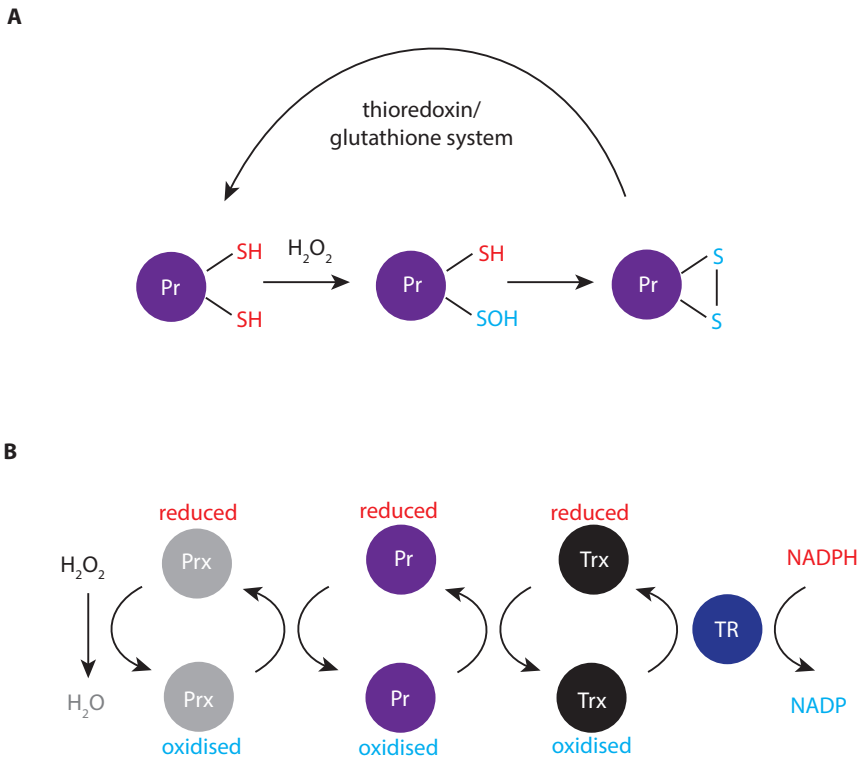

Figure 1.7 Protein thiol oxidation by (A) direct interaction with H_2O_2 or (B) a possible disulfide relay mechanism. *H_2O_2 can modify proteins **(A)** directly, e.g. disulphide formation, or **(B)** indirectly, via disulfide formation with ROS scavaging proteins. Both mechanisms can temporarily alter protein function. Pr, protein.*

1.4.5 Redox regulated proteins

Whether a redox signal emanates from mitochondria as H_2O_2, a redox relay or another signalling molecule, this will ultimately have to act on a target protein and lead to a biological effect. Interesting examples of this include cytosolic stabilisation of hypoxia-inducible factor-1α (HIF-1α) in response to mitochondrial ROS during hypoxia and inflammation (leading to transcriptional adaptation) (Sanjuan-Pla et al., 2005, Mills et al., 2016) and mitochondrial ROS-induced oligomerisation of

mitochondrial antiviral signalling (MAVS) protein in immune cells in response to viral infection, enhancing production of pro-inflammatory cytokines (Buskiewicz et al., 2016). Many proteins have been claimed to be targets for mitochondrial redox signals but often the evidence is circumstantial or indirect. The development of redox proteomic methods should enable theses targets to be picked up more definitively (Rinalducci et al., 2008, Kumar et al., 2013, Menger et al., 2015). However, it may be a recurring problem that these changes are a series of reversible redox changes that have multiple small effects that may be challenging to detect definitively. Going forward, our lab is particularly interested in investigating the down stream effects of mitochondrial ROS production by RET, particularly the response of signalling enzymes that have the ability to modify mitochondrial function and cellular metabolism, including AMP-activated protein kinase (AMPK).

1.5 AMP-activated protein kinase: a metabolic sensor and regulator

1.5.1 Mitochondrial respiratory control

The evolution of mitochondria as efficient generators of ATP has enabled the development of complex life. Mitochondria can acutely respond to short-term energy demand by increasing or decreasing ATP synthesis by OXPHOS, a phenomenon known as respiratory control (Brown, 1992, Murphy and Brand, 1987, Chance and Williams, 1956). Mechanistically, respiration can be controlled at several steps in the OXPHOS process, including: 1) ATP synthesis by the F_OF_1-ATP synthase is limited by the availability of ADP and Pi, which are imported into the mitochondria from the cytosol (ADP in exchange for ATP). If ATP usage (hydrolysis) in the cytosol is increased, the breakdown products ADP and Pi will thus increase and favour increased ATP synthesis in the mitochondria. If ATP use in the cytosol is decreased, the supply of ADP and Pi for further ATP synthesis will also decrease (Chance and Williams, 1956); 2) Increased ATP synthesis will decrease the ΔP across the IMM (due to the H^+ influx into the matrix from the IMS) and this will also stimulate respiration in the short-term (Brown et al., 1990); 3) Respiration can be controlled by the supply of electrons to respiratory complexes, mainly from NADH, therefore an increased mitochondrial NADH/NAD^+ ratio (perhaps from increased flux through the CAC or fatty acid oxidation) will enhance OXPHOS by raising the ΔP (Brown et al., 1990); 4) increased calcium levels can increase respiration by stimulating calcium-sensitive matrix dehydrogenases which increase NADH supply (McCormack et al., 1990); 5) F_OF_1-ATP synthase can be inhibited by proteins, such as IF_1, although the physiological role of these inhibitory proteins are unclear (Nakamura et al., 2013); 6) ATP production can also be inhibited by the degree of proton leak, such as occurs in brown adipose tissue when potential energy is dissipated as heat (Brown, 1992).

1.5.2 Signaling between mitochondria and the rest of the cell

While mitochondrial respiratory control ensures that ATP synthesis can rapidly adapt to meet demand, this adaptation is limited in the short-term by substrate availability and in the long-term by the number and mass of mitochondria in the cell. To increase flux through catabolic pathways or to increase mitochondrial biogenesis under conditions of chronic ATP demand, mitochondria signal to several regulatory systems in the cell. AMP-activated protein kinase (AMPK) plays a key role in energy sensing and is considered to be one of the cell's master regulators of energy metabolism (Carling et al., 2011, Hardie et al., 2012, Garcia and Shaw, 2017, Hardie et al., 2016). AMPK senses energy demand as an increase in cellular AMP and ADP relative to ATP and then adapts a broad range of cellular processes to promote ATP production and inhibit ATP expenditure. AMPK exerts control over several signalling pathways that affect mitochondrial function.

In quiescent cells performing mainly catabolic processes the main source of ATP is the efficient OXPHOS process (O'Neill and Hardie, 2013). Fatty acid oxidation is a major contributor of electrons to the ETC (via NADH and $FADH_2$) and so promotes OXPHOS. Fatty acids are transported from the cytosol into the mitochondria for oxidation as acyl-coA, via the Carnitine/Palmitoyl-Transferase 1 (CPT1) (Schreurs et al., 2010). Proliferating cells on the other hand, such as some activated immune cells, require increased anabolic processes such as fatty acid and protein synthesis, required for cell growth and division. Switching from OXPHOS to glycolysis favours NADPH production necessary for these anabolic processes (Hamanaka and Chandel, 2012, O'Neill and Hardie, 2013). Increased fatty acid synthesis has the effect of simultaneously inhibiting fatty acid oxidation. Both processes are largely controlled by acetyl CoA carboxylase (ACC) isoforms 1 and 2, respectively, whose activity is sustained by citrate emanating from the mitochondrial CAC cycle for biosynthetic purposes at the expense of electron donation to the ETC (Schreurs et al., 2010). ACC1 (cytosolic) converts cytosolic acetyl CoA (from citrate) to malonyl CoA, a requirement for fatty acid biosynthesis.

ACC2 (associated with the cytosolic face of the OMM) also converts acetyl CoA to malonyl CoA, which inhibits CPT1 transport of acyl-coA into the mitochondria for oxidation. Thus, when both isoforms are activated, fatty acid biosynthesis is promoted and fatty acid oxidation is inhibited. Under conditions of ATP demand, however, fatty acid metabolism is switched back to favour oxidation, and AMPK plays a key role in this metabolic switch (Hardie, 2011, O'Neill and Hardie, 2013, Schreurs et al., 2010). AMPK, when activated under conditions of ATP demand, phosphorylates and inhibits both ACC isoforms. This adaptation inhibits fatty acid synthesis (as malonyl CoA production is now inhibited) and promotes fatty acid oxidation (with increased mitochondrial acyl-coA import via uninhibited CPT1). Thus, AMPK, by exerting control over the activity of ACC1 and 2 (amongst other pathways), can acutely control electron donation to the ETC for OXPHOS to meet the ATP demand of the cell.

The volume of mitochondria and the area of the IMM in a cell varies greatly depending on cell type and energy demand (Jornayvaz and Shulman, 2010). Continuously working muscles, such as the heart, have greater mitochondrial content and activity than sporadically contracting muscle, e.g. back muscles (Paul and Sperling, 1952). Chronic exercise, cold exposure, dietary restriction, cell division and differentiation are all associated with increased mitochondrial biogenesis in cells (Puigserver et al., 1998, Civitarese et al., 2007, Holloszy, 1967, Jornayvaz and Shulman, 2010), i.e. the growth and division of pre-existing mitochondria. Mitochondrial biogenesis requires the cytosolic synthesis and mitochondrial import of ~ 1000 – 1500 proteins encoded by the nuclear genome, as well as the mitochondrial synthesis of proteins encoded by mtDNA. Peroxisome-proliferator-activated receptor γ co-activator-1α (PGC-1α) is a transcriptional coactivator that facilitates mitochondrial biogenesis by activating different transcription factors: nuclear respiratory factor (NRF) 1 and 2, which activate nuclear transcription of mitochondrial genes and also activate mitochondrial transcription factor A (Tfam), which drives transcription and replication of mitochondrial DNA. PGC-1α also regulates mitochondrial antioxidant defence

systems. PGC-1α expression and activity is regulated by several signalling pathways in the cell, including AMPK which, when activated by energy chronic demand, upregulates PGC-1α activity through phosphorylation (Jornayvaz and Shulman, 2010, Hardie, 2011, Jager et al., 2007). Thus, AMPK can bring about long-term adaptation of cells to a higher ATP demand by increasing the mass of mitochondria in the cell.

1.5.3 Sensitivity to ATP/AMP and ATP/ADP ratios as an energy sensing strategy in the cell

Cells require a high ratio of ATP/ADP (i.e. 10 - 20) in order to perform energy-requiring processes typically involving ATP hydrolysis (usually to ADP and Pi) (Hardie and Hawley, 2001). Adenylate kinase in cells (which catalyses the interconversion of ATP, ADP and AMP) maintains the reaction 2ADP ↔ ATP + AMP close to equilibrium. In healthy cells, the high ATP/ADP ratio ensures the adenylate kinase reaction is shifted towards ADP production, with AMP levels maintained low. During acute or chronic energy demand, when ATP synthesis is inhibited or ATP consumption increases, this decrease in ATP (measured as lowered ATP/ADP ratio) is countered by the adenylate kinase reaction shifting towards ATP production to promote maintenance of a high ATP/ADP ratio. This shift will also cause AMP levels to increase. As the ATP/AMP ratio varies as the square of the ATP/ADP ratio (Hardie and Hawley, 2001) (**Figure 1.8**), small decreases in the ATP/ADP ratio translate to much larger relative decreases in the ATP/AMP ratio. Thus, enzyme regulation by the ATP/AMP ratio has evolved as a highly sensitive, energy sensing strategy in the cell. A number of metabolic enzymes are regulated by AMP, including glycogen phosphorylase, and fructose-1,6-bisphosphatase, which switch on catabolic or switch off anabolic pathways, respectively (Hardie, 2011). AMPK is also activated by decreased ATP/AMP and ATP/ADP ratios and this results in downregulation of anabolic (ATP-consuming) pathways in the cell and upregulation of catabolic (ATP-generating) pathways.

Thus, activated AMPK works with adenylate kinase to maintain the high ATP/ADP ratios in cells needed for survival.

$$2ADP \xleftrightarrow{\text{adenylate kinase}} ATP + AMP$$

$$\frac{[ATP]\,[AMP]}{[ADP]^2} = K \text{ (equilibrium constant)}$$

$$\therefore [ATP]\,[AMP] = K\,[ADP]^2$$

$$\frac{[ATP]\,[AMP]}{[ATP]^2} = \frac{K\,[ADP]^2}{[ATP]^2}$$

$$\therefore \frac{[AMP]}{[ATP]} \propto \left(\frac{[ADP]}{[ATP]}\right)^2$$

Figure 1.8 The cell ATP/AMP ratio varies as the square of the ATP/ADP ratio. *Adapted from (Hardie and Hawley, 2001).*

1.5.4 Discovery of AMPK

AMPK is a highly conserved serine/threonine kinase with orthologs found in all eukaryotes except *Encephalitozoon cuniculi*, an obligate intracellular parasite that has also lost its mitochondria during evolution (Miranda-Saavedra et al., 2007). Its ubiquity highlights the importance of AMPK in integrating mitochondrial function with the rest of the cell. AMPK is not found in prokaryotes, but the β subunit carbohydrate-binding module (CBM), which binds glycogen and can facilitate allosteric inhibition of AMPK (McBride et al., 2009), is similar to that found in prokaryotic enzymes that metabolise starch and glycogen (Machovic and Janecek,

2006, Hardie, 2011), suggesting that the function of AMPK may have origins in glucose sensing. The key experiments that led to the discovery of AMPK were performed in *Saccharomyces cerevisiae.* Inactivating mutations in (or knockouts of) genes of the SNF1 complex (later labelled as orthologs of mammalian AMPK subunits) resulted in failure of the yeast to grow on substrates other than glucose (Hardie, 2011). SNF1 is insensitive to activation by AMP (Zhang et al., 2017). Thus, AMPK orthologs are essential to survival and proliferation of complex life, but mainly conferred protection from glucose starvation in lower order eukaryotes. The discovery of AMPK in mammalian cells came about as phosphorylation-induced inactivation of enzymes involved in fatty acid biosynthesis (ACC and HMG-CoA reductase) were found to be caused by one enzyme that was activated by AMP, leading to the renaming of the enzyme as AMP-activated protein kinase (Hardie et al., 2011). Importantly, knockout of the AMPK catalytic α subunit (both isoforms simultaneously) causes embryonic lethality in mice (Ross et al., 2016), highlighting the essential role of AMPK in complex life. Recent studies have re-emphasised the role of AMPK as a glucose sensor as well as an energy sensor, with the discovery of an AMP/ADP-independent mechanism for AMPK activation during glucose starvation before the onset of energy stress (Zhang et al., 2017, Zhang et al., 2014). For the remainder of this chapter I will focus on how AMPK functions as a metabolic sensor in mammalian cells, and the potential role of ROS in AMPK regulation.

1.5.5. Structure of AMPK

AMPK is a heterotrimeric serine/threonine kinase **(Figure 1.9)**. The complex is composed of a catalytic α subunit and regulatory β and γ subunits, with seven mammalian genes encoding different subunit isoforms: α1 and α2, β1 and β2, and γ1, γ2 and γ3 (Ross et al., 2016). The α subunit contains an N-terminal kinase domain (α-KD), containing an activation loop that is phosphorylated (at T172) by upstream kinases, including LKB1 and CaMKKβ, which is required for activation. The α subunit contains C-terminal regulatory domains: auto-inhibitory domain (α-AID), which associates either with the α-KD (inactive conformation) or the γ subunit

(active conformation); α-linker, which connects the α-AID to the C-terminal domain (α-CTD), essential for allosteric regulation by adenine nucelotides; serine/threonine-rich loop (ST-loop), which mediates inhibitory phosphorylation and signalling by PI3K/Akt and glycogen synthase kinase 3 (at S487). The β subunit contains a regulatory carbohydrate-binding module (CBM), which is phosphorylated (at S108) and makes up the allosteric drug and metabolite (ADaM) binding pocket along with the α-KD N-lobe. The β subunit also contains and an N-terminal myristoylation site, which is also regulatory and required for activation during glucose starvation. The γ subunit contains four nucleotide-binding cystathionine-β-synthase (CBS) domains, which allow the enzyme to sense and respond to changing levels of adenine nucleotides (ATP, ADP and AMP) as a readout of the energy status of the cell (Xiao et al., 2007). In structural studies, only three of these sites have been found occupied: one molecule of AMP binds irreversibly at CBS4 and molecules of AMP, ADP or ATP can bind reversibly at CBS1 and CBS3 (Xiao et al., 2007, Xiao et al., 2011). It is considered that each of the different subunit isoforms can recombine with any of the partner subunit isoforms to form functional enzymes (12 combinations in total), but some isoform combinations are more favoured in different cell and tissue types, e.g. predominant α2/β2/γ3 activation in skeletal muscle (Ross et al., 2016, Birk and Wojtaszewski, 2006). However, isoform specificity is not fully understood and variation in isoform combination is not fully characterised.

A

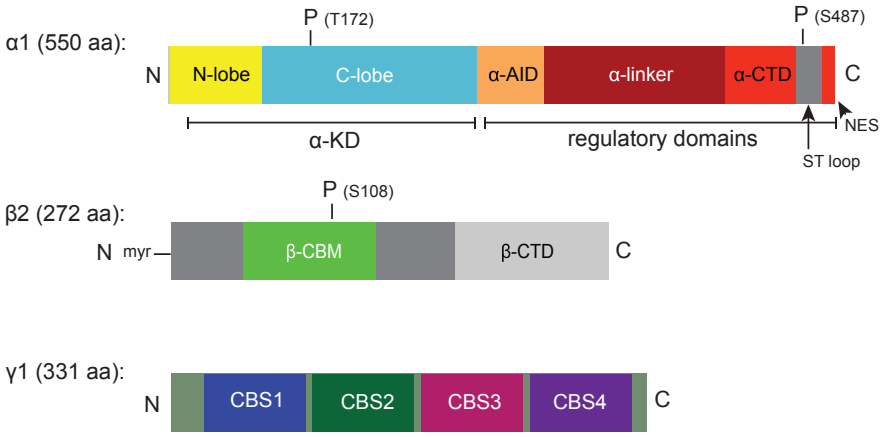

B

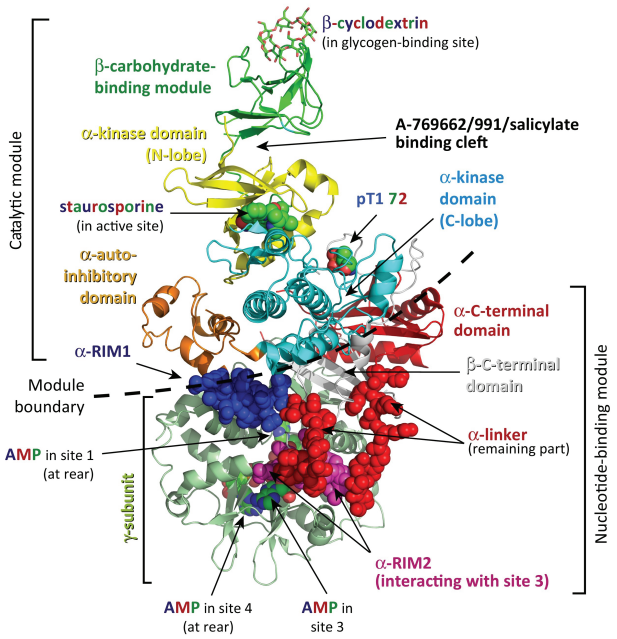

Figure 1.9 Domain map and structure of human AMPK α1/ β2/ γ1. (A) *Domain map of AMPK α1/β2/γ1. α-KD, kinase domain; α-AID, auto-inhibitory domain; CTD, C-terminal domain; ST loop, serine/threonine rich loop; NES, nuclear export sequence; CBM, carbohydrate binding module; CBS, cystathionine-β-synthase domain.* ***(B)*** *Structure of human AMPK α1β2γ1 complex. The CBM and catalytic sites are occupied by cyclodextrin and staurosporine, respectively. The ADaM site is empty. The 'module boundary' shows the approximate boundary between the 'catalytic module' (containing the α-KD and the β-CBM) and the 'nucleotide-binding module' (containing the γ subunit and the α and β CTD). Extracted from (Hardie et al., 2016).*

1.5.6. Downstream targets of AMPK

In response to activating phosphorylation, AMPK in turn phosphorylates and modifies the activity of a wide range of downstream proteins (over 50 proteins cited in the literature), with the general effect of increasing and conserving ATP levels in the cell. Situations that induce AMPK activation in cells and tissues include skeletal muscle contraction during exercise (Winder and Hardie, 1996, O'Neill et al., 2011, Jager et al., 2007), glucose deprivation (Zhang et al., 2017), hypoxia and ischaemia (Marsin et al., 2000, Hardie, 2011). **Table 1.1** lists a selection of enzymes, transcription factors/activators and transporters under the control of AMPK (Garcia and Shaw, 2017, Carling et al., 2011, Hardie, 2017, O'Neill and Hardie, 2013, Hardie et al., 2012).

Target	Target function	Effect of AMPK activation on target function
Anabolic pathways		
ACC1	Fatty acid synthesis	Inhibition
SREBP1c	Transcription of lipogenic genes	
ChREBP		
HMGR	Sterol synthesis	
mTORC1	Protein synthesis	
GS	Glycogen synthesis	
Catabolic pathways		
ACC2	Fatty acid oxidation	Activation/induction
PGC1α	Mitochondrial biogenesis, OXPHOS, antioxidant defence	
GLUT1/4	Glucose uptake	
ULK1	Autophagy	
CD36	Fatty acid uptake	
FOXO	Antioxidant defence	
PFK1/2	Glycolysis	

Table 1.1 Selection of enzymes, transcription factors/activators and transporters under the control of AMPK. *ACC, acetyl CoA carboxylase; SREBP1c, sterol regulatory element-binding protein 1c; ChREBP, carbohydrate-responsive element-binding protein; HMGR, 3-hydroxy-3-methylglutaryl coenzyme A reductase; mTORC1, mammalian target of rapamycin complex 1; GS, glycogen synthase; PGC1α, peroxisome proliferator-activated receptor gamma coactivator 1- α; GLUT1/4, glucose transporter 1/4; ULK1, unc-51-like autophagy-activating kinase 1; CD36, cluster of differentiation 36 (fatty acid translocase); FOXO, forkhead box O; PFK1/2, phosphofructokinase 1/2.*

1.5.7. Regulation of AMPK by adenine nucleotides

In general terms, AMPK senses energy stress as increased cellular AMP and ADP relative to ATP. This leads to allosteric activation of AMPK by AMP, which binds to the CBS domains of the γ subunit and induces a conformational change that promotes phosphorylation of AMPK by upstream kinases (which induces high levels of kinase activity), leads to allosteric activation and also protects AMPK from inactivating dephosphorylation (Xiao et al., 2007). Activated AMPK phosphorylates and turns on or off a broad range of enzymes, generally shifting metabolic pathways toward ATP production and conservation (Carling et al., 2011, Hardie et al., 2012). As cellular ATP levels rise again, increased binding of ATP to the γ subunit removes the positive allosteric effect of AMP and AMPK activity is decreased in an elegant feedback mechanism (Oakhill et al., 2011, Hardie et al., 2011).

In greater detail, when in a basal state (assuming a high cellular ATP/ADP ratio) AMPK is bound by one molecule of AMP at γ subunit CBS4 and most likely two molecules of magnesium-bound ATP (MgATP) (at CBS1 and CBS3) (Xiao et al., 2011). Binding of MgATP maintains interaction between the AID and α-KD, inhibiting kinase activity. During moderate energy stress (with rising AMP and ADP concentrations relative to ATP), AMP replaces MgATP bound at CBS3, disengaging the AID from the α-KD, putting AMPK in an 'active' conformation (Cheung et al., 2000). This promotes phosphorylation of threonine 172 (Thr172) within the α-KD activation loop by upstream kinases, which stabilises enzyme in the active conformation and results in up to several hundred-fold increase in AMPK activity (Oakhill et al., 2010). Binding of AMP (or ADP at CBS3) also protects AMPK from inactivating dephosphorylation by protein phosphatases (e.g. PP2A, PP2C) (Oakhill et al., 2011, Xiao et al., 2011, Davies et al., 1995). During more severe energy stress, binding of AMP to CBS1 results in additional allosteric activation of phosphorylated AMPK (Xiao et al., 2011, Gowans et al., 2013, Xiao et al., 2007).

In healthy cells, concentrations of free adenine nucleotides are reported to be in the following ranges: 3 – 8 mM ATP, 50 – 200 µM ADP and 0.5 – 5 µM AMP (Xiao et al., 2011). ATP is greatly in excess, but as most ATP in cells is bound to Mg (and AMP and ADP are not) AMPK binds AMP and ADP significantly more strongly than ATP in cells. As ADP is typically in excess of AMP, ADP is more effective than AMP at displacing CBS-bound MgATP and protecting AMPK from dephosphorylation, suggesting that this may be the main physiological mechanism of AMPK activation (Hardie et al., 2011, Xiao et al., 2011). But only AMP induces allosteric activation of AMPK and promotes phosphorylation-dependent high levels of activity (Xiao et al., 2011). Thus, AMPK can sensitively sense and respond to varying levels of energy demand, ranging from mild to severe. In a feedback mechanism, when cell ATP/ADP and ATP/AMP ratios are high, increased binding of MgATP to CBS1 and CBS3 inhibits allosteric activation of the complex or protection from dephosphorylation (Carling et al., 2011, Xiao et al., 2011).

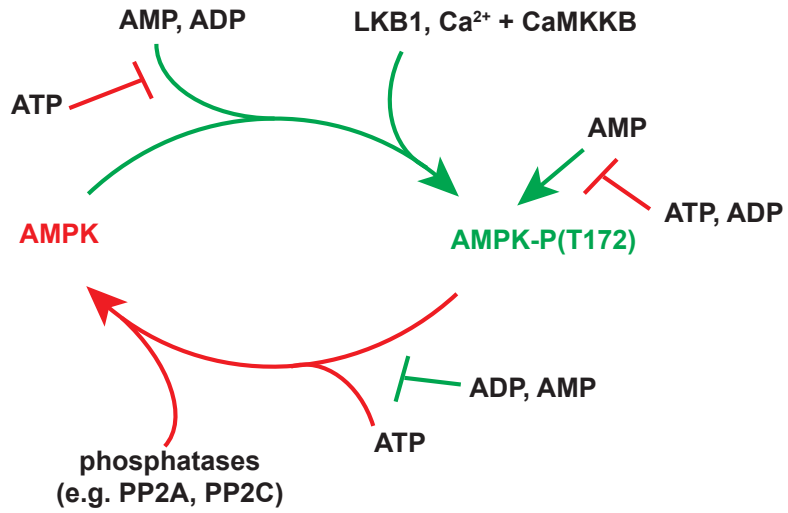

Figure 1.10 AMPK is regulated by adenine nucleotides in a tripartite mechanism. *Binding of AMP or ADP induces conformational change, which promotes phosphorylation and activation of AMPK by upstream kinases and protects against dephosphorylation by phosphatases. Further binding of AMP to phosphorylated AMPK allosterically activates the enzyme. Adapted from (Hardie and Alessi, 2013).*

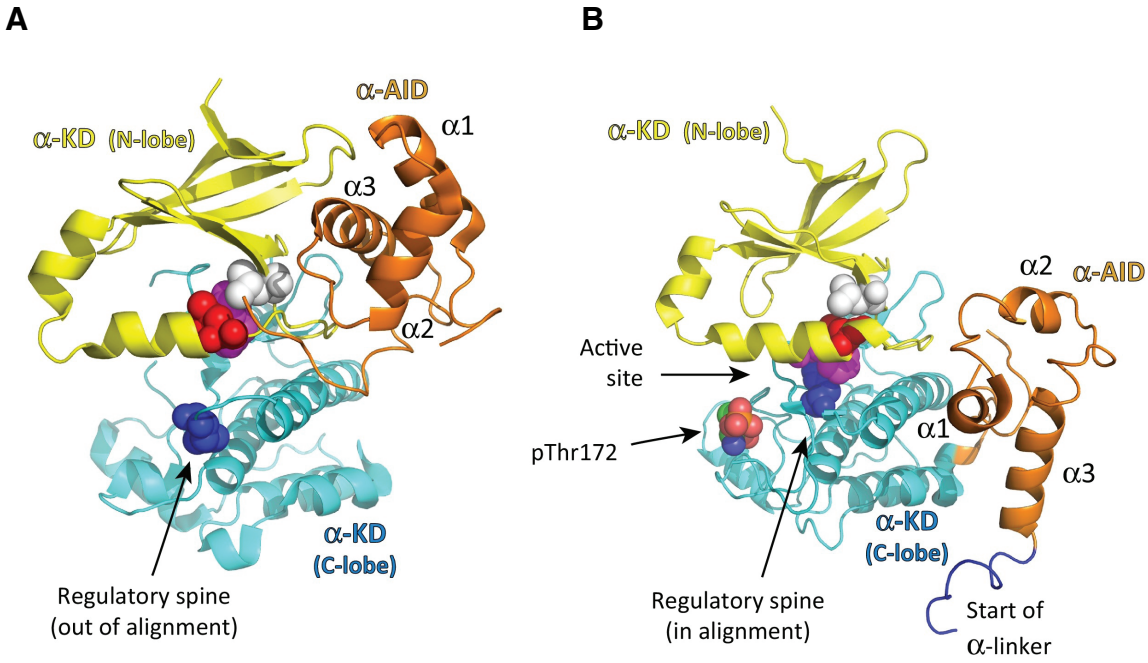

Figure 1.11 Structure of human AMPK α1 in (A) 'inactive' and (B) 'active' conformations. (A) *Binding of MgATP to the γ subunit CBS domains maintains the interaction between the AID and α-KD, inhibiting kinase activity.* ***(B)*** *When AMP replaces MgATP, the AID disengages from the α-KD, putting AMPK in an 'active' conformation. Side chains of the regulatory spine: Leu81, white; Leu70, red; Phe160, magenta; His139, blue. Extracted from (Hardie et al., 2016).*

1.5.8. Regulation of AMPK by co- and post-translational modifications

For AMPK to phosphorylate and regulate other enzymes, AMPK itself needs to be phosphorylated at the conserved Thr172 residue of the α catalytic subunit, which locks the enzyme in an active conformation. (Hawley et al., 1996). This phosphorylation is promoted and protected by the effects of AMP (Davies et al., 1995) and also protected by AMP and ADP (Xiao et al., 2011). The tumour suppressor Liver Kinase B1 (LKB1) is the main upstream AMPK kinase (Hawley et al., 2003, Hong et al., 2003, Shaw et al., 2004). Furthermore, C-terminal farnesylation of LKB1 is required for maximal AMPK activation in response to energy stress (Houde et al., 2014). Binding of ADP or AMP to AMPK protects AMPK from dephosphorylation by protein phosphatases (e.g. PP2A, PP2C) (Oakhill et al., 2011, Xiao et al., 2011, Davies et al., 1995). Increases in cytosolic calcium levels can also induce AMPK phosphorylation and activation via

Ca^{2+}/calmodulin-activated protein kinase kinase β (CAMKKB) (Hawley et al., 2005, Woods et al., 2005). AMPK activity can be inhibited by phosphorylation of the α subunit at Ser487 by Akt during insulin signalling (Ross et al., 2016). The AMPK β subunit also contains a co-translational N-myristoylation site, which is required for AMPK phosphorylation and perinuclear AMPK accumulation during glucose starvation (Oakhill et al., 2010). β subunit N-myristoylation may also play a role in mitophagy (i.e. the destruction of damaged mitochondria by autophagy), possibly by enabling association between AMPK and mitochondrial membranes (Liang et al., 2015). The AMPK β subunit is also phosphorylated, which is important for AMPK activation by compounds that bind the allosteric drug and metabolite (ADaM) binding site (Hardie, 2016).

1.5.9 AMPK as a clinical target

As AMPK can inhibit anabolic pathways required for cell proliferation, AMPK has become an attractive target in the study of cancer metabolism. Whereas some AMPK subunit isoforms tend to be mutated in certain cancers (i.e. α2 and β1) perhaps conferring a loss of function, other AMPK subunit isoforms tend to be amplified in certain cancers (α1 and β2), suggesting they confer a pro-survival advantage (Ross et al., 2016). This discrepancy points towards different subunit isoforms having different substrate or cell type specificities that are not fully understood, and this complicates the interpretation of the role of AMPK in cancer development and progression. Further complicating matters is the characterization of the main AMPK kinase, LKB1, as a tumour suppressor, suggesting that at least some of its tumour suppressing function is mediated by AMPK signalling (Hardie and Alessi, 2013). Similarly, AMPK is inhibited via α subunit phosphorylation by Akt in cancers in which the tumour suppressor PTEN is non-functional and whole-body AMPK α1 knock-out mice have accelerated B cell lymphoma development driven by Myc over-expression (Ross et al., 2016). Thus, the role of AMPK in cancer metabolism is highly complicated and factors such as the cell type, cancer stage (early or invasive) and tumour microenvironment (i.e. sufficient or deficient oxygen

and/or nutrient availability) likely play a role in characterizing AMPK as an oncogene or a tumour suppressor (Ross et al., 2016).

AMPK has become an attractive target in protection against inflammation. Activated immune cells that promote inflammation are highly proliferative and thus have a glycolytic phenotype (O'Neill and Hardie, 2013). Non-proliferating, anti-inflammatory immune cells instead preferentially make ATP by OXPHOS. As AMPK promotes oxidative metabolism, AMPK has emerged as drug target for inflammatory diseases. Furthermore, the long-used anti-inflammatory drug salicylate (which also arises from aspirin metabolism) is now known to directly bind and activate AMPK via the ADaM binding site (Hawley et al., 2012). AMPK activation has also been protective in models of cardiac ischaemia reperfusion injury (IRI), possibly mediating some of the effects of the phenomenon of ischaemic preconditioning by upregulating antioxidant defence systems and pro-survival pathways in the heart (Greer et al., 2007, Zaha et al., 2016, Qi and Young, 2015, Kim et al., 2011, Shao et al., 2014).

AMPK is also a potential drug target in treatment of type-2 diabetes (T2D) (Hardie, 2016). Metformin is a widely-prescribed drug treatment for T2D that helps to normalise blood glucose levels without causing hypoglycaemia or lactic acidosis in otherwise healthy patients. Metformin (and the more hydrophobic biguanide, phenformin) non-specifically inhibit complex I in isolated mitochondria and in cells *in vitro* at mM concentrations (Owen et al., 2000, Bridges et al., 2014). The concurrent activation of AMPK at these concentrations has been considered to be largely due to decreased ATP/ADP ratios resulting from inhibition of respiration (Zhou et al., 2001). Although the exact mechanism(s) of metformin action are not completely understood, there is evidence that AMPK activation contributes to some of the beneficial effects of metformin (Fullerton et al., 2013, Hardie, 2016). AMPK α2 knockout mice are insulin-resistant and glucose-intolerant, and exercise, which activates AMPK, also helps to maintain and normalise blood glucose levels. Thus,

selective AMPK activators are being investigated as therapeutic agents for T2D (Hardie, 2017).

1.5.10 AMP/ADP-independent regulation of AMPK

The small molecule AMPK activators A-769662 and 991, and salicylate (a metabolite of aspirin), bind at one site at the interface of the phosphorylated β subunit CBM and the N-lobe the α subunit kinase domain, which is known as the allosteric drug and metabolite (ADaM) binding site (Langendorf and Kemp, 2015, Xiao et al., 2013). Binding of compounds at this site increases AMPK activity independently of adenine nucleotide-binding to the y subunit by inducing a conformational change that puts AMPK into the 'active' conformation (i.e. the kinase domain is unblocked by the AID). This conformational change does not require Thr172 phosphorylation but the phosphorylation appears to enhance AMPK activity (Willows et al., 2017). This AMP/ADP-independent allosteric activation can also act in synergy with AMP, as combined A-769662 and AMP binding have an additive effect on AMPK activity (Xiao et al., 2013). There are currently no known naturally occurring metabolites that bind the ADaM site. Binding of glycogen and cyclodextran to the β subunit CBM may have an inhibitory effect on AMPK (McBride et al., 2009). However, an alternative hypothesis is that the binding of glycogen enables co-localization of AMPK with glycogen synthase, which is inactivated by AMPK phosphorylation (Ross et al., 2016). It is possible that glycogen binding may also regulate AMPK activation by an as yet unknown natural ADaM-site activator. All the known allosteric activators that bind this site have a much higher affinity for complexes containing β1 rather than β2 (Ross et al., 2016). Furthermore, it is reported that the β2 subunit binds glycogen more strongly than the β1 subunit (Koay et al., 2010). Ultimately, the importance of glycogen binding remains somewhat unclear and remains an interesting area of investigation. AMPK activity can also be inhibited by Compound C (also known as dorsomorphin), however, the mechanism by which Compound C inhibits AMPK is unclear and the compound has been reported to inhibit several other kinases (Liu et al., 2014).

AMPK is also activated in an ADP/AMP-independent manner by glucose deprivation. Previously, AMPK activation during glucose deprivation has been considered an adenine nucleotide-dependent event. As glucose is a key source of ATP in the cell, generated via either glycolysis or OXPHOS, historically it was thought that glucose deprivation would be an energy stress on the cell, causing decreased ATP/ADP and/or AMP/ATP ratios (Salt et al., 1998). However, glucose deprivation has not always been accompanied by measurable decreases in ATP/ADP or ATP/AMP ratios. Recently, it has been found that glucose deprivation activates AMPK by an alternative mechanism (Zhang et al., 2017). Briefly, as extracellular glucose deceases, so too do intracellular levels of fructose-1,6-bisphosphate (FBP), an intermediate in the glycolysis pathway. Aldolase, a glycolytic enzyme that catalyses the reversible conversion of FBP to glyceraldehyde 3-phosphate and dihydroxyacetone phosphate, senses the fall in levels of FBP. When unbound by FBP, aldolase promotes formation of a multi-enzyme lysosomal complex that has previously been shown to be necessary for AMPK activation. The complex contains at least: v-ATPase, ragulator, axin, LKB1 and AMPK (Zhang et al., 2014, Zhang et al., 2013). Binding of aldolase by FBP promotes dissociation of LKB1 and AMPK from the multi-enzyme scaffold, which inhibits AMPK phosphorylation by LKB1. Thus, high glucose has an inhibitory effect on AMPK activation and low glucose promotes AMPK activation by an AMP/ADP and ADaM-binding site – independent mechanism.

1.5.11 Evidence for and against redox-regulation of AMPK

ROS have also been investigated as an atypical regulator of AMPK as a further way of relaying information about the metabolic state or demands of the cell and thus promoting pro-survival adaptation (Shao et al., 2014, Emerling et al., 2009, Hart et al., 2015, Zmijewski et al., 2010, Mungai et al., 2011, Hawley et al., 2010, Auciello et al., 2014). It is conceivable that redox-regulation of AMPK may enable feedback about the redox state of the cell and promote upregulation of antioxidant defense systems (Greer et al., 2007, Zaha et al., 2016, Qi and Young, 2015, Kim et

al., 2011). Below I will discuss the key findings from the published articles that have most influenced the experimental goals of this thesis.

One of the first papers to examine the role of ROS in AMPK regulation in detail was presented by (Zmijewski et al., 2010) in which the authors described an AMP/ADP-independent redox mechanism for AMPK activation in HEK 293 cells. The authors detected redox changes to cysteine residues in the AMPK α catalytic subunit (specifically glutathionylation of C299 and C304) in response to exogenous H_2O_2 delivered as a bolus (250 μM) and also in response to H_2O_2 generated by glucose oxidase (10 milliunits/ml). The authors observed concurrent activation of AMPK in these experiments, measured as increased AMPK(T172) and ACC(S79) phosphorylation (a downstream target). Although the authors described observing decreased cell ATP/ADP ratios in cells treated with 250 μM H_2O_2, they did not observe decreases in cell ATP/ADP ratios in cells treated with glucose oxidase, which generates H_2O_2 in cell culture media gradually. The authors also observed increased AMPK activity in extracellular experiments when recombinant AMPK was incubated with H_2O_2 or H_2O_2 + GSH, with effects negated when C299 and C304 were mutated. Thus, the authors concluded that H_2O_2 was activating AMPK by a redox-dependent mechanism.

Building upon this and other previous studies, Auciello et al. (2014) also utilised the glucose oxidase method of extracellular H_2O_2 generation, testing the effects of H_2O_2 on HEK 293 cells expressing the AMP/ADP-insensitive AMPK γ subunit R531G (RG) mutant, which renders AMPK unable to be allosterically activated by AMP or allosterically protected from dephosphorylation by AMP or ADP. In this study, the authors observed decreases in cell ATP/ADP ratios after treatment with glucose oxidase. The high level of AMPK activity observed in wild-type (WT) cells was abrogated in RG cells, indicating that the H_2O_2 was primarily acting by an AMP/ADP-dependent mechanism. The authors did observe low-grade but statistically significant increases in AMPK activity with time, suggesting that H_2O_2 may play a minor role in AMPK regulation by inhibiting AMPK dephosphorylation,

potentially by H_2O_2-induced inhibition of upstream phosphatases.

The authors of (Shao et al., 2014) described a different mechanism of AMPK redox regulation, in which AMPK activity was inhibited by cysteine thiol oxidation. AMPK α was identified as a target of Trx 1, which prevented oxidation of AMPK α cysteine thiols (C130 and C174 in the α-KD) and so prevented AMPK inhibition during glucose deprivation and cardiac ishaemia, both associated with increased cellular ROS. It is plausible that immortalised cell lines have upregulated antioxidant defence systems compared to primary cells and tissues (e.g. high expression of Trxs and a highly reduced NADPH/NADP pool, a key reducing modality in the cell (Murphy, 2015)), which may explain why this remains the only report of redox-dependent AMPK inhibition that I have observed to date.

The role of mitochondrial ROS in AMPK activity is less studied and interpretation of results is more complicated. It has been reported that ROS produced during hypoxia (Emerling et al., 2009, Mungai et al., 2011) can increase AMPK activity in different AMP/ADP-independent ways, e.g. involving LKB1, or via ROS-induced increases in cytosolic calcium (which activates the alternative AMPK kinase, CAMKKB). It is reported that during hypoxia, mitochondrial superoxide is generated from complex III, and can be liberated directly to the mitochondrial matrix or to the IMS (Murphy, 2009). Superoxide generated to the IMS would bypass the protein-dense barrier of the IMM and theoretically provide an easier pathway to transfer to the cytosol than mitochondrial superoxide generated to the matrix only. Mitochondrial ROS has also been reported to play a role in AMPK activation via MnSOD upregulation in cancer cells, however the exact mechanism of the pathway, reported to involve CAMKKB, remains unclear (Hart et al., 2015).

The highly varied reports of AMP/ADP-dependent or AMP/ADP-independent AMPK regulation by ROS indicate that there is still much that is not known about the factors that affect AMPK activity in cells. There are a number of possible technical and biological reasons for the above and other diverse reports of AMPK regulation.

it is possible that varying sensitivities in methods of measuring adenine nucleotides can affect the interpretation of AMP/ADP-dependent or AMP/ADP-independent mechanisms. Different levels of ROS scavenging proteins in different cell types (and other factors that affect the redox state of the cell) may affect AMPK redox state and thus activity. Different expression levels of AMPK subunit isoforms and enzymes which co- or post-translationally modify AMPK may affect how AMPK responds to different ROS. Different cellular nutrient availability (e.g. high or low [glucose]) may also differentially affect AMPK responses to ROS. With regard to mitochondrial ROS, the site of ROS production may determine how the ROS affects cellular signaling pathways, including AMPK (e.g. ROS production from complex I versus that from complex III, or ROS production produced by forward or reverse electron transfer). Due to the vital role played by AMPK in metabolic regulation and cell survival, it is vital that the diverse mechanisms governing AMPK regulation are elucidated.

1.6 Summary and aims

Above, I have introduced the key steps in mitochondrial energy metabolism and highlighted the importance of mitochondria to complex life as we know it. As a by-product of energy metabolism, mitochondria can also produce ROS from several sources within mitochondria, including from respiratory complexes of the electron transport chain, in our view mainly from complex I (Murphy, 2009). These ROS can overwhelm the multitude of antioxidant defence systems within the mitochondrial matrix and cause oxidative damage, which can contribute to cell death (Smith et al., 2012). ROS may also behave as signalling molecules, by reversibly oxidising proteins at cysteine residues that are important for protein function (Collins et al., 2012, Gough and Cotter, 2011, Holmstrom and Finkel, 2014). Historically, mitochondrial ROS production was considered to be an unregulated process, produced by dysfunctional mitochondria. More interesting is the recent view that for mitochondrial ROS to behave as a signal to the rest of the cell it should be regulated and responsive to mitochondrial status (Holmstrom and Finkel, 2014, Finkel, 2012, Janssen-Heininger et al., 2008). Thus, mitochondrial ROS produced by RET has emerged as a potentially biologically relevant signal, as it is a tightly-regulated process dependent on a highly-reduced mitochondrial Q pool and high mitochondrial ΔP (Chouchani et al., 2016). Mitochondrial ROS production by RET is reported to play a role in metabolic adaptation of immune cells during inflammation (Mills et al., 2016), the immune response to viral infection (Buskiewicz et al., 2016) and lifespan extension (Scialo et al., 2016), as well as being a key source of ROS during ischaemia-reperfusion (IR) injury, highlighted in a study that enabled greater understanding of the metabolic requirements necessary for RET to occur in biology (Chouchani et al., 2014). One way in which mitochondrial ROS may behave as a signal is by altering the activity of AMPK, a key metabolic sensor and regulator of cell metabolism (Carling et al., 2011, Hardie et al., 2012, Garcia and Shaw, 2017, Hardie et al., 2016). AMPK is primarily regulated by adenine nucleotides, mainly AMP, which, when levels rise relative to ATP during energy stress, binds to and activates the enzyme. When activated, AMPK generally

enhances ATP generating pathways and inhibits ATP consuming pathways to promote cell survival. As mitochondria are key generators of ATP, they can signal to AMPK via the magnitude of the cellular ATP/AMP and ATP/ADP ratios. Mitochondria may also signal to AMPK via ROS. AMPK exerts control over several transcriptional responses in the cell, including PGC1α and NRF 1 and 2, and FOXO3, which upregulate the expression of genes required for mitochondrial biogenesis and antioxidant defence, respectively (Jager et al., 2007, Greer et al., 2007). Thus, the role of ROS in AMPK activity has been investigated in recent years. Several important papers have helped to clarify the role of exogenously-generated or cytosolic ROS in AMPK regulation. However, the role of mitochondrial ROS, including that produced by RET, remains unclear. Thus, the main focus of this thesis has been to build upon previous work in the field and work towards characterising the effects of ROS, specifically mitochondrial ROS, on AMPK activity in cells. This goal was divided into three individual but interrelated sub-projects, which I discuss in detail in the following three chapters, and introduce briefly below.

Aim 1. An important step in determining if a protein is potentially redox regulated is monitoring the redox state of the protein itself in response to ROS (Requejo et al., 2010). Proteins can be oxidatively modified at cysteine residues (specifically at the thiol group), which can affect the functioning of that protein. There are several mass spectrometry techniques that can enable a screen of the redox state of the proteome (Held et al., 2010, Leichert et al., 2008, Menger et al., 2015), but the readouts are often biased towards abundant proteins that can be easily detected. Complementary methods utilise targeted approaches that enable the redox state of candidate proteins to be determined. In **Chapter 3**, I describe a method of candidate protein redox state analysis, which I developed in collaboration with co-first author Lucie A.G. van Leeuwen and corresponding author Helena M Cochemé (both of MRC London Institute of Medical Sciences, Du Cane Road, London W12 0NN, UK; Institute of Clinical Sciences, Imperial College London, Hammersmith Hospital Campus, Du Cane Road, London W12 0NN, UK), and others. The

chapter describes the steps involved in optimising the new method (which offers more flexibility than previous methods), for which we used a known redox-regulated protein, GAPDH, as a model. I then discuss adapting the method to analyse purified AMPK, with the ultimate aim of analysing the redox state of AMPK in cell lysates. Progress was made in this regard, suggesting future optimisations will enable AMPK redox state in cells to be analysed. Results emerging from experiments discussed in **Chapter 4** then shifted the focus away from redox state analysis and towards analysis of AMPK regulation.

Aim 2. The second aim of this thesis was to characterise the effects of exogenous or selective, mitochondrially-derived ROS on AMPK activity, cell ATP/ADP ratios and subcellular redox state to determine if the effects of different sources of ROS on AMPK activity can be explained as AMP/ADP-dependent regulation or AMP/ADP-independent (redox) regulation. These results are presented in **Chapter 4.** It remains unclear to what extent mitochondrial ROS can transfer to the cytosol and affect signalling processes there. While mitochondrial ROS is often implicated in cytosolic or nuclear signalling pathways, there is often limited data showing a biological effect of mitochondrially-derived ROS in other cellular compartments. Thus, an aim was to use peroxiredoxin dimerisation as a biologically relevant measure of the oxidation state of multiple subcellular compartments in response to different sources of ROS (Sobotta et al., 2013). As AMPK is a predominantly cytosolic protein, a reversible change in the redox state of a cytosolic protein involved in antioxidant defence and redox signalling would likely be required for there to be any potential biologically relevant redox regulation of AMPK. An irreversible change in redox state would be indicative of oxidative damage. By combining cellular sub-compartment redox state analysis with measures of AMPK activity and cell ATP/ADP ratios, I aimed to clarify the effects of ROS on endogenous AMPK activity, using screening methodology that can be readily adapted to any cell type.

Aim 3. The third aim of this thesis was to create a cell system for further investigating the downstream effects of mitochondrial ROS produced by RET, hypothesised to be a natural way in which mitochondria signal to the rest of the cell. To do this I aimed to stably express the alternative respiratory enzymes, NDI1 and the alternative oxidase, AOX (introduced in detail in **Chapter 5**) in mammalian cell lines, as there is evidence that these enzymes (when co-expressed alongside mammalian respiratory complexes) increase or decrease, respectively, ROS production by RET (Scialo et al., 2016, El-Khoury et al., 2013). This is reported to occur because the enzymes hyper-reduce or oxidise the Q pool, respectively, and Q pool redox state is a key determinant of RET. I aimed to express the genes in a tetracycline-inducible cell system so that a gradient of protein expression could be consistently achieved. As RET is also dependent on the magnitude of the ΔP, high expression levels of IMM-associated proteins could potentially negatively affect the ΔP or inhibit ATP production in different ways, complicating the interpretation of results. Thus, a gradient of protein expression would be desirable in using these enzymes to modulate ROS production by RET. The preliminary results of this project are discussed in **Chapter 5.** Future aims involve investigating the downstream targets of ROS production by RET in cells, including the response of AMPK.

Chapter 2

Materials and Methods

2.1 General materials and methods

2.1.1 Chemicals and consumables

All chemicals and consumables were obtained from Sigma-Aldrich, UK or Merck unless otherwise stated.

2.1.2 Quantitative and qualitative protein assays and reagents

2.1.2.1 Antibodies

All antibodies used were purchased from Sigma-Aldrich, UK unless otherwise stated, and were polyclonal antibodies unless otherwise stated as being monoclonal.

2.1.2.1.1 Primary antibodies and Western blot working dilution

- ***rabbit-acetyl coA carboxylase (ACC) isoform 1/2:*** (Cell Signalling Technology (CST): 3662), 1:1,000 (dilution);
- ***rabbit-ACC1/2-phosphoS79:*** (CST: 3661), 1:1,000;
- ***rabbit-AMP-activated protein kinase (AMPK) subunit α isoform 1/2:*** (CST: 2532), 1:1,000;
- ***rabbit-AMPKα1/2-phosphoT172 monoclonal (mAb) 40H9:*** (CST: 2535), 1:1,000;
- ***rabbit-AMPKβ1/2 mAb 57C12:*** (CST: 4150), 1:1,000;
- ***rabbit-AMPKγ1:*** (CST: 4187), 1:1,000;
- ***rabbit-AOX:*** from Professor Howy Jacobs, Institute of Biotechnology, University of Helsinki (originally supplied by 21st Century Biochemicals (Marlboro, MA))(Fernandez-Ayala et al., 2009), 1:50,000;
- ***mouse-FLAG® M2 mAb:*** (F1804), 1:1,000;
- ***rabbit-glyceraldehyde 3-phosphate dehydrogenase (GAPDH):*** (G9545), 1:10,000;
- ***rabbit-manganese superoxide dismutase (MnSOD):*** (Abcam: ab13534), 1:5,000;
- ***mouse-Myc mAb 4A6:*** (Merck Millipore: 05-724), 1:1,000;
- ***rabbit-myogenin mAb [EPR4789]:*** (Abcam: (ab124800), 1:1,000;

- ***rabbit-NDI1:*** from Professor Takao Yagi, The Scripps Research Institute, Department of Molecular and Experimental Medicine, San Diego, California, USA (Seo et al., 1998), 1:1,000;
- ***mouse-peroxiredoxin 2 (Prx 2):*** (Abcam: ab50862), 1:4,000;
- ***rabbit-Prx 3:*** (Abcam: ab73349), 1:500;
- ***rabbit-Prx-SO_3:*** (Abcam: ab16830), 1:2,000;
- ***rabbit-Sip2 (yeast ortholog of mammalian AMPKβ) mAb:*** from Professor David Carling, MRC Clinical Sciences Centre, Hammersmith Hospital Campus, London, UK (Woods et al., 1996), used for immunoprecipitation (0.3 µl serum/100-200 µg whole cell protein);
- ***mouse-α-tubulin mAb B-5-1-2:*** (T5168), 1:8,000;
- ***rabbit-voltage-dependent anion channel (VDAC):*** (Abcam: ab15895), 1:1,000;
- ***mouse-VDAC mAb 20B12AF2:*** (Abcam: ab14734), 1:5,000.

2.1.2.1.2 Secondary antibodies and Western blot working dilution

- ***IRDye® 800 goat-anti-rabbit IgG (H&L):*** (Rockland Antibodies and Assays: 611-132-003), 1:20,000;
- ***IRDye® 680RD goat anti-mouse IgG (H+L):*** (LI-COR Biosciences: 926-68070); 1:40,000.

2.1.2.2 Bicinchoninic acid assay

Concentrations of purified protein or cell lysate were determined using a Bicinchoninic acid (BCA) assay kit (Pierce ™), for use with 96-well microplates (Costar®) and a microplate reader (SpectraMax® Plus 384 Microplate Reader), recording absorbance at 562 nm. Samples were diluted in 1% (v/v) Triton X-100 (Tx100) and measured against a 7-part standard curve of Bovine Serum Albumin (BSA) (diluted 0 – 1 mg/ml in 1% (v/v) Tx100). Diluted protein samples were normalised against a 1% (v/v) Tx100 blank reaction spiked with protein reconstitution buffer or cell lysis buffer. All samples, standards and blanks were loaded in triplicate wells.

2.1.2.3 SDS-polyacrylamide gel electrophoresis (SDS-PAGE)

Purified protein or cell lysate (mass of protein as indicated in the individual experiment) was heated in an appropriate volume of 4X Laemmli sample buffer (125 mM Tris (pH 6.8), 4% (w/v) sodium dodecyl sulphate (SDS), 40% (v/v) glycerol, 25 mg bromophenol blue and freshly added reducing agent (50 mM DTT or 10 mM TCEP)) for 5 min at 95˚C. For non-reducing SDS-PAGE, reducing agents were omitted from the sample buffer. Samples were loaded on Mini-PROTEAN® TGX™ Precast 7.5%, 10%, 12% or 4-20% gradient gels (BIO-RAD), depending on the molecular weight of the target protein(s). Proteins were electrophoresed at 100 V (until the loading dye had just run off the gel) using a running buffer containing 25 mM Tris (pH 8.3), 192 mM glycine, 0.1% (w/v) SDS. Protein standards (5 µl) were loaded and electrophoresed alongside samples so that sample protein sizes could be estimated from the gel. Precision Plus Protein Dual Color standards (BIO-RAD) were loaded on all gels: all bands are visible and stained blue except two reference bands (25 kDa and 75 kDa), which are stained pink. For gels with which Western blots would later be performed, MagicMark™ XP Western Protein Standard (ThermoFisher) was also loaded on gels, which can be visualized by colorimetric detection (e.g. Coomassie protein stain) or fluorescent detection (e.g. Odyssey® CLx Infrared Imaging System).

2.1.2.4 Western blotting

Electrophoresed proteins were transferred to Immobilon®-FL Polyvinylidene difluoride (PVDF) membranes (Merck Millipore: IPFL00010) by wet transfer performed at 100 V for 1 h at 4˚C. PVDF membranes were activated in methanol for 15 s prior to pre-equilibration of the membranes, gels, filter paper and fiber pads in pre-chilled transfer buffer (25 mM Tris, 192 mM glycine, 20% (v/v) methanol, pH 8.4 (unadjusted) at 4˚C). Post-transfer, the membranes were blocked with Odyssey® Blocking Buffer (PBS) (LI-COR Biosciences: 927-40003) for 1 h at RT with gentle shaking (Bibby Stuart Platform Rocker STR6 at 30 revolutions/min (rpm)). Membranes were incubated in primary antibodies in 4% (v/v) blocking buffer in PBST (137 mM NaCl, 2.7 mM KCl, 10 mM Na_2HPO_4, 1.8 mM KH_2PO_4,

0.05% (v/v) Tween-20) or TBST (20 mM Tris, 150 mM NaCl, 0.1% (v/v) Tween-20) (both pH 7.4 at RT (adjusted with HCl)) overnight at 4˚C. Membranes were incubated in secondary antibodies in 4% (v/v) blocking buffer/PBST or TBST (1 h at RT, protected from light). Both the primary and secondary antibody dilutions used were specific for the antibody, see ***2.1.2.1 Antibodies***. All primary antibodies were raised in rabbit or mouse. All secondary antibodies were raised in goat and specific for either rabbit or mouse IgG. Membranes were washed before and after secondary antibody incubations in PBST or TBST at RT (4 – 5 buffer changes in 1 h). Incubations and washings were performed with gentle shaking (30 rpm). Final washings were performed in PBS or TBS (without Tween-20). The signal intensities of target bands were measured as fluorescence emission at 680 nm or 800 nm (depending on the secondary antibody used) with the Odyssey® CLx Infrared Imaging System. The signal intensities of target bands were quantified with LI-COR Biosciences Image Studio™ Lite software and were normalised against those of a suitable protein loading control, such as a protein located in same cell subcompartment as the target protein, whose levels in cells tend to remain stable and for which there is a sensitive and specific primary antibody. For normalisation, the signal intensity of target band was divided by the signal intensity of the control band of the same lane so that small differences in total protein loaded between samples did not affect the quantification of the target band. Transfer buffer was re-used up to five times and stored at 4˚C. Blocking buffers and antibody buffers were reused up to five times and up to three times, respectively, and stored at -20˚C.

2.1.2.5 Coomassie Protein Stain

Coomassie Brilliant Blue R-250 (BIO-RAD: 161-0436) or QC Colloidal Coomassie protein stain (BIO-RAD: 161-0803) was used to visualise protein separation on SDS-PAGE gels, according to the manufacturer's guidelines (http://www.bio-rad.com/en-uk/sku/1610436-coomassie-brilliant-blue-r-250-staining-solution) or (http://www.biorad.com/webroot/web/pdf/lsr/literature/10032602.pdf), respectively. Gels were scanned using an Epson perfection V750 Pro scanner.

2.1.2.6 **Ponceau S *reversible protein stain***

To visualise protein transfer to PVDF membranes (and any transfer inefficiencies due to air bubbles etc.), PVDF membranes (prior to blocking) were incubated in *Ponceau S* reversible protein stain for 10 min at RT with gentle shaking. The stain was decanted and the membranes washed 3 – 5 times in Milli-Q (MQ) H_2O to remove background stain and allow visualisation of protein bands. Protein bands were destained with further washings in MQ H_2O before incubating the membranes in blocking buffer and continuing with Western blotting.

2.2 Mammalian cell culture

2.2.1 Cell culture media, buffers, reagents and cell lines

- ***Standard medium:*** Dulbecco's Modified Eagle's Medium (DMEM) (Gibco™): high glucose (4.5 g/l) or low glucose (1.0 g/l), GlutaMAX™ (2 mM), sodium pyruvate (110 mg/ml); supplemented with 10 % (v/v) fetal bovine serum (FBS) (E.U.-approved, South American origin, Gibco™), 100 U/ml penicillin and 100 µg/ml streptomycin (Gibco™);
- ***C2C12 differentiation medium:*** DMEM: high glucose (4.5 g/l), GlutaMAX™ (2 mM), sodium pyruvate (110 mg/ml); supplemented with 1 % (v/v) FBS, 100 U/ml penicillin and 100 µg/ml streptomycin;
- ***Tetracycline (Tet) - free medium:*** DMEM: high glucose (4.5 g/l) or low glucose (1.0 g/l), GlutaMAX™ (2 mM), sodium pyruvate (110 mg/ml); supplemented with 10 % (v/v) tetracycline-free FBS (Clontech), 100 U/ml penicillin and 100 µg/ml streptomycin;
- ***Cell freezing medium:*** 90% (v/v) FBS, 10% (v/v) dimethyl sulfoxide (DMSO) (Fisher BioReagents);
- ***Phosphate-buffered saline (PBS)***: Dulbecco's phosphate-buffered saline (Gibco™) without calcium, magnesium or phenol red;
- ***Trypsin:*** Trypsin-EDTA (0.25%), phenol red (Gibco™);
- ***Cell lines:*** C2C12 mouse myoblast cell line (American Type Culture Collection (ATCC)); Human Embryonic Kidney (HEK 293) cell line (ATCC); Flp-In™ T-REx™ 293 cell line (Thermo Fisher Scientific);

  Flp-In™ T-REx™ 293-NDI1 stable cell line & Flp-In™ T-REx™ 293-AOX stable cell lines (both generated in this body of work); C2C12-mito-roGFP-ORP1 & C2C12-cyto-roGFP-ORP1 stable cell lines (laboratory stocks generated by Andrew R. Hall, (MRC Mitochondrial Biology Unit, University of Cambridge, Wellcome Trust/MRC Building, Cambridge Biomedical Campus, Hills Road, Cambridge CB2 0XY, UK)). See **Appendix A** for expression vectors used in generation of stable cell lines.

2.2.2 Growth and maintenance of cell lines

Cell lines were typically cultured in T75 or T125 (Thermo Scientific™, Nunclon™ Delta treated, vented) flasks in standard DMEM medium (high glucose), unless otherwise stated. Cells were incubated in a humidified atmosphere (5% CO_2/95% air) at 37 °C and routinely subcultured (at ~ 70% confluency). For subculturing, standard medium and PBS were pre-warmed from 4°C to 37°C in a water bath and trypsin was pre-warmed from 4°C to RT. In the cell culture hood, medium was aspirated and cells were washed in 5 ml PBS. PBS was aspirated and 5 ml trypsin was added to cells. For adherent cells (e.g. C2C12 cells), excess trypsin was aspirated, leaving ~ 1 ml trypsin and cells were incubated at 37°C for 3 - 5 min. Cells were then resuspended by gentle pipetting up and down after addition of 9 ml standard medium. For semi-adherent cells (e.g. HEK 293 cells), cells were incubated in 5 ml trypsin at 37°C for 3 - 5 min before resuspension by gentle pipetting up and down after addition of 5 ml standard medium. The cell suspension was centrifuged in a 15 ml Falcon tube (1,000 X g for 3 min at RT) to pellet the cells. The supernatant was aspirated and cells were gently resuspended in 10 ml standard medium by pipetting. Fresh T75 or T125 flasks (containing 10 ml or 25 ml standard medium, respectively) were seeded with a 1/10 – 1/50 dilution of cell suspension. Media in subconfluent flasks was replaced every 2 - 3 days.

2.2.3 Freezing, storing and re-thawing cell lines

Cells in T75 or T125 flasks were trypsinised, resuspended and counted by a Trypan Blue Exclusion assay. Cell suspension (10 µl) was mixed with the same vol. of Trypan Blue stain 0.4% (Invitrogen™) and the mix was loaded on a Countess™ cell counting chamber slide (10 µl per chamber). The concentration of live cells (capable of excluding the stain) per ml and the concentration of dead cells (where the stain had permeated the plasma membrane) per ml were counted using a Countess™ II FL hemocytometer (Invitrogen™). After live cell quantification, the cells were pelleted by centrifugation (described above). The supernatant was aspirated and cells were gently resuspended in cell freezing medium (described above) at a density of 1 - 5 x 10^6 cells/ml. 1 ml cell suspensions were transferred to

cryovials and placed in a Nalgene® Mr. Frosty freezing container (pre-warmed at 37°C), containing isopropyl alcohol to facilitate a slow (~1°C/min) cooling rate required for cell cryopreservation. The container was stored at - 80°C for a minimum of 24 h, after which cryovials were transferred to liquid N_2 for long-term storage. To re-thaw and culture cells, frozen cell stocks were thawed rapidly in a 37°C water bath before transferring the cell suspension to a fresh T75 flask containing 20 ml standard medium (pre-warmed at 37°C). After cell adherence had occurred (time depending on the cell line, e.g. ~ 4 h for C2C12s, ~ 24 h for HEK 293 cells), cell medium was replaced with 10 ml fresh standard medium.

2.2.4 Differentiation and treatment of C2C12 cells

C2C12 mouse myoblast cells were terminally differentiated to myotubes by serum depletion with C2C12 differentiation medium for seven days (Yoshiko et al., 2002, Leary et al., 1998), with media changes every 2 days. Cells were seeded at a density of 20,000 cells/cm^2 on 6 cm plates or 6-well plates (Nunclon Delta Surface, Thermo Scientific) in 3 ml or 2 ml standard medium (respectively) and cultured to ~ 90 % confluency prior to serum depletion. Experiments were performed 7 or 8 days after serum depletion and for these experiments fresh differentiation medium or serum-free medium (for H_2O_2 experiments) was added. Differentiation was confirmed by cell shape changes detected by microscopy (single, rounded cells changing to elongated, fused cells (Andres and Walsh, 1996, Elkalaf et al., 2013)) and Western blotting for a marker of differentiation, myogenin, which is expressed from initiation of differentiation (Yoshiko et al., 2002, Andres and Walsh, 1996). Although in the initial days of serum depletion protein expression levels of myogenin varied between batches, expression levels became stable from day 5 of serum depletion (**Figure 2.1**).

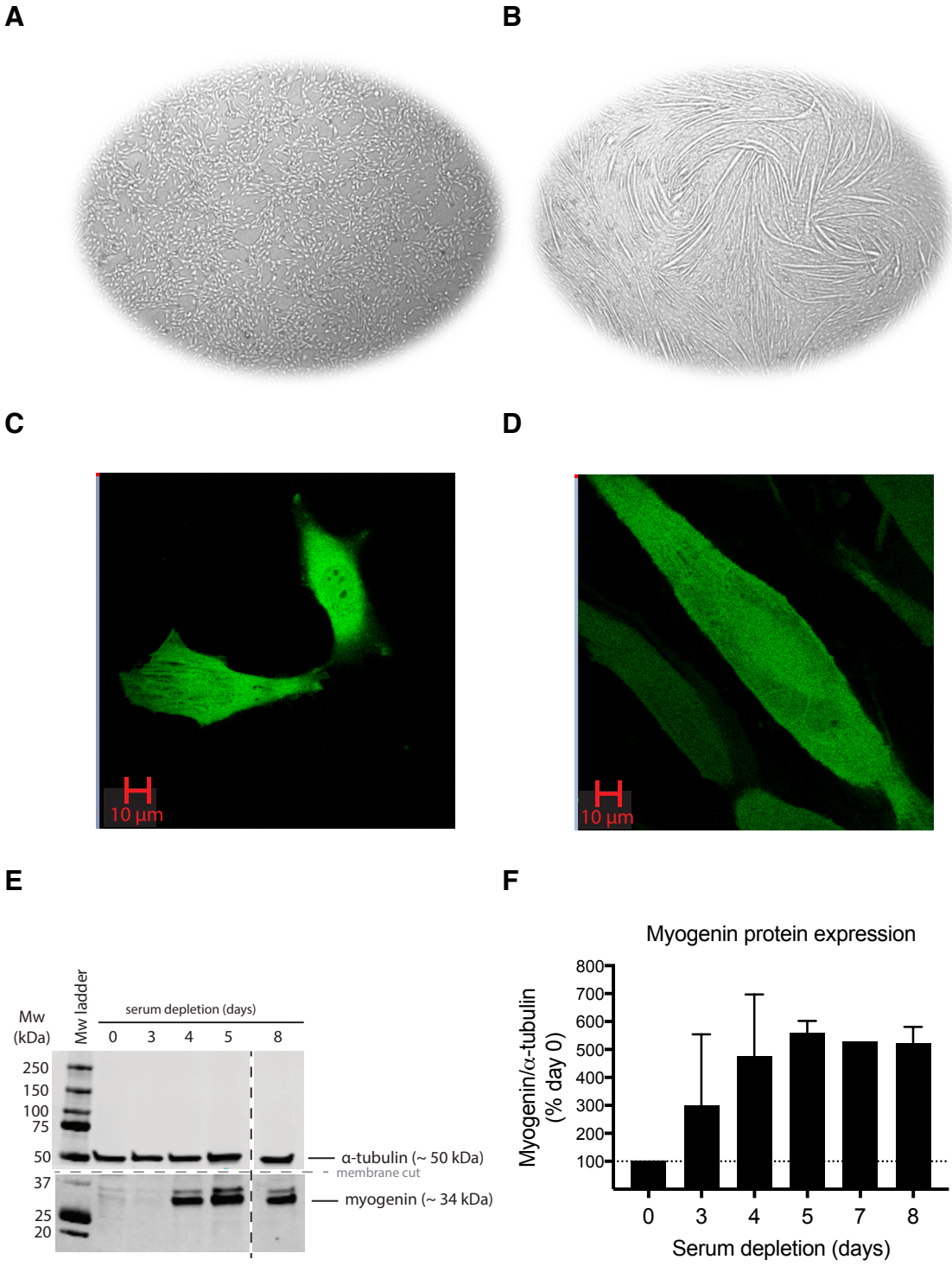

Figure 2.1 C2C12 myoblast to myotube differentiation is accompanied by cell shape and protein profile changes. (A & B, E & F) *C2C12 myoblasts were plated on 6 cm plates at 20,000 cells/cm^2 in high glucose standard medium. When cells reached ~ 90% confluency (day 0), myoblast to myotube differentiation was induced by serum depletion (replacing standard medium with differentiation medium). Cells were cultured for a further 8 days with differentiation medium changes every 2 days.* ***(A & B)*** *C2C12 myoblasts photographed* ***(A)*** *prior to differentiation (day 0) or* ***(B)*** *after differentiation (day 8 of differentiation media)****.*** *Cells were visualised in bright-field using a*

Nikon Eclipse TS100 inverted routine microscope (10X lens X 4X objective) and photographed using a QImaging QIClick™ digital CCD camera attachment. Photographs show whole field of view; ***(C & D)*** *Cells were plated and treated as described in* ***2.7 Live cell confocal microscopy and imaging****. Undifferentiated* ***(C)*** *and differentiated* ***(D)*** *C2C12-cyto-roGFP-ORP1 cells imaged using a Zeiss LSM 880 confocal microscope (63X objective, oil lens), excitation: 488 nm, emission: 500 – 550 nm* ***(E)*** *Cells were lysed in Hepes lysis buffer supplemented with DTT and protease inhibitors (see* ***2.4.1 Buffers/reagents for AMPK assays****). SDS-PAGE (~ 25 µg protein per well) and Western blots were performed as previously described. Post blocking, PVDF membranes were cut horizontally with a razor blade (as indicated by the grey dotted line) and each section was individually incubated with the appropriate primary antibody for the Mw range of that section, indicated by band descriptions (see* ***2.1.2.1.1 Primary antibodies)****. Rabbit and mouse primary antibodies were differentially labeled with fluorescent secondary antibodies (****see 2.1.2.1.2 Secondary antibodies****). Western blots were imaged using the Odyssey® CLx Infrared Imaging System (fluorescence emission at 800 nm for myogenin or 680 nm for α-tubulin);* ***(F)*** *The Western blot signal intensity of myogenin (quantified with LI-COR Biosciences Image Studio™ Lite software) was normalised to that of α-tubulin as a loading control and expressed as % day 0. Graphed data represents mean ± range of n = 2 biological replicates, except day 7 (n = 1).*

2.2.5 Maintenance of the Flp-In™ T-REx™ 293 host cell line

Flp-In™ T-REx™ 293 host cells were cultured in T75 flasks in 10 ml standard medium. 24 h after seeding, cell medium was replaced with fresh standard medium supplemented with 100 µg/mL zeocin (Invitrogen) to select for cells that contain a Flp Recombination Target (FRT) recombination site in the genome, linked to the lacZ-Zeocin™ fusion gene which confers zeocin resistance. The medium was also supplemented with 15 µg/ml blasticidin (Invitrogen) to select for cells that stably express the tetracycline (Tet) repressor gene. The Tet repressor gene in the host cell genome is under the same transcriptional control as a gene conferring blasticidin resistance. Therefore, cells resistant to both zeocin and blasticidin have the genetic properties that allow Flp-recombinase dependent gene integration and tetracycline-dependent gene expression. Cell medium was replaced every 2 – 3 days with standard medium supplemented with freshly added blasticidin and zeocin.

2.2.6 Exogenous gene expression in cells

2.2.6.1 Standard transfection procedure

For transfection, cDNA vectors were diluted to the desired concentration in Opti-MEM I Reduced Serum Media (Gibco™), (see for further details: **2.2.6.2 Transient gene expression**, and **2.2.6.3 Transfection, selection and maintenance of stable, inducible Flp-In™ T-REx™ 293 cell lines**). The final vol. of DNA/ Opti-MEM I mix = 150 µl per 6 cm cell plate to be transfected. In parallel, Lipofectamine® 2000 (Thermo Fisher Scientific) was diluted in Opti-MEM I (Lipofectamine® 2000 (15 µl) + Opti-MEM I (135 µl) per 6 cm cell plate). The DNA/ Opti-MEM I mix (150 µl) was added to the Lipofectamine® 2000/Opti-MEM I mix (150 µl). The final 300 µl mix was mixed gently and allowed to rest at RT for 5 min. The final mix was then pipetted drop-wise (using a Gilson P1,000 Pipetman) over 5 – 10 s onto plated cells in 3 ml standard medium (~ 70 % confluent at time of transfection) and the plates were swirled gently before replacing in the incubator.

2.2.6.2 Transient gene expression

HEK 293 cells were plated at a density of 20,000 cells/cm^2 on 6 cm plates in 3 ml standard media. At 60 - 70% confluency, cells were transfected with 1 µg DNA of each cDNA vector. 24 h after transfection, cells were lysed and assayed by Western blot to confirm translation of the novel or over-expressed protein of interest.

2.2.6.3 Transfection, selection and maintenance of stable, inducible Flp-In™ T-REx™ 293 cell lines

Flp-In™ T-REx™ 293 host cells were plated on 6 cm plates at a seeding density of 20,000 cells/cm^2 in 3 ml Tet-free medium. When ~ 60 - 70% confluent, cells were transfected with a total of 3 µg DNA per plate (2.7 µg pOG44 Flp recombinase expression plasmid + 0.3 µg pcDNA5/FRT/TO expression vector (containing the gene of interest)), see **Appendix A** for sequences. 24 h later, cells were trypsinised and transferred to a T75 flask in 10 ml Tet-free medium. 24 – 48 h later, cell medium was replaced with 10 ml Tet-free medium supplemented with 15 µg/ml

blasticidin and 100 µg/ml hygromycin (Invitrogen) to select for cells in which integration of pcDNA5/FRT/TO expression vector had occurred (at a Flp-recombinase dependent site), conferring hygromycin resistance and zeocin sensitivity to the cells. Due to low levels of integration, typically > 90% of the cells die 2 - 3 days after the initial hygromycin treatment. 3 days post-selection, the cell medium was replaced with fresh Tet-free medium supplemented with blasticidin and hygromycin, removing the dead cells and allowing the resistant cells to repopulate. Medium was replaced every 2 days until 2 – 3 stable cell colonies were apparent. Cells were trypsinised and transferred to a T25 flask in 5 ml Tet-free medium supplemented with blasticidin and hygromycin to allow the polyclonal cell repopulation to proceed. When 70% confluency was reached, cells were subcultured and maintained as standard in Tet-free medium supplemented with blasticidin and hygromycin. Cells were frozen in 90% (v/v) Tet-free FBS, 10% (v/v) DMSO.

2.3 Click-PEGylation

2.3.1 Buffers and reagents

- ***HEND buffer:*** 25 mM HEPES, 1 mM EGTA, 10 µM neocuproine, 100 µM DPTA, 2% (w/v) SDS, pH 7.4 with NaOH;
- ***Purified glyceraldehyde 3-phosphate dehydrogenase (GAPDH) (from rabbit muscle):*** Sigma: G2267, 1 mg protein/ml stock in HEND buffer (freshly made before use);
- ***Purified AMP-activated protein kinase (AMPK) (α1/β1/γ1), active, His tagged human:*** Sigma: A1233
- ***Tris (2-carboxyethyl)phosphine hydrochloride (TCEP):*** (Thermo Fisher Scientific: 20490), 500 mM stock in HEND buffer, adjusted to pH 7.4 with NaOH, aliquoted and stored at -20°C;
- ***Diamide:*** (Sigma: D3648), 25 mM stock in HEND buffer, aliquoted and stored at -20°C;
- ***Spin columns:*** Micro Bio-Spin 6, 6,000 MW limit, Tris-buffered (BIO-RAD: 732–6222); pre-equilibrated in HEND buffer prior to use according to the manufacturer's guidelines;
- ***Propargyl-malemide:*** (Jena Bioscience: CLK-TA113 or Click Chemistry Tools: TA113), 100 mM stock in HEND buffer (freshly made before use);
- ***N-ethylmaleimide (NEM):*** (Sigma: E1271), 200 mM stock in HEND buffer (freshly made before use);
- ***Tris buffer:*** 50 mM Tris-HCl (pH 7.4), 0.5% (w/v) SDS;
- ***Methoxypolyethylene glycol azide (azide-PEG):*** azide-$PEG_{5,000}$ (5 kDa) (Sigma: 689475 or Creative PEGworks: PLS-2024), 50 mM in Tris buffer (freshly made before use);
- ***L-Ascorbic acid:*** (Sigma: A5960), 125 mM in Tris buffer (freshly made before use), then just before use this was diluted (to minimize pipetting error) to 23 mM in Tris buffer containing 10 mM azide-$PEG_{5,000}$;
- ***Tris[(1-benzyl-1H-1,2,3,-triazol-4-yl)methyl]amine (TBTA):*** (Sigma: 678937); 1.7 mM in 80% (v/v) *t*-butanol:20% (v/v) DMSO, then just before

use this was diluted (to minimize pipetting error) to 0.94 mM in Tris buffer containing 10 mM azide-$PEG_{5,000}$;

- ***$CuSO_4 \cdot 5H_2O$:*** (Sigma: C7631), 50 mM in Tris buffer (freshly made before use), then just before use this was diluted (to minimize pipetting error) to 9.3 mM in Tris buffer containing 10 mM azide-$PEG_{5,000}$.

2.3.2 Sample preparation

Purified protein was reconstituted in HEND buffer at a protein concentration of 0.1 mg/mL (for GAPDH) or 20 or 10 µg/ml (for AMPK to be detected by Coomassie protein staining or by Western blot, respectively), based on the protein concentration stated on product information sheets/lot numbers. Protein concentration of GAPDH HEND stock was confirmed by BCA assay, as previously described. Protein concentration of AMPK HEND stock was not confirmed by BCA assay, due to limited availability of stock. To obtain maximally reduced and oxidised controls, samples (100 µl starting vol.) were pre-treated with either TCEP (10 mM) or diamide (1 mM), respectively, and incubated at 37°C for 30 min with gentle shaking (500 rpm, Eppendorf ThermoMixer). Reduced controls were bubbled through with N_2 gas for 30 s and sealed with Parafilm prior to incubation. Afterwards, excess TCEP and diamide was removed by applying samples to a spin column.

2.3.3 Labelling of reduced cysteine residues by Click-PEG_{red}

The Click-PEG_{red} protocol facilitates labelling of reduced cysteine residues. Samples were incubated with 5 mM propargyl-maleimide at 37°C for 30 min with agitation (1,000 rpm). Excess propargyl-maleimide was then removed by passing samples through a spin column. Optionally, oxidised thiols can then be reduced with TCEP (10 mM), and alkylated by reaction with NEM (100 mM), followed by a spin column step to remove excess NEM.

2.3.4 Labelling of oxidised cysteine residues by Click-PEG_{ox}

The Click-PEG_{ox} protocol facilitates labelling of reversibly oxidised cysteine residues. Samples were first incubated with NEM (100 mM) at 37°C for 30 min with

agitation (1,000 rpm) to alkylate reduced thiols. Excess NEM was removed by passing the samples through a spin column. The flow-through was treated with TCEP (10 mM) to reduce reversibly oxidised thiols, and N_2 gas was bubbled through the samples for 30 s prior to incubation at 37°C for 30 min with gentle shaking (500 rpm). Excess TCEP was removed from the samples by passing through a spin column. Samples were then reacted with propargyl-maleimide (5 mM) at 37°C for 30 min with agitation (1,000 rpm), after which excess propargyl-maleimide was removed by passing samples through a spin column.

2.3.5 Click reaction

It is important to remove chelating agents from the above Click-PEG_{red} and Click-PEG_{ox} samples as they would impede the copper-catalysed Click reaction between propargyl-maleimide and azide-PEG. To do this, the protein was precipitated by adding ice-cold acetone (4 – 6 vol.) and storing the protein samples at –20°C for a minimum of 2 h. Precipitated protein was pelleted by centrifugation (30 min at 17,000 X g at 4°C) and then the pellet was washed once with ice-cold acetone. The resulting pellet was air-dried at 37°C, then resuspended in Tris buffer (28 µl), containing azide-$PEG_{5,000}$ (10 mM). A range of other azide-PEG moieties of different sizes are available including: azide-$PEG_{10,000}$ (10 kDa), azide-$PEG_{2,000}$ (2 kDa) and azide-$PEG_{1,000}$ (1 kDa). The optimal PEG size depends on the molecular weight of the protein target and the number of redox-sensitive cysteine residues. The sample was then divided into 2 X 12.5 µl aliquots; upon one of which the Click reaction would be performed (+ catalyst) with the other serving as a negative control (- catalyst).

To initiate the Click reaction, the copper catalyst is added to the solution to a final concentration of 10% (v/v) (or Tris-HCl buffer for the '– catalyst' control). The catalyst is composed of 3 reagents, typically added in the following order and proportions (Kolb et al., 2001): 125 mM L-ascorbic acid (1 vol.): final concentration = 2.5 mM, 1.7 mM TBTA (3 vol.): final concentration = 0.1 mM, and 50 mM copper sulphate (1 vol.): final concentration = 1 mM. For a starting sample vol. of 12.5 µl,

the vol. of each catalyst reagent to be added would be 0.28 µl, 0.84 µl and 0.28 µl, respectively. To avoid pipetteing small volumes that may have high error, catalyst components were first diluted into Tris buffer containing 10 mM azide-$PEG_{5,000}$ (to minimise further diluting the azide-$PEG_{5,000}$ concentration), such that 2 µl of each catalyst component (6 µl in total, containing 6.7 mM azide-$PEG_{5,000}$) were added without altering the final concentrations of each catalyst component. Tris-HCl buffer containing 6.7 mM azide-$PEG_{5,000}$ (6 µl) was added for the '– catalyst' control. Samples were incubated at 37°C for 1 h at 1,000 rpm. The reaction was stopped by adding the appropriate vol. of reducing gel loading buffer to the samples (4X Laemmli buffer, supplemented with DTT (50 mM) or TCEP (10 mM)) and heating for 5 min at 95 °C, followed by brief centrifugation. Samples were assayed immediately or stored at –20°C until required for mass shift analysis by SDS-PAGE and coomassie staining/Western blot.

2.3.6 Preparation of cell lysate samples for Click-PEGylation

C2C12 mouse myoblast cells were lysed in ice-cold HEND buffer containing 5 mM propargyl-maleimide (ClickPEG$_{red}$ protocol) or 100 mM NEM (ClickPEG$_{ox}$ protocol), incubated at 37 °C for 30 min with agitation (1,000 rpm), sonicated (10 X 1 s pulse; Q700 sonicator, Qsonica), centrifuged (13,000 X *g* for 20 min at 4°C), and the protein concentration of the resulting supernatant adjusted to 0.5 mg protein /mL. The protein concentration was estimated by lysing a plate of cells from the same batch in HEND buffer without propargyl-maleimide or NEM and performing a BCA assay on this lysate (propargyl-maleimide and NEM can interfere with the BCA assay). For maximal denaturation of complex biological samples, 6 M urea was added to the HEND buffer. The Click-PEG$_{red}$ and Click-PEG$_{ox}$ protocols were then performed as described above for the purified protein samples (100 µl starting vol.).

2.3.7 SDS PAGE and Western blotting for Click-PEGylation

SDS-PAGE and Western blotting were performed as standard. Samples (~ 2 – 5 µg for purified GAPDH, ~ 0.5 - 1µg for purified AMPK; ~ 25 µg whole cell protein

for complex biological samples) in reducing loading buffer were separated by SDS-PAGE (typically on a 10% PAGE gel for GAPDH or 7.5% PAGE gel for AMPK), the % PAGE gel depending on the size of the target protein and the number of redox-reactive cysteine residues. Protein bands were either stained directly (with Coomassie Brilliant Blue R-250 or QC Coomassie stain for purified protein samples) or detected by Western blotting. To quantify redox-dependent mobility shifts, Coomassie stained gels or Western blot images were analysed for profile plots of lanes or relative band signal intensities, measured using FIJI or Li-Cor Image Studio Lite software, respectively.

2.4 AMPK assays

2.4.1 Buffers and reagents

- ***Hepes buffer:*** 50 mM Hepes, 50 mM sodium fluoride, 5 mM sodium pyrophosphate, 1 mM EDTA, 10 % (v/v) glycerol, pH 7.4 at 4°C. To this was added just before use: 1 mM dithiothreitol (DTT) (from a 1 M stock made in MQ H_2O) and protease inhibitors: 4 µg/ml soybean trypsin-chymotrypsin inhibitor (from a 4 mg/ml stock made in Hepes buffer), 1 mM benzamidine (from a 1 M stock made in Hepes buffer) and 0.1 mM phenylmethanesulfonyl fluoride (PMSF) (from a 0.1 M stock made in EtOH);
- ***Hepes lysis buffer (HLB):*** Hepes buffer, 1 % (v/v) Tx-100. To this was added just before use: DTT and protease inhibitors (as above);
- ***SAMStide (peptide):*** (Signal Chem: S07-58) 1 mM stock made in Hepes buffer containing DTT and protease inhibitors as above, aliquoted, snap frozen and stored at -80°C.
- ***Kinase assay mix (15 µl per reaction):*** 333.3 µM AMP (5 µl 1 mM stock made in Hepes buffer), 333.3 µM SAMStide (5 µl 1 mM stock made in Hepes buffer), HLB (5 µl). Hepes buffer and HLB contained DTT and protease inhibitors as above;
- ***SAMStide blank assay mix (15 µl per reaction):*** 333.3 µM AMP (5 µl of 1 mM stock made in Hepes buffer), Hepes buffer (5 µl), HLB (5 µl). Hepes buffer and HLB contained DTT and protease inhibitors as above;
- ***radiolabelled ATP mix (5 µl per reaction):*** 100 µCi/ml [γ-^{32}P]ATP (Perkin Elmer), 1 mM ATP (from 100 mM stock made in Hepes buffer), 25 mM $MgCl_2$ (from 100 mM stock made in Hepes buffer), made up to 5 µl with Hepes buffer. Hepes buffer contained DTT and protease inhibitors as above.

2.4.2 Cell lysis

Immediately after media aspiration, cells for AMPK assays were washed rapidly (within seconds) in ice-cold PBS (using a plastic 2 ml Pasteur pipette) on an ice-cold aluminium block. The PBS was then aspirated and cells were lysed rapidly

(within seconds) in ice-cold HLB (250 µl from a Gilson p1000 Pipetman per 6 cm plate). Cells were scraped from the plate surface using plastic cell scrapers (Sarstedt, 25 cm). Scraped lysate was transferred to ice-cold Eppendorf tubes and centrifuged (17,000 X g for 10 min at 4°C). Supernatants were stored on ice for immediate use or aliquoted, snap-frozen on dry ice and stored at - 80°C.

2.4.3 AMPK SAMS kinase assay on whole cell lysates

The specific kinase activity of AMPK can be determined by the radiometric SAMS peptide assay, which measures the incorporation of radiolabelled phosphate from [$_{\gamma}$-^{32}P]ATP into the SAMS peptide (SAMStide) as it undergoes phosphorylation by active AMPK (Hardie et al., 2000). The SAMStide is a synthetic peptide substrate of AMPK, derived from the amino sequence of ACC1 (mouse) (https://www.signalchem.com/shared_product_sheets/R339-3.pdf), a natural phosphorylation target of AMPK. The SAMStide (HMRSAMSGLHLVKRR) consists of residues corresponding to those at positions 73 – 85 of the full-length mouse ACC1 protein, with the following modifications: a serine residue at position 77 is replaced with alanine (to prevent phosphorylation by cAMP-dependent protein kinase) and two arginine residues (which have positively charged side-chains) are incorporated at the C-terminal end of the peptide to facilitate binding to negatively charged P81 phosphocellulose paper, enabling the removal of unincorporated MgATP in washing steps. The SAMStide is phosphorylated by AMPK at the serine residue that corresponds to position 79 in the full length mouse ACC1 protein.

Kinase assays were performed on AMPK immunoprecipitated from 100 - 200 µg whole cell lysate protein using 0.3 µl Sip2 serum (yeast AMPKβ ortholog antibody) and 30 µl protein A (from *Staphylococcus aureus*) - Sepharose® beads (Sigma: **P9424)** (50 % (v/v) slurry in Hepes buffer). The beads were pipetted with cut-off pipette tips (~ 3 mm was cut off the narrow end of the pipette tips with a clean razor blade) to avoid trapping beads in the pipette tips. Immunoprecipitation was performed in a total vol. of 250 µl (made up with HLB) in 1.5 mL Eppendorf tubes at 4˚C for 2 h with overhead rotation. Washings were performed by addition of 1 X 1

ml HLB (followed by centrifugation (1,000 x g for 1 min at 4˚C) and supernatant aspiration (using gel loading tips to avoid pipetting the beads)), and then 2 x 500 µl Hepes buffer washings (as above). The beads were then resuspended in 40 µl Hepes buffer (with cut-off pipette tips) and divided into 4 x 10 µl aliquots in 1.5 ml Eppendorf tubes, each equivalent to ¼ of the whole cell protein from which AMPK was immunopreciptated.

Kinase assays were performed on duplicate aliquots alongside one blank assay (without SAMStide). Kinase assays were performed with the addition of 15 µl kinase assay mix (or blank assay mix without SAMStide) and initiated with 5 µl radiolabelled ATP mix. Reactions were incubated at 37˚C for 30 min before spotting 25 µl onto P81 phosphocellulose paper (Whatman). The papers were washed to quench the reaction and wash off any unbound $_{\gamma}$-^{32}P, first with 1% (v/v) phosphoric acid (3 x 500 ml) with vigorous stirring (decanted in the sink), then MQ H_2O (2 x 500 ml). The papers were then added to 3 ml organic scintillant (Ultima Gold™ AB) and phosphorylation of the SAMS peptide by active AMPK was measured by scintillation counting, measured as counts per minute.

The specific radioactivity of the radiolabelled ATP mix was measured by spotting 5 µl radiolabelled ATP mix (5 nmol ATP) onto P81 paper (in duplicate) followed by immediate scintillation counting (no washings). The mean specific kinase activity of AMPK (nmol $_{\gamma}$-^{32}P/µg cell protein/min) was measured as follows, where counts per minute = CPM; specific radioactivity = SR (CPM.nmol^{-1}); incubation time = T (min); kinase reaction vol. = V (µl):

$$\frac{\textit{CPM (mean kinase – blank) X total V (30 µl)}}{\textit{SR (CPM.nmol}^{-1}\textit{) X pipetted V (25 µl) X T (30 min) X cell protein (25 - 50 µg)}}$$

2.4.4 AMPK and ACC phosphorylation assays

The kinase activity of AMPK can also be assayed by Western blot, where phosphorylation at T172 of the AMPKα1/2 catalytic subunit and phosphorylation of the downstream target ACC1/2 at S79 can be detected with antibodies to the phospho-specific epitopes (Hardie et al., 2000). Total AMPK and ACC levels can be monitored with antibodies to the AMPKβ1/2 subunits and to the ACC1/2 protein, respectively. For same-gel signal intensity normalization, the signal intensity of the phospho-specific epitopes of AMPK and ACC can both be normalised to the signal intensity of the AMPKβ1/2 subunit to control for changes in total expression of AMPK. Whole cell lysate (25 µg protein) was electrophoresed in reducing, denaturing conditions on 4 – 20 % gradient SDS-PAGE gels as described in **2.1.2.4 SDS-PAGE**. Following wet transfer to PVDF membranes and blocking as described in **2.1.2.5 Western blotting,** membranes were sectioned (with a clean razor blade) at the 50 kDa molecular weight marker and at the 100 kDa molecular weight marker (Precision Plus Protein™ Dual Color Standards (BIO-RAD)). The '0 – 50 kDa' membrane section was incubated with rabbit-AMPKβ1/2 primary antibodies (AMPKβ1 ~ 38 kDa, AMPKβ2 ~ 30 kDa), the '50 – 100 kDa' membrane section was incubated with rabbit-AMPKα1/2-phosphoT172 primary antibodies (~ 62 kDa) and the '> 100 kDa' membrane section was incubated with rabbit-ACC1/2-phosphoS79 (ACC1 ~ 265 kDa, ACC2 ~ 280 kDa) primary antibodies. Antibody catalogue numbers and Western blot dilutions are listed in **2.1.2.1.1 Primary antibodies**. Following overnight incubation and washings, the membrane sections were incubated with the same goat-α-rabbit fluorescent secondary antibodies (see **2.1.2.1.2 Secondary antibodies)** and washed as previously described. TBS was used instead of PBS for all buffers and washings. Membrane sections were visualized simultaneously using the Odyssey® CLx Infrared Imaging System (fluorescence emission at 800 nm) and target bands quantified using the LI-COR Biosciences Image Studio™ Lite software. The signal intensity of AMPKα1/2-phosphoT172 and ACC1/2-phosphoS79 bands were normalised to the signal

intensity of AMPKβ2 bands to control for changes in AMPK protein expression after a given treatment.

2.5 Measuring cell and tissue ATP/ADP ratios by bioluminescence

2.5.1 Background

The luciferase/luciferin bioluminescence reaction can be utilised in a sensitive assay to measure adenosine triphosphate (ATP) and adenosine diphosphate (ADP) in extracts from cells and tissues (Strehler, 1974). The concentrations of luciferin and luciferase are fixed, allowing the ATP concentrations in unknowns to be determined against ATP standards by measuring light production in a luminometer. Furthermore, ADP in cells and tissues can be measured by first degrading the endogenous ATP with ATP sulfurylase and then enzymatically converting endogenous ADP to ATP using a pyruvate kinase/phosphoenolpyruvate mix **(Figure 2.2).**

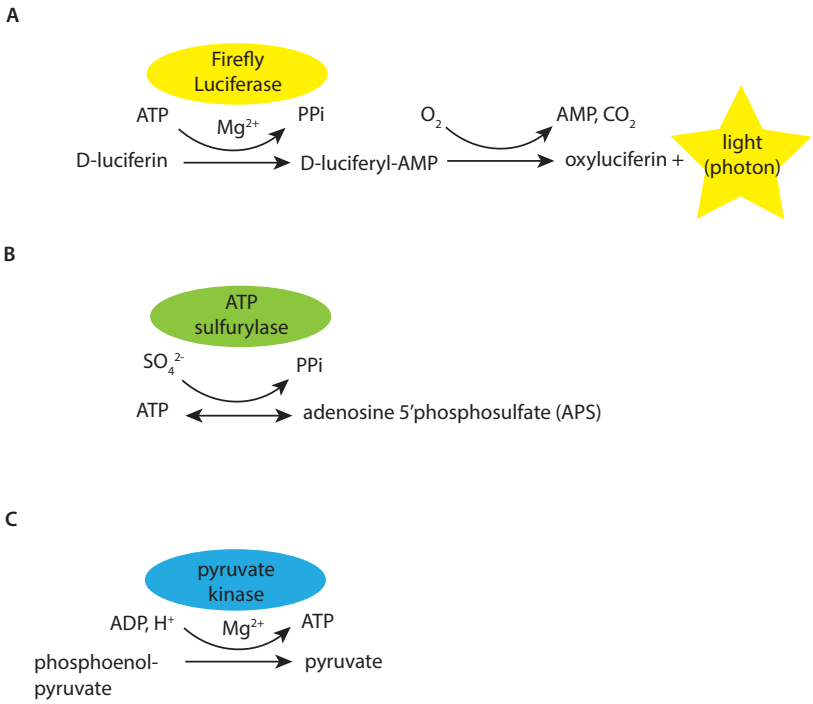

Figure 2.2 Reactions involved in measurement of ATP and ADP by luciferase/luciferin bioluminescence. (A) *Photons are produced in proportion to ATP, D-luciferin and luciferase concentrations;* ***(B)*** *ATP sulfurylase catalyses the adenylation of sulfate using ATP, producing APS and PPi;* ***(C)*** *Pyruvate kinase catalyses the phosphorylation of ADP, forming ATP and pyruvate.*

Nucleotides are extracted from cells or snap-frozen tissue samples using perchloric acid to rapidly denature any endogenous proteins that may alter the relative levels of ATP, ADP and adenosine monophosphate (AMP) *in vitro*, primarily adenylate kinase, and to stabilise pH-labile adenine nucleotides. The acidified, deproteinised extract is then neutralised with potassium hydroxide (in the presence of the pH buffer MOPS), forming a $KClO_4$ precipitate. Enzymatic reactions are then performed on the neutralised supernatant.

2.5.2 Stock Solutions

- ***ADP and ATP stock solutions:*** 20 mM stocks (sodium salts) in HCl-acidfied H_2O (pH 1 – 2), snap frozen in 100 µl aliquots, stored at -80°C;
- ***Perchloric acid ($HClO_4$) extractant (PCA):*** 3% (v/v) $HClO_4$, 2 mM Na_2EDTA, 0.5% (v/v) Triton X-100**,** stored at 4°C;
- ***Potassium hydroxide solution (KOH):*** 2 M KOH, 2 mM Na_2EDTA, 50 mM MOPS, stored at 4°C;
- ***Tris-acetate (TA) buffer:*** 100 mM Tris, 2 mM Na_2EDTA, 50 mM $MgCl_2$ (pH 7.75 with glacial acetic acid), stored at 4°C;
- ***D-Luciferin sodium salt:*** 2 mM in TA buffer, snap frozen in 200 µl aliquots in opaque Eppendorf tubes and stored at -80°C;
- ***Luciferase from Photinus pyralis (firefly)***: 1 mg lyophilised preparation (~150 µg luciferase protein) in 1.86 ml TA buffer (25% (v/v) glycerol) (~ 80 µg protein/ml), snap frozen in 100 µl aliquots in opaque Eppendorf tubes and stored at -80°C;
- ***Phosphoenoylpyruvate cyclohexylammonium salt (PEP):*** 114 mM in TA buffer, snap frozen in 150 µl aliquots and stored at -80°C;
- ***Tris-HCl buffer:*** 100 mM Tris-HCl, 10 mM $MgCl_2$ (pH 8.0) stored at 4°C;
- ***Guanosine 5′-monophosphate disodium salt hydrate (GMP):*** 100 mM in Tris-HCl buffer, stored at 4°C;
- ***Sodium molybdate (Na_2MoO_4):*** 1 M in MQ H_2O, stored at 4°C;
- ***Bovine serum albumin (BSA) fatty acid free (Sigma):*** 100 mg/ml in TA buffer snap frozen and stored at -80°C;

2.5.3 Working solutions (prepared just before use)

- ***2X ATP sulfurylase assay buffer (250 µl per reaction):*** 20 mM Na_2MoO_4, 5 mM GMP, 0.2 U ATP sulfurylase (New England Biolabs), Tris-HCl buffer to 250 µl, stored on ice until use;
- ***Pyruvate kinase / PEP mix (10 µl per reaction):*** 100 mM PEP, 6 U pyruvate kinase suspension (type II, from rabbit muscle: P1506), stored on ice until use;
- ***Luciferase/Luciferin mix (100 µl per reaction):*** 7.5 mM DTT (from 1 M stock made in MQ H_2O), 0.4 mg/ml BSA, 1.92 µg luciferase/ml, 120 µM luciferin, TA buffer (25% (v/v) glycerol) to 100 µl, stored at RT (protected from light).

2.5.4 Preparation of ATP and ADP standard curves

ATP and ADP (20 mM stocks) were thawed quickly at 37°C and then serially diluted in ice-cold PCA to make 10-part standard curves, typically ranging between 0 (100 % v/v PCA) and 20 µM in 1 ml aliquots. Standards were stored on ice and 400 µl of each standard was carried forward to the neutralization step.

2.5.5 Nucleotide extraction from cells

C2C12 cells were plated at a density of 20,000 cells/cm^2 on 6 cm plates and differentiated as previously described. Cells were washed rapidly in ice-cold PBS on an ice-cold aluminium block (as for AMPK assays) and rapidly lysed in ice-cold PCA (500 µl per 6 cm plate). Lysed cells were scraped from the plate surface with a plastic cell scraper and lysate was transferred to 1.5 ml Eppendorf tubes stored on ice. Tubes were vortexed and centrifuged (17,000 X g for 10 min at 4°C) to pellet the insoluble material. Supernatants were diluted 1:5 in 1 ml PCA and maintained on ice for immediate use or snap frozen (along with undiluted PCA extracts) and stored at -80°C. 400 µl of the diluted PCA extracts were carried forward to the neutralization step.

2.5.6 Nucleotide extraction from tissues

2.5.6.1 Porcine heart tissue biopsy freezing, storage and homogenization: Core needle biospies (Celero vacuum assisted biopsy device) (diameter: ~ 1 mm, length: 5 – 10 mm, weight: ~ 5 mg) were excised immediately (within ~ 5 s), snap frozen in liquid nitrogen (suspended from a clean forceps) for ~ 15 s and transferred to pre-chilled cryotubes (Nunc®, 1.8 ml) on dry ice. Biopsies were transferred and stored at – 80°C until further preparation. Prior to nucleotide extraction, biopsies were mechanically homogenised using a pestle and mortar (Haldenwanger™ 5500, unglazed, 20 ml). A pestle, mortar, forceps and spatula were pre-chilled on dry ice for 30 min. Wearing cryogloves and safety glasses, liquid nitrogen was poured into the mortar (maintained on dry ice in a Styrofoam container) and the frozen biopsy was transferred into the liquid nitrogen in the mortar. The frozen biopsy was rapidly homogenised (5 – 10 s) in the mortar with the pestle, under liquid nitrogen. After the liquid nitrogen had evaporated, the resulting frozen powder was scraped into a pre-chilled cryovial (on dry ice) with a spatula and maintained on dry ice. The pestle, mortar and spatula were washed thoroughly in ethanol and MQ H_2O between biopsy homogenizations. On a fine balance (Sartorius®, CP124S), samples of frozen homogenate (1 - 5 mg) were rapidly weighed into pre-chilled (on dry ice) Eppendorf tubes, using a pre-chilled spatula and forceps to transfer and handle the homogenate and cold tubes, respectively. The weighed homogenate was rapidly returned to dry ice until nucleotide extraction.

2.5.6.2 Nucleotide extraction from tissue homogenate: Ice-cold PCA (1 ml) was added to weighed homogenate (on dry ice) and the solution was vortexed immediately for ~10 s until the sample was fully dissolved. Tubes were centrifuged (17,000 X g for 20 min at 4°C). Acidified supernatants were stored on ice and diluted to 1 mg frozen homogenate extract /ml PCA in 500 µl aliquots. Diluted PCA extracts were used immediately or snap frozen (along with the remaining undiluted PCA extracts) and stored at -80°C.

2.5.7 Neutralisation of PCA extracts and standards

Ice-cold PCA extracts, ATP and ADP standards (400 µl) had their pH adjusted to pH 7 – 7.5 by addition of ice-cold KOH solution (containing MOPS as a pH buffering agent) of about 110 – 118 µl (vol. optimised on test samples). Each tube was vortexed immediately after KOH addition for 5 s until formation of a white precipitate ($KClO_4$). Samples were replaced on ice to allow the precipitate to settle. The pH of the neutralised supernatant was tested by pipetting 2 µl of each sample onto pH indicator strips (Sigma, pH 4.5 – 10.0). If a sample remained too acidic, a further 4 µl of KOH was added, the sample vortexed and the pH re-checked. This step was repeated until the optimum pH was achieved. Samples with a pH > 8 were discarded in favour of fresh acidified extracts/standards, as nucleotides are unstable in basic solutions. After neutralization was confirmed, the white $KClO_4$ precipitate in all samples was pelleted by centrifugation (1,000 X g for 1 min at 4°C) and supernatants were stored on ice. The vol. KOH added to the standards (initially 400 µl) was noted so as to later calculate nucleotide concentrations. As cell and tissue ATP and ADP content is expressed as a ratio, the differences in vol. of the KOH additions between samples do not affect the ratio.

2.5.8 ATP/ADP measurements

Light emission from the luciferase/luciferin reaction in the presence of ATP (from standards and extracts) was recorded using a luminometer (Berthold Technologies AutoLumat LB 953 Multi-Tube luminometer; software: Eg&g Berthold Tubemaster Version 1.0 (1997-99)) fitted with an autoinjector to deliver the luciferase/luciferin solution to individual tubes. Samples were loaded in luminometer tubes (Sarstedt Rohren tubes (5 ml, 75 X 12 mm, PS)). TA buffer (400 µl) was added to all luminometer tubes (and maintained at RT) before sample additions, as follows:

- ***ATP measurement in ATP standards:*** neutralised ATP standard supernatant (100 µl) was added to TA buffer (400 µl) in luminometer tubes (in duplicate or triplicate);
- ***ATP measurement in samples:*** neutralised sample supernatant (100 µl) was added to TA buffer (400 µl) in luminometer tubes;

- ***ADP → ATP measurement in ADP standards:*** neutralised ADP standard supernatant (100 µl) was added to TA buffer (400 µl) in luminometer tubes (in duplicate). PK/PEP cocktail (10 µl) to be added later to convert the ADP to ATP;
- ***ADP →ATP measurements in samples:*** neutralised sample supernatant (250 µl) was added to 2X ATP sulfurylase assay buffer (250 µl), vortexed briefly and incubated at 30°C for 20 min with gentle shaking. Samples were centrifuged (17,000 X g for 1 min at RT), boiled at 100°C for 5 min and cooled on ice. ATP sulfurylase-treated sample (the ATP should now be degraded) (200 µl) was added to TA buffer (400 µl) in luminometer tubes (in duplicate). PK/PEP cocktail (10 µl) to be added later to one of the duplicate tubes to convert the ADP to ATP. The other duplicate tube (without addition of PK/PEP cocktail) serves as an ATP 'blank' value.

Luminometer preparation: The autoinjector was washed (6 x 100 µl injections) with 0.5 M HCl, then washed with 0.5 M NaOH and finally washed three times with MQ H_2O. The washings (collected in luminometer tubes) were discarded. Just before running the samples, the autoinjector was primed (6 x 100 µl injections) with freshly made Luciferase/Luciferin mix. The mix was collected in a clean luminometer tube and recycled back into the working stock Falcon tube for use in the assay.

Sample running: Prepared luminometer tubes containing samples and standards were placed in the luminometer. PK/PEP cocktail (10 µl) was added to all tubes requiring an ADP → ATP conversion. The tubes were mixed gently and replaced in the luminometer in the correct order. All tubes were incubated in the luminometer for 30 min at 30°C to allow the ADP → ATP conversion to proceed. The assay was commenced with the following settings: read time: 30 s, background read time: 5 s, cycle time: 40 s, post-injection delay: 5 s, total time: 80 s, temp.: 30°C, injection vol.: 100 µl.

Signal quantification and analysis: Emitted light, recorded as Relative Light Units (RLU) was analysed using Microsoft Excel and GraphPad Prism 5.0. Vol.-corrected ATP standard curve values (pmol ATP per tube) were plotted against corresponding RLU values (expressed as mean and range/SEM of duplicates/triplicates). A linear regression was performed to assess the linearity of the standard curve (see **Figure 2.3** for typical standard curves). Then the RLU values of the samples (for ATP and ATP 'blank' measurements) were plotted against the standard curve and unknown values (pmol ATP) were interpolated from a linear regression analysis. The unknown pmol ATP values of the vol.- corrected ADP standards were similarly interpolated from this standard curve. The linearity of the ADP → ATP conversion standard curve was assessed by plotting these interpolated pmol ATP values against their corresponding mean RLU values and performing a linear regression. The RLU values corresponding to ADP → ATP conversion measurements from samples were then plotted against this linear ADP → ATP conversion standard curve and unknown pmol ATP values were interpolated from this data set by performing a linear regression analysis. Finally, the ratio of ATP/ADP in the samples was calculated as follows:

$$\frac{\text{Sample ATP values (pmol ATP)}}{\text{Sample ADP values (pmol ATP) – sample ATP 'blank' values (pmol ATP).}}$$

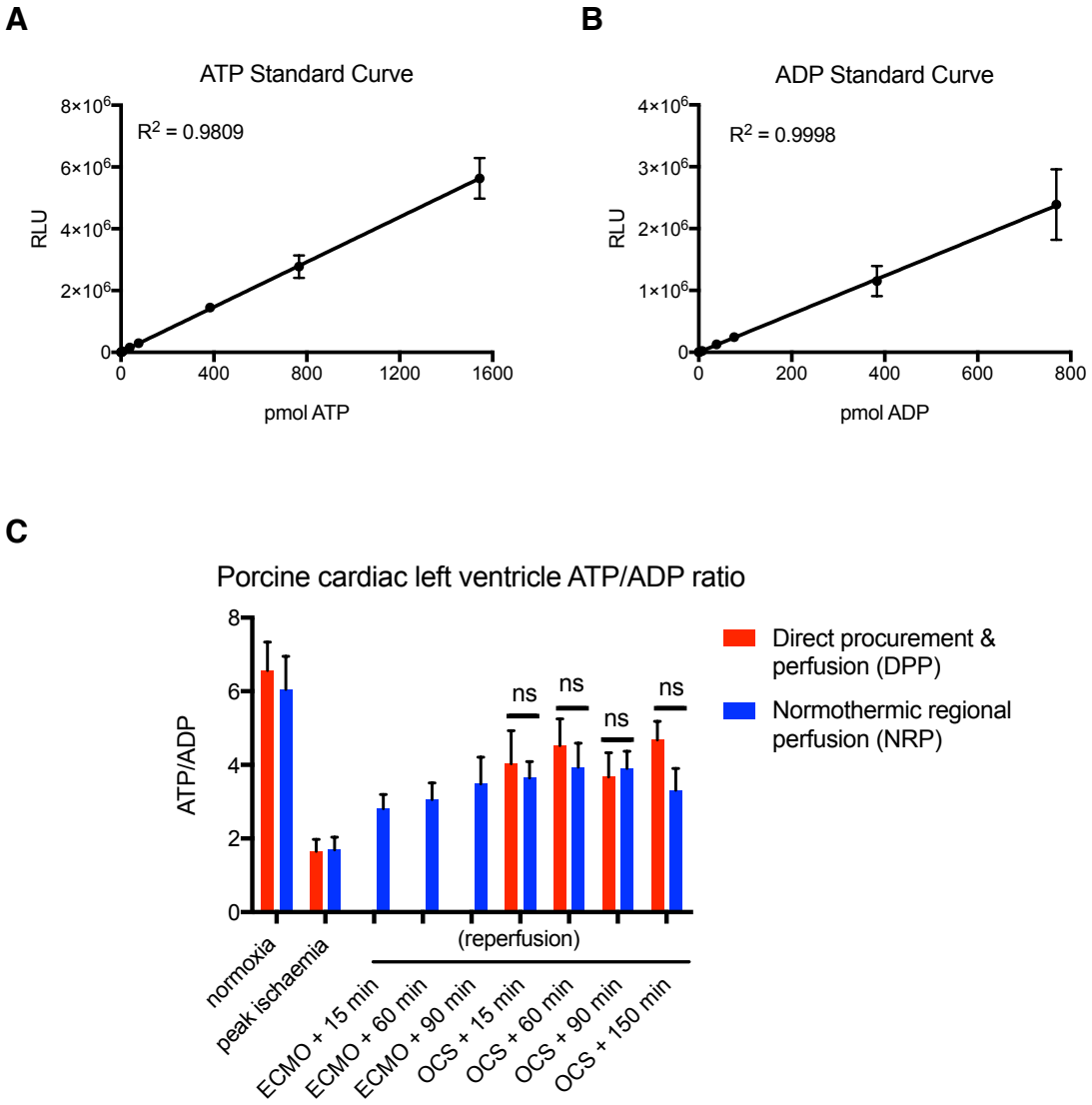

Figure 2.3 Example of an ATP/ADP ratio measurement experiment: comparing cardiac left ventricle ATP/ADP ratios before and after alternate methods of organ reperfusion in a preclinical model of deceased circulatory donation (DCD) heart transplantation. (A & B) *Typical ATP and ADP standard curves. Data points are mean ± range of n = 2 technical replicates.* ***(C)*** *In a side project with collaborator Simon J. Messer (Department of Cardiovascular Surgery, Papworth Hospital NHS Foundation Trust, Cambridge, UK) et al.: Functional and biochemical comparisons of alternate methods of DCD heart transplantation in a pig model (research article in submission), I measured ATP/ADP ratios in left ventricle core needle biopsies. Data is expressed as mean ± SEM of n = 6 biological replicates. Statistical analysis was performed using two-way ANOVA with a Bonferroni multiple comparisons post test comparing ATP/ADP ratio recovery during reperfusion by DPP or NRP (method) over different time-points (OCS + 15 to 150 min). There was no statistically significant difference between the two methods of reperfusion. Method: P = 0.2470, Time: P = 0.8955. DPP: direct procurement and perfusion; NRP: normothermic regional perfusion; ECMO: Extracorporeal membrane oxygenation; OCS: Organ Care System (TransMedics™).*

2.6 Peroxiredoxin dimerisation assays

2.6.1 Buffers and reagents

- ***Radioimmunoprecipitation (RIPA) buffer:*** 150 mM sodium chloride, 1.0 % (v/v) Triton X-100, 0.5 % (w/v) sodium deoxycholate, 0.1 % (w/v) SDS, 50 mM Tris, pH 8.0 at 4°C;
- ***methyl methanethiosulfonate (MMTS):*** 500 mM in PBS (freshly made in fume hood before use);
- ***Prx lysis buffer (working stock):*** RIPA buffer containing 80 mM freshly made MMTS. To this was added protease inhibitors, as previously described.

2.6.2 Cell treatment and lysis

After desired cell treatments, MMTS was added directly to cell medium to a final concentration of 80 mM (from 500 mM stock) to alkylate thiols and prevent artificial oxidation occurring during lysis (Sobotta et al., 2013). Cells were incubated for 10 min in an externally vented hood. Then, transferred onto an ice-cold aluminium block, medium was aspirated and cells were washed rapidly in ice-cold PBS (as for **2.4 AMPK assays**). Ice-cold Prx lysis buffer (250 µl per 6 cm plate) was rapidly added to cells. Cells were scraped from the surface with a plastic scraper, transferred to pre-chilled Eppendorf tubes and stored on ice. Tubes were centrifuged (17,000 X g for 10 min at 4°C) to pellet undissolved material.

2.6.3 Non-reducing SDS-PAGE and Western blotting

The protein concentration in the supernatants was estimated by performing a BCA assay on a control cell plate without MMTS treatment, because the high concentration of MMTS in the sample lysates can interfere in protein quantification. Test sample supernatant (~ 25 µg protein) was then added to 4X Laemmli sample buffer without reductant. Samples were heated at 95°C for 5 min. Samples were electrophoresed on 4-20% SDS-PAGE gels. Western blot was performed with primary antibodies to Prx 2 (mouse) and Prx 3 (rabbit) on the same membrane or

individually on duplicate membranes, and then differential labeling using goat-α-mouse and goat-α-rabbit secondary antibodies, respectively (see **2.1.2.1 Antibodies** for catalogue numbers and Western blot dilutions). The Western blot signal intensities (SI) of Prx 2 and Prx 3 dimers were quantified using LI-COR Biosciences Image Studio™ Lite software, normalised against those of their respective monomer bands and expressed as % dimer (% dimer = (SI dimer / (SI dimer + SI monomer)) x 100). Absolute SI for both monomer and dimer (total of one or multiple bands where present) were used for quantification (i.e. dimer signal intensity was not halved).

2.7 Live cell confocal microscopy and imaging

2.7.1 Background

C2C12-mito-roGFP-ORP1 and C2C12-cyto-roGFP-ORP1 stable cell lines were generated by Andrew R. Hall (MRC Mitochondrial Biology Unit, University of Cambridge, Wellcome Trust/MRC Building, Cambridge Biomedical Campus, Hills Road, Cambridge CB2 0XY, UK). The cells stably express redox-sensitive Green Fluorescent Protein (roGFP) coupled to Orp1 (glutathione peroxidase*, S. cerevisiae*) to improve sensitivity to H_2O_2. The mito-roGFP-ORP1 probe is targeted to the mitochondria by a mitochondria targeting sequence (MTS) so detects mitochondrial H_2O_2 and cyto-roGFP-ORP1 detects cytosolic H_2O_2 (Gutscher et al., 2009). The presence of a dithiol/disulphide switch alters the excitation spectra of GFP (488 nm (green label) and 405 nm (blue label), respectively) enabling a ratiometric fluorescent read-out of thiol oxidation by H_2O_2.

2.7.2 Cell preparation and imaging

C2C12-mito-roGFP-ORP1 cells or C2C12-cyto-roGFP-ORP1 cells were plated on glass coverslips in 6-well plates (20,000 cells per cm^2) in 2 ml standard media. Cells were terminally differentiated to myotubes as previously described and imaged on day 8 of serum depletion. Undifferentiated cells (myoblasts) were plated at the same density and imaged 24 h later. Prior to imaging, coverslips were placed in Attofluor cell chambers (Thermo Fisher) and 1 ml standard media was added. Cells were imaged using a Zeiss LSM 880 confocal microscope (63X objective, oil lens) with imaging intervals every 30 s for 1 h. Emitted light was collected between 500 – 550 nm for both excitation wavelengths. Videos were exported as uncompressed avi files and processed in FIJI. Single time-point images were exported as tiff files.

2.8 Seahorse XF96 Respirometry

2.8.1 Background

The Seahorse XF96 Analyser measures respiration in live cells in real time in a multi-well plate. The respiration calculations are automated, as are plate calibrations, compound injections and mixing. Cell respiration (measured as oxygen consumption rate (OCR)) is measured following sequential injections of selective inhibitors of respiratory chain complexes or F_OF_1ATP synthase, and can thus be used to measure key parameters of respiration (**Figure 2.4**). Respiration can be measured with and without test conditions or additions of test compounds to interrogate the effects of the variables on cellular respiration.

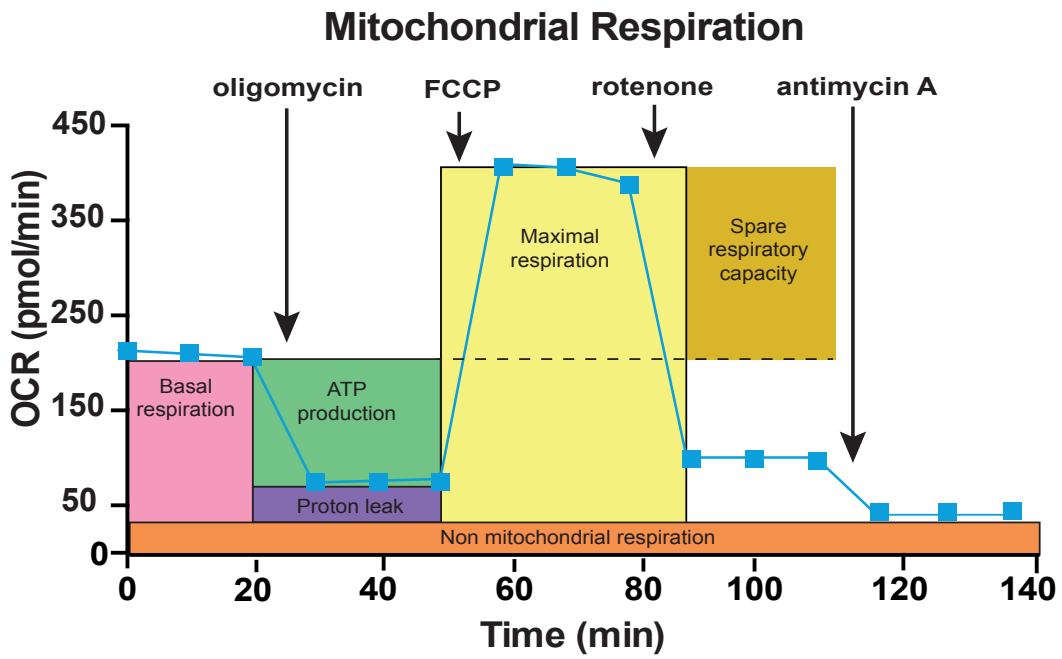

Figure 2.4 Model of mitochondrial respiration as measured by the Seahorse XF96 Analyser. *Measurable parameters of mitochondrial function: basal respiration, ATP production, proton leak, maximal respiration and spare respiratory capacity.*

2.8.2 Buffers and reagents

- ***Seahorse assay medium:*** DMEM base (Sigma) (4.15 g/l), glucose (1 g/l), GlutaMAX™ supplement (2 mM), sodium pyruvate (110 mg/l), phenol red (15 mg/l), HEPES (20 mM), pH 7.4 at 37°C with NaOH. Assay medium was supplemented with Tet-free FBS (0.4% (v/v), 100 U/ml penicillin and 100 µg/ml streptomycin.
- ***Seahorse XF96 well culture plates (Agilent)***
- ***Seahorse XF96 sensor cartridges (Agilent)***
- ***Calibrant solution (Agilent)***
- ***Stock solutions:*** oligomycin (126 mM), rotenone (10 mM), FCCP (10 mM), antimycin A (90 mM) (all made in EtOH).

2.8.3 Cell preparation

Flp-In™ T-REx™ 293 - NDI1 (Doxycycline inducible) cells were plated at a density of 50,000 cells/ well of a Seahorse XF96 well culture plate in low glucose (1 g/l) Tet-free medium (see **2.2.1 Cell culture media, buffers, reagents and cell lines**), supplemented with blasticidin (15 µg/ml) and hygromycin (100 µg/ml) (200 µl/well). Cells were plated ± Doxycycline (1 µg/ml). 24 h later, cell medium was replaced with Seahorse assay medium (180 µl/well), following a cell wash in the same medium. The cell plate was incubated in a CO_2-free incubator for 1 h at 37ºC prior to assay.

2.8.4 Seahorse XF96 Analyser preparation and running

Sensor cartridges were incubated in calibrant solution overnight in a CO_2-free incubator at 37ºC (200 µl/well). On day of assay, injector ports were loaded with compounds (diluted in Seahorse assay medium), and incubated at 37ºC, see **Table 2.1**. Assays were performed at 37°C according to the manufacturer's guidelines: http://www.agilent.com/en-us/products/cell-analysis-%28seahorse%29/seahorse-analyzers/seahorse-xfe96-analyzer/basic-procedures-to-run-an-xf96-assay.

Port	Compound	Conc. (10 X)	Injection vol. (µl) (10% of well vol.)
A	oligomycin	10 µM	20
B	FCCP	10 µM	22
C	rotenone	2 µM	24
D	antimycin A	50 µM	27

Table 2.1 Seahorse XF96 port injections.

2.9 Molecular cloning

2.9.1 *Escherichia coli* growth media

All media was prepared and autoclaved in the Media Kitchen, MRC/Wellcome Trust Building, Cambridge Biomedical Campus, Hills Road, Cambridge, UK.

- **LB broth + Ampicillin (AMP):** 0.5% (w/v) yeast extract, 1% (w/v) tryptone, 0.1 mM NaCl, pH 7.0, 100 µg/ml ampicillin;
- **LB agar + AMP:** 0.5% (w/v) yeast extract, 1% (w/v) tryptone, 0.14 mM NaCl, 1.5% (w/v) agar, pH 7.4, 100 µg/ml ampicillin;
- **SOC transformation media:** 0.5% (w/v) yeast extract, 2% (w/v) tryptone, 10 mM NaCl, 2.5 mM KCl, 10 mM $MgCl_2.6H_2O$, 20 mM glucose, pH 7.0

2.9.2 cDNA vectors

pWPI-NDI1 and pWPI-AOX vectors were a gift from Dr. Alberto Sanz (Institute for Cell and Molecular Biosciences & Newcastle University Institute for Ageing, Newcastle University, Newcastle, UK)(Scialo et al., 2016). AMPK subunit expression vectors pcDNA3-AMPKα2-CT-FLAG, pcDNA3-AMPKβ1 and pcDNA3-AMPKγ1-NT-Myc were a gift from Professor David Carling (MRC Clinical Sciences Centre, Hammersmith Hospital Campus, London, UK). See **Appendix A** for sequences.

2.9.3 Molecular subcloning strategy

Mammalian cell expression vectors containing different genes of interest were created by molecular subcloning, strategy outlined in (**Figure 2.5**). Methods described below are accompanied by examples from a project that involved subcloning a cDNA sequence for a single subunit NADH dehydrogenase, NDI1 or an alternative oxidase, AOX (both alternative respiratory enzymes) from a pWPI donor plasmid into a pcDNA5/FRT/TO recipient expression vector. All scale plasmid maps and annotations were created using SerialCloner 2-6-1 and restriction sites were confirmed using NEBCutter V2.0. Molecular cloning of AOX was perfomed by Aonghus McCarthy (MRC Mitochondrial Biology Unit, University of Cambridge, Wellcome Trust/MRC Building, Cambridge Biomedical Campus,

Hills Road, Cambridge CB2 0XY, UK) in the course of a summer studenship sponsored by the Amgen Scholars programme, Cambridge 2016.

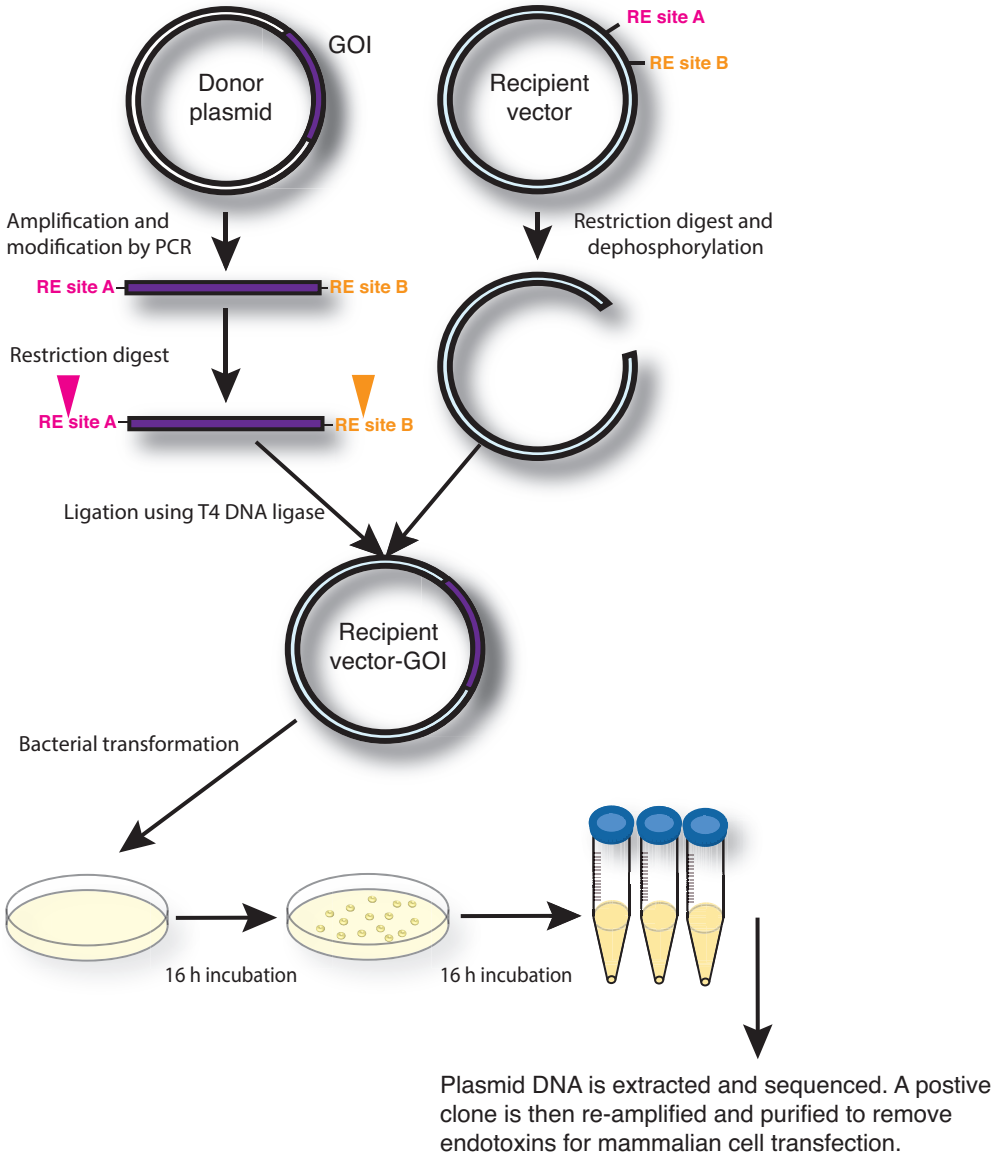

Figure 2.5: A mammalian cell expression vector containing a novel gene of interest (GOI) created by molecular subcloning. *This was performed using enzymatic restriction digest to cut a double-stranded (ds) recipient expression vector (plasmid) of choice at two different sites in the Multiple Cloning Site (MCS) and then inserting a ds cDNA gene of interest (flanked by compatible restriction sites) into the MCS of the expression vector in the correct orientation and reading frame, creating a novel expression vector. The ds cDNA gene of interest was initially amplified from a donor plasmid by PCR and modified to include flanking restriction sites.*

2.9.4 Agarose Gel Electrophoresis

Linear dsDNA (plasmid fragments) were separated according to size (bp) by agarose gel electrophoresis. Agarose gels (0.8 % (w/v) or 1.0 % (w/v)) were made by heating (in a microwave) agarose in a conical flask in 100 ml (per gel) TAE buffer (40 mM Tris (pH 7.6), 20 mM acetic acid, 1 mM EDTA) until fully dissolved. GelRed™ (Biotium) was added to the agarose (cooled enough so that the flask could be held comfortably) to allow visualisation of DNA under UV light. The agarose was poured into horizontal gel chambers (Engineering & Design Plastics Ltd - Laboratory Equipment and Electrophoresis Division: EM100 - Mini Gel Unit) and a 10-well comb was inserted. After the gel had set, TAE buffer was poured over the gel in the chamber until both gel and electrodes were fully submerged and the well combs were then removed. Samples were loaded in Purple Loading Dye without SDS (NEB) and electrophoresed at 100 V for ~ 30 min to separate DNA fragments of different sizes. A 1 kbp DNA ladder (Invitrogen: 15615-016) was loaded along with the samples to estimate fragment size. According to the manufacturer's guidelines (tool.thermofisher.com/content/manuals/15615016.pdf), the ladder has an upper range composed of 1 – 12 repeats of a 1018 bp DNA fragment, combined with a lower range of plasmid DNA fragments ranging between 75 and 1636 bp, and is suitable for sizing DNA fragments between 500 bp and 12 kbp. DNA was visualised using a UV Transilluminator (ChemiDoc™ XRS+ System (BIO-RAD) with Image Lab™ Software).

2.9.5 DNA quantification

2.9.5.1 Circular DNA quantification

Plasmid DNA was quantified with a NanoDrop™ 8,000 Spectrophotometer. The instrument was initially zeroed with DNAase-free H_2O (Qiagen) and then blanked with DNA elution buffer (10 mM Tris-HCl, pH 8.5) or TE buffer (10 mM Tris-HCl, 1 mM disodium EDTA, pH 8.0). A ratio of absorbance at 260 nm to that at 280 nm of ~1.8 was considered pure for DNA. The 260/230 ratio is a secondary measure of

purity, with 2.0-2.2 considered pure for DNA, whereas a lower ratio indicates contaminants.

2.9.5.2 Linear DNA quantification (approximation)

Linear dsDNA was approximately quantified by densitometry using Image Lab™ software **(Figure 2.6)**. A serial dilution of DNA sample of unknown mass was electrophoresed on an agarose gel alongside a serial dilution of 1 kbp DNA ladder (Invitrogen) of known concentration (1 µg DNA/µl). The ~1.6 kbp band contains ~ 10% of the mass applied to the gel, according to the manufacturer's guidelines (https://tools.thermofisher.com/content/sfs/manuals/15615016.pdf). Therefore, a serial dilution of 1 kbp ladder can be used to assess the approximate mass of DNA present in samples of unknown concentration.

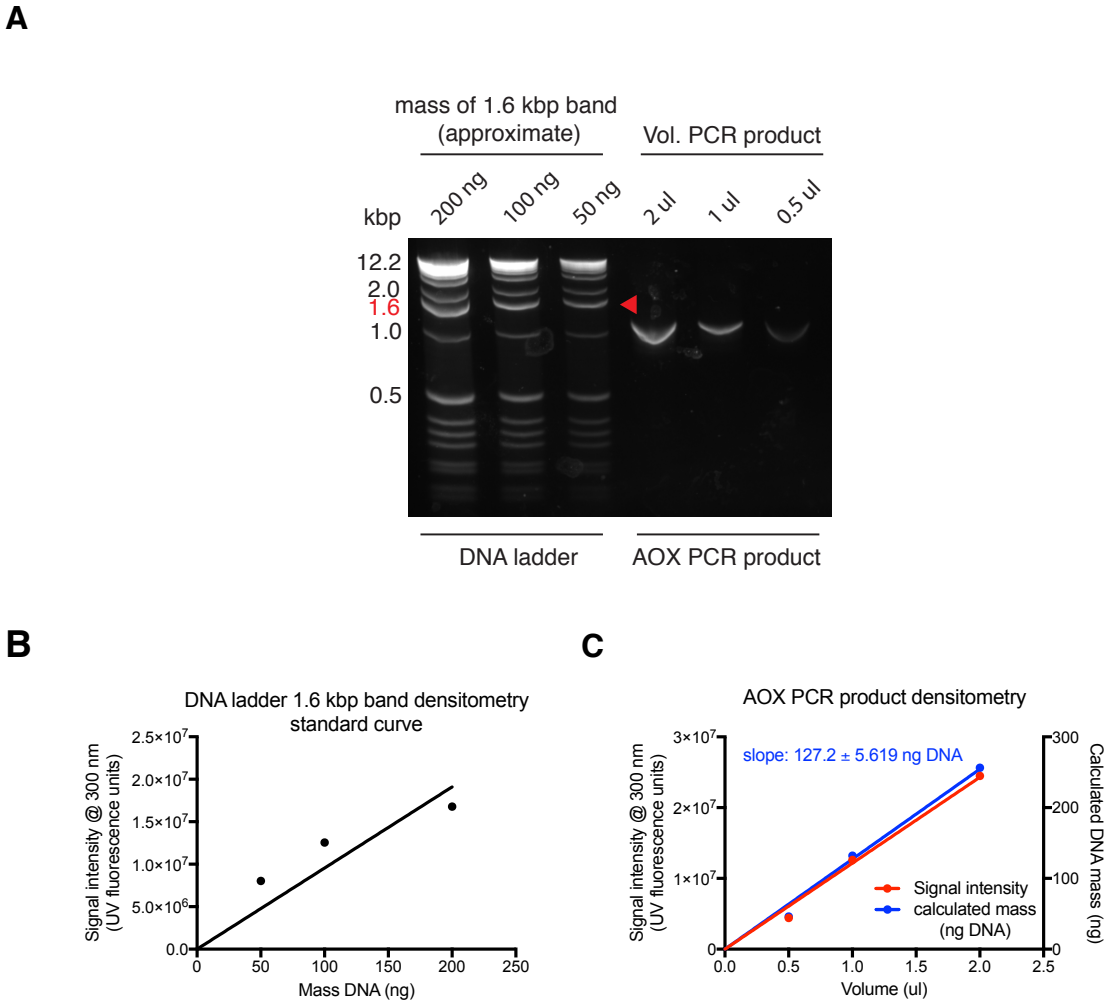

Figure 2.6. Linear dsDNA quantification (approximation) by densitometry. (A) *A serial dilution of 1 kbp ladder of known concentration (1 µg/µl) was applied to the gel, (following dilution in DNAase-free H_2O and addition of an appropriate vol. of 6X loading buffer). The ~1.6 kbp band (highlighted in red) contains ~ 10% of the mass loaded on the gel (e.g. 2 µl equivalent of 1 kbp ladder = 2 µg DNA in total; ~1.6 kb band ~ 200 ng DNA). Known vol. of linear PCR product (unknown concentration) were also loaded on the gel. After electrophoresis, the DNA in the gel was visualized using a UV transilluminator (at 300 nm, appropriate for GelRed™ nucleic acid stain) and the image scanned and exported. The image was imported into Image Lab™ and signal intensities (SI) of the 1.6 kbp bands of the DNA ladder of known mass (standard curve) were recorded.* ***(B)*** *These values were exported to GraphPad Prism 5.0 and a linear regression was performed: SI versus DNA mass (ng).* ***(C)*** *The SI of the PCR product bands were then recorded (in Image Lab™) and plotted (in GraphPad Prism 5.0) alongside vol. to assess SI-vol. linearity (in red). The mass of the PCR product bands were then interpolated from the standard curve (expressed as SI) by linear regression. The calculated masses were then plotted alongside their equivalent volumes (linear regression through zero), with the slope of the line estimating the PCR product DNA concentration (ng/µl ± standard error). All data points are n = 1.*

2.9.6 Enzymatic restriction digest

All restriction enzymes (RE) and buffers were purchased from New England Biolabs (NEB). Cohesive-end RE digest of plasmid or PCR-amplified DNA was performed in a total vol. of 20 or 50 µl in the presence of DNAase-free H_2O, compatible buffer (CutSmart® where appropriate, containing 50 mM potassium-acetate, 20 mM Tris-acetate, 10 mM magnesium-acetate, 100 µg/ml BSA, pH 7.9 at 25°C) and 10 U of each RE per 1 µg DNA. Reactions were performed at 37°C for 1 h at 500 rpm (unless otherwise indicated). When restriction sites were selected **(Figure 2.7)**, the online resource, NEBCloner™ (http://nebcloner.neb.com/#!/redigest) was referred to for buffer compatibility and reaction time guidelines. Typically, RE digests were performed on small amounts of plasmid DNA (diagnostic tests) **(Figure 2.8)** before digesting larger amounts for ligation reactions, to assess the ability of selected REs to cut the DNA at expected sites. Plasmid DNA (250 ng) was digested by 1 or 2 REs (for single and double-digests, respectively) for diagnostic tests and plasmid DNA or PCR product (1 µg) was double-digested for ligation preparation. Post digest, reactions were heated at 65 or 80°C for 20 min (where indicated) to heat inactivate the REs prior to ligation.

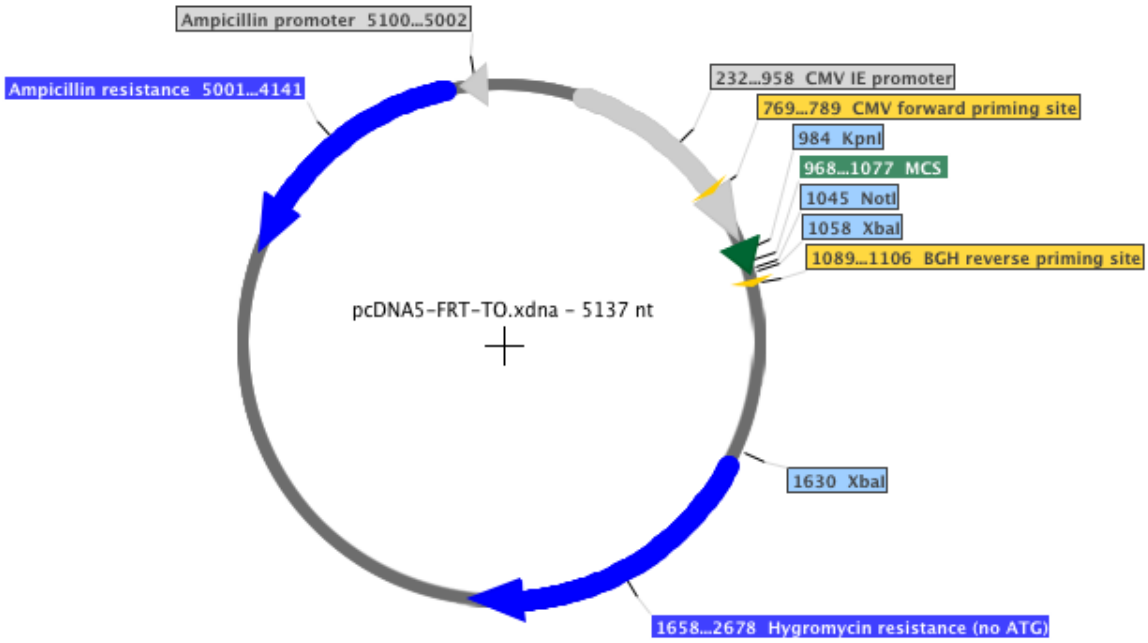

Figure 2.7. Scale map of pcDNA5/FRT/TO expression vector highlighting restriction sites. *Restriction sites KpnI and NotI are present in the Multiple Cloning Site (MCS) and XbaI is present in the MCS and at one other site in the vector. RE digest with enzymes KpnI-HF or NotI-HF would linearise the vector (cutting one time each), resulting in dsDNA fragments of 5.137 kbp. A double digest with KpnI-HF and NotI-HF would create orientation specific ligation sites for a compatible insert (5'KpnI, 3'NotI). The restriction site XbaI can be used to aid identification of the vector, as RE digest with enzyme XbaI would result in two linear dsDNA fragments, one of 0.572 kbp and one of 4.57 kbp, and thus the electrophoretic migration pattern of these fragments would act as a signature. The scale map was created using SerialCloner 2-6-1, with the pcDNA5/FRT/TO DNA sequence imported from the manufacturer's online resource (https://tools.thermofisher.com/content/sfs/vectors/pcdna5frtto_seq.txt). See also* ***Appendix A*** *for sequence.*

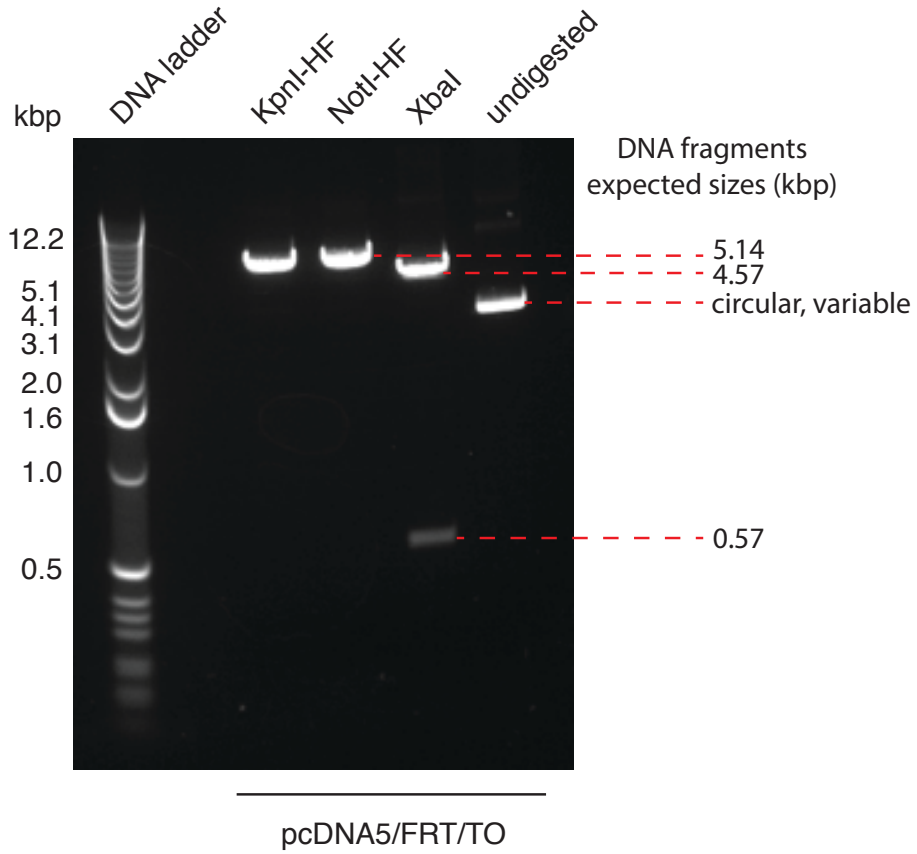

Figure 2.8. Diagnostic 1% (w/v) agarose gel of pcDNA5/FRT/TO vector (250 ng per lane) digested with REs KpnI-HF, NotI-HF, XbaI or undigested. *KpnI-HF and NotI-HF REs efficiently digested the vector (presenting as different DNA band migration compared to undigested vector), cutting once each as expected (no other DNA bands were visible) and creating bands of the same size, although suggesting a higher than expected plasmid size. However, this was likely artifactual due to gel heat warping at the top of the middle lanes (not visible). XbaI digested the plasmid DNA at two sites as expected, generating two bands that electrophoresed approximately according to expected sizes (0.572 kbp and 4.57 kbp). Undigested vector, which can exist in varying circular or pseudo-linear conformations (e.g. supercoiled) each affecting gel migration differently, electrophoresed further than linear vector.*

2.9.7 Polymerase Chain Reaction (PCR)

Target cDNA sequences in plasmids were amplified by PCR **(Figure 2.9 - 2.11)** in a TProfessional Basic Gradient Thermocycler (Biometra). PCR was performed in a total vol. of 20 µl (in DNAase-free H_2O) with 10 ng template (plasmid) DNA, Phusion™ High Fidelity DNA Polymerase (final concentration 0.02 U/ml), GC buffer and dNTPs (final concentration 200 µM per dNTP) (Thermo Scientific). Custom extension/amplification primers were synthesised by Sigma Genosys Biotechnologies and used at a final concentration of 0.5 µM (see **Appendix B** for sequences). Routine PCR was performed as described below **(Table 2.2).** Samples from post-PCR reactions were electrophoresed on agarose gels to confirm DNA amplification of product of the desired size **(Figure 2.11)**.

Step	Sub-step	Temperature (°C)	Time (s)
Initial denaturation		98	30
Thermocycling	Denaturation	98	10
	Primer annealing	varied	30
	Extension	72	30 (per kbp)
Final extension		72	600
Hold		4	Indefinitely

Table 2.2 Routine PCR settings. *Primer annealing temperature varied depending on the size of the primers. Primer melting temperatures (T_m) were calculated from only the nucleotides complementary to the target sequence (NDI1) by referring to the online resource, NEB Tm Calculator (http://tmcalculator.neb.com/#!/) which takes into account optimum temperatures for the specific polymerase and buffer in the PCR reaction (simplified equation: T_m (°C) = 2° X (A + T) + 4° X (G + C)); Primers greater than 20 nucleotides in length were annealed at 3°C above the T_m of the lower T_m primer; primers less than 20 nucleotides in length were annealed at the T_m of the lower T_m primer. All other PCR settings remained constant.*

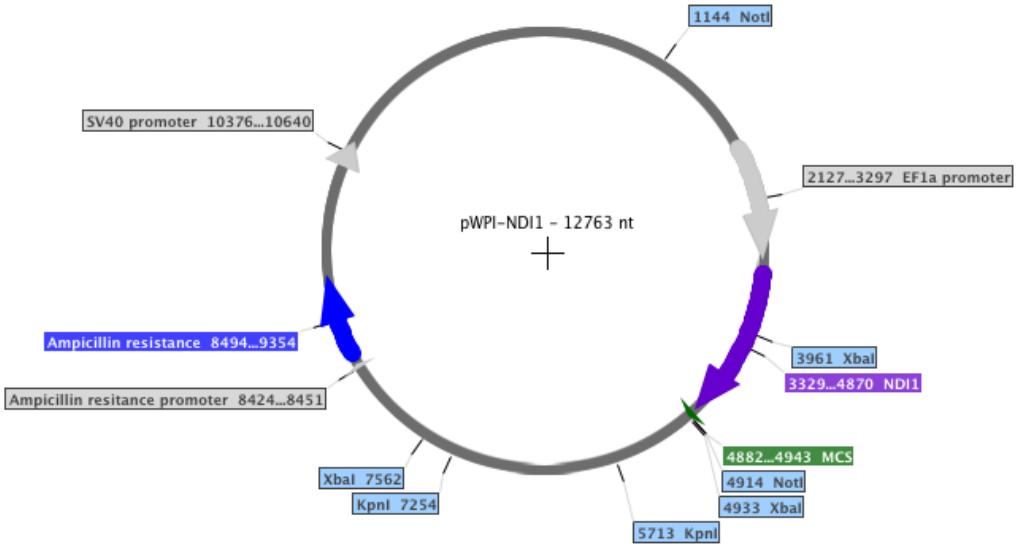

Figure 2.9. Scale map of pWPI plasmid containing the NDI1 template sequence to be PCR-amplified. *The NDI1 sequence (1541 nt) did not contain internal KpnI or NotI restriction sites (to be incorpated onto the 5' and 3' ends, respectively, of the NDI1 sequence during PCR to allow orientation specific ligation with the pcDNA5/FRT/TO recipient vector). The NDI1 sequence did contain an internal XbaI restriction site which was used to help confirm the identity of the eventual PCR product. RE digest of the PCR product with enzyme XbaI would result in two linear ds DNA fragments (917 bp and 651 bp) whose electrophoretic mobility pattern would aid identification of the PCR product. The scale map was created using SerialCloner 2-6-1, using the pWPI-NDI1 DNA template imported from Dr. Alberto Sanz (Institute for Cell and Molecular Biosciences & Newcastle University Institute for Ageing, Newcastle University, Newcastle, UK) (see* ***Appendix A****), who gifted me the vector.*

A

NDI1 PCR primers:	Description/legend:	Tm:
Forward: TTA ATC GGT ACC GCC ACC ATG CTA TCG AAG AAT TTG TAT	5'-KpnI-Kozak-Start-NDI1-3'	54°C
Reverse: CG GGT AGC GGC CGC CTA TAA TCC TTT AAA AAA GTC TCT T	5'-NDI1-Stop-NotI-3'	55°C

B

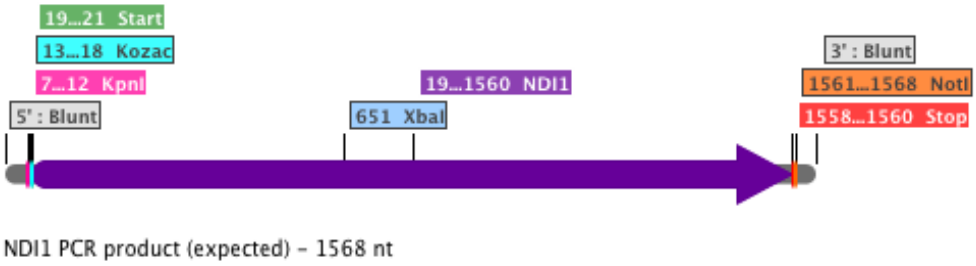

Figure 2.10 Description of NDI1 PCR primers and the expected PCR product. (A) *The forward primer was designed to introduce a 5' KpnI restriction site and a modified Kozak consensus sequence (to aid initiation of translation) before the start codon (ATG) of NDI1; the reverse primer was designed to introduce a NotI restriction site after the NDI1 stop codon;* ***(B)*** *the expected PCR product size was 1568 bp. The scale map was created using SerialCloner 2-6-1, using the NDI1 DNA template from the previously described source.*

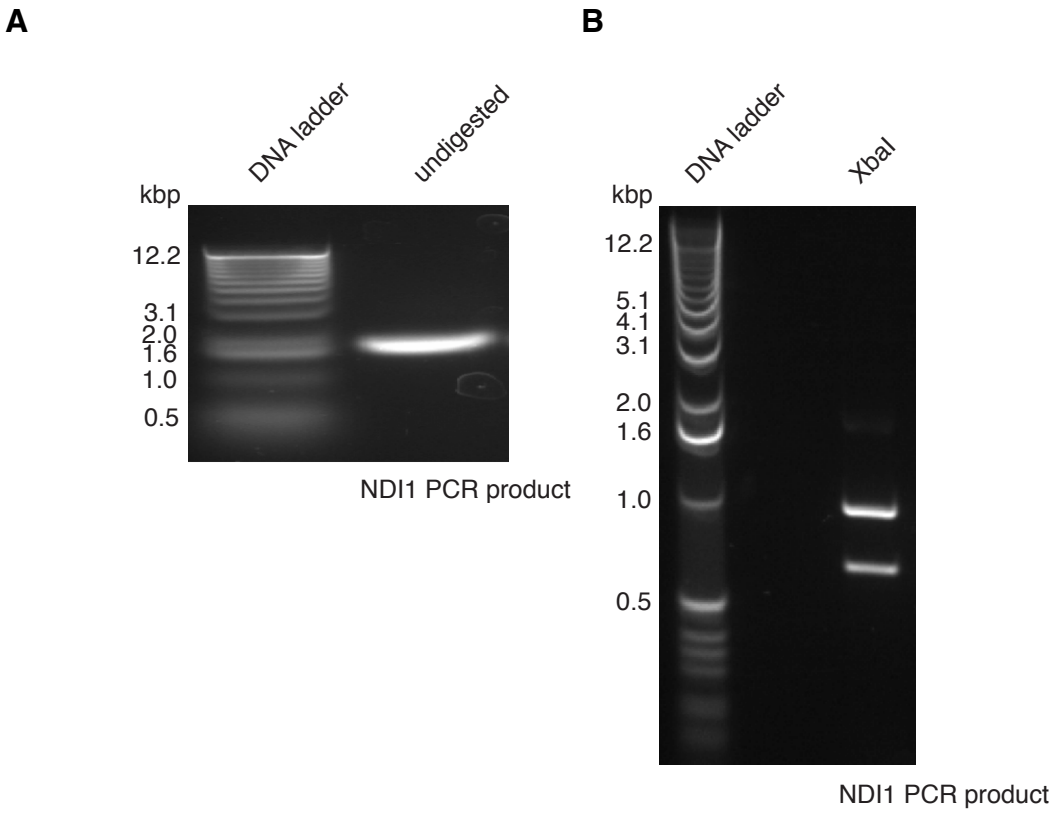

Figure 2.11 Diagnostic agarose gels of the NDI1 PCR product. (A) *Diagnostic 1% (w/v) agarose gel of 1 µl of NDI1 post-PCR mix which confirmed amplification of a single product which electrophoresed to the ~ 1.6 kbp DNA marker.* ***(B)*** *Diagnostic 1% (w/v) agarose gel of 1 µl of NDI1 post-PCR mix restriction digested with XbaI which cut the PCR product into two fragments (expected: 917 bp and 651 bp) due to the XbaI site in the middle of the NDI1 sequence, the electrophoretic mobility pattern offering evidence of the identity of the PCR product.*

2.9.8 Dephosphorylation of recipient vector

RE digest introduces 5' phosphate groups, which are required for ligation to occur. In order to inhibit recipient vector self-ligation (in cases where double-digestion was incomplete) and promote ligation between the recipient vector and a 5' phosphorylated insert, the double-digested recipient vector was dephosphorylated with Antarctic Phosphatase (NEB). Typically, 1 µg DNA was desphosphorylated with 5 U Antarctic Phosphatase in the presence of Antarctic Phosphatase Reaction Buffer (50 mM Bis-Tris-Propane HCl, 1 mM $MgCl_2$, 0.1 mM $ZnCl_2$, pH 6.0 @ 25°C). Samples were incubated at 37°C for 1 h and then heat inactivated at 65°C for 5 min or at the temperature and time required to heat inactivate any active REs still present (according to the manufacturer's guidelines).

2.9.9 Gel purification

PCR amplified cDNA sequences or linear RE-digested vectors were gel purified prior to further processing (RE-digestion or ligation). This was done to isolate and purify linear cDNA of a specific size from a PCR reaction or vector backbone and also to remove primers and other contaminants which may inhibit further enzymatic reactions. Samples were loaded onto 0.8 % (w/v) agarose gels, as previously described, and visualised using UV light. DNA bands were cut from the gel using a clean razor blade and placed in a pre-weighed, sterile 1.5 ml Eppendorf tube. The Eppendorf tube was weighed again to calculate the gel mass and DNA was purified from the gel using a QIAquick Gel Extraction Kit (Qiagen), according to the manufacturer's instructions. Briefly, the gel slice (containing DNA) was melted (65°C, 10 min) in a high salt, acidic buffer (3 vol. buffer QG : 1 vol. gel) to provide the optimum pH (pH ≤ 7.5) for DNA binding to the silica spin column provided in the same kit. DNA was then washed on the column, first with QG buffer (to remove agarose), then with an ethanol-containing buffer that removes salts and other contaminants that do not bind to the column. DNA was eluted from the column in a low salt, basic elution buffer (10 mM Tris·Cl, pH 8.5).

2.9.10 DNA ligation

Double digested, dephosphorylated recipient vector and double digested, 5' phosphorylated PCR product were ligated in a 3 : 1 (insert : vector) molar ratio calculated as follows:

Required mass insert (ng) = desired insert : vector molar ratio (3) x mass of vector (50 ng) x ratio of insert : vector lengths (variable).

Ligation was performed in a total vol. of 20 µl, containing vector DNA (50 ng) and insert DNA (variable), T4 DNA Ligase Buffer (50 mM Tris-HCl, 10 mM $MgCl_2$, 1 mM ATP, 10 mM DTT, pH 7.5 @ 25°C (NEB)), DNAase-free H_2O and 5 U T4 DNA ligase (NEB). The reaction was mixed gently, centrifuged (1,000 X g for 1 min) and incubated at RT overnight. The ligation mix was heat inactivated at 65°C for 10 min prior to transformation.

2.9.11 Bacterial transformation

In order to isolate and amplify the novel ligated vector, 40 µl XLI-Blue electrocompetant *E. coli* (Aligent Technologies) were transformed with 1 µl ligation mix by electroporation in an electroporation cuvette (2 mm gap, Flowgen Bioscience). Warm SOC media (960 µl) was then added to the bacteria in the electroporation cuvette and incubated at 37°C for 1 h. The *E.coli*/SOC broth was then plated (20 µl) on LB-agar plates containing 100 *µ*g/ml ampicillin and incubated at 37°C overnight in order to select for bacterial colonies resistant to ampicillin (conferred by the intact vector). The transformation efficiency of the ligation mix was compared to that of 1 µl circular, undigested vector as a positive control **(Table 2.3)**. *E. coli* were also transformed with 1 µl ' – insert' ligation mix (double-digested dephosphorylated vector (50 ng), T4 DNA Ligase Buffer, DNAase-free H_2O and 5 U T4 DNA ligase (NEB), total vol. 20 µl, incubated for the same time as the ' + insert' ligation mix) as a negative control to assess the background presence of undigested vector or self-ligated vector, as only circular plasmids and not linear DNA fragments are taken up by *E.coli* during transformation.

Plate	Plasmid	Insert (NDI1 PCR product, double-digested)	Colonies per plate
1	Undigested pcDNA5/FRT/TO	-	> 1,000
2	Double-digested, dephosphorylated pcDNA5/FRT/TO	-	19
3	Double-digested, dephosphorylated pcDNA5/FRT/TO	+	~ 70

Table 2.3. Example of analysis of transformation efficiency. *XLI-Blue electrocompetant* E. coli *were transformed with 1 µl of undigested pcDNA5/FRT/TO vector as a positive control (plate 1), plated on an LB-agar plate containing 100 µg/ml ampicillin and incubated overnight at 37°C as described above. Colony growth (> 1,000 colonies) was evidence of viability of the* E.coli *and the effectiveness of the transformation protocol. As a negative control (plate 2),* E. coli *were transformed with 1 µl of '- NDI1 insert' ligation mix to assess the relative amount of undigested vector or self-ligated vector. The presence of 19 colonies was evidence of some intact vector present in mix, suggesting that there might be some false positives on the test plate;* E. coli *were transformed with 1 µl of the '+ NDI1 insert' ligation mix (plate 3). The presence of ~ 70 colonies suggested that there would be ~ 3.5 times more positive colonies (containing NDI1-ligated vector) on the test plate than false-positive colonies (containing undigested or self-ligated vector).*

2.9.12 Isolating plasmid DNA from bacterial colonies for diagnostic tests

Plasmid DNA was purified from bacterial colonies by the QIAprep Spin Miniprep Kit (Qiagen), according to manufacturer's instructions. Briefly, 3 ml aliquots of LB broth + AMP (in 15 ml Falcon tubes) were inoculated with individual bacterial colonies from LB agar + AMP plates (typically 20 colonies per batch). Cultures were grown overnight at 37°C with agitation. Cultures were pelleted by centrifugation (5,000 X g for 5 min at RT). Supernatant was decanted and pellets were resuspended in a buffer containing RNAase A, which degrades single-stranded RNA. 1 vol. of alkaline lysis buffer was added to the resuspension and mixed thoroughly. After 3 - 5 min, the solution was pH neutralised by addition of neutralisation buffer, which has a high salt content to promote DNA binding to the silica column. The neutralised solution was centrifuged (17,000 X g for 10 min at RT) to separate DNA-containing supernatant from the precipitate. The supernatant was passed through a silica spin column. Salts were removed from the silica-bound

DNA with an ethanol-containing buffer. Finally, DNA was eluted in a low salt elution buffer (10 mM Tris·Cl, pH 8.5).

2.9.13 Identification of plasmid DNA in transformed *E.coli* by RE-digest

Samples of mini-prep plasmid stocks from transformed *E.coli* were RE double-digested with the same REs used to ligate the insert to the vector backbone (KpnI-HF and NotI-HF). Samples were electrophoresed alongside a DNA ladder. Samples that linearized into 2 fragments (one having the approximate size of the vector backbone and the other having the approximate size of the desired insert **(Figure 2.12 & 2.13)**) were marked as potential positive samples. Potential positive samples were sent for DNA sequence analysis to confirm the identity of the plasmid and to rule out any *de novo* mutations (see **Appendix A**).

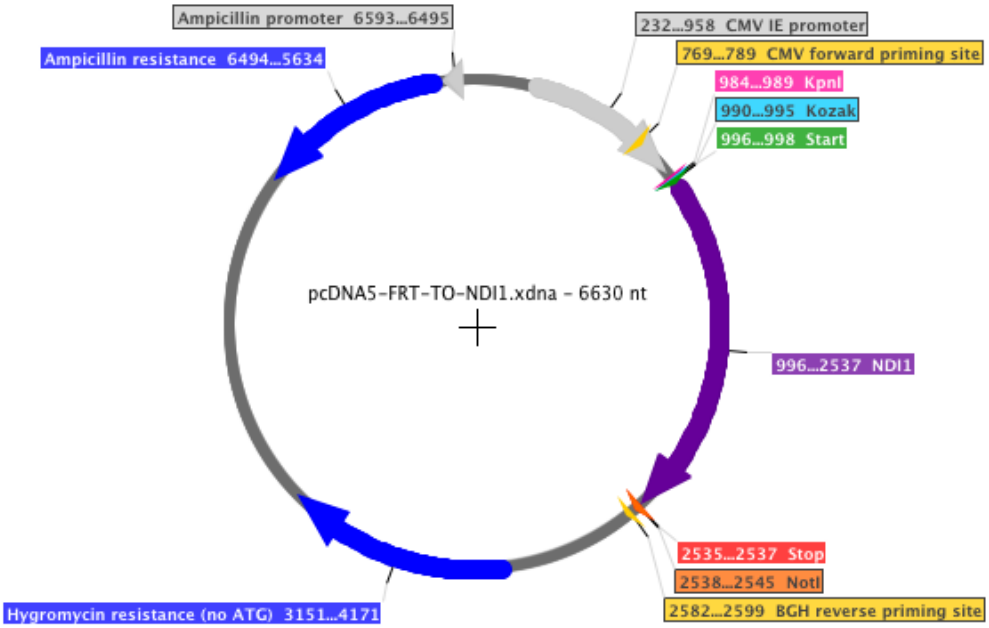

Figure 2.12 Scale map of the expected pcDNA5/FRT/TO plasmid containing the NDI1 gene. *The pcDNA5/FRT/TO recipient vector was double digested at the KpnI and NotI RE sites and dephosphorylated (with Antarctic phosphatase) prior to ligation (with T4 DNA ligase) to a PCR-amplified NDI1 insert double digested at flanking 5'KpnI and 3'NotI RE sites (introduced by PCR). Ligation was performed overnight at RT. To isolate ligated vector, XL1 Blue electrocompetant* E.coli *were transformed with 1 ul of ligation mix. Transformed E.coli were selected on LB plates + AMP (overnight at 37°C) and propogated in LB broth + AMP (overnight at 37°). Plasmid DNA was isolated by Qiagen Miniprep. Positive clones were identified first by RE digest and then confirmed by DNA sequence analysis. The scale map was created using SerialCloner 2-6-1, using the pcDNA5/FRT/TO template (digested* in silico *at the KpnI and NotI RE sites) and the expected NDI1 PCR product (digested* in silico *at the KpnI and NotI RE sites).*

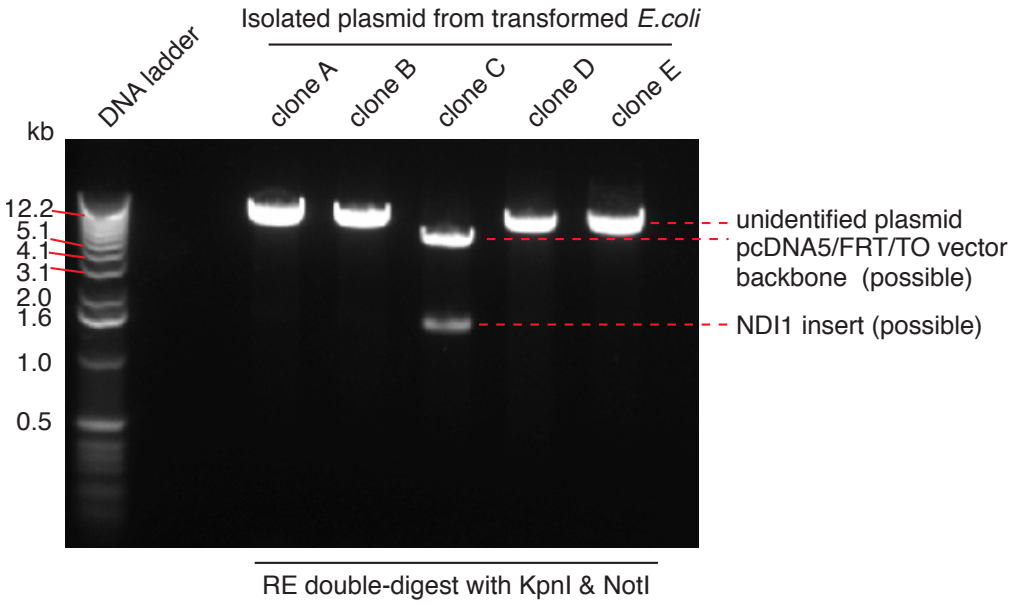

Figure 2.13 Isolated plasmid DNA extracted from transformed E.coli diagnosed by RE double digest followed by agarose gel electrophoresis. *Unidentified plasmid DNA from transformed* E.coli *(250 ng) was double digested by RE enzymes KpnI-HF and NotI-HF and electrophoresed on a 1% (w/v) agarose gel. Plasmid DNA that digested into two fragments, one of ~1.6 kbp, was marked as a potential positive clone (pcDNA5/FRT/TO-NDI1) and sent for Sanger DNA sequencing for confirmation.*

2.9.14 DNA sequence analysis

Plasmid DNA was sequenced by Sanger sequencing (Source Bioscience), using stock primers or custom primers (see **Appendix B** for sequences) where necessary. Samples were diluted to 100 ng DNA /µl in TE buffer before sample submission.

2.9.15 Isolating endotoxin-free vector for mammalian cell transfection

In order to prepare a large quantity of endotoxin-free vector for mammalian cell transfection, bacteria were retransformed with the plasmid of interest and isolated as described above. New colonies that formed after plating on LB-agar + AMP plates were picked and grown in LB broth + AMP and DNA was isolated according to the Qiagen Midi-prep protocol (below), quantified by Nano-drop and sent for Sanger sequencing analysis. (qiagen.com/cn/resources/resourcedetail?id=c164 c4ce-3d6a-4d18-91c4-f5763b6d4283&lang=en).

2.9.16 Creation of bacterial glycerol stocks for long-term storage

An overnight culture of transformed bacteria in LB broth + AMP (500 µl) was mixed with 500 µl of 50 % (v/v) glycerol (in MQ H_2O) in a cryovial. Glycerol stocks were snap frozen on dry ice and stored at -80°C.

2.10 Statistical analysis

Data analysis was performed with GraphPad Prism 5.0. Results (n = 2) were expressed as mean ± range. Results (n ≥ 3) were analysed by unpaired, one-tailed t-tests (2 groups) or one-way analysis of variance (ANOVA) (> 2 groups), typically with Dunnet's post-tests (comparing all columns to control) (unless otherwise stated) and expressed as mean ± standard error of the mean (SEM). *P*-values < 0.05 were considered statistically significant.

Chapter 3

Click-PEGylation - a mobility shift approach to assess the redox state of cysteines in candidate protein

3.1 Introduction

The redox state of cysteine thiols is critical for protein function. Whereas cysteines play an important role in the maintenance of protein structure through the formation of internal disulfides, their nucleophilic thiol groups can become oxidatively modified in response to diverse redox challenges and thereby function in signalling and antioxidant defences. These oxidative modifications occur in response to a range of agents and stimuli, and can lead to the existence of multiple redox states for a given protein. To assess the role(s) of a protein in redox signalling and antioxidant defence, it is thus vital to be able to assess which of the multiple thiol redox states are present and to investigate how these alter under different conditions.

As discussed in **Chapter 1**, AMPK, a master regulator of cell metabolism and mitochondrial biogenesis, has been a focus of interest in the redox biology field. ROS have been investigated as an atypical regulator of AMPK by several potential redox mechanisms, including by direct cysteine oxidation of the catalytic subunit. However, direct redox-regulation of AMPK in cells is not uniformly observed (Emerling et al., 2009, Auciello et al., 2014, Hawley et al., 2010). Also, the effects on AMPK redox-state and activity by different sources of ROS (i.e. cytosolic versus mitochondrially-derived ROS) have not yet been compared. As previously discussed, mitochondrially-derived ROS is of particular interest as a redox signal, with several labs including our own having described how ROS production by RET could be a potential way in which mitochondria relay information about the metabolic state and demands of the cell. Thus, it remains necessary to be able to readily measure the redox state of AMPK in cells and tissues (as well as measuring AMPK activity and cell adenine nucleotide ratios) in order to determine if different sources of ROS directly alter AMPK activity (e.g. through cysteine thiol oxidation) or if ROS only alters AMPK activity indirectly (e.g. by decreasing ATP levels or by inhibiting upstream phosphatases).

A number of methods are available to assess the redox state of protein thiols, the

most quantitative of which are redox proteomic approaches utilising mass spectrometry, such as OxICAT (Held et al., 2010, Leichert et al., 2008). These untargeted approaches can both identify the cysteine residues affected and quantify the extent of oxidation. However, these screens are time-consuming and coverage is often biased towards abundant proteins. In addition, detection of cysteine residues by mass spectrometry can be complicated by their location within regions that are challenging to access using currently available proteases (Verrastro et al., 2015). Therefore, candidate protein approaches based on antibody binding are often used in parallel to enable low abundance proteins to be interrogated (e.g. specific kinases), or to obtain a more complete redox profile of the protein of interest. Typically, the redox-altered protein thiols are selectively tagged to a large group, such as a polyethylene glycol (PEG) moiety connected to a maleimide compound (Burgoyne et al., 2013). Maleimide compounds react relatively selectively and irreversibly with thiol groups through the formation of a thioether bond. Samples can then be separated by electrophoresis, and probed with an antibody against the protein of interest, avoiding the need to purify proteins prior to analysis. PEGylated cysteines will cause a mobility shift, and the result will typically show a series of bands corresponding to different redox forms of the protein interrogated. Providing an appropriate antibody is available for the protein itself or for an epitope tag on the protein (if existing), the extent of the redox modification for even low abundance proteins can be quantified quickly and cheaply. However, a limitation of this approach is that the reaction of a cysteine residue with a large (typically ~2 – 5 kDa) reactive PEG moiety can be slow, leading to incomplete reaction with protein thiols.

3.2 Aims and strategy

To investigate redox modifications of AMPK in cells, my aim was to develop a more robust and flexible method for redox-selective PEGylation. Here I have utilised a Click chemistry approach, where free thiol groups are first labelled with a small and reactive reagent modified to contain an alkyne moiety, which is subsequently Click-reacted with a PEG molecule containing a complementary azide function **(Figure 3.1)**. This strategy can be adapted to study reduced or reversibly oxidised cysteines. Separation of the thiol labelling step from the PEG conjugation enhances the fidelity and flexibility of this candidate protein approach. The method was initially optimised using purified glyceraldehyde-3-phosphate dehydrogenase (GAPDH) as an exemplar protein, then adapted to analyze GAPDH in cell lysates, and finally AMPK became the focus of continued Click-PEGylation experiments.

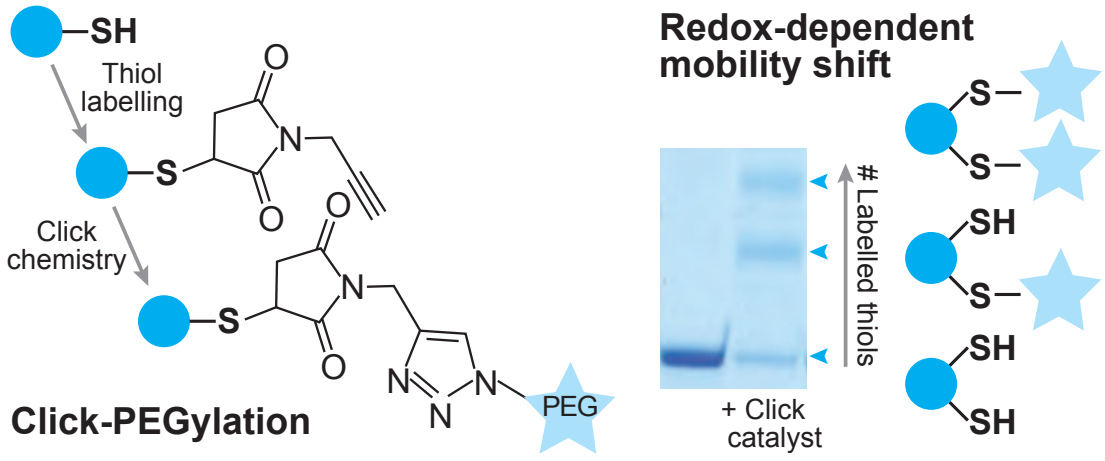

Figure 3.1. Click-PEGyation concept. *Reduced thiols are first labeled with an alykating agent containing an alkyne group. Then using Click chemistry, a large PEG molecule containing an azide group is conjugated to the alkyne. Oxidised thiols are reduced and remain unlabeled by PEG. The net effect is electrophoretic mobility shift dependent on the number of PEG-bound thiols groups.*

3.3 Collaborations and publications

This work led to a publication: Click-PEGylation – A mobility shift approach to assess the redox state of cysteines in candidate proteins (2017) (*Free Radic Bio Med,* **108**, 374 – 382) in collaboration with the co-first author Lucie A.G. van Leeuwen (LvL hereafter), corresponding author Helena M. Cochemé (both of MRC London Institute of Medical Sciences, Du Cane Road, London W12 0NN, UK; Institute of Clinical Sciences, Imperial College London, Hammersmith Hospital Campus, Du Cane Road, London W12 0NN, UK) and Ellen L. Robb and Michael P. Murphy (MRC Mitochondrial Biology Unit, University of Cambridge, Wellcome Trust/MRC Building, Cambridge Biomedical Campus, Hills Road, Cambridge CB2 0XY, UK)(van Leeuwen et al., 2017) (see **Appendix C**).

The experimental work discussed below (excluding **3.5 Method Application**) was divided between LvL and me (the division is described in each figure legend) with preliminary experiments performed by Ellen L. Robb (data not shown). All experiment design, troubleshooting and optimisation decisions discussed below were made by both LvL and me. Prior to publication, I presented a poster of this work at the Gordon Research Conference: Thiol-Based Redox Regulation & Signalling, 2016 (Stoweflake Conference Center, Stowe, VT, USA) and gave a short talk at the associated Gordon Research Seminar for PhD students and post-doctoral researchers.

3.4 Method development and results

3.4.1 Choosing a model protein

We set out to optimise and assess the potential utility of the Click-PEG protocols using GAPDH as an exemplar protein. GAPDH is one of the most well-characterised redox sensitive proteins. It is the most abundant S-thiolated protein during conditions of oxidative stress in yeast, with the thiol oxidation reversibly decreasing the enzyme's activity and therefore acting as a redox switch in regulating glycolysis (Grant et al., 1999, Shenton et al., 2002). Initially, we utilised purified GAPDH protein from rabbit, which contains 4 cysteine residues, enabling

the effectiveness of the Click-PEG reactions to be directly assessed by SDS-PAGE and Coomassie protein staining. To test if the Click-PEGylation method is applicable to a broad range of proteins of differing sizes, we also tested another candidate protein, catalase, which has a higher molecular weight (~ 60 kDa) and 4 cysteine residues. Having validated the Click-PEGylation technique with purified GAPDH and catalase as a proof-of-principle, we next wanted to demonstrate that the Click-PEGylation approach can be applied to detect redox state changes of target proteins within complex biological samples, such as cell lysates and tissue extracts. I looked at GAPDH from lysates of C2C12 mouse myoblast cells, noting that mouse GAPDH contains 5 cysteine residues, and not 4 as in rabbit.

3.4.2 Basic Click-PEGylation protocol

The basic Click-PEGylation reaction scheme is shown in **Figure 3.2**. The essence of the assay is to differentially label cysteine residues that are unmodified (i.e. reduced) and those that are reversibly oxidised, with either a low molecular weight thiol alkylating agent, or with one that can be further conjugated to a high molecular weight PEG polymer, containing an azide group. In Click chemistry, azide and alkyne groups are selectively reacted with each other in the presence of a Cu^{1+} catalyst (Rostovtsev et al., 2002, Tornoe et al., 2002). This assay can be designed to PEGylate either the reduced or reversibly oxidised thiols, described as Click-PEG_{red} and Click-PEG_{ox}, respectively.

To label reduced cysteine residues by Click-PEGylation (Click-PEG_{red} **Figure 3.2 (B)**), reduced thiols are initially reacted with a maleimide compound containing a Click-reactive alkyne moiety (propargyl-maleimide), then subsequently conjugated to a large PEG molecule containing a complementary Click-reactive azide moiety (azide-PEG), to selectively PEGylate the Click-tagged thiols. The sample can then be separated by electrophoresis, and analysed by protein staining or by Western blotting. Thus, in Click-PEG_{red}, proteins with reduced cysteine residues undergo a mobility shift and appear as higher molecular weight bands, enabling the redox state of the protein to be inferred. This basic protocol can also be altered to Click-

PEGylate reversibly oxidised cysteine residues (Click-PEG$_{ox}$**, Figure 3.2 (C)**), providing complementary information. In this case, reduced thiol groups are first blocked with *N*-ethylmaleimide (NEM), before reducing any reversibly oxidised thiols with TCEP or DTT and subjecting these to Click-PEGylation. There are potential advantages to both approaches depending on the protein of interest and its inherent redox status (e.g. if a protein's thiols exist in a mostly reduced state, more obvious redox shifts may be observed by performing Click-PEG$_{ox}$ than Click-PEG$_{red}$ and vice versa). Most importantly, analysing a sample in parallel by Click-PEG$_{red}$ and Click-PEG$_{ox}$ should generate complementary information that enhances confidence in the redox state determined.

Other advantages of this Click-PEGylation approach are: 1) it can be applied simply to the experimental sample, avoiding the slow and difficult direct reaction of a bulky maleimide-PEG polymer with cysteine residues; 2) the method could be adapted to detect a specific cysteine residue modification selectively, by exploiting a particular biochemical reactivity at the labelling stage - e.g. treatment with Cu/ascorbate to identify *S*-nitrosation, dimedone for *S*-sulfenylation, or hydroxylamine for *S*-acetylation (Jaffrey et al., 2001, Benitez and Allison, 1974, Drisdel and Green, 2004); 3) this Click chemistry approach to label cysteine thiol groups can be extended by substituting the azide-PEG moiety for any desired azide-containing tag to allow other modes of detection, e.g. fluorescence.

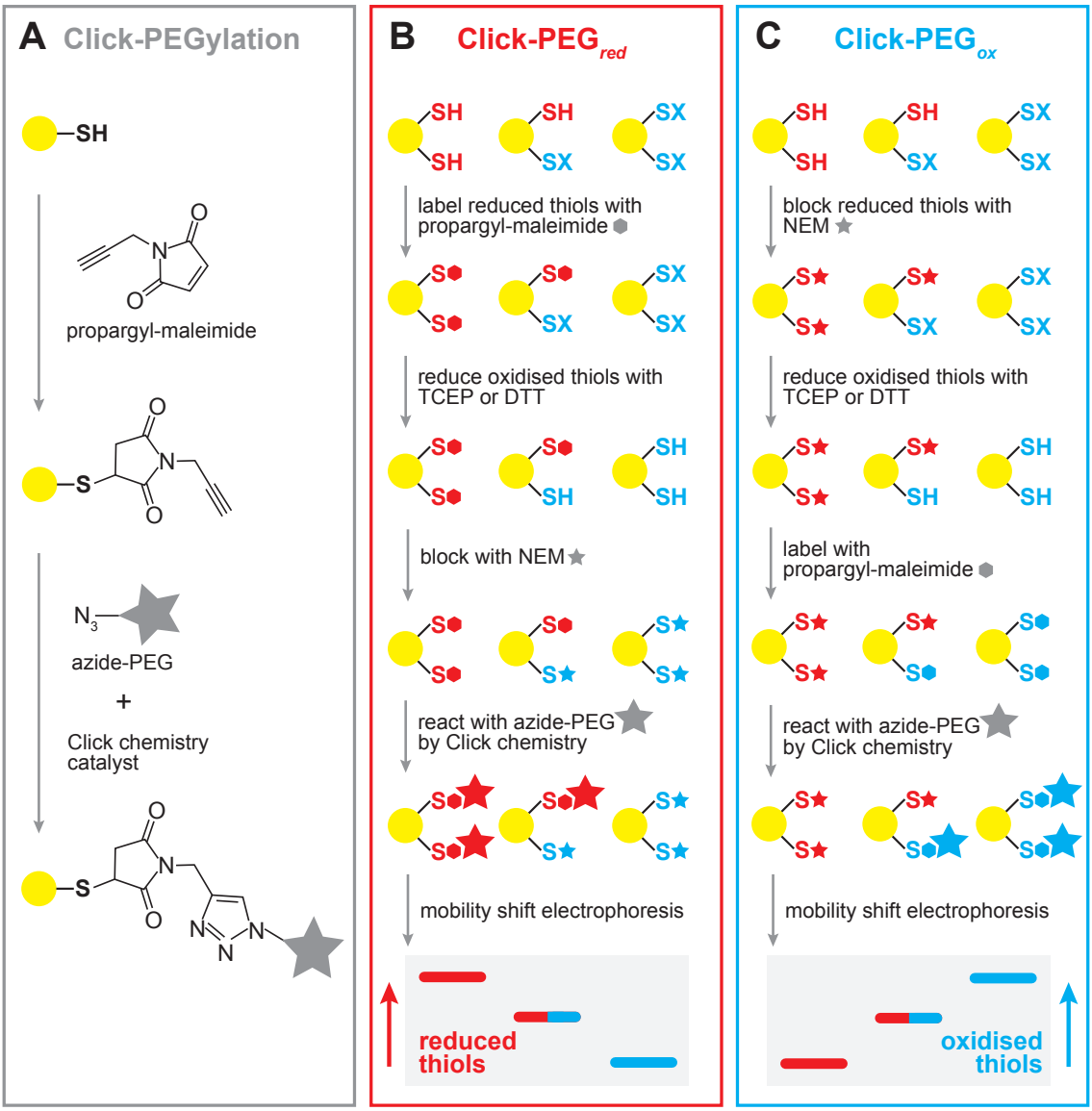

Figure 3.2. Click-PEGylation schemes. (A) *Principle of the Click-PEGylation reaction. A reduced thiol is alkylated with propargyl-maleimide, then conjugated with an azide-PEG of high molecular weight (e.g. 5 kDa) using copper-catalysed Click chemistry.* ***(B)*** *Click-PEG$_{red}$ reaction to label reduced thiols. A protein with two potentially reversibly oxidisable cysteine residues is shown. For Click-PEG$_{red}$, the sample is reacted with propargyl-maleimide to label reduced cysteines, which are subsequently derivatised with azide-PEG via Click chemistry. Optionally, oxidised cysteines can then be reduced and blocked with NEM before separation by electrophoresis.* ***(C)*** *Click-PEG$_{ox}$ reaction to label oxidised thiols. Conversely, for ClickPEG$_{ox}$, the sample is first reacted with NEM to block any reduced cysteine residues. Next, previously oxidised thiols are reduced, allowing their reaction with propargyl-maleimide and derivatisation with azide-PEG. Finally, samples are separated by electrophoresis to determine the resulting redox mobility shifts.*

3.4.3 Assessing the Click-PEGylation protocols using purified GAPDH

The Click-PEG_{red} protocol, designed to facilitate the selective labelling and gel shifts of reduced protein thiols, was tested on purified GAPDH. The GAPDH was reacted with propargyl-maleimide and derivatised with azide-$PEG_{5,000}$ (~5 kDa) in a Click reaction step, then visualised by Coomassie staining after SDS-PAGE **(Figure 3.3)**. For the Click reaction step, samples were split and treated in parallel with and without Click catalyst, to visualise the redox-dependent mobility shift ('+ catalyst'). The unshifted lane ('– catalyst') serves as a loading control, indicating total levels of a particular target protein, which is important for quantification purposes.

We compared untreated GAPDH (i.e. reflecting the endogenous redox state), with GAPDH that was either treated with reductant or oxidant to highlight the redox range extremes. For all conditions, GAPDH samples in the absence of Click catalyst were present only as a single band, confirming that PEGylation is fully catalyst-dependent. In samples treated with the reductant TCEP, Click-PEGylation resulted in a redox-dependent mobility shift of GAPDH relative to the untreated condition, visible as the appearance of higher molecular weight bands. Conversely, in response to pre-treatment with the thiol oxidant diamide, loss of PEGylation was observed relative to the untreated condition. This experiment confirmed that GAPDH was present in a range of redox forms with 0–4 reduced thiols groups that were responsive to the redox environment. The redox-dependent PEGylation-induced mobility shifts can easily be visualised by plotting the densitometry profiles for each '+ catalyst' lane (profile plot). Individual PEGylated bands can also be quantified by densitometry, to show the relative distribution of GAPDH thiol redox states in response to the various treatments.

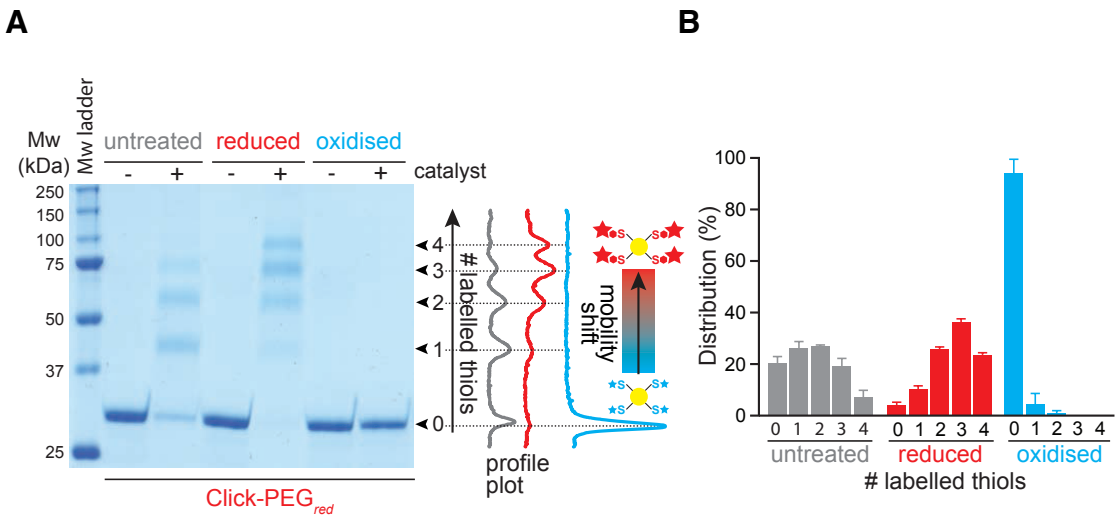

Figure 3.3. Assessment of Click-PEGylation by Coomassie staining using purified GAPDH. ***(A)*** *Click-PEG$_{red}$ of purified rabbit GAPDH, which contains 4 cysteine residues, and can therefore exist as 5 possible bands on a gel: 0 to 4 labelled cysteine thiols. Coomassie-stained mobility shift gel of GAPDH under untreated (i.e. endogenous), reduced (10 mM TCEP), and oxidised (1 mM diamide) conditions, showing redox-dependent band shifting. Profile plots of the '+ catalyst' lanes were performed in FIJI.* ***(B)*** *Quantification of GAPDH cysteine redox state distribution from* ***(A).*** *Band densitometry was performed in FIJI and expressed as a % of total band intensity per lane. Data are means ± SEM of n = 4 independent experiments. The gel and densitometry was provided by LvL.*

In addition, we confirmed that purified GAPDH in its different redox states could similarly be assessed by Western blotting **(Figure 3.4)**, obtaining similar results to the direct protein staining. We also tested the efficacy of the Click-PEG$_{red}$ and Click-PEG$_{ox}$ protocols performed in parallel using purified GAPDH, comparing reduced and oxidised samples. These approaches provided complementary information on redox state. Reduced GAPDH displayed strong band shifting when detected by Click-PEG$_{red}$ but not by Click-PEG$_{ox}$, and vice versa for oxidised GAPDH.

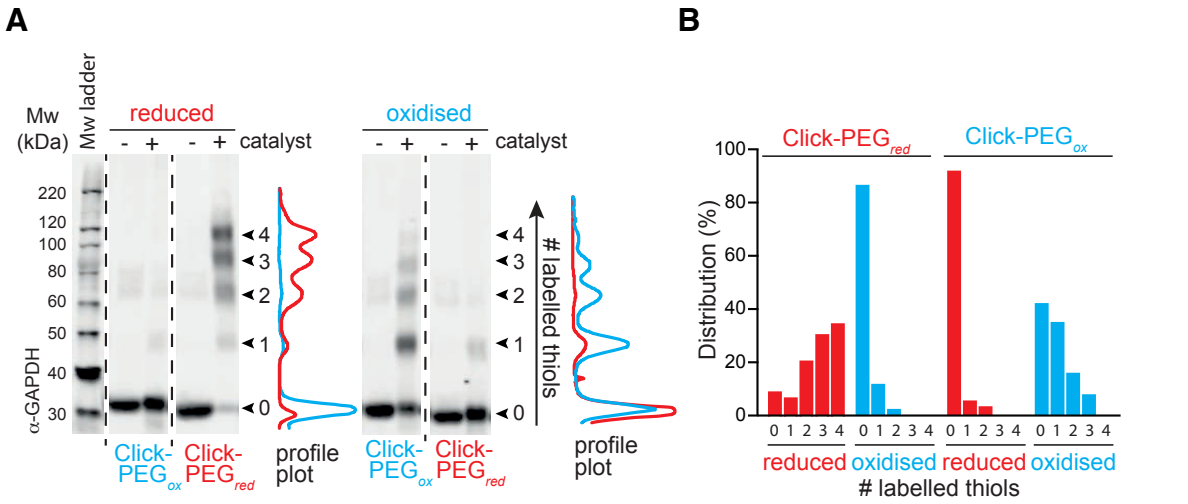

Figure 3.4. Assessment of Click-PEGylation by Western blotting using purified GAPDH. (A) *Parallel Click-PEG$_{red}$ and Click-PEG$_{ox}$ of purified GAPDH under reduced (10 mM TCEP), and oxidised (1 mM diamide) conditions, detected by Western blotting, showing redox-dependent band shifting. The Western blot sections shown are from 1 PVDF membrane. After the Western blot was imaged, the image was cropped vertically and sections were separated or rearranged (as indicated by the black dotted lines) for clarity. After imaging, the profile plots of the '+ catalyst' lanes were performed in FIJI.* ***(B)*** *Quantification of GAPDH cysteine redox state distribution from* ***(A)****. Band densitometry was performed in FIJI and expressed as a % of total band intensity per lane (n=1). I provided the Western blot and the densitometry was provided by LvL.*

3.4.4 Effect of azide-PEG size on redox-dependent band shifts

To test the effect of azide-PEG polymer size, we compared the Click-PEGylation response of purified GAPDH reacted with propargyl-maleimide and then conjugated to a range of PEG moieties including 1, 2, and 5 kDa **(Figure 3.5).** Using samples of reduced GAPDH to focus on maximal shifting, the densitometry profile plots illustrate how varying the PEG size results in a corresponding shifting of the bands, with 5 kDa (azide-$PEG_{5,000}$) providing the best band separation and resolution for the Click-PEGylation of GAPDH. However, regardless of the azide-PEG size selected, the resulting distribution pattern of GAPDH thiol redox state was not affected. Therefore, depending on the overall molecular weight of the candidate protein, as well as the total number of cysteine residues present, the optimal PEG size can be established. Other azide-PEG sizes, e.g. 10 kDa, are also commercially available.

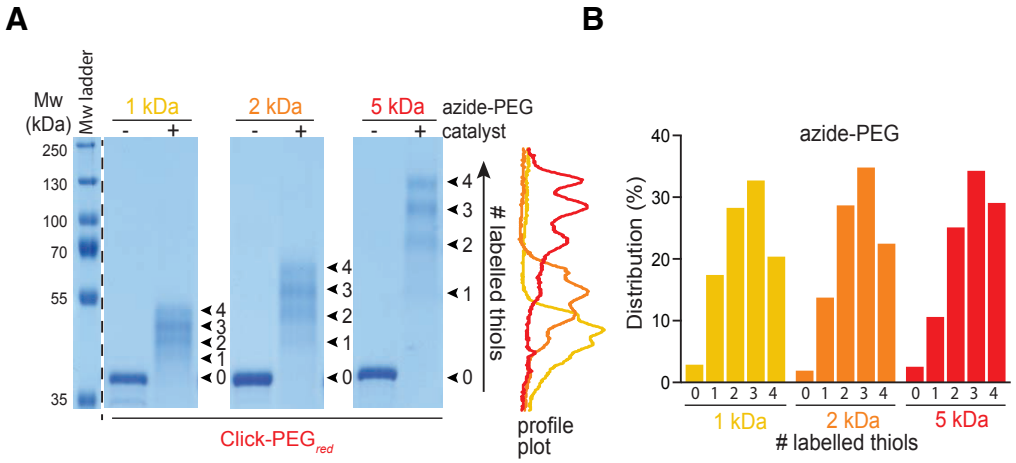

Figure 3.5. Effect of azide-PEG size on redox-dependent band shifts using purified GAPDH. ***(A)*** *Effect of different azide-PEG sizes on the Click-PEG_{red} band shifting. Coomassie-stained mobility shift gel of purified GAPDH under reduced conditions (10 mM TCEP) derivatised with either 1, 2 or 5 kDa azide-PEG. The gel sections shown are from 1 gel. After the gel was imaged, the image was cropped vertically and sections were separated or rearranged (as indicated by the black dotted line) for clarity. Profile plots of the '+ catalyst' lanes were performed in FIJI.* ***(B)*** *Quantification of band shifting distribution from* ***(A).*** *Band densitometry was performed in FIJI and expressed as a % of total band intensity per lane (n = 1). The gel and densitometry was provided by LvL.*

We found no loss of sample upon PEGylation comparing total protein content between the '– and + catalyst' lanes both in the case of direct protein detection by Coomassie staining and Western blotting (although Western blotting was more variable) **(Figure 3.6).**

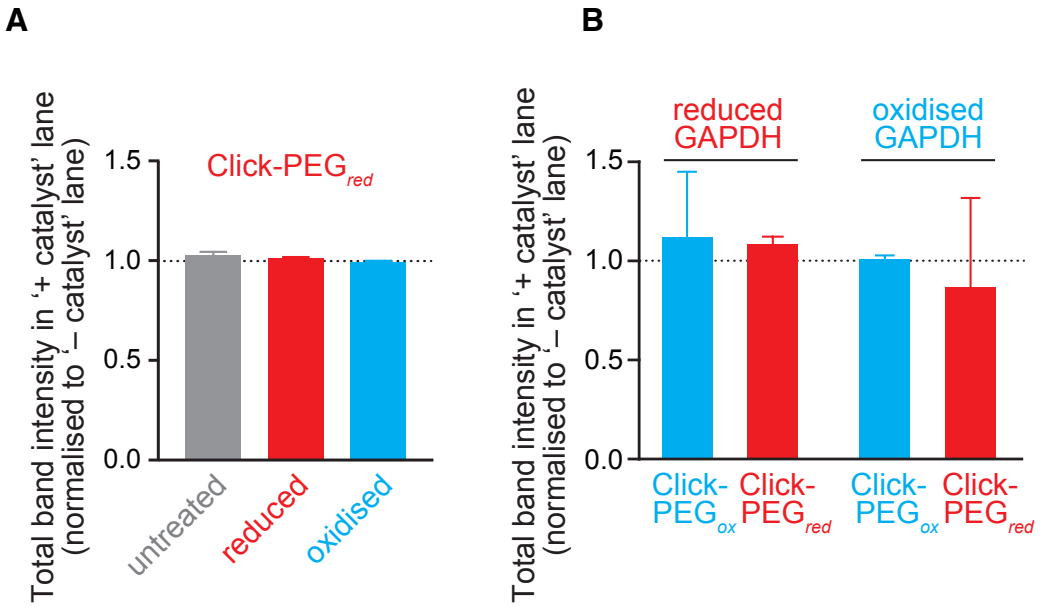

Figure 3.6. Assessment of sample recovery following the Click-PEG reaction. (A) *Quantification of total band intensity for the '+ catalyst' lane of the Coomassie-stained gel in* ***Figure 3.3 (A),*** *assessed using FIJI and normalised to the '– catalyst' lane as a loading control. Data are means ± SEM of n = 3 independent experiments (data provided by LvL).* ***(B)*** *Quantification of total band intensity for the '+ catalyst' lane of the Western blot in* ***Figure 3.4 (A),*** *assessed using LiCor Image Studio software and normalised to the '– catalyst' lane as a loading control. Data are means ± SEM of n = 3 independent experiments (data provided by me).*

3.4.5 Optimisation of the Click-PEGylation protocols

To optimise labelling conditions during the Click-PEGylation protocols, we performed a number of control experiments. First, we considered sample protein concentration, and found that PEGylation efficiency was significantly improved by decreasing the starting protein concentration from 1 to 0.1 mg/mL **(Figure 3.7).** This is consistent with previous findings for redox proteomic sample preparation (Menger et al., 2015), and indicates the need to optimise the ratio of protein thiol content to tag compound in order to ensure complete labelling and therefore an accurate representation of protein redox status.

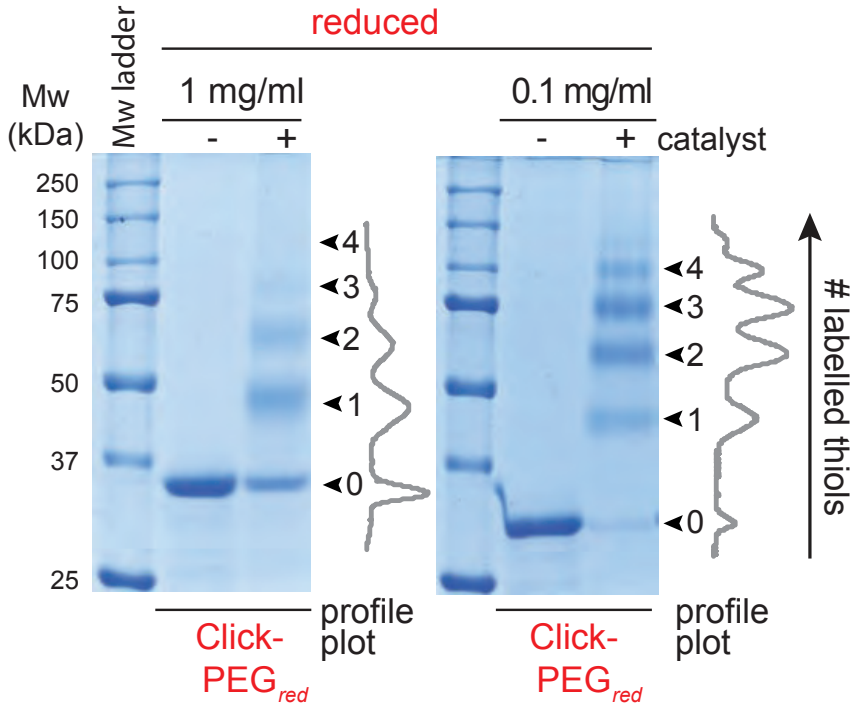

Figure 3.7 Effect of protein concentration on labelling efficiency during the Click-PEG reaction. *Coomassie-stained mobility shift gels of purified GAPDH under untreated conditions reacted by Click-PEG$_{red}$, comparing starting concentrations of 1 and 0.1 mg protein/mL. Profile plots of the '+ catalyst' lanes were performed in FIJI. Data was provided by LvL.*

Next, we optimised the duration of the propargyl-maleimide reaction step to ensure complete labelling, comparing 10, 30 and 120 min incubation times **(Figure 3.8).** We confirmed by both direct protein staining and Western blotting that propargyl-maleimide labelling was complete by 10 min incubation, with no further changes at subsequent time points. This was true for both Click-PEG_{red} and Click-PEG_{ox} labeling.

In examining the effects of the propargyl-maleimide timecourse on purified GAPDH labeling, 2 different stocks of GAPDH were used: a new stock in **(A – D)** and an older stock in **(E – F)**. We determined that the older stock had likely become hyperoxidised as we observed incomplete labeling of GAPDH (for equivalent starting protein concentrations) indicating the increased presence of irreversibly oxidised thiols in the older stock that would not become labeled. Thus, we determined that the experiments should be performed on fresh protein stocks if possible.

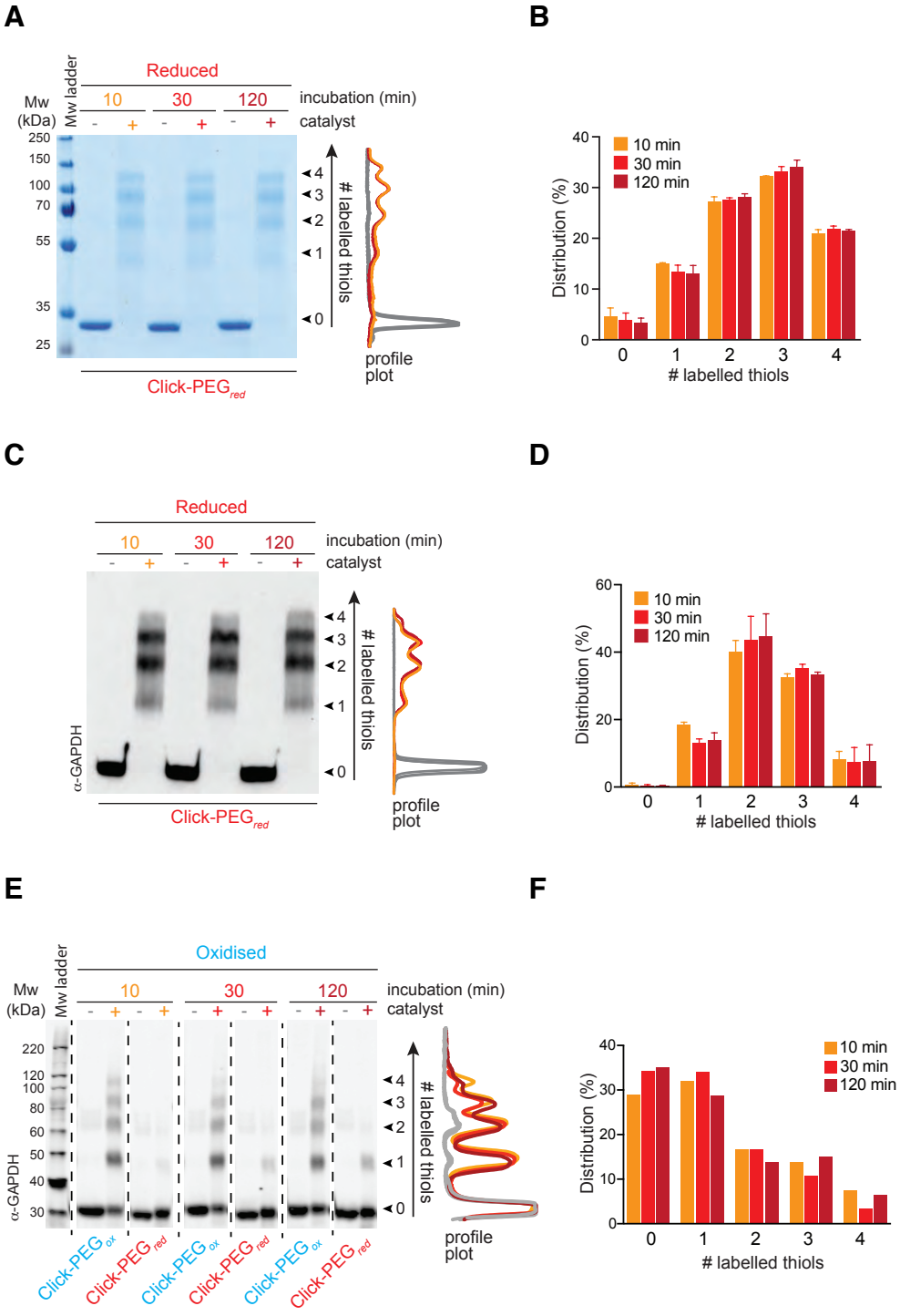

Figure 3.8. Effect of propargyl-maleimide incubation time on Click-PEG labelling. (A) *Coomassie-stained gel of purified GAPDH under reduced conditions (10 mM TCEP) reacted by Click-PEG$_{red}$, comparing propargyl-maleimide (50 mM) incubation times of 10, 30 and 120 min. Profile plots of the '–/+ catalyst' lanes were performed in FIJI.* ***(B)*** *Quantification of GAPDH thiol redox state distribution from* ***(A).*** *Band densitometry was performed in FIJI and expressed as a % of total band intensity per lane. Data are means ± range of n = 2 independent experiments. Gel and*

densitometry provided by LvL. ***(C)*** *Western Blot of purified GAPDH under reduced conditions (10 mM TCEP) reacted by Click-PEG$_{red}$, comparing incubation times of 10, 30 and 120 min. Profile plots of the '–/+ catalyst' lanes were performed in FIJI.* ***(D)*** *Quantification of GAPDH thiol redox state distribution from* ***(C).*** *Band densitometry was performed in FIJI and expressed as a % of total band intensity per lane. Data are means ± range of n = 2 independent experiments. Gel and densitometry provided by LvL.* ***(E)*** *Western Blot of purified GAPDH (older stock) under oxidised conditions (1 mM diamide) reacted by Click-PEG$_{ox}$ or Click-PEG$_{red}$, comparing incubation times of 10, 30 and 120 min. The Western blot sections shown are from 1 PVDF. After the Western blot was imaged, the image was cropped vertically (as indicated by the black dotted lines) and sections were rearranged for clarity. Profile plots of the '–/+ catalyst' lanes were performed in FIJI.* ***(F)*** *Quantification of GAPDH thiol redox state distribution from* ***(E).*** *Band densitometry was performed in Image Studio and expressed as a % of total band intensity per lane (n = 1). I provided the Western blot and densitometry.*

Furthermore, we optimised the concentration of propargyl-maleimide during the initial labelling of redox-reactive free thiols **(Figure 3.9)**. While an excess of propargyl-maleimide at this step is desirable to ensure complete labelling, previous studies have shown that excessive maleimide to thiol ratio leads to non-specific protein labeling of residues other than cysteines (Tyagarajan et al., 2003, Pretzer and Wiktorowicz, 2008). Previously, it has been difficult to observe any off-target labeling of purified GAPDH by 50 mM propargyl-maleimide because purified GAPDH doesn't exist in 100% reduced or 100% reversibly oxidised states, instead existing in a range of redox states. This is perhaps due to some irreversible oxidation that occurred during preparation of the purified protein, which increased with duration of storage, as previously suggested. Thus, any redox-insensitive (off-target) band shifting, if existing, was difficult to identify. However, to minimize the risk of off-target labeling we reduced the concentration of propargyl-maleimide (50 mM to 5 mM) and found comparable target band labeling (30 min incubation). Therefore, in following experiments 5 mM propargyl-maleimide was used for labelling to minimize the risk of off-target labeling by higher concentrations. With this lower concentration of propargyl-maleimide I observed that 10 min was now insufficient for complete labeling, however, complete labeling could be achieved with longer incubations (≥ 30 min). Therefore, the majority of experiments presented in this study were performed with a 30 min propargyl-maleimide incubation.

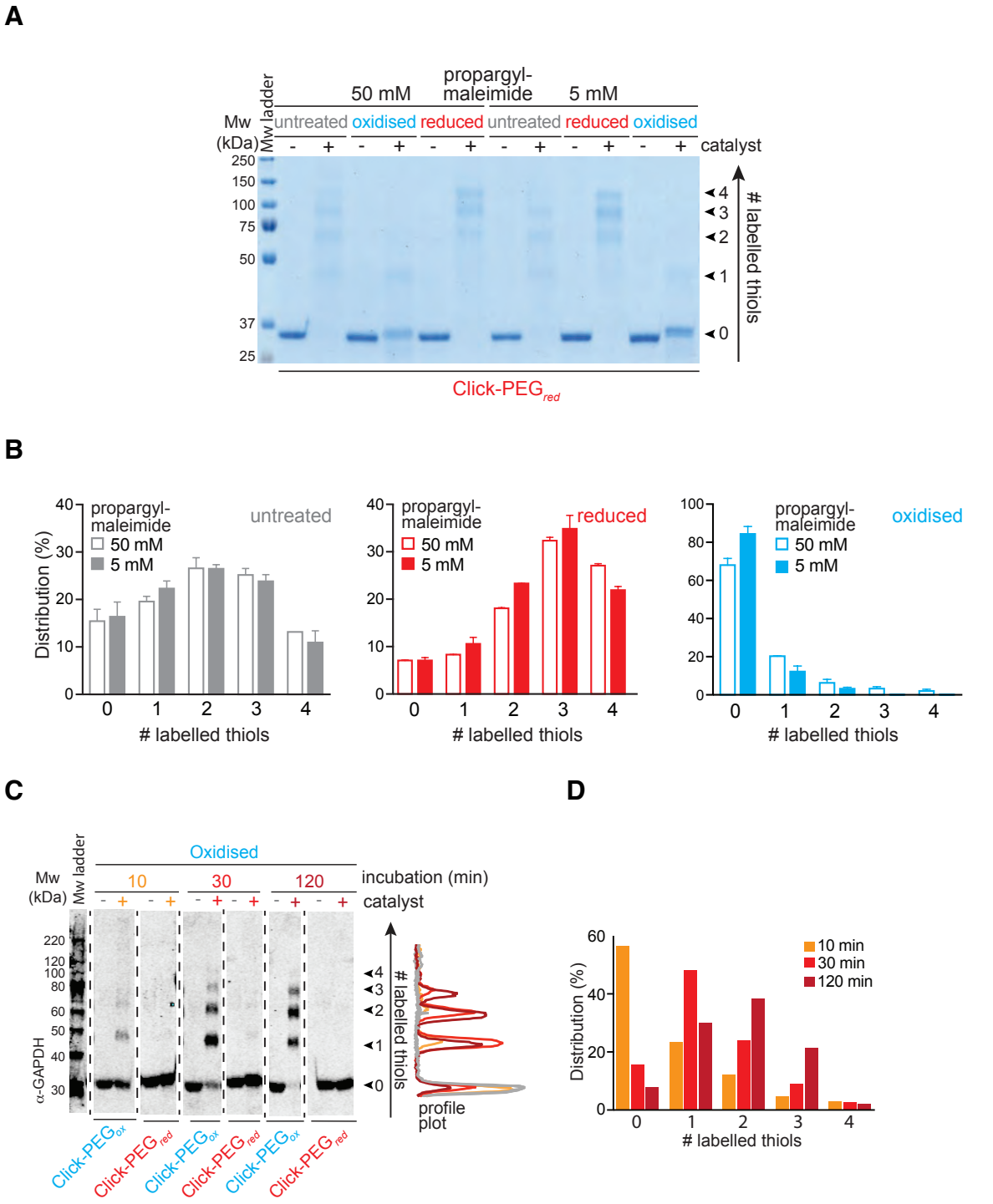

Figure 3.9 Effect of propargyl-maleimide concentration on Click-PEG labelling. (A) *Coomassie-stained mobility shift gel of purified GAPDH reacted by Click-PEG$_{red}$ comparing 5 or 50 mM propargyl-maleimide under untreated, reduced (10 mM TCEP) and oxidised (1 mM diamide) conditions.* ***(B)*** *Quantification of GAPDH thiol redox state distribution from* ***(A).*** *Band densitometry was performed in FIJI and expressed as a % of total band intensity per lane. Data are means ± range of n = 2 independent experiments. Gel and densitometry was provided by LvL.* ***(C)*** *Western Blot of purified GAPDH under oxidised conditions (1 mM diamide) reacted by Click-PEG$_{ox}$ or Click-*

PEG_{red}, comparing the labeling of 5 mM propargyl-maleimide after incubation times of 10, 30 and 120 min. After the Western blot was imaged, the image was cropped vertically (as indicated by the black dotted lines) and sections were rearranged for clarity. Profile plots of the '–/+ catalyst' lanes (Click-PEG_{ox}) were performed in FIJI. ***(D)*** *Quantification of GAPDH thiol redox state distribution reacted by Click-PEG_{ox} from* ***(C).*** *Band densitometry was performed in Image Studio and expressed as a % of total band intensity per lane (n = 1). I provided the Western blot and densitometry.*

3.4.6 Assessing the redox state of higher molecular weight proteins by Click-PEGylation: catalase

So far the Click-PEGylation assay has been used effectively with purified GAPDH, which has a molecular weight of ~36 kDa. To confirm that the Click-PEGylation method is widely applicable to a broad range of proteins with differing sizes, we also tested another candidate, catalase **(Figure 3.10),** with a higher molecular weight (~60 kDa predicted) and 4 cysteine residues (Sevinc et al., 1995). Comparable to experiments with GAPDH, we found that purified catalase was increasingly Click-PEGylated upon reduction and that this was decreased upon oxidation. Again we compared the effect of different sized azide-PEGs (1 kDa, 2 kDa, and 5 kDa) on the band shifting resolution of fully reduced catalase by Click-PEG_{red}. Unlike with GAPDH, we found that only azide-$PEG_{5,000}$ was able to resolve the different redox-shifted bands sufficiently whereas the 1 and 2 kDa sizes were ineffective, as evident from the unresolved profile plots. This highlights the importance of optimising the size of the azide-PEG moiety for a given protein of interest.

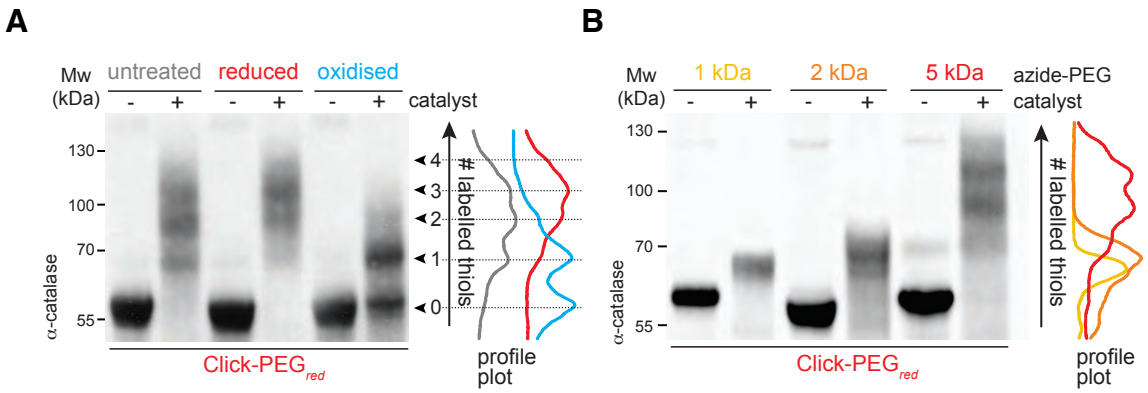

Figure 3.10. Application of Click-PEGylation to purified catalase. (A) *Click-PEG_{red} of purified catalase under untreated, reduced (10 mM TCEP) and oxidised (1 mM diamide) conditions,*

detected by Western blotting. Profile plots of the '+ catalyst' lanes were performed in FIJI. ***(B)*** *Effect of different azide-PEG sizes on the Click-PEG$_{red}$ band shifting. Western blot of purified catalase under reduced conditions (10 mM TCEP) derivatised with either 1, 2 or 5 kDa azide-PEG. Profile plots of the '+ catalyst' lanes were performed in FIJI. Western blots were provided by LvL.*

3.4.7 Assessing the redox state of GAPDH in complex biological samples by Click-PEGylation

To assess endogenous redox state for a given target, the Click-PEGylation reaction is performed on the complex protein sample, and then specific detection of the redox mobility shifting for the protein of interest is achieved by Western blotting. Therefore, the redox state of multiple proteins can be assessed from the sample by parallel/successive Western blotting using appropriate antibodies. Tagged proteins (e.g. Flag, HA) could also be assessed, using antibodies against the relevant tag.

Here, we consider the response of endogenous GAPDH in cell culture. We applied the Click-PEGylation technique to label GAPDH in mouse C2C12 myoblast lysates **(Figure 3.11).** I performed parallel Click-PEG$_{red}$ and Click-PEG$_{ox}$ protocols on TCEP- and diamide-treated cell lysates, and observed complementary redox-dependent band shifting for these reduced and oxidised conditions. I also considered untreated cell lysates, and found that endogenous GAPDH in cell culture is present in a range of redox states, which is consistent with reports in the literature for GAPDH *in vivo* (Menger et al., 2015, Brandes et al., 2009). Therefore, the Click-PEG$_{red}$ and Click-PEG$_{ox}$ protocols are useful techniques when used individually or in parallel to determine protein redox state by mobility shift electrophoresis in complex biological samples.

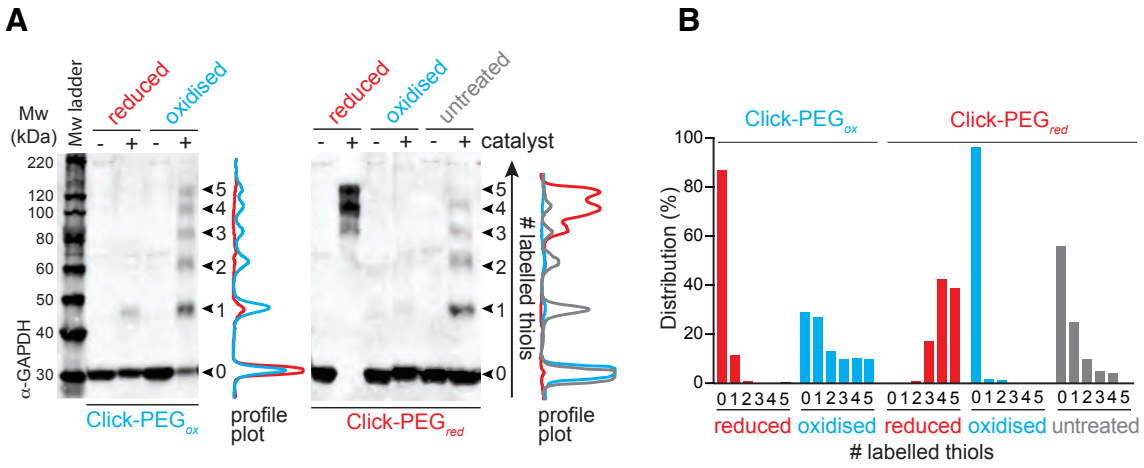

Figure 3.11. Analysis of endogenous GAPDH from cell lysates (C2C12 mouse myoblast) by Click-PEG$_{ox}$ and Click-PEG$_{red}$ detected by Western blotting. (A) *Cell lysates were Click-PEGylated after reduction (10 mM TCEP) or oxidation (1 mM diamide).* In situ *analysis of GAPDH redox status (untreated) was also performed by lysing the cells in the presence of 5 mM propargyl-maleimide. The Western blot sections shown are from 1 PVDF membrane. After the Western blot was imaged, the image was cropped vertically and separated for clarity.* ***(B)*** *Quantification of band shifting in* ***(A)****. Band densitometry was performed in FIJI and expressed as a % of total band intensity per lane (n=1). I performed the cell experiment and Western blot, densitometry was performed by LvL.*

3.5 Method application

3.5.1 Towards assessing AMPK redox shifts using the Click-PEGylation protocols

In working towards elucidating any possible direct redox-regulation of AMPK, a series of experiments were performed on purified AMPK and AMPK in cell lysates to test if the Click-PEG protocols could resolve redox shifts in the enzyme. Although promising advancements were made in optimising the Click-PEG protocols to suit AMPK analysis, activity experiments conducted in parallel (discussed in **Chapter 4**) indicated that AMPK activity changes in response to ROS in C2C12 myotubes correlated with changes to cell ATP/ADP ratios, suggesting indirect effects. Thus, optimisation of the AMPK redox-state analysis was halted in favor of further characterizing AMPK regulation and cellular redox state by different sources of ROS cells. However, it remains of critical importance to be able to analyze the redox state of AMPK to further confirm indirect regulation by ROS in the C2C12 cell model. Also, as AMPK redox-regulation could potentially be cell type specific (or dependent on other variables), further optimisation of AMPK redox-state analysis by Click-PEGylation will advance the experimental techniques available to our and other labs in determining the nature of AMPK regulation in response to ROS in different cell types. Discussed below are the steps I took towards optimising AMPK redox-state analysis by Click-PEGylation, initially using purified AMPK and then continued with AMPK in cell lysates.

Initially, prior to any Click-PEGylation reactions, a serial dilution of purified AMPK was performed and then separated by SDS-PAGE to identify the limit of detection by Coomassie protein staining **(Figure 3.12)**. The 3 subunits of AMPK: α1-His tag (~62 kDa), β1-His tag (~38 kDa), γ1-His tag (~ 40 kDa) (Sigma: A1233 (human), data sheet size estimations) were visible upon SDS-PAGE and Coomassie Brilliant Blue R-250 staining of ≥ 0.5 µg protein. Considering that for Click-PEGylation the initial starting protein would be halved before the Click catalyst reaction and assuming some loss of protein would occur during the different Click-PEGylation

reaction steps, I decided to use a starting protein concentration of 2 µg/100 µl for Click-PEGylation of purified AMPK to be detected by Coomassie protein staining. I also decided to switch to QC Colloidal Coomassie protein stain for future gels in order to maximise the sensitivity of detection.

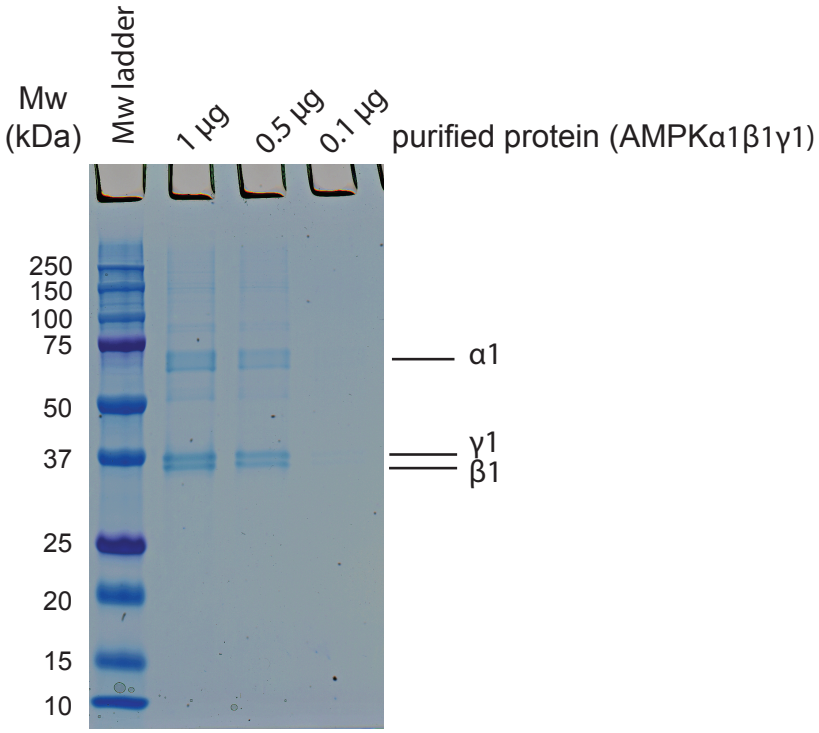

Figure 3.12. Serial dilution of purified AMPK α1/ β1/ γ1 (-His tagged) followed by SDS-PAGE and Coomassie protein staining to determine the limit of detection. *Purified human AMPK was serially diluted, loaded on a 12% SDS-PAGE gel electrophoresed in reducing conditions. The gel was stained with Coomassie Brilliant Blue R-250 and destained according to the manufacturer's instructions. The gel was scanned using an Epson perfection V750 Pro scanner.*

Next, purified AMPK was reacted by Click-PEG$_{red}$ and derivatised with azide-PEG$_{5,000}$ followed by SDS-PAGE and QC Colloidal Coomassie protein staining to see if redox-dependent shifts could be observed **(Figure 3.13)**. The gel and profile plot showed that catalyst-dependent labelling was occurring and there were obvious differences in the labelling pattern between pre-reduced (10 mM TCEP) and pre-oxidised (1 mM diamide) protein. A complication of detecting Click-PEG$_{red}$ – labelled purified AMPK by SDS-PAGE and Coomassie protein staining is that all 3 subunits are detected, so it is impossible to identify individual subunit mobility

shifts with any clarity. Also, the α1 subunit is cysteine-rich (11 cysteine residues in human) and combined with the β1 and γ1 subunits (3 cysteines each in human) **(Figure 3.14)**, a total of potentially 20 bands could potentially be observed (unlabelled α1, β1 and γ1 + 17 cysteine residues that could potentially be labeled). In spite of the technical limitations, this experiment did confirm that catalyst-dependent labelling had occurred and that broad redox-dependent shifts had also occurred.

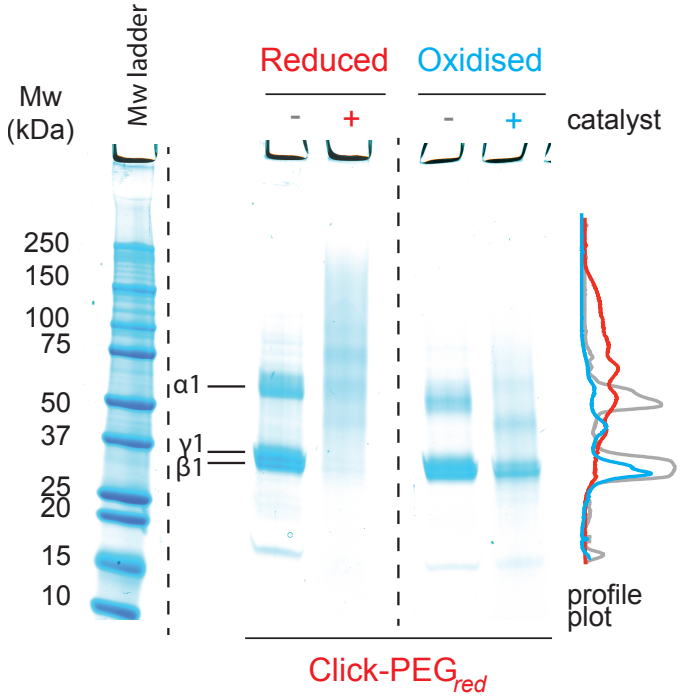

Figure 3.13. Purified AMPK α1/ β1/ γ1 reacted by Click-PEG$_{red}$ followed by SDS-PAGE and Coomassie protein staining. *QC Colloidal Coomassie stained gel (12%) of purified human his-tagged AMPK (starting concentration: 2 µg protein /100 µl) reacted by Click-PEG$_{red}$ under reduced (10 mM TCEP) or oxidised (1 mM diamide) conditions. In '- catalyst ' lanes, all subunits of AMPK were detected: α1, β1 and γ1. The gel was scanned and the image was cropped vertically (as indicated by the black dotted lines) and sections were rearranged for clarity. Profile plots of the '–/+ catalyst' lanes were performed in FIJI.*

A

5'-AMP-activated protein kinase catalytic subunit alpha-1 isoform 1 [Homo sapiens]

11 cysteines in α1 subunit

001 MRRLSSWRKM ATAEKQKHDG RVKIGHYILG DTLGVGTFGK VKVGKHELTG HKVAVKILNR
061 QKIRSLDVVG KIRREIQNLK LFRHPHIIKL YQVISTPSDI FMVMEYVSGG ELFDYICKNG
121 RLDEKESRRL FQQILSGVDY CHRHMVVHRD LKPENVLLDA HMNAKIADFG LSNMMSDGEF
181 LRTSCGSPNY AAPEVISGRL YAGPEVDIWS SGVILYALLC GTLPFDDDHV PTLFKKICDG
241 IFYTPQYLNP SVISLLKHML QVDPMKRATI KDIREHEWFK QDLPKYLFPE DPSYSSTMID
301 DEALKEVCEK FECSEEEVLS CLYNRNHQDP LAVAYHLIID NRRIMNEAKD FYLATSPPDS
361 FLDDHHLTRP HPERVPFLVA ETPRARHTLD ELNPQKSKHQ GVRKAKWHLG IRSQSRPNDI
421 MAEVCRAIKQ LDYEWKVVNP YYLRVRRKNP VTSTYSKMSL QLYQVDSRTY LLDFRSIDDE
481 ITEAKSGTAT PQRSGSVSNY RSCQRSDSDA EAQGKSSEVS LTSSVTSLDS SPVDLTPRPG
541 SHTIEFFEMC ANLIKILAQ

B

5'-AMP-activated protein kinase subunit beta-1 [Homo sapiens]

3 cysteines in β1 subunit

001 MGNTSSERAA LERHGGHKTP RRDSSGGTKD GDRPKILMDS PEDADLFHSE EIKAPEKEEF
061LAWQHDLEVN DKAPAQARPT VFRWTGGGKE VYLSGSFNNW SKLPLTRSHN NFVAILDLPE
121 GEHQYKFFVD GQWTHDPSEP IVTSQLGTVN NIIQVKKTDF EVFDALMVDS QKCSDVSELS
181 SSPPGPYHQE PYVCKPEERF RAPPILPPHL LQVILNKDTG ISCDPALLPE PNHVMLNHLY
241 ALSIKDGVMV LSATHRYKKK YVTTLLYKPI

C

5'-AMP-activated protein kinase subunit gamma-1 isoform 1 [Homo sapiens]

3 cysteines in γ1 subunit

001 METVISSDSS PAVENEHPQE TPESNNSVYT SFMKSHRCYD LIPTSSKLVV FDTSLQVKKA
061 FFALVTNGVR AAPLWDSKKQ SFVGMLTITD FINILHRYYK SALVQIYELE EHKIETWREV
121 YLQDSFKPLV CISPNASLFD AVSSLIRNKI HRLPVIDPES GNTLYILTHK RILKFLKLFI
181 TEFPKPEFMS KSLEELQIGT YANIAMVRTT TPVYVALGIF VQHRVSALPV VDEKGRVVDI
241 YSKFDVINLA AEKTYNNLDV SVTKALQHRS HYFEGVLKCY LHETLETIIN RLVEAEVHRL
301 VVVDENDVVK GIVSLSDILQ ALVLTGGEKK P

Figure 3.14. Amino acid sequences of AMPK α1, β1 and γ1 subunit isoforms (human) from the National Center for Biotechnology Information (NCBI). *Cysteine residues are highlighted in red.* ***(A)*** *Amino acid sequence of AMPK α1 (human) containing 11 cysteine residues. NCBI Reference Sequence: NP_006242.5;* ***(B)*** *amino acid sequence of AMPK β1 (human) containing 3 cysteine residues. NCBI Reference Sequence: NP_006244.2;* ***(C)*** *amino acid sequence of AMPK γ1 (human) containing 3 cysteine residues. NCBI Reference Sequence: NP_002724.1.*

In order to detect redox shifts in only the AMPKα catalytic subunit, purified AMPK α1/ β1/ γ1 was reacted by Click-PEG$_{ox}$ and then analysed by SDS-PAGE and Western blotting with a primary antibody to the α subunit **(Figure 3.15)**. A lower % SDS-PAGE gel (7.5%) was selected in order to maximize the area of the gel to where AMPKα bands were expected to migrate. The Click-PEG$_{ox}$ reaction showed that catalyst and redox-dependent mobility shifting had occurred. Band resolution was improved from Coomassie detection, but remained imperfect. The large number of cysteine residues (which would present as up to 12 potential bands) combined with the relatively large molecular weight of the subunit (similar to catalase) are likely the reasons for the resolution difficulties. However, broad redox shifts could be identified with the purified protein suggesting similar shifts could also be detected in biological samples.

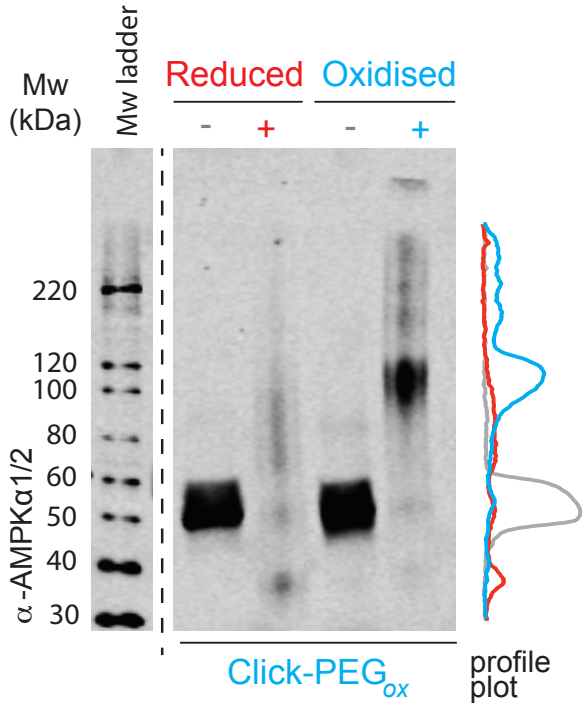

Figure 3.15. Purified AMPK α1/ β1/ γ1 reacted by Click-PEG$_{red}$ or Click-PEG$_{ox}$ followed by SDS-PAGE and Western blotting with a primary antibody to the α subunit. *Purified human his-tagged AMPK (starting concentration: 1 µg protein /100 µl) reacted by Click-PEG$_{ox}$ under reduced (10 mM TCEP) or oxidised (1 mM diamide) conditions. Samples were loaded on a 7.5 % gel and SDS-PAGE was performed in reducing conditions. In the '- catalyst' lanes, only AMPKα was detected. The gel was scanned and the image was cropped vertically (as indicated by the black dotted line) and sections were rearranged for clarity. Profile plots of the '–/+ catalyst' lanes were performed in FIJI.*

3.5.2 Optimising Click-PEGylation on endogenous AMPK in cells

Optimisation of Click-PEGylation for detecting redox shifts in purified AMPK was limited by the need for relatively large quantities of expensive purified stock in each reaction. Thus, I decided to continue the optimisation using cell lysates, as the goal of the experiment is to detect redox shifts in AMPK in complex biological samples, not in purified protein. The cell lysates I used were from a C2C12 mouse myoblast cell line in the proliferating, undifferentiated state. The primary antibody to AMPKα detects isoforms 1 and 2. Mouse AMPKα1 has high homology to human AMPKα1 and all the cysteine residues are conserved **(Figure 3.16)**, meaning that potentially 12 bands could be observed following a Click-PEGylation reaction (unlabeled AMPKα1 + 11 cysteine residues that could be labeled). Mouse AMPKα2 has 11 cysteine residues (compared to 10 in human). However, there is evidence that the protein expression of AMPK subunits changes during myogenesis with only AMPKα2 being detected in proliferating, undifferentiated C2C12 myoblast cells and protein expression of AMPKα1 occurring during differentiation (Niesler et al., 2007).

A

AMPKα1 amino acid sequence alignment: Human v Mouse

```
Human   1    MRRLSSWRKMATAEKQKHDGRVKIGHYILGDTLGVGTFGKVKVGKHELTGHKVAVKILNR   60
Mouse   1    MRRLSSWRKMATAEKQKHDGRVKIGHYILGDTLGVGTFGKVKVGKHELTGHKVAVKILNR   60

Human   61   QKIRSLDVVGKIRREIQNLKLFRHPHIIKLYQVISTPSDIFMVMEYVSGGELFDYICKNG   120
Mouse   61   QKIRSLDVVGKIRREIQNLKLFRHPHIIKLYQVISTPSDIFMVMEYVSGGELFDYICKNG   120

Human   121  RLDEKESRRLFQQILSGVDYCHRHMVVHRDLKPENVLLDAHMNAKIADFGLSNMMSDGEF   180
Mouse   121  RLDEKESRRLFQQILSGVDYCHRHMVVHRDLKPENVLLDAHMNAKIADFGLSNMMSDGEF   180

Human   181  LRTSCGSPNYAAPEVISGRLYAGPEVDIWSSGVILYALLCGTLPFDDDHVPTLFKKICDG   240
Mouse   181  LRTSCGSPNYAAPEVISGRLYAGPEVDIWSSGVILYALLCGTLPFDDDHVPTLFKKICDG   240

Human   241  IFYTPQYLNPSVISLLKHMLQVDPMKRATIKDIREHEWFKQDLPKYLFPEDPSYSSTMID   300
Mouse   241  IFYTPQYLNPSVISLLKHMLQVDPMKRAAIKDIREHEWFKQDLPKYLFPEDPSYSSTMID   300

Human   301  DEALKEVCEKFECSEEEVLSCLYNRNHQDPLAVAYHLIIDNRRIMNEAKDFYLATSPPDS   360
Mouse   301  DEALKEVCEKFECSEEEVLSCLYNRNHQDPLAVAYHLIIDNRRIMNEAKDFYLATSPPDS   360
```

```
Human   361  FLDDHHLTRPHPERVPFLVAETPRARHTLDELNPQKSKHQGVRKAKWHLGIRSQSRPNDI  420
Mouse   361  FLDDHHLTRPHPERVPFLVAETPRARHTLDELNPQKSKHQGVRKAKWHLGIRSQSRPNDI  420

Human   421  MAEVCRAIKQLDYEWKVVNPYYLRVRRKNPVTSTYSKMSLQLYQVDSRTYLLDFRSIDDE  480
Mouse   421  MAEVCRAIKQLDYEWKVVNPYYLRVRRKNPVTSTFSKMSLQLYQVDSRTYLLDFRSIDDE  480

Human   481  ITEAKSGTATPQRSGSVSNYRSCQRSDSDAEAQGKSSEVSLTSSVTSLDSSPVDLTPRPG  540
Mouse   481  ITEAKSGTATPQRSGSISNYRSCQRSDSDAEAQGKPSDVSLTSSVTSLDSSPVDVAPRPG  540

Human   541  SHTIEFFEMCANLIKILAQ  559
Mouse   541  SHTIEFFEMCANLIKILAQ  559
```

B

AMPKα2 amino acid sequence alignment: Human v Mouse

```
Human   1    MAEKQKHDGRVKIGHYVLGDTLGVGTFGKVKIGEHQLTGHKVAVKILNRQKIRSLDVVGK  60
Mouse   1    MAEKQKHDGRVKIGHYVLGDTLGVGTFGKVKIGEHQLTGHKVAVKILNRQKIRSLDVVGK  60

Human   61   IKREIQNLKLFRHPHIIKLYQVISTPTDFFMVMEYVSGGELFDYICKHGRVEEMEARRLF  120
Mouse   61   IKREIQNLKLFRHPHIIKLYQVISTPTDFFMVMEYVSGGELFDYICKHGRVEEVEARRLF  120

Human   121  QQILSAVDYCHRHMVVHRDLKPENVLLDAHMNAKIADFGLSNMMSDGEFLRTSCGSPNYA  180
Mouse   121  QQILSAVDYCHRHMVVHRDLKPENVLLDAQMNAKIADFGLSNMMSDGEFLRTSCGSPNYA  180

Human   181  APEVISGRLYAGPEVDIWSCGVILYALLCGTLPFDDEHVPTLFKKIRGGVFYIPEYLNRS  240
Mouse   181  APEVISGRLYAGPEVDIWSCGVILYALLCGTLPFDDEHVPTLFKKIRGGVFYIPDYLNRS  240

Human   241  VATLLMHMLQVDPLKRATIKDIREHEWFKQDLPSYLFPEDPSYDANVIDDEAVKEVCEKF  300
Mouse   241  VATLLMHMLQVDPLKRATIKDIREHEWFKQDLPSYLFPEDPSYDANVIDDEAVKEVCEKF  300

Human   301  ECTESEVMNSLYSGDPQDQLAVAYHLIIDNRRIMNQASEFYLASSPPSGSFMDDSAMHIP  360
Mouse   301  ECTESEVMNSLYSGDPQDQLAVAYHLIIDNRRIMNQASEFYLASSPPSGSFMDDSAMHIP  360

Human   361  PGLKPHPERMPPLIADSPKARCPLDALNTTKPKSLAVKKAKWHLGIRSQSKPYDIMAEVY  420
Mouse   361  PGLKPHPERMPPLIADSPKARCPLDALNTTKPKSLAVKKAKWHLGIRSQSKACDIMAEVY  420

Human   421  RAMKQLDFEWKVVNAYHLRVRRKNPVTGNYVKMSLQLYLVDNRSYLLDFKSIDDEVVEQR  480
Mouse   421  RAMKQLGFEWKVVNAYHLRVRRKNPVTGNYVKMSLQLYLVDSRSYLLDFKSIDDEVVEQR  480

Human   481  SGSSTPQRSCSAAGLHRPRSSFDSTTAESHSLSGSLTGSLTGSTLSSVSPRLGSHTMDFF  540
Mouse   481  SGSSTPQRSCSAAGLHRARSSFDSSTAENHSLSGSLTGSLTGSTLSSASPRLGSHTMDFF  540
```

```
Human   541   EMCASLITTLAR   552
Mouse   541   EMCASLITALAR   552
```

Figure 3.16. Amino acid sequence alignments of AMPK α1 and α2 subunit isoforms, comparing the human and mouse homologues. (A) *Amino acid sequence alignment of AMPK α1 comparing human (NP_006242.5) and mouse (NP_001013385.3) α1. Alignments were performed by NCBI protein BLAST® (NCBI protein sequence ID numbers in parentheses). Sequence differences are highlighted in yellow. Cysteine residues are highlighted in red. Both human and mouse AMPKα1 contains 11 cysteine residues;* ***(B)*** *amino acid sequence alignment of AMPKα2 comparing human (NP_006243.2) and mouse (NP_835279.2) α2. Alignments were performed by NCBI protein BLAST® (NCBI protein sequence ID numbers in parentheses). Sequence differences are highlighted in yellow. Cysteine residues are highlighted in red. Human AMPKα1 contains 10 cysteine residues and mouse AMPKα1 contains 11 cysteine residues.*

Prior to Click-PEGylation experiments, I first tested if the thiol-alkylating agents used in Click-PEGylation would affect antibody-epitope (AMPKα1/2) recognition in cell lysates **(Figure 3.17)**. Although AMPKα1 Western blot signal was easily detected with purified protein, reduced antibody-epitope recognition due to alkylating agents could be more detrimental to an experiment on cell lysate due to smaller amounts of target protein likely to be detected on a Western blot. C2C12 cells were lysed in the presence of DTT and then reacted with NEM or propargyl-maleimide before sample analysis by SDS-PAGE and Western blotting with a primary antibody to AMPKα1/2. Firstly, AMPKα1/2 bands of the appropriate size were observed after all treatments, confirming that the antibody was compatible with these thiol modifications. It was also observed that the higher concentration of propargyl-maleimide (50 mM) did result in the appearance of a non-specific band, a risk discussed previously. The non-specific band was not visible in lysate treated with a lower concentration of propargyl maleimide (5 mM), confirming that this concentration would be preferable. A non-specific band was also visible in lysate treated with NEM (100 mM) so a lower concentration of NEM should also be considered in future optimisation steps.

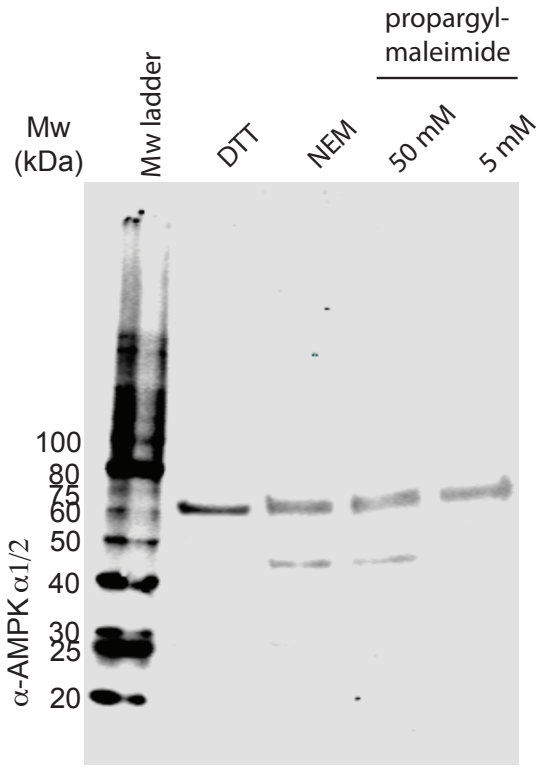

Figure 3.17. Endogenous AMPKα1/2 from C2C12 cell lysate detected by Western blotting following cell lysate incubations with Click-PEGylation thiol-alkylating agents. *C2C12 cells were plated at 20,000 cells per cm^2 on 6 cm plates and cultured to ~ 80% confluency. Cells were lysed in the presence of DTT (50 mM), and then diluted to a concentration of 500 µg protein/ml (determined by BCA assay) to maximize labeling potential. Lysates were then reacted with NEM (100 mM) or propargyl-maleimide (50 mM or 5 mM) or remained untreated (DTT only) and incubated for 30 min at 37°C with shaking (1,000 rpm). Samples (~ 25 µg protein) were analysed by SDS-PAGE (7.5% gel) in reducing conditions followed by Western blotting using the AMPKα1/2 primary antibody.*

Click-PEGylation was then performed in C2C12 cell lysates **(Figure 3.18)**. Cells were lysed in the presence of NEM (for Click-PEG$_{ox}$) or propargyl-maleimide (for Click-PEG$_{red}$). Thus, the *in situ* or 'untreated' endogenous AMPKα was being tested to see if Western blot signal would be observed after PEGylation. Compared to **Figure 3.17**, the AMPKα1/2 Western blot signal in the '- catalyst' lanes for both Click-PEG protocols was greatly reduced. The Click-PEGylation reactions were performed on a starting amount of 50 µg whole cell protein (100 µl of 500 µg protein/ml), a previously optimised amount and concentration of whole cell protein for Click-PEGylation of endogenous GAPDH from cell lysates. The total protein,

when halved at the catalyst addition stage, would result in theoretically 25 µg whole cell protein to be analysed by SDS-PAGE (equivalent to the amount of protein loaded on the gel per lane in **Figure 3.17**, from which AMPKα1/2 was readily detectable by Western Blot)**.** However, this calculation did not take into account the possibility for protein loss during the Click-PEGylation steps and it does appear that the final amount of AMPKα1/2 in the '- catalyst' lanes (**Figure 3.18**) was much less than in **Figure 3.17**. Furthermore, there was no AMPKα1/2 signal in the '+ catalyst' lanes, suggesting that there was further protein degradation during the catalyst reaction or else perhaps the azide-PEG labeling was affecting the antibody-epitope recognition.

Ultimately, further optimisation steps are needed to use this technique to assess AMPK redox state in cell lysates, including increasing the starting amount of whole cell lysate protein, investigating the use of protease inhibitors in the catalyst incubation that may inhibit protein degradation and investigating the use of AMPK expression vectors to overexpress epitope-tagged AMPK in cells.

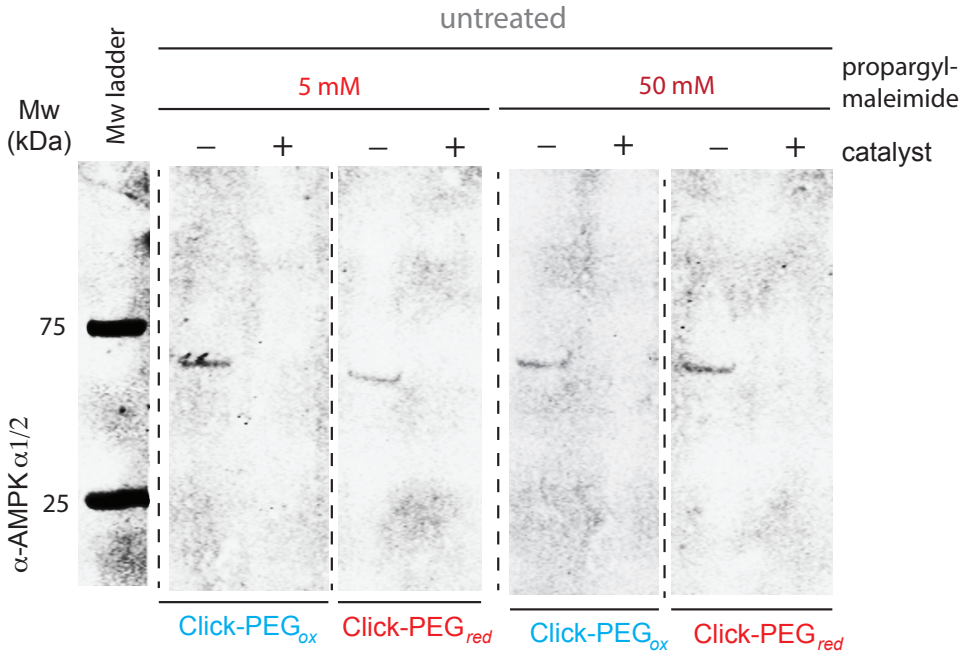

Figure 3.18. Endogenous AMPKα1/2 from C2C12 cell lysate reacted by Click-PEG$_{ox}$ or Click-PEG$_{red}$ and detected by Western blotting. *C2C12 myoblast cells were plated at 20,000 cells per cm^2 on 6 cm plates and cultured to ~ 80% confluency. Cells were lysed in the presence of 100 mM NEM (Click-PEG$_{ox}$) or 5 or 50 mM propargyl-maleimide (Click-PEG$_{red}$). Lysate was diluted to a concentration of ~500 µg whole cell protein/ml and Click-PEGylation was performed on 100 µl aliquots. Samples were analysed by SDS-PAGE (7.5% gel) in reducing conditions followed by Western blotting using the AMPKα1/2 primary antibody. The Western blot sections shown are from 1 PVDF membrane, analysed using Image Studio. After the Western blot was imaged, the image was cropped vertically (indicated by the black dotted lines) and separated for clarity.*

3.5.3 Overexpressing epitope-tagged AMPK in cells as an alternative approach for optimising Click-PEGylation of AMPK in cells

An alternative approach to optimising Click-PEGylation of AMPK in cell lysates was to overexpress AMPK in cells. Overexpressed AMPK would be more readily detected on a Western blot of whole cell lysate. A further benefit would be the option to perform Western blots with primary antibodies to N- or C- terminal epitope tags if engineered onto the AMPK subunits. This would avoid any possible inhibitory effect of the bulky azide-PEG on AMPK antibody-epitope recognition, provided the new epitope tags did not contain any cysteine residues.

Expression vectors containing cDNA sequences of the AMPK subunits were a gift from Professor David Carling, MRC Clinical Sciences Centre, Hammersmith Hospital Campus, London, UK (see **Appendix A** for sequences). The sequence for AMPKα2 contained a C-terminal (CT) FLAG tag and the sequence for AMPKγ1 contained an N-terminal Myc tag. The sequence for AMPKβ1 was untagged. The subunit sequences were independently encoded in individual expression vectors and were transiently transfected into cells simultaneously. As a proof of concept, a number of Western blots were performed to assess the protein expression of the AMPK subunits in untransfected and transfected cells and also to test the detection of the epitope tags, where present (**Figure 3.19 & 3.20**). I chose to test the transfection and detection on HEK293 cells initially, as they are readily compatible with transient transfection.

The protein expression of AMPKα2-CT-FLAG (~ 62 kDa) in HEK293 cells was analysed first. Western blot **(A)** was performed with a primary antibody to the FLAG tag. I also simultaneously probed for AMPKβ1/2 (38/30 kDa) to confirm increases in AMPK protein expression and for ACC1/2 (265/280 kDa) as a loading control. The FLAG-BAP™ protein was detected by the FLAG antibody, confirming the compatibility of the antibody with the FLAG tag. AMPKβ1 was overexpressed in

transfected cells (relative to ACC1/2), confirming that this transfection was effective. However, AMPKα2-CT-FLAG signal was poor. Western blot **(B)** was performed with a primary antibody to AMPKα1/2, and also simultaneously probed for ACC1/2 and AMPKβ1/2 as before. Again, AMPKβ1 was overexpressed in transfected cells (relative to ACC1/2). AMPKα1/2 signal was also increased (relative to ACC1/2) confirming that both AMPKα1/2 and AMPKβ1 were successfully overexpressed. The reason for the poor detection of AMPKα2-CT-FLAG by the FLAG antibody is unclear, but it is possible that some cleavage of the FLAG-tag occurred in the cells, possibly if the serum in the cell culture media contained excessive enteropeptidase, which cleaves the FLAG tag (Zhao et al., 2013). It was also clear from the Western blots and quantification that transfection of cells with 1 µg expression vector DNA (per vector) offered more α and β subunit overexpression than cells transfected with 10 µg DNA. As an aside, it can be observed from both Western blots that AMPKβ1 (~ 38 kDa) is the dominantly expressed β subunit in HEK293 cells, with the Western blot signal of β1 in untransfected cells being much stronger than β2 (~ 30 kDa).

Next, I tested the protein expression of AMPKγ1-NT-Myc (~ 38 kDa). Western blot **(C)** was performed with a primary antibody to the Myc tag and simultaneously probed for AMPKα1/2 to confirm increases in AMPK protein expression and for ACC1/2 as a loading control. AMPKγ1-NT-Myc Western blot signal was easily visible in transfected cells and not in untransfected cells, confirming that the overexpression was successful and that the Myc-antibody was compatible with the tag. In parallel, the Western blot in **(D)** was performed with a primary antibody to AMPKγ1/2, and also simultaneously probed for ACC1/2 and AMPKα1/2 as before. The Western blot showed that the AMPKγ1/2 antibody was poor and so for detecting overexpressed AMPKγ1-NT-Myc, the Myc antibody is preferable. To summarize, the AMPK subunit expression vectors can be used to increase AMPK protein expression in cells. The AMPKα1/2 antibody was more effective than the FLAG antibody at detecting AMPKα2-CT-FLAG and the Myc antibody was more effective than the AMPKγ1/2 antibody at detecting AMPKγ1-NT-Myc. The AMPKβ1

vector did not encode an epitope tag but the AMPKβ1/2 antibody is effective at detecting endogenous and overexpressed protein. Cells transfected with 1 µg expression vector DNA (per vector) offered more protein overexpression than cells transfected with 10 µg DNA (per vector).

Above, I have assessed the functionality of the expression vectors and confirmed the appropriate antibodies to use for detection of each of the overexpressed AMPK subunits. In future experiments, Click-PEGylation could be performed on these lysates containing overexpressed and tagged AMPK subunits. However, extensive work conducted in **Chapter 4** indicated that all AMPK activity changes in response to different sources of ROS in C2C12 myotubes correlated with changes to cell ATP/ADP ratios, suggesting indirect effects. Thus, optimisation of the AMPK redox-state analysis was temporarily halted in this body of work.

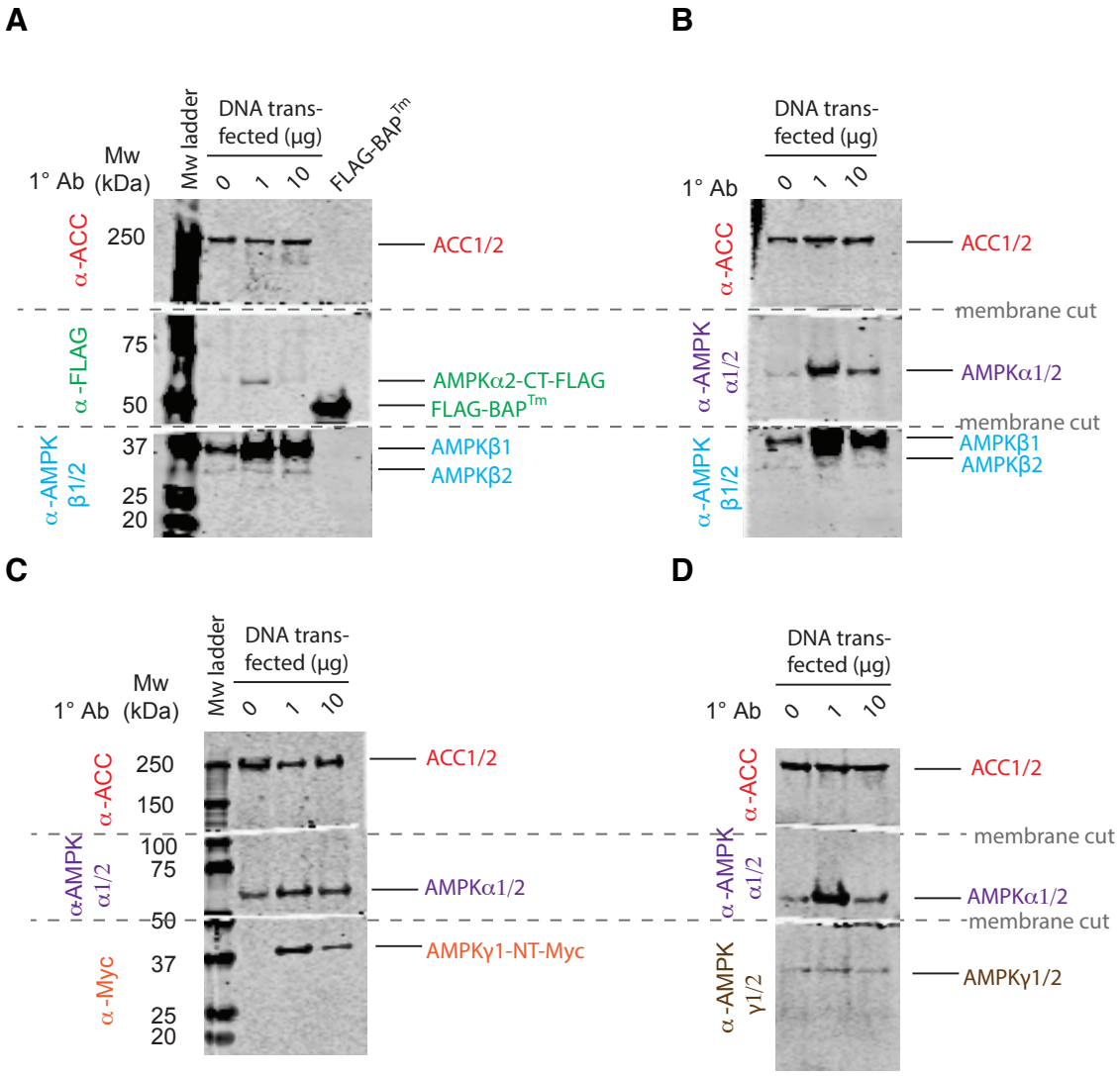

Figure 3.19. Epitope-tagged and untagged AMPK subunits overexpressed in HEK293 cells, detected by Western blotting. (A - D) *HEK 293 cells were plated at a density of 20,000 cells/cm^2 on 6 cm plates in 3 ml standard media. At 50 – 70 % confluency, cells were transfected with 1 µg or 10 µg of each cDNA vector. 24 h after transfection, cells were lysed in Hepes lysis buffer (see* ***2.4 AMPK assays****) and assayed by Western blot (25 µg protein per well) to confirm translation of overexpressed proteins of interest. For method details, see* ***2.2.6.1 Standard transfection procedure.*** *Samples from untransfected and transfected cells were loaded on quadruplicate 4 – 20% SDS-PAGE gels,* ***(A)*** *alongside a sample of purified FLAG-BAP™ protein (Sigma) (~ 49 kDa): a positive control for the FLAG antibody. Post blocking, membranes were sectioned (grey dotted lines) and each section was incubated with the appropriate primary antibody for the Mw range of that section (indicated by descriptions). Western blots were performed as standard (****2.1.2.5 Western blotting).***

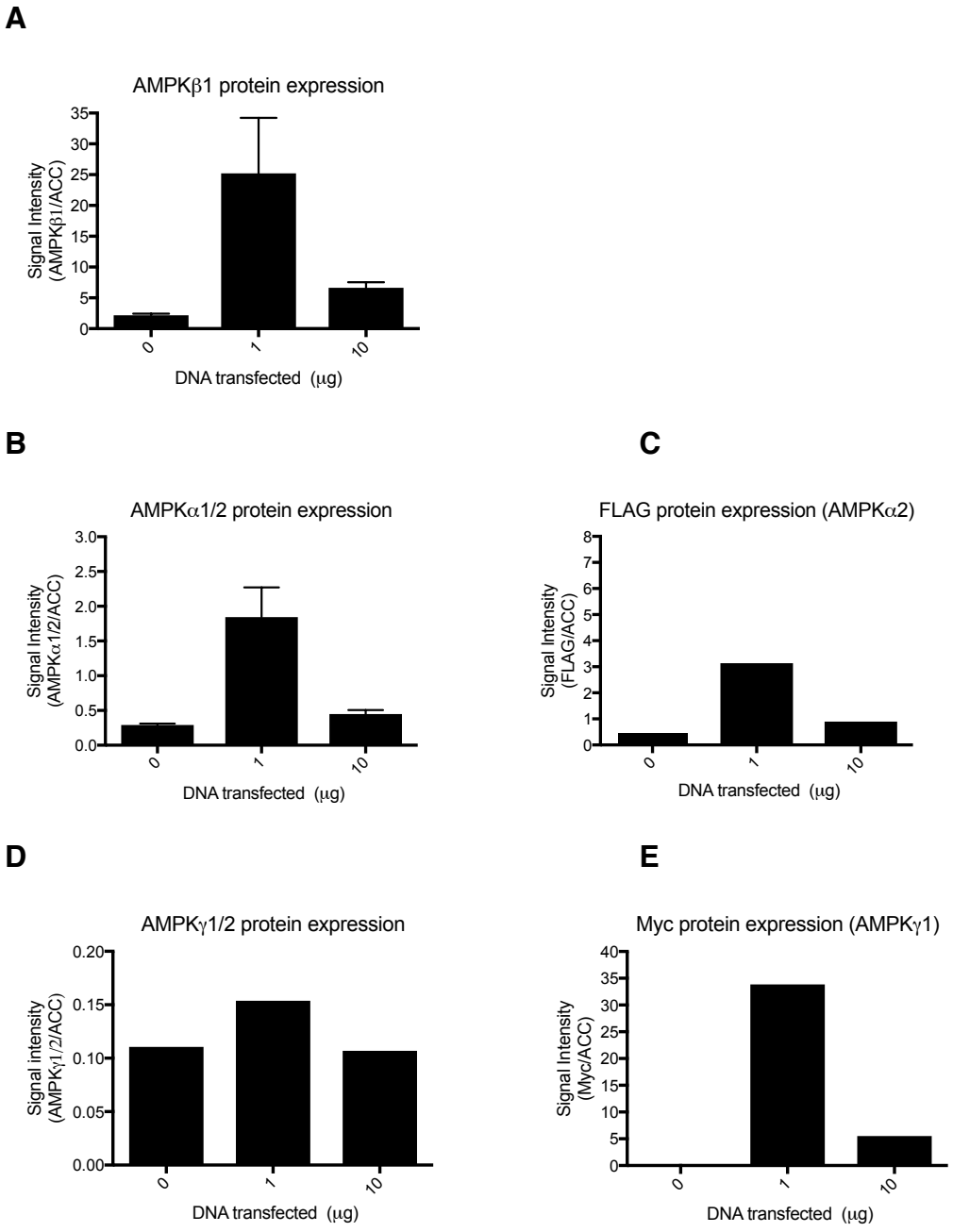

Figure 3.20. Quantification of epitope-tagged and untagged AMPK subunits overexpressed in HEK293 cells, detected by Western blotting. (A – E) *Signal intensities of target bands (from* ***Figure 3.19****) were normalized to those of ACC1/2 as a loading control.* ***(A & B)*** *Graphed data represents mean ± SEM n = 3 or 4 technical replicates.* ***(C – E)*** *Graphed data is n = 1.*

3.6 Discussion and future work

The above experiments describe an approach to differentially label cysteine residues according to thiol redox state, which is assessed by mobility shift electrophoresis. In Click-PEGylation, the thiol labelling step by maleimide derivatisation is separated from the PEG labelling, via a Click chemistry conjugation reaction, which gives improved flexibility over existing single-step strategies (e.g. the PEG-switch assay from which Click-PEGylation drew inspiration) (Burgoyne et al., 2013, van Leeuwen et al., 2017). Thiol labelling, particularly of proteins in their native state, can be impaired by the bulkiness of the PEG polymers, which can limit them from reaching their target sites. For this reason, the Click-PEGylation approach - utilising a Click chemistry intermediate linking step between the labelling and the tagging – is a useful alternative method.

Click-PEGylation can also be adapted to incorporate different tags. One could for example react samples with propargyl-maleimide and, as well as PEGylating some of them, react the remaining samples with other tags (e.g. a fluorescent label or biotin) for further enrichment, mass spectrometry or other downstream applications. Compared to other electrophoretic gel-based redox assays, thiol PEGylation has the advantage of providing the user with details about the contribution of different redox states of a protein whereas other assays, such as fluorescent labelling, generally result in a measure of overall protein oxidation.

The Click-PEGylation approach complements redox proteomics-based techniques as it is quicker and can, depending on the antibody, also facilitate a targeted assessment of candidate proteins, including proteins that are low in abundance or proteomically challenging. In **3.4 Method development and results**, as a proof-of-principle and to optimise the Click-PEGylation protocol, we used purified GAPDH. However, we also showed that the protocol can be applied to complex samples (cell lysates) and to thiol-containing proteins of a higher molecular weight, like catalase. Click-PEGylation would be useful to assess the effects of a range of

different conditions on the redox state of candidate proteins, with interesting findings followed up by using complementary mass spectrometry-based redox methods to identify the specific cysteine residues involved. Click-PEGylation also allows the redox state of multiple targets to be interrogated from a single sample by detection with different antibodies.

Above we focused on differentially labelling reduced and reversibly oxidised thiols. To distinguish between the various possible oxidised modifications more selectively, additional steps can be incorporated into the standard Click-PEGylation protocol at the initial thiol labelling stage. For instance, S-nitrosated thiols could be selectively reduced using Cu/ascorbic acid, or S-sulfenylation specifically studied by labelling with a dimedone-containing alkyne group (e.g. DYn-2 (Yang et al., 2015)). With the increasing use of Click chemistry as a selective and efficient conjugation strategy, the range of available azide-tagged probes is constantly expanding, which will allow further enhancement of the Click-PEGylation approach.

In establishing and optimising this method, we discovered a number of important points that need to be considered before adapting the method to a new protein of interest. In some cases, depending on the proximity of cysteine residues, conjugation of the target protein with PEG polymers may obstruct the epitope recognition site of some antibodies, leading to loss of Western blot signal upon Click-PEGylation, but not in the '– catalyst' control. If this occurs, alternative antibodies (particularly polyclonal) can be explored, where PEGylation will not interfere with antibody recognition of the protein.

The molecular weight shifts obtained upon Click-PEGylation are not directly additive to the combined size of the PEG moieties. This is due to drag and steric hindrance for the migration of branched Click-PEGylated proteins through a gel compared to unlabelled linear proteins during electrophoresis. The PEG labeling also affects the SDS-coating of the protein, which also alters how the proteins migrate on an SDS-PAGE gel.

We showed that the Click-PEGylation protocols can be used to detect redox shifts in complex biological samples by lysing the cells in the presence of NEM or propargyl-maleimide to alkylate the reduced thiols during lysis. As thiol oxidation can occur rapidly during cell lysis, cell protein can potentially be acid-precipitated prior to Click-PEGylation to prevent any artefactual oxidation (Held and Gibson, 2012). Future work with the Click-PEGylation protocols can include testing the benefits of this step.

From my work on AMPK, and also further work by others in the lab to which this method has been applied, I observed that it is more difficult to resolve individual bands of proteins with a large number of cysteine residues. In this instance, it is worth considering the structure of the protein and whether or not some cysteine residues may be involved in internal structures (e.g. Fe-S clusters) that may render them unlikely to be reversibly modified physiologically in the context of redox-signalling. If this is the case, native labeling of only the easily accessible cysteines (labeling without initial denaturation of the protein by SDS, urea or heat) can be attempted which will decrease the number of thiols PEGylated and importantly focus on the thiols which are most likely to be biologically relevant in redox signaling. Similarly, in other applications of this method in the lab it has been found that with some proteins, maleimides can react with groups other than thiols or cross-react with certain antibodies (although I did not observe any evidence of this with the model protein GAPDH or with AMPK after the propargyl maleimide concentration had been optimised). In this instance, the thiol alkylating agent iodoacetamide can be used instead of maleimide to good effect (Hill et al., 2009), and propargyl-iodoacetamide compounds exist commercially to use with this Click-PEGylation method.

Investigating AMPK redox states by Click-PEGylation would require further experiments. For testing endogenous AMPK, the starting protein amount needs to first be increased and protease inhibitors and antioxidants in the catalyst addition stage can also be investigated to prevent protein degradation. In parallel,

overexpressing AMPK subunits in cells, some with epitope tags, may also prove to be useful in optimising the Click-PEGylation reactions. However, as discussed in greater detail in **Chapter 4**, it does remain to be seen just how relevant AMPK redox states are in the context of AMPK regulation by ROS in cells.

Chapter 4

AMPK activation in C2C12 myotubes by H_2O_2 and mitochondrially-derived ROS

4.1 Introduction and aims

AMPK is a key sensor and regulator of cellular and whole-body energy metabolism which promotes cell survival by adapting metabolic pathways to energy demand (Carling et al., 2011, Hardie et al., 2012). The enzyme has been identified as a potential therapeutic target in T2 diabetes (Cool et al., 2006, Coughlan et al., 2014, Hardie, 2017), inflammation (O'Neill and Hardie, 2013) and cardiac ischaemia reperfusion injury (Kim et al., 2011, Zaha et al., 2016, Shao et al., 2014, Qi and Young, 2015). The enzyme's activity is directly regulated by adenine nucleotides (Oakhill et al., 2011, Hardie et al., 2011), primarily by AMP, which, when levels increase relative to ATP (measured as a decreased ATP/AMP or ATP/ADP ratio), binds the γ subunit and allosterically activates the enzyme. However, reactive oxygen species (ROS) have also been investigated as an atypical regulator of AMPK by several potential redox mechanisms. The role of mitochondrial ROS in AMPK activity is of particular interest. Mitochondria are key regulators of the adenine nucleotide pool and so play an important role in ADP and/or AMP-dependent AMPK regulation (hereafter, AMP/ADP-dependent regulation). Mitochondria are also important producers of ROS and their generation, particularly by RET, is now suggested by us and other labs to be a potential way in which mitochondria may signal to the rest of the cell during periods of metabolic adaptation (Chouchani et al., 2014, Mills et al., 2016, Scialo et al., 2016, Chouchani et al., 2016).

The prospect that ROS may alter AMPK activity as a further way of relaying information about the metabolic state or demands of the cell and thus promoting pro-survival adaptation has been investigated in a number of ways (Shao et al., 2014, Zmijewski et al., 2010, Emerling et al., 2009, Hart et al., 2015, Mungai et al., 2011, Hawley et al., 2010, Auciello et al., 2014). However, as discussed in **1.5.11 Evidence for and against redox-regulation of AMPK**, while AMPK can be allosterically activated in an AMP/ADP-independent mechanism (Xiao et al., 2013, Hawley et al., 2012, Zhang et al., 2017, Garcia and Shaw, 2017) **(Figure 4.1)**, AMP/ADP-independent AMPK activation by ROS is not uniformly observed

(Auciello et al., 2014, Hawley et al., 2010). It is possible that varying sensitivities in methods of measuring adenine nucleotides, different expression levels of ROS scavenging proteins in different cell types and possibly different cellular glucose availability (Auciello et al., 2014, Shao et al., 2014, Zhang et al., 2017) are causes for the lack of consensus. Although AMPK redox state in response to exogenous oxidants has been investigated by different methods and found to be altered (Zmijewski et al., 2010, Shao et al., 2014), it has not been determined to what extent the ROS tested alter the redox state of the cells. As AMPK is localised in the cytosol, a reversible change in the redox state of the cytosol (particularly to known ROS scavenging and ROS signaling proteins) would likely be required for any potential redox-regulation of AMPK to occur physiologically as a signalling mechanism. An irreversible change in redox state would be indicative of oxidative damage. Furthermore, the effects on AMPK activity by different sources of ROS (i.e. cytosolic versus mitochondrially-derived ROS) have not been compared in detail, nor what effect compartmentalisation of ROS has on the redox state of the cytosol and on AMPK activity.

To address these uncertainties, my aim was to characterise the effects of exogenous and selective, mitochondrially-derived ROS on AMPK activity and cell ATP/ADP ratios to determine if the effects of different sources of ROS on AMPK activity could be explained as AMP/ADP-dependent regulation or AMP/ADP-independent regulation. If confirmed, I aimed to determine the nature of AMP/ADP-independent regulation, which could be evidence of 1) direct redox effects on AMPK activity in cells (e.g. due to redox changes to key cysteine thiols on AMPK) or 2) indirect redox effects on AMPK activity in cells (e.g. ROS-induced inhibition of upstream phosphatases or ROS-induced increases in cytosolic calcium, etc.). As well as measures of AMPK activity and cellular ATP/ADP ratios, I aimed to use peroxiredoxin dimerisation as a biologically relevant measure of the oxidation state of multiple subcellular compartments. I used differentiated C2C12 myotubes as the cell model (for reasons discussed below), treated on day 7 or 8 post initiation of differentiation. In greater detail, I first measured the dynamic range of AMP/ADP-

dependent and AMP/ADP-independent AMPK activation caused by several control compounds that alter AMPK activity by known mechanisms. This enabled the creation of a set of calibration graphs with which to determine the mode of action of other AMPK activating treatments whose mechanism is unclear. I then measured the effects on AMPK activity and ATP/ADP ratios of cellular oxidation by exogenous H_2O_2, which I confirmed was sufficient to oxidise the cytosol (where AMPK is localized) and also the mitochondria. Then to investigate the effects of selective, mitochondria-generated ROS on AMPK and ATP/ADP ratios, I utilised the mitochondria-targeted redox-cycler, MitoParaquat (MPQ) (Robb et al., 2015), confirming that ROS was generated and contained within mitochondria only and not transferred to the cytosol. Using the calibration graphs and other supporting data, I aimed to infer the mechanisms of action of both the exogenous and mitochondria-generated ROS on endogenous AMPK activity using a screening methodology that can be readily adapted to any cell type.

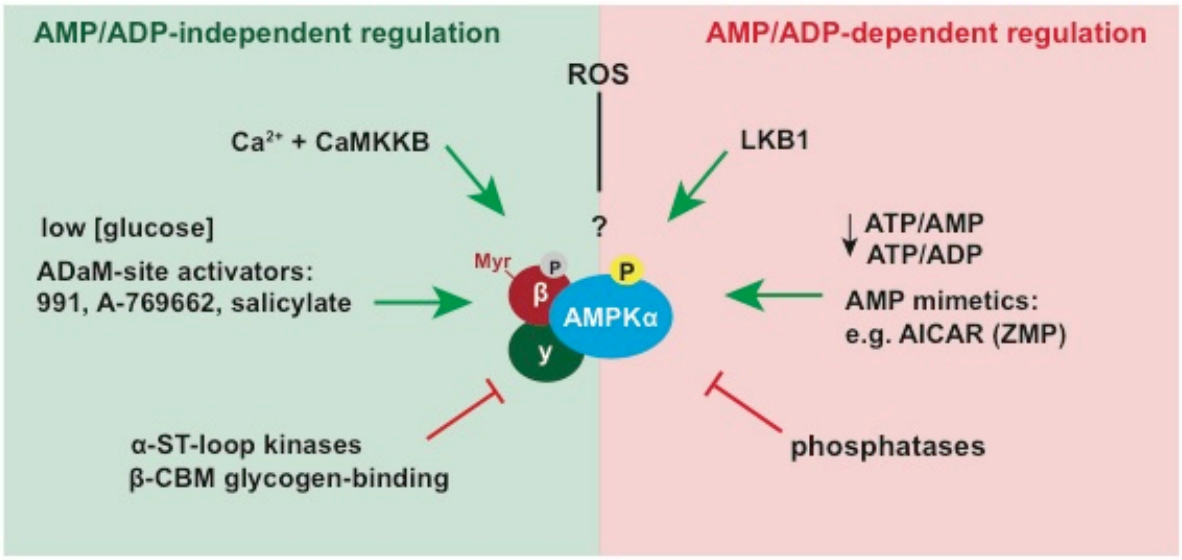

Figure 4.1 Known and potential regulators of AMPK activity by AMP/ADP dependent or AMP/ADP independent mechanisms. *ADaM-site, allosteric drug and metabolite binding site; α-ST-loop, α subunit C-terminal domain serine/threonine-rich loop; β-CBM, β subunit carbohydrate binding module.*

4.2 Methods and results

4.2.1 Cell model background and characterization

C2C12 cells are a mouse skeletal muscle (myoblast) cell line, which I chose as the cell model for this project for several reasons: 1) C2C12s have sufficient levels of mitochondria to be able to study mitochondrial function (Leary et al., 1998, Elkalaf et al., 2013); 2) C2C12 myoblasts can be terminally differentiated to myotubes to provide an alternative set of biological parameters (discussed in greater detail below); 3) C2C12s are a useful model to study AMPK activity as AMPK plays an important role in skeletal muscle function, regulating glucose uptake, fatty acid oxidation and mitochondrial biogenesis (O'Neill et al., 2011, Jager et al., 2007).

C2C12 myoblasts are typically cultured in a high glucose (4.5g/l or 25 mM) DMEM GlutaMAX media, supplemented with 10% fetal bovine serum (FBS) that provides mitogens that maintain the cells in an undifferentiated, myoblast state (Yoshiko et al., 2002). As a highly proliferative cell line, C2C12 myoblasts are typically glycolytic (Leary et al., 1998). For investigating mitochondria - AMPK cross-talk, I chose to differentiate the myoblasts to myotubes as there is evidence that myotubes are more dependent on mitochondrial ATP production (OXPHOS) than myoblasts (Leary et al., 1998, Sin et al., 2016). Myotubes are thus a more physiologically relevant model than myoblasts because being terminally differentiated, they are more similar in morphology and bioenergetics to skeletal muscle fibers than are myoblasts. Differentiation also provides a useful quality control system, as there is evidence that cells with dysfunctional mitochondria do not differentiate (Wagatsuma and Sakuma, 2013). Finally, differentiation allows easier and more direct comparisons of short and long (i.e. 24 h) treatment time-points without the cell density changing (as myotubes are non-proliferating, compared to highly proliferative myoblasts).

C2C12 myoblasts can be differentiated to myotubes by two main methods: 1) changing the serum in the media from 10% (v/v) FBS to 2% (v/v) adult horse serum

(Andres and Walsh, 1996) or 2) decreasing the FBS in the media from 10% (v/v) to 1% (v/v) (Yoshiko et al., 2002). Both methods decrease the amount of mitogens present in the culture media. This induces endogenous expression of insulin-like growth factors (IGFs), which halts proliferation and promotes differentiation (Yoshiko et al., 2002). As reasons for and against both methods of differentiation are not well characterized and preference is likely due to individual lab traditions, I chose FBS serum-depletion as the method of C2C12 differentiation as it negates the need for an additional reagent (horse serum) whose components (like FBS) are unclear and variable from batch to batch.

C2C12 differentiation is accompanied by cell shape and protein expression changes (Andres and Walsh, 1996, Elkalaf et al., 2013, Yoshiko et al., 2002, Leary et al., 1998) which I confirmed by microscopy and Western blotting for myogenin, a marker of differentiation which is expressed from initiation of differentiation (see **2.2.4 Differentiation and treatment of C2C12 cells**). I also observed apparent increases in protein expression of a mitochondrial membrane protein, VDAC, in differentiated cells compared to undifferentiated cells, an indicator of increased mitochondrial content **(Figure 4.2).** This is consistent with literature indicating mitochondrial biogenesis is upregulated during C2C12 differentiation (Leary et al., 1998, Sin et al., 2016, Elkalaf et al., 2013). I observed a change in protein expression of the AMPKβ subunit isoforms **(Figure 4.2)**. In undifferentiated cells, AMPKβ1 was the dominant AMPKβ isoform expressed, but there was increased protein expression of AMPKβ2 from day 5 of differentiation. This is consistent with literature indicating that AMPKβ2 is mainly expressed in muscle (Birk and Wojtaszewski, 2006). It has been found that AMPKβ2 can bind glycogen (a potential negative regulator of AMPK activity) tighter than AMPKβ1 (Koay et al., 2010) and so targeting AMPKβ2 for activation may be a way of selectively increasing AMPK activity in muscle for blood glucose-lowering benefit to diabetic patients (Koay et al., 2010, Hardie, 2017).

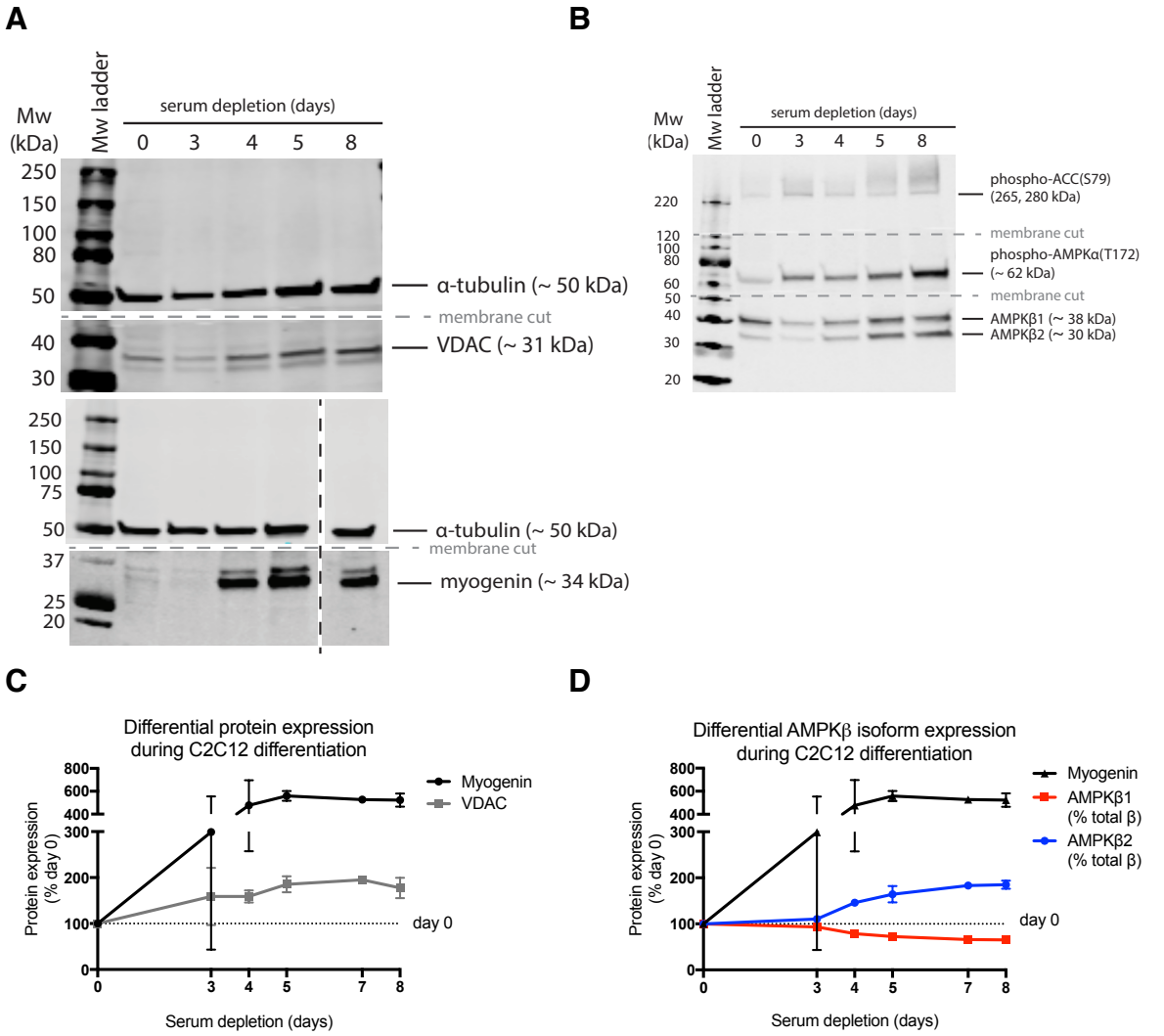

***Figure 4.2. Differential protein expression profiles during C2C12 differentiation**. **(A - D)** C2C12 myoblasts were plated at 20,000 cells/cm^2 in high glucose standard medium. When cells reached ~ 90% confluency (day 0), myoblast to myotube differentiation was induced by serum depletion (see **2.2.4 Differentiation and treatment of C2C12 cells**). Cells were rapidly lysed in Hepes lysis buffer supplemented with DTT and protease inhibitors (see **2.4 AMPK assays**). SDS-PAGE (~ 25 µg protein per well) and Western blot were performed as described in 2.1.2.4 Western blotting or **2.4 AMPK assays**. Post blocking, PVDF membranes were cut horizontally with a razor blade (as indicated by the grey dotted lines) and each section was individually or dual incubated with the appropriate primary antibody(s) for the Mw range of that section, indicated by band descriptions (see **2.1.2.1.1 Primary antibodies**). Rabbit and mouse primary antibodies were differentially labelled with fluorescent secondary antibodies (see 2.1.2.1.2 Secondary antibodies).* Western blots were imaged using the *Odyssey® CLx Infrared Imaging System (**(A)** fluorescence emission at 800 nm for myogenin or 680 nm for VDAC and α-tubulin and **(B)** fluorescence emission at 800 nm for all proteins). **(C)** The Western blot signal intensities of* myogenin *and VDAC (quantified with LI-COR Biosciences Image Studio™ Lite software) were normalised to that of α-tubulin as a loading control. Results were expressed as % day 0. **(D)**. The Western blot signal intensities* AMPKβ1 or AMPKβ2 were calculated as % total AMPKβ1+2 and then expressed as *% day 0. All data points represent mean ± range of n = 2 biological replicates, except day 7 (n = 1).*

4.2.2 Characterizing AMP/ADP-dependent and AMP/ADP-independent AMPK activity in C2C12 myotubes

The cellular adenine nucleotide pool (consisting of ATP, ADP and AMP) is the primary regulator of AMPK (Oakhill et al., 2011, Hardie et al., 2011). Increases in cellular AMP and ADP relative to ATP (measured as decreased ATP/AMP or ATP/ADP ratios) (Carling et al., 2011) occur during acute and chronic energy demand and promote AMPK activation by an allosteric mechanism. To characterize the cell line-specific dynamic range of this regulation of AMPK in response to energy stress (AMP/ADP-dependent activation), C2C12 myotubes were treated with mitochondrial respiratory chain inhibitors or an uncoupler that inhibit mitochondrial ATP production in different ways, thereby increasing AMP and ADP levels. Initially, phosphorylation of the AMPK catalytic α subunit at T172 and of a downstream target, Acetyl Co-A carboxylase (ACC) at S79, were assayed by Western blotting (**Figure 4.3**). Rotenone and phenformin (specific and non-specific inhibitors, respectively, of mitochondrial complex I), FCCP (mitochondrial uncoupler) and oligomycin (inhibitor of ATP synthase) all significantly increased AMPK and ACC phosphorylation after 30 min treatment.

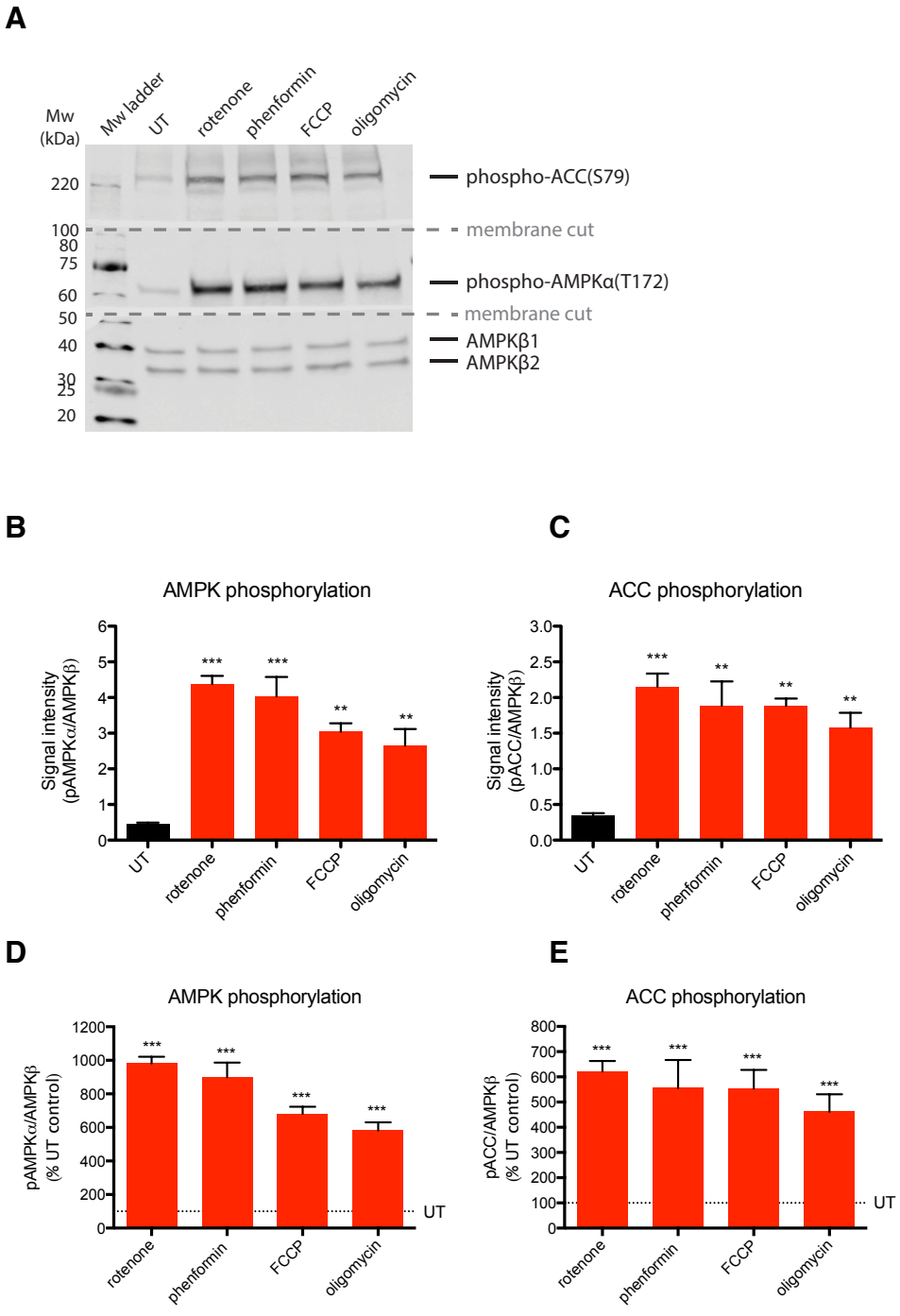

Figure 4.3. AMPK activity markers (phospho-AMPKα(T172) and phospho-ACC(S79)) in C2C12 myotubes in response to inhibitors of mitochondrial ATP production, assessed by Western blotting. (A) *C2C12 myotubes were treated with mitochondrial respiratory chain inhibitors or an uncoupler (FCCP) for 30 min to inhibit ATP production and activate AMPK. Cells were treated in fresh medium (1% (v/v) FBS) with rotenone (2 μg/ml), phenformin (5 mM), FCCP (1 μM) or oligomycin (100 ng/ml). Cells were rapidly lysed in ice-cold Hepes lysis buffer: 250 μl lysis buffer per 6 cm plate (see* ***2.4 AMPK assays****). Western blotting (25 μg protein) was performed as previously described.* **(B & C)** *The Western blot signal intensities of* AMPKα1/2-phosphoT172 and ACC1/2-phosphoS79 *target bands were normalised to those of AMPKβ2 as a loading control.*

Graphed data is mean ± SEM of n = 3 biological replicates; ***(D & E)*** *Graphed data is mean ± SEM of n = 3 biological replicates (from* ***(B & C)****), expressed as % untreated (UT) control. Statistical analysis was performed by one-way analysis of variance (ANOVA) with Dunnett's Multiple Comparison post-test comparing all treatments to UT control. Means were considered significantly different when P < 0.05. **P < 0.01, *** P < 0.001.*

AMPK specific activity in response to these inhibitors of mitochondrial ATP production was then measured by the radiometric SAMS kinase assay (**Figure 4.4**). In agreement with the phosphorylation assays, AMPK specific activity was increased in response to treatment with the different compounds that inhibit mitochondrial ATP production.

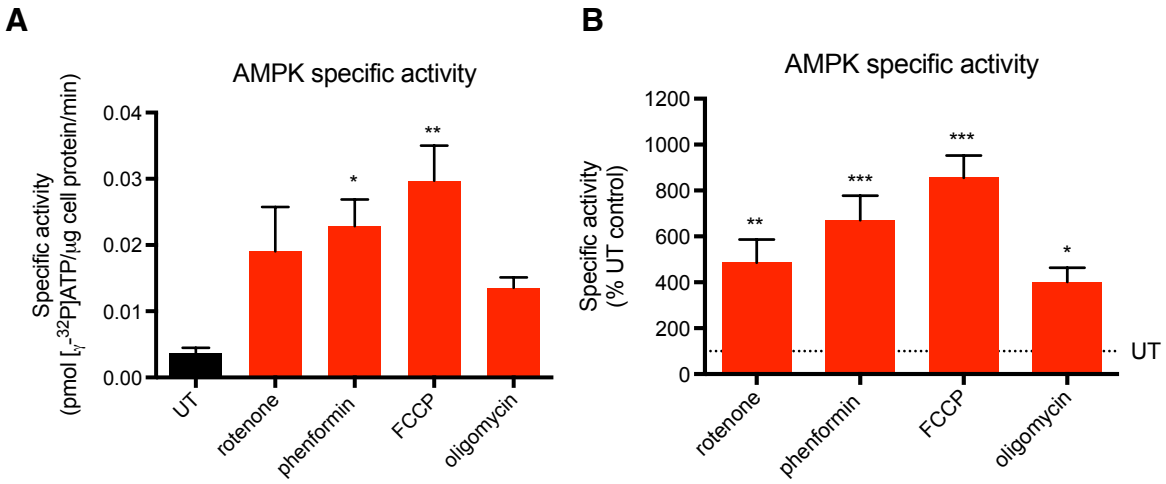

Figure 4.4 AMPK specific activity in C2C12 myotubes in response to inhibitors of mitochondrial ATP production, assessed by the AMPK SAMS kinase assay. (A) *AMPK was immunoprecipitated from 200 µg protein from freshly thawed whole cell lysate aliquots (described in* ***Figure 4.3****), and then divided into 4 X 10 µl aliquots. SAMS kinase assays were performed as described in* ***2.4 AMPK assays*** *on duplicate aliquots (equivalent to 50 µg whole cell protein) in Hepes buffer with AMP (167 µM) and SAMS peptide (167 µM) (final concentrations). A 'blank' reaction was performed on a third aliquot (without SAMS peptide). All kinase reactions were initiated with* radiolabelled ATP mix*: [γ-^{32}P]ATP (*16.7 *µCi/ml), ATP (167 µM) and $MgCl_2$ (4.2 mM) (final concentrations). SAMS peptide phosphorylation (radiolabelled) by AMPK was measured by scintillation counting and quantified by measuring the specific radioactivity (SR) of a known amount of radiolabelled ATP (5 nmol). The mean specific activity of AMPK was calculated as follows: (mean kinase – blank counts per min (CPM)) X total V (30 µl))/(SR (CPM.nmol^{-1}) X pipetted V (25 µl) X T (30 min) X cell protein (50 µg)). Graphed data is mean ± SEM of n = 3 biological replicates presented as pmol [γ-^{32}P]ATP /µg cell protein/min;* ***(B)*** *Graphed data is mean ± SEM of n = 3 biological replicates from* ***(A)*** *expressed as % untreated (UT) control. Statistical analysis was performed by one-way ANOVA with Dunnett's Multiple Comparison post-test comparing all treatments to UT control. Means were considered significantly different when P < 0.05. *P < 0.05, **P < 0.01, *** P < 0.001.*

In parallel, the ATP/ADP ratio of C2C12 myotubes was measured in response to the respiratory chain inhibitors (**Figure 4.5**). The cell ATP/ADP ratio is readily measurable using a luciferase/luciferin-based bioluminescence assay (Strehler, 1974), see **2.5 Measuring cell and tissue ATP/ADP ratios by bioluminescence**. The ATP/ADP ratio was measured instead of the ATP/AMP ratio because the concentration of AMP in cells tends to be one or two orders of magnitude lower than those of ADP and ATP (Hardie, 2011) so it can be difficult to measure AMP reliably. As the cell ATP/AMP ratio varies as the square of the ATP/ADP ratio (Hardie and Hawley, 2001), small decreases in the ATP/ADP ratio translate to larger relative decreases in the ATP/AMP ratio. Thus, even small decreases in the ATP/ADP ratio can enable allosteric activation of AMPK by AMP. Furthermore, increased cell ADP levels relative to ATP also activate AMPK by protecting AMPK from dephosphorylation (and thus inactivation) by upstream phosphatases. The ATP/ADP ratiometric measurement avoids discrepancies in absolute quantification of ATP or ADP that can occur due to slight changes in cell numbers. Absolute ATP/ADP ratios in untreated (UT) cells averaged at 16.1 ± 2.1 (mean ± SEM of n = 3 biological replicates). As it is thought that healthy cells require a ratio of ATP/ADP of ~ 10 - 20 in order to perform energy-requiring processes (Hardie and Hawley, 2001), the average ratio I measured in untreated cells suggests that the cells were healthy and also that the method of nucleotide measurement was sensitive and offered results comparable with literature. ATP/ADP ratios in treated cells ranged between 7.4 ± 0.7 (rotenone) and 11.4 ± 1.8 (FCCP), ~ 46 and ~ 71% of UT cells, respectively, confirming that ATP production was inhibited. Decreased cell ATP/ADP ratios combined with the increased AMPK activity shown above is characteristic of AMP/ADP-dependent regulation of AMPK activity by these control compounds.

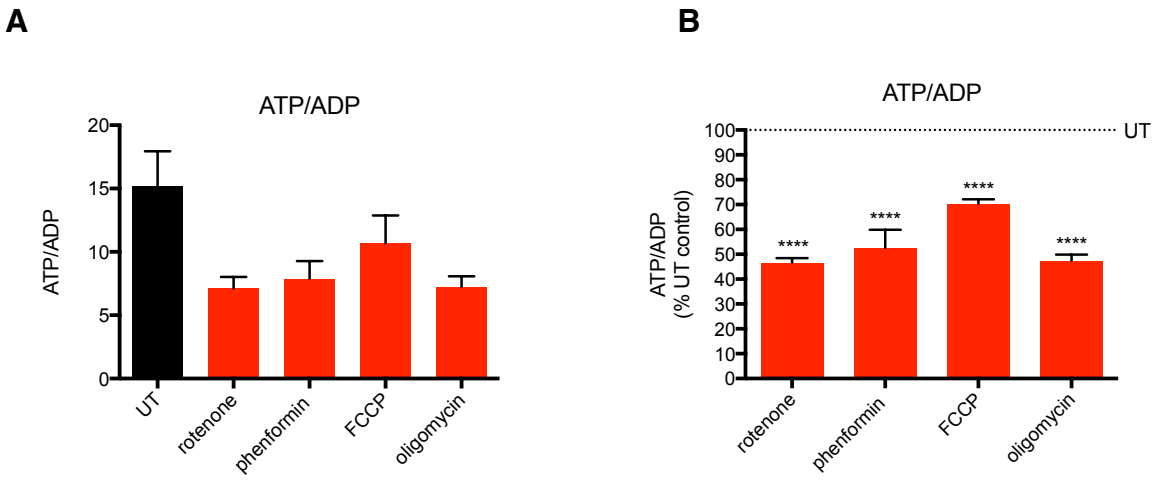

Figure 4.5 ATP/ADP ratios in C2C12 myotubes in response to inhibitors of mitochondrial ATP production, measured by a luciferase/luciferin bioluminescence assay. (A) *C2C12 myotubes were treated with compounds as described in* ***Figure 5.3.*** *Cells were rapidly lysed in ice-cold perchloric acid extractant (PCA). For ATP measurements, pH neutralised sample (100 µl) was added to 400 µl Tris-Acetate buffer in luminometer tubes. ATP was measured by light emission in a luminometer (Berthold AutoLumat LB 953 Multi-Tube) following addition of luciferase/luciferin solution (100 µl per tube, delivered by autoinjector, protected from light). For ADP measurements, endogenous ATP was first degraded by ATP sulfurylase and then endogenous ADP was converted to ATP using a pyruvate kinase/ phosphoenoylpyruvate solution. Newly converted ATP was then measured by luciferase/luciferin solution as previously described. ATP and ADP values were quantified from standard curves. Sample ATP and ADP values were expressed as ratios, calculated as follows: ATP (pmol ATP)/(ADP (as pmol ATP) – 'blank' (pmol ATP)). Graphed data is mean ± SEM of n = 3 biological replicates. For detailed methods and buffers see* ***2.5 Measuring ATP/ADP ratios by bioluminescence. (B)*** *Graphed data is mean ± SEM of n = 3 biological replicates (from* ***(A)****) expressed as % untreated (UT) control. Statistical analysis was performed by one-way ANOVA with Dunnett's Multiple Comparison post-test comparing all treatments to UT control. Means were considered significantly different when $P < 0.05$. **** $P < 0.0001$.*

AMPK can also be directly activated in an AMP/ADP-independent manner by a number of small molecules: the synthetic AMPK activators A-769662 and 991 and the naturally occurring plant compound, salicylate (a metabolite of aspirin) (Xiao et al., 2013, Hawley et al., 2012). These compounds bind at one site at the interface of the α subunit kinase domain and the β subunit carbohydrate-binding module (CBM), known as the allosteric drug and metabolite (ADaM)-binding pocket (Langendorf and Kemp, 2015), and increase AMPK activity independently of adenine nucleotide-binding. This AMP/ADP-independent allosteric activation can also act in synergy with AMP, with combined A-769662 and AMP binding having an additive effect on AMPK activity (Xiao et al., 2013). Treatment of C2C12

myotubes with 991 increased AMPKα(T172) phosphorylation and ACC(S79) phosphorylation dose-dependently (**Figure 4.6**). Compound C, a non-specific inhibitor of AMPK by an unclear mechanism (Liu et al., 2014) was also tested on cells (**Figure 4.6**). The inhibitor had no effect on phosphorylation markers compared to untreated cells, suggesting that the untreated cells already had low levels of AMPK activation. Although not tested, Compound C may have an inhibitory effect on above-basal AMPK activation in cells, caused either due to energy stress (AMP/ADP-dependent activation) or following pre-treatment with 991 (AMP/ADP-independent activation).

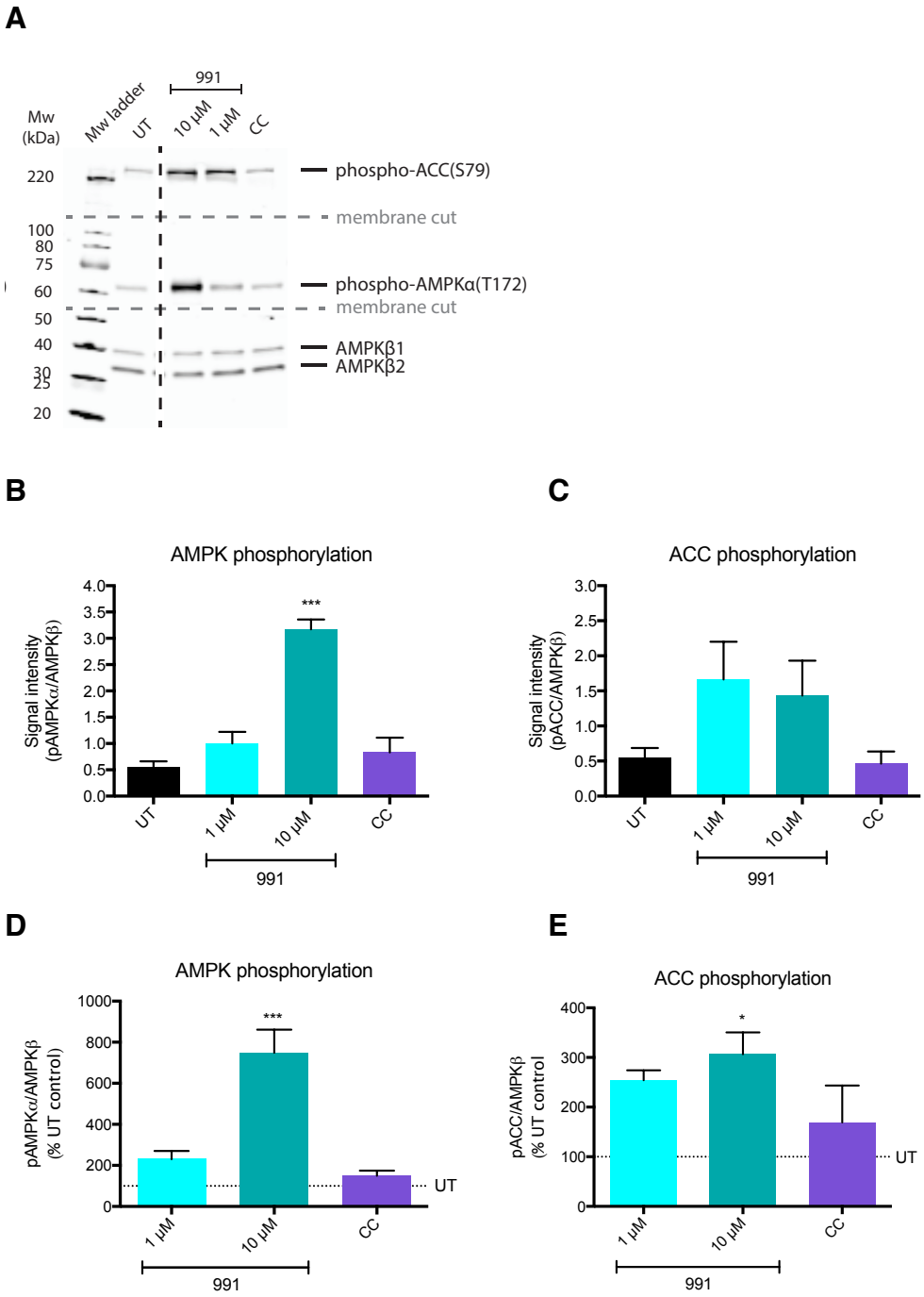

Figure 4.6 AMPK activity markers (phospho-AMPKα(T172) and phospho-ACC(S79)) in C2C12 myotubes in response to a selective AMPK activator or inhibitor, assayed by Western blotting. (A) *C2C12 myotubes were treated with the selective AMPK activator, 991 or the AMPK inhibitor, Compound C (CC) to activate or inhibit AMPK by an AMP/ADP-independent mechanism. Cells were treated in fresh medium (1% (v/v) FBS) with 991 (1 or 10 µM) or CC (10 µM) and incubated for 30 min. Cells were rapidly lysed in ice-cold Hepes lysis buffer and Western blots were performed on freshly thawed aliquots as previously described. After the representative Western blot was imaged, the image was cropped vertically and merged (as indicated by the black dotted line) to exclude middle lanes that were not relevant for this experiment;* ***(B & C)*** *The Western blot signal*

intensities of AMPKα1/2-phosphoT172 and ACC1/2-phosphoS79 *target bands were normalised against those of* AMPKβ2 *as a loading control. Graphed data is mean ± SEM of n = 3 or 4 biological replicates;* ***(D & E)*** *Graphed data is mean ± SEM of n = 3 or 4 biological replicates (from* ***(B & C)***), *expressed as % untreated (UT) control. Statistical analysis was performed by one-way ANOVA with Dunnett's Multiple Comparison post-test comparing all treatments to UT control. Means were considered significantly different when P < 0.05. *P < 0.05, **P < 0.01, *** P < 0.001.*

AMPK specific activity in response to 991 and Compound C was measured by the radiometric SAMS kinase assay (**Figure 4.7**). 991 induced dose-dependent AMPK activation and Compound C had no effect (compared to untreated cells), all in agreement with the previous Western blot analyses.

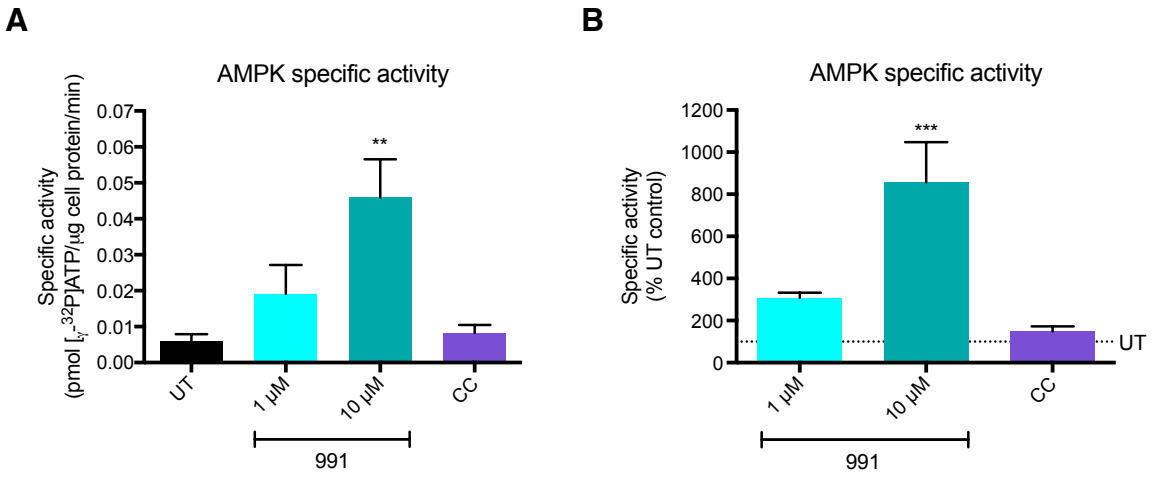

Figure 4.7 AMPK specific activity in C2C12 myotubes in response to a selective AMPK activator or inhibitor, assessed by the AMPK SAMS kinase assay. (A) *SAMS kinase assays were performed as previously described on AMPK immunoprecipitated from 200 µg protein from freshly thawed lysate aliquots, described in* ***Figure 4.6. (A)*** *Graphed data is mean ± SEM of n = 3 biological replicates presented as pmol [γ-32P]ATP/µg cell protein/min;* ***(B)*** *Graphed data is mean ± SEM of n = 3 biological replicates from* ***(A)*** *expressed as % untreated (UT) control. Statistical analysis was performed by one-way ANOVA with Dunnett's Multiple Comparison post-test comparing all treatments to UT control. Means were considered significantly different when P < 0.05. **P < 0.01, *** P < 0.001.*

The ATP/ADP ratio of C2C12 myotubes was then measured in response to the activator, 991 or inhibitor, Compound C **(Figure 4.8).** 991 did not decrease cell ATP/ADP ratios, consistent with this mode of AMPK activation being independent of AMP or ADP levels. Instead, a low dose of 991 increased ATP/ADP ratios above untreated cells, possibly evidence of metabolic changes induced by low-grade AMPK activation in the absence of energy stress (promotion of ATP generating pathways and inhibition of ATP consuming pathways). The higher dose of 991 did not significantly affect ATP/ADP ratios, perhaps due to off-target effects or effects caused by very high levels of AMPK activity. The inhibitor, Compound C, also had no significant effect on ATP/ADP ratios.

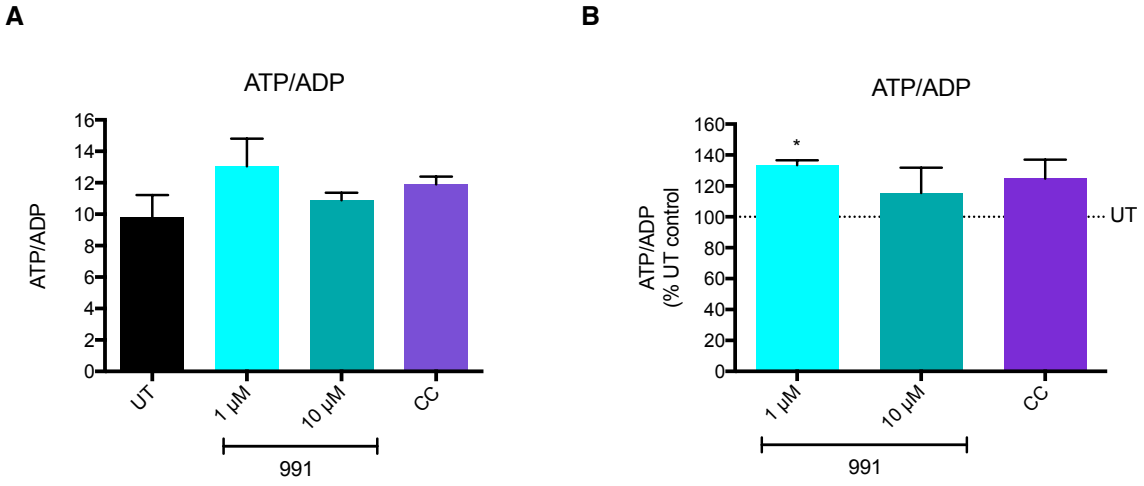

Figure 4.8 ATP/ADP ratios in C2C12 myotubes in response to a selective AMPK activator or inhibitor, measured by a luciferase/luciferin bioluminescence assay. (A) *C2C12 myotubes were treated with compounds as described in Figure 4.6. Cells were rapidly lysed in ice-cold PCA and ATP/ADP assays were performed as previously described. Graphed data is mean ± SEM of n = 3 biological replicates;* ***(B)*** *Graphed data is mean ± SEM of n = 3 biological replicates (from* ***(A)****) expressed as % untreated (UT) control. Statistical analysis was performed by one-way ANOVA with Dunnett's Multiple Comparison post-test comparing all treatments to UT control. Means were considered significantly different when P < 0.05. *P < 0.05.*

I next combined all the data derived from testing AMP/ADP-dependent and AMP/ADP-independent AMPK activators (or inhibitor) on C2C12 myotubes, creating calibration graphs. Using these graphs I aimed to determine the mechanism of other AMPK-activating treatments, either AMP/ADP-dependent or

AMP/ADP-independent. The relationship between the three AMPK activity markers (AMPK phosphorylation, ACC phosphorylation and AMPK specific activity) and ATP/ADP ratios after cell treatments were compared (with all data presented as % untreated (UT) control, so that UT control for all variables = 100 %) **(Figure 4.9).** Plotting all the data together in this way allowed me to clearly visualize the dynamic range of the variables in response to control compounds for both AMP/ADP-dependent and AMP/ADP-independent activation. It was apparent that these differing forms of AMPK activation have distinct signatures: AMP/ADP-dependent activators induce AMPK activation while decreasing ATP/ADP ratios (red background); the AMP/ADP-independent activator induces AMPK activation without decreasing ATP/ADP ratios (green background).

A

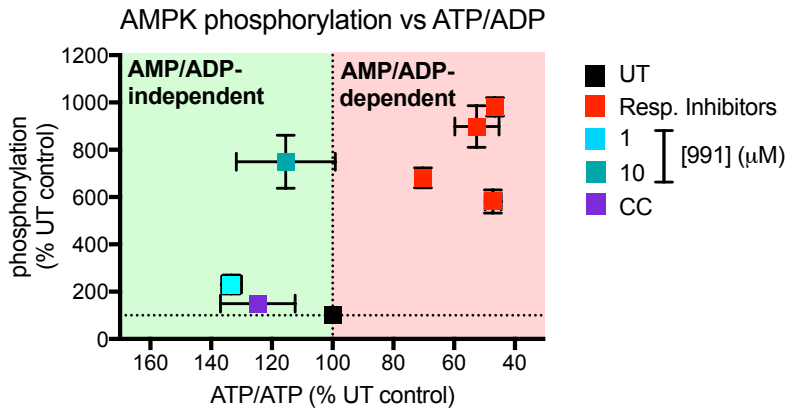

B

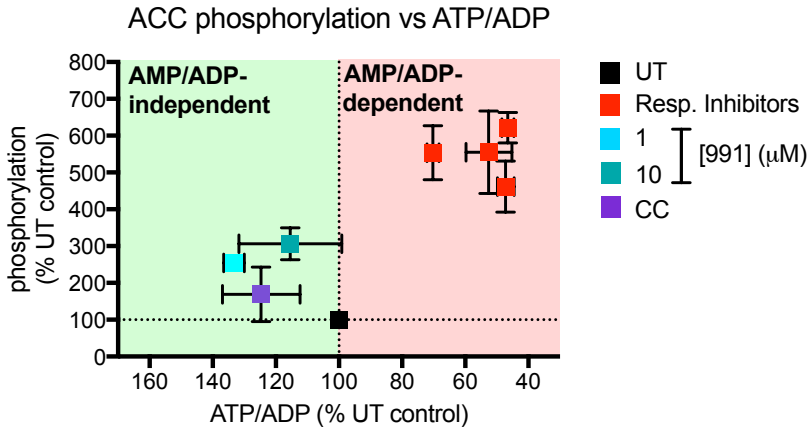

C

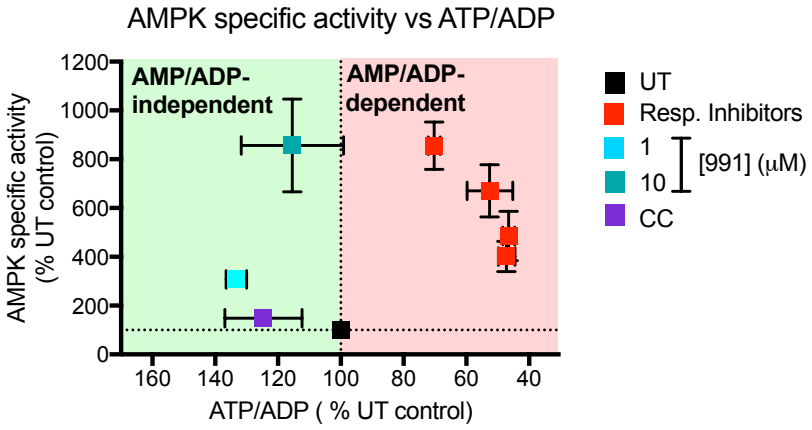

Figure 4.9 Calibration graphs showing the relationship between AMPK activation markers and ATP/ADP ratios in C2C12 myotubes. (A - C) *Graphed data shows AMPK activation markers:* ***(A)*** *AMPKα(T172) phosphorylation* ***(B)*** *ACC(S79) phosphorylation and* ***(C)*** *AMPK specific activity plotted against their respective cell ATP/ADP ratios. Data points are mean ± SEM of n ≥ 3 biological replicates. All values are expressed as % UT control.*

4.2.3 Effects of H_2O_2 on cellular redox state, AMPK activity and ATP/ADP ratios

Having established the calibration graphs with control compounds that affect AMPK activity by AMP/ADP-dependent or AMP/ADP-independent mechanisms, I tested the effects of exogenous H_2O_2 on AMPK activity and ATP/ADP ratios, to determine whether: 1) exogenous H_2O_2 has AMP/ADP-independent effects on AMPK activity in cells (e.g. via a redox dependent mechanism) or 2) the effects on AMPK are indirect, by altering ATP/ADP ratios (AMP/ADP-dependent activation). C2C12 myotubes were treated with serially diluted boluses of H_2O_2 for 10 or 30 min, ranging from 7.5 µM to 750 µM, which spans the reported limit of physiological concentrations in cells and *in vivo* (300 nM - 10 µM) (Mueller and Arnhold, 1995, Sobotta et al., 2013) to supra-physiological concentrations (> 10 µM). Boluses were delivered in serum-free media to minimize extracellular catalase (in serum), which catalyzes the rapid decomposition of H_2O_2 to H_2O. I first tested if the bolus concentrations were sufficient to alter the redox state of the cells, with particular interest in changes in the cytosol as that is where AMPK is localized. Consequently, a requirement of potential AMPK redox-regulation in cells would be a reversible change in the redox state of this subcompartment. I was also interested in the redox state of the mitochondria as increased oxidation here could potentially impact ATP production, affecting AMPK indirectly (by an AMP/ADP-dependent mechanism).

Biological effects of oxidation can be monitored by measuring peroxiredoxin (Prx) dimerisation (see **1.3.3.1 The peroxiredoxin/thioredoxin system, 1.4.2 Regulation of mitochondrial ROS** and **2.6 Peroxiredoxin dimerisation assays**). Prx are a family of thiol peroxidases that help to maintain the redox balance of the cell by reducing H_2O_2 to H_2O. When oxidised, Prx can form intermolecular reversible disulfide bridges (-S-S-), resulting in Prx homodimerisation and inactivation. These inactive dimers (measurable by Western blotting with an antibody to Prx, which recognises both the monomer and the dimer) are relevant in

redox signalling as they are readily reversible. Thus, the activity of Prx is modulated by the ratio of its active to reversibly inactive form, due to disulfide bond formation in response to oxidation (Cox et al., 2009, Cox et al., 2008), and increased formation of dimer relative to monomer can be used as a measure of extracellular, submicromolar concentrations of H_2O_2 (Sobotta et al., 2013). Extended oxidation can cause thiol modifications that do not lead to Prx dimerisation (sulfinic acid ($–SO_2H$), sulfonic acid ($–SO_3H$)), more likely associated with oxidative damage than redox signalling as they are not readily reversible. This hyper-oxidation presents on a Western blot as loss of peak dimerisation, but can be visualised using an antibody to the sulfonic acid modification: Prx-SO_3 (Riquier et al., 2014). To summarise, Prx dimerisation tends to follow an inverted U-shaped curve in response to H_2O_2: dimerisation increases as H_2O_2 level increase reaching a peak (typically measurable as 80 – 90 % dimer), then as H_2O_2 levels further increase, dimerisation decreases due to hyper-oxidation (Sobotta et al., 2013). A second benefit of Prx-dimerisation as a measure of cellular oxidation/ extracellular H_2O_2 level is that the redox state of different subcellular compartments can be analysed simultaneously. As previously discussed, different Prx isoforms are located in different subcellular compartments. Using antibodies specific to Prx 2 and Prx 3, I was able to monitor the effects of H_2O_2 boluses on both the cytosol and the mitochondrial matrix, respectively, at the same time **(Figure 4.10 and 4.11)**. Cells were treated with diamide (thiol-specific oxidant (Kosower and Kosower, 1995) as a positive control for both Prx 2 and Prx 3 dimerisation, showing the dynamic range of dimerisation that is possible to measure in both subcompartments simultaneously.

I found that both Prx 2 and Prx 3 dimerisation started to increase in response to H_2O_2 boluses between 7.5 and 75 µM, measured at 10 min post bolus addition. Prx 2 dimerisation (cytosol) peaked after treatment with the 75 µM bolus, reaching 44.3 ± 9.3% dimer (mean ± SEM of n = 3), compared to 19.4 ± 4.1% dimer in the UT control. Then % dimer decreased with higher bolus concentrations of H_2O_2. This suggests hyper-oxidation to sulfinic or sulfonic acid was occurring at or higher

than this 75 µM bolus. It is possible that hyper-oxidation would have occurred between the 7.5 and 75 µM boluses, as other literature has shown peak Prx 2 dimerisation of ~ 80% dimer after treatment with a 25 µM H_2O_2 bolus measured at 5 min post bolus addition (Sobotta et al., 2013). However, this bolus concentration was not tested in this experiment. Peak Prx 3 (mitochondrial matrix) dimerisation occurred after treatment with the 375 µM H_2O_2 bolus (80.7 ± 8.5% dimer, compared to 46.1 ± 6.0% dimer in the UT control), measured 10 min post-bolus addition. % dimer started to decrease after treatment with the 750 µM bolus (72.9 ± 10.8% dimer) suggesting that hyper-oxidation was occurring between the 375 and 750 µM boluses. That peak Prx 3 dimerisation occurred after a higher bolus of H_2O_2 than peak Prx 2 dimerisation suggests several possibilities: 1) Prx-H_2O_2 oxidation is slower in the mitochondrial matrix compared to the cytosol for equivalent [H_2O_2]; 2) it takes longer for the H_2O_2 to transfer into the mitochondrial matrix than the cytosol, making the local [H_2O_2] in the matrix lower than in the cytosol; 3) some H_2O_2 metabolism occurred in the cytosol before reaching the matrix. A loss of both Prx 2 and Prx 3 dimer signal was observed at 30 min post bolus addition. There are several possible reasons for this: 1) the H_2O_2 was being rapidly metabolised to H_2O by peroxidases; 2) Prx dimerisation was being rapidly enzymatically reversed (by Trx); 3) hyper-oxidation to sulfinic and/or sulfonic acid was occurring across the range, presenting as loss of dimerisation. Prx 3 dimers were visible as double bands, due to the different electrophoretic mobility of dimers linked by one or two disulfide bridges (Dietz et al., 2002, Hall et al., 2009).

Although a number of interpretations can be made from this data set, I have come to the following conclusions: 1) the H_2O_2 boluses tested had a sufficient range to reversibly oxidise monomer Prx to dimers (biologically relevant in redox signaling) and at higher boluses to hyper-oxidise Prx with loss of dimerisation (consistent with oxidative damage); 2) both Prx 2 and Prx 3 formed dimers, confirming that the cytosol was oxidised, and so was the mitochondrial matrix; 3) the dimerisation subsided at 30 min, possibly as the H_2O_2 was metabolised from the cell. Although Prx-SO_3 Western blots to test for formation of hyper-oxidised Prxs (with a pan-Prx

antibody specific to the sulfonic acid modification, see **2.1.2.1.1 Primary antibodies**) were attempted at both time-points, but the antibodies were poor and so this will require further analysis in future work.

A

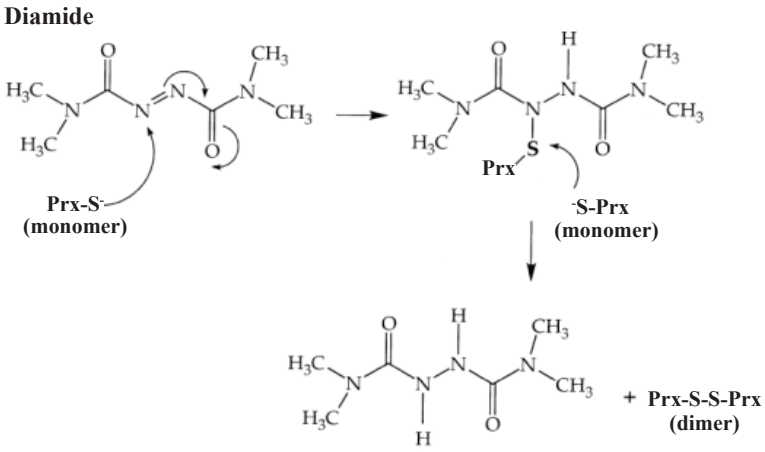

B

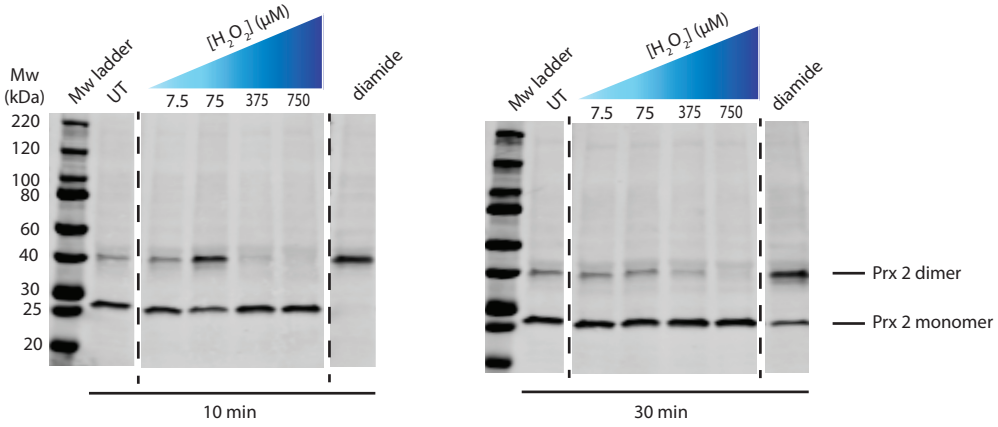

C

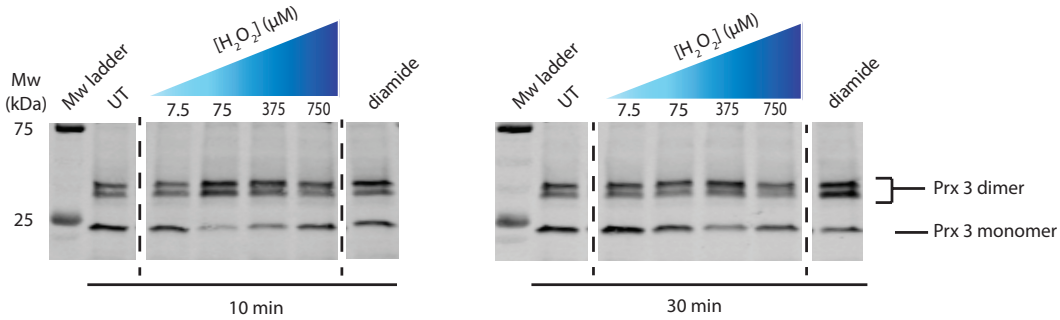

Figure 4.10. Prx 2 (cytosol) and Prx 3 (matrix) dimerisation in C2C12 myotubes in response to boluses of H_2O_2, assayed by Western blot. (A) *Diamide oxidises protein thiols forming*

disulfide bonds (adapted from (Tortorella et al., 1998). ***(B & C)*** *C2C12 myotubes were treated with serially diluted boluses of H_2O_2 (7.5, 75, 375 or 750 µM) or diamide (500 µM) in serum-free media for 10 or 30 min to oxidise cells. Prior to treatment, cells were washed once in 3 ml serum free media. After treatment, cells were incubated in methyl methanethiosulfonate (MMTS) (80 mM) for 10 min at RT to alkylate thiols. Cells were rapidly lysed in ice-cold RIPA buffer supplemented with 80 mM MMTS (250 µl lysis buffer per 6 cm plate). Non-reducing SDS-PAGE (~ 25 µg protein) and Western blotting was performed, see* ***2.6 Peroxiredoxin dimerisation assays.*** *Representative Western blots of Prx 2 and Prx 3 were imaged using the Odyssey® CLx Infrared Imaging System (fluorescence emission at 680 nm (Prx 2) or 800 nm (Prx 3)). After imaging, the middle sections outlined above by vertical black dotted lines were reflected so that lanes containing H_2O_2 treated lysates were arranged low (7.5 µM) to high (750 µM), from left to right for clarity.*

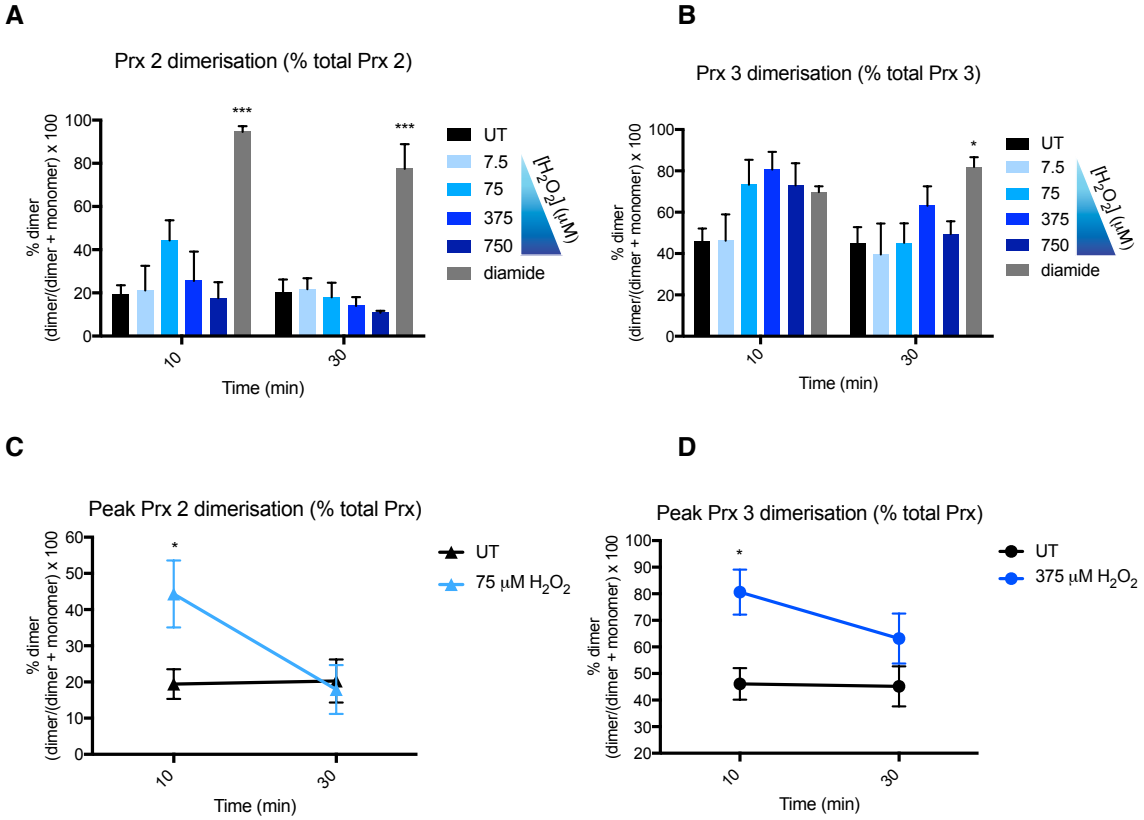

Figure 4.11 Prx 2 (cytosol) and Prx 3 (matrix) dimerisation in C2C12 myotubes in response to boluses of H_2O_2: Western blot quantification. (A - D) *The Western blot signal intensities (SI) of* Prx 2 and Prx 3 dimers *(quantified from* ***Figure 4.10****) were normalised to those of their respective monomer bands and expressed as % dimer (% dimer = (SI dimer / (SI dimer + SI monomer)) x 100). Graphed data is mean ± SEM of n = 3 or mean ± range of n = 2 biological replicates. Statistical analysis was performed by one-way ANOVA (where n ≥ 3) with Dunnett's Multiple Comparison post-test comparing H_2O_2 treatments to UT control, at 10 or 30 min. Means were considered significantly different when P < 0.05. * P < 0.05, ***P < 0.001.* ***(C & D)*** *Graphed data highlights the peak Prx2 and Prx3 dimerisation measured after treatment with 75 µM or 375 µM H_2O_2 boluses, respectively. Data is presented as mean ± SEM of n = 3 biological replicates,*

*expressed as % dimer and analysed by unpaired, one-tailed t tests. Means were considered significantly different when P < 0.05. * P < 0.05.*

AMPK activity markers (AMPKα(T172) and ACC(S79) phosphorylation) were measured in response to cell treatments with serially diluted boluses of H_2O_2 in serum-free media for 10 or 30 min **(Figure 4.12)**. H_2O_2 induced dose-dependent increases in both AMPK and ACC phosphorylation at both time-points, with the 750 µM dose effect being statistically significant and peaking at 30 min.

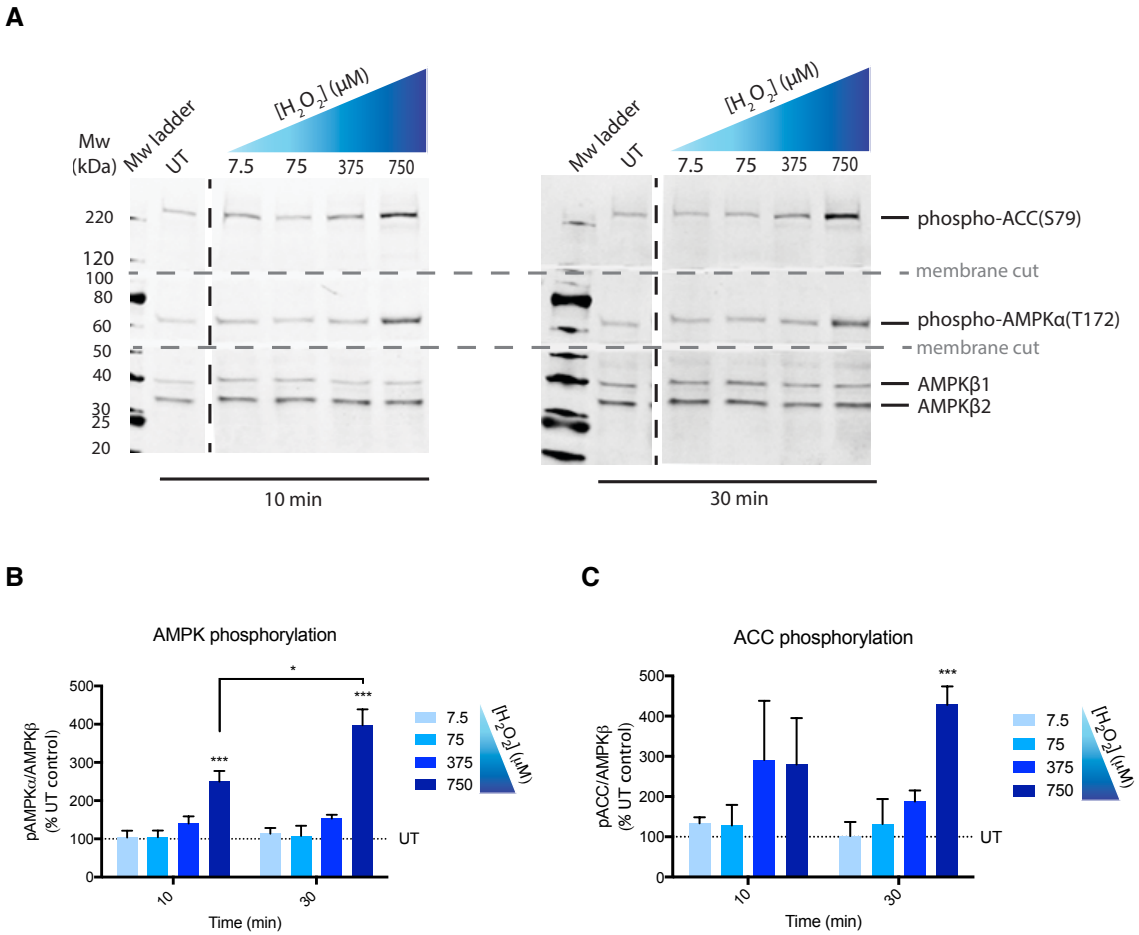

Figure 4.12 AMPK activity markers (phospho-AMPKα(T172) and phospho-ACC(S79)) in C2C12 myotubes in response to boluses of H_2O_2, assayed by Western blot. (A) *C2C12 myotubes were treated with serially diluted boluses of H_2O_2 in serum-free media for 10 or 30 min as described in* ***Figure 4.10****. Cells were lysed in ice-cold Hepes lysis buffer and Western blots were performed as previously described.* ***(B & C)*** *The Western blot signal intensities of* AMPKα1/2-phosphoT172 and ACC1/2-phosphoS79 *target bands (from* ***(A)****) were normalised to those of* AMPKβ2 *as a loading control. Graphed data is mean ± SEM of n = 3 biological replicates expressed as % untreated (UT) control. Statistical analysis was performed by one-way ANOVA with Dunnett's Multiple Comparison post-test comparing H_2O_2 treatments to UT control, at 10 or 30 min. The difference in AMPK phosphorylation at 10 and 30 min was analysed by unpaired, one-tailed t test. Means were considered significantly different when $P < 0.05$. * $P < 0.05$; *** $P < 0.001$.*

In parallel, AMPK specific activity was measured in response to H_2O_2 treatment **(Figure 4.13)**. H_2O_2 induced dose-dependent increases in specific activity at both time-points (with the 750 µM dose effect reaching statistical significance), but the effect was diminished at 30 min. These overall results largely agree with the phosphorylation assays, but differ in that specific activity peaked at 10 min but AMPK phosphorylation peaked at 30 min. It was also apparent that increasing AMPK specific activity at 10 min coincided with loss of Prx 2 dimerisation (a proxy of cytosolic hyper-oxidation) at high [H_2O_2] (> 75 µM). AMPK specific activity also somewhat correlated with increased Prx 3 dimerisation (mitochondrial matrix oxidation). Across the markers of AMPK activation tested, statistically significant AMPK activation only occurred at supra-physiological concentrations of H_2O_2.

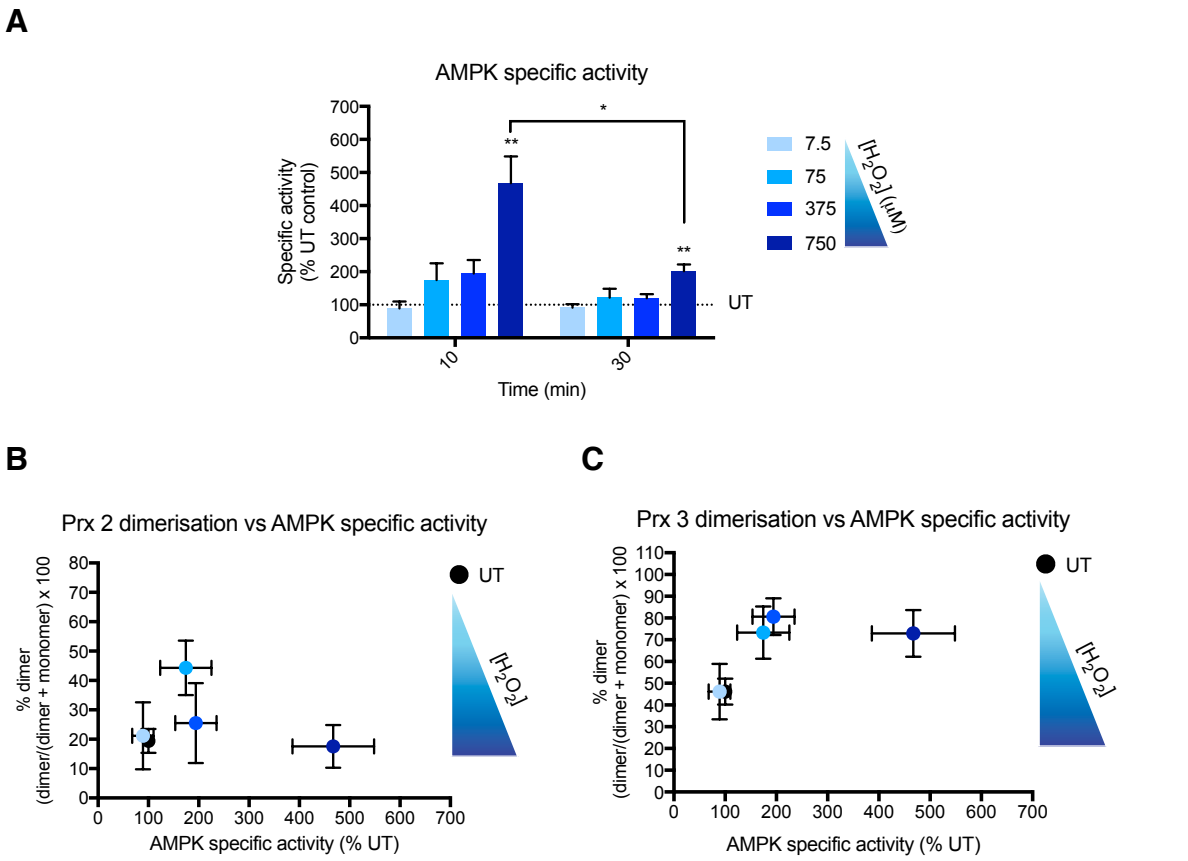

Figure 4.13 AMPK specific activity in C2C12 myotubes in response to boluses of H_2O_2, assessed by the AMPK SAMS kinase assay. (A) *SAMS kinase assays were performed on AMPK immunoprecipitated from 100 µg protein from freshly thawed cell lysate aliquots, described in* ***Figure 4.12****. Graphed data is mean ± SEM of n = 3 or mean ± range of n = 2 biological replicates, measured as pmol [γ-^{32}P]ATP/µg cell protein/min and expressed as % untreated (UT) control.*

*Statistical analysis performed by one-way ANOVA (where n ≥ 3) with Dunnett's Multiple Comparison post-test comparing H_2O_2 treatments to UT control, at 10 or 30 min. The difference in AMPK specific activity at 10 and 30 min was analysed by unpaired, one-tailed t test. Means were considered significantly different when P < 0.05. * P < 0.05; ** P < 0.01.* ***(B)*** *Graphed data shows that loss of Prx 2 dimerisation (hyper-oxidation) in response to high [H_2O_2] (>75 µM) (from* ***Figure 4.11 (10 min)****), coincides with increasing AMPK specific activity.* ***(C)*** *Graphed data shows that increasing Prx 3 dimerisation (from* ***Figure 4.11 (10 min)****) coincides with increasing AMPK specific activity. Data is presented as mean ± SEM of n = 3 or mean ± range of n = 2 biological replicates.*

Next, ATP/ADP ratios were measured in cells treated with the H_2O_2 boluses **(Figure 4.14)**. H_2O_2 appeared to have a dose-dependent effect on ATP/ADP ratios: the 750 µM bolus decreased the cell ATP/ADP ratios at 10 min to 73.1 ± 8.2 % UT control (mean ± SEM of n = 3 biological replicates) but the ATP/ADP ratios appeared to recover at 30 min (94.2 ± 6.5 % UT control). It also became apparent that the decreasing ATP/ADP ratios at 10 min coincided with loss of Prx 2 dimerisation and increasing Prx 3 dimerisation, as did AMPK specific activity **(Figure 4.13)**. Although cytosolic oxidation (Prx 2 dimerisation) occurred in response to H_2O_2 boluses lower than 750 µM without appearing to decrease the cell ATP/ADP ratios, AMPK activity did not significantly change, suggesting that AMPK activity only responds to the cell ATP/ADP ratio and not directly to the H_2O_2.

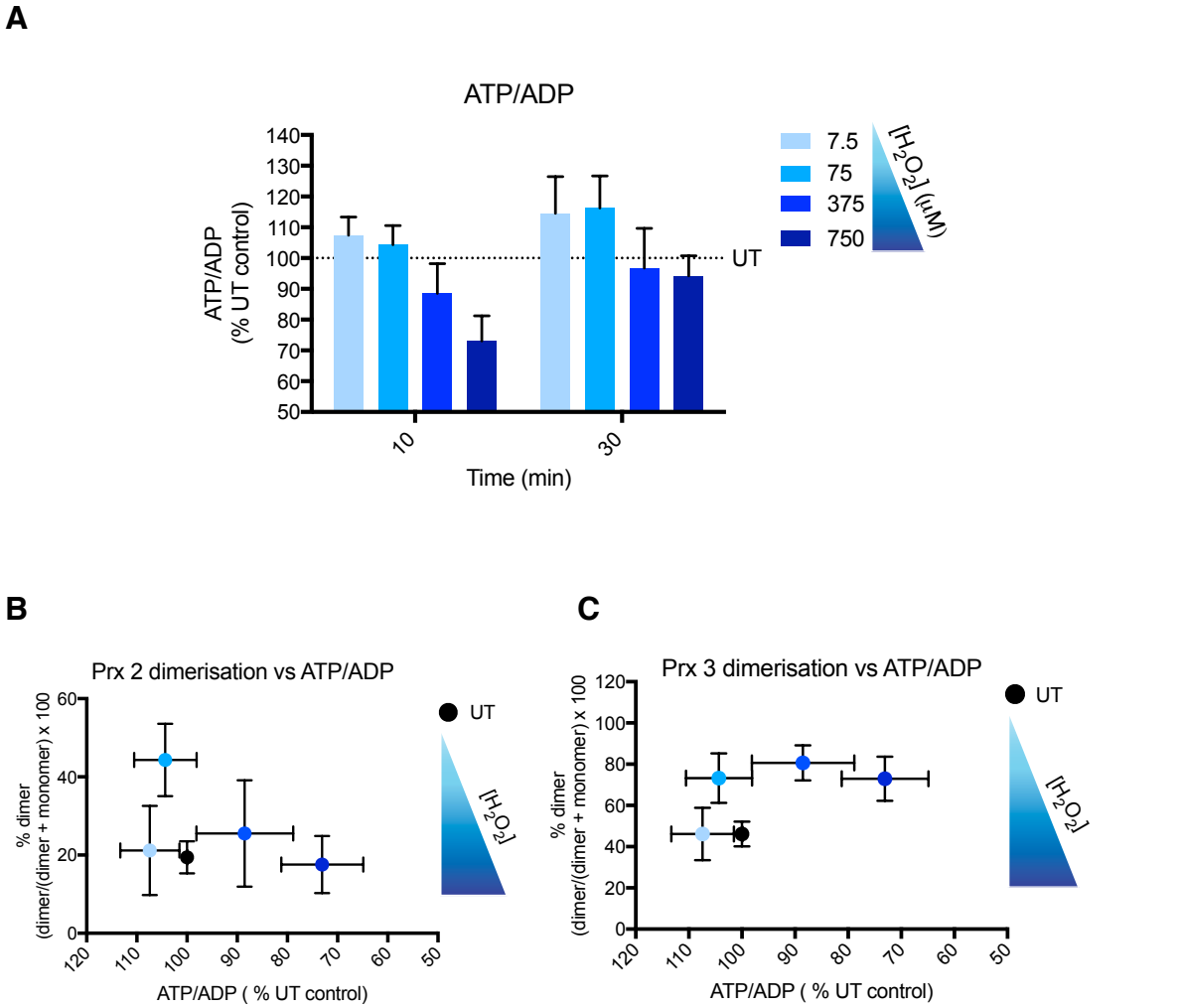

Figure 4.14 ATP/ADP ratios in C2C12 myotubes in response to boluses of H_2O_2, measured by a luciferase/luciferin bioluminescence assay. (A) *C2C12 myotubes were treated with serially diluted boluses of H_2O_2 in serum-free media for 10 or 30 min as described in* ***Figure 4.10****. Cells were rapidly lysed in ice-cold PCA and ATP/ADP assays were performed as previously described. Graphed data is mean ± SEM of n = 3 biological replicates, expressed as % untreated (UT) control. Statistical analysis was performed by one-way ANOVA with Dunnett's Multiple Comparison post-test comparing H_2O_2 treatments to UT control, at 10 or 30 min. Means were considered significantly different when $P < 0.05$. $[H_2O_2]$ at 10 min (750 μM): $P = 0.0589$.* ***(B & C)*** *Graphed data shows loss of Prx 2 dimerisation (hyper-oxidation) at 10 min in response to high $[H_2O_2]$ (>75 μM) or increasing Prx 3 dimerisation coincides with decreasing ATP/ADP ratios in cells. Data is presented as mean ± SEM of n = 3 or mean ± range of 2 biological replicates.*

Further comparison of AMPK activity and ATP/ADP ratios from H_2O_2-treated cells to those treated with control compounds using the calibration graphs **(Figure 4.15)** confirmed that the increase in AMPK activity markers correlated with decreasing ATP/ADP ratios. The specific activity spike and high phosphorylation at 10 min might thus be considered AMP/ADP-dependent events due to a ~ 27% decrease in the cell ATP/ADP ratio at this time-point, which approached recovery at 30 min. At this later time-point the specific activity of AMPK was also partially ablated. The maintained high phosphorylation of AMPK at 30 min might be evidence of ROS-induced inhibition of dephosphorylation, previously shown to play a minor role in AMPK activation in response to H_2O_2 (Auciello et al., 2014). Under this assumption, it could be possible that hyper-oxidation from the 750 μM H_2O_2 bolus maintained and increased AMPK phosphorylation, even as the allosteric activation decreased when cell ATP/ADP ratios recovered. The spike in AMPK specific activity at 10 min might also be evidence of a small effect of the cysteine thiol oxidation mechanism proposed by (Zmijewski et al., 2010). These possibilities are currently speculative and are further detailed in **4.3 Discussion and future work**. From the combined results, however, I concluded that the cell ATP/ADP ratio is the key determinant of AMPK activity in H_2O_2-treated C2C12 myotubes, impacted on by cellular hyper-oxidation in response to supra-physiological concentrations of H_2O_2. There is no evidence of AMPK activation by biologically relevant concentrations of H_2O_2 in the absence of energy stress.

A

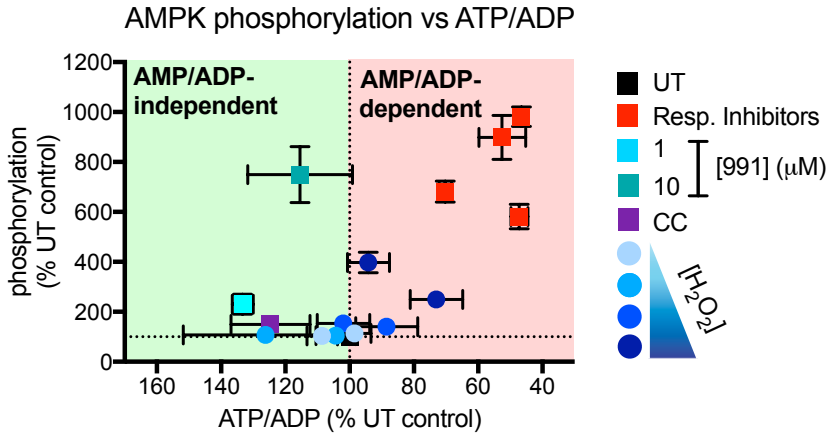

B

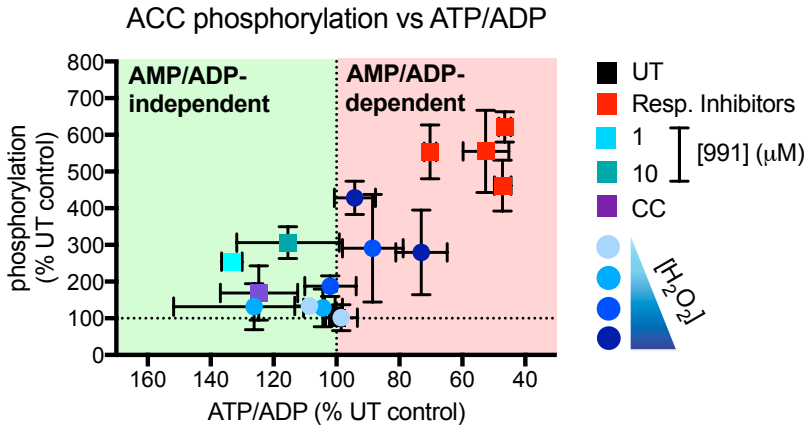

C

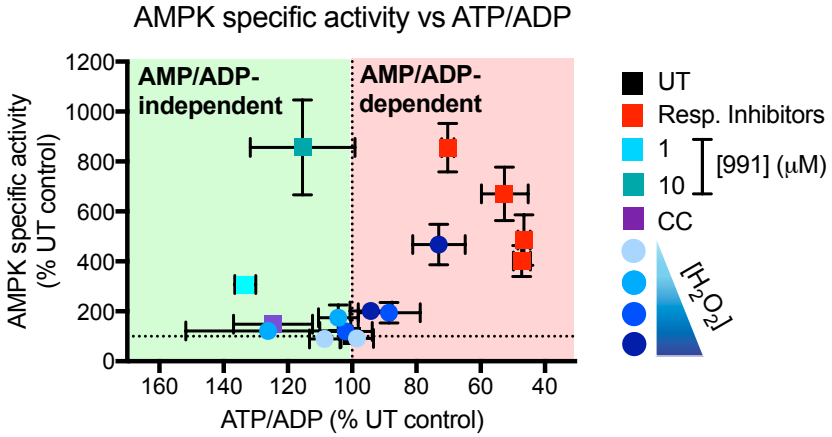

Figure 4.15 Calibration graphs showing the relationship between AMPK activation markers and ATP/ADP ratios in C2C12 myotubes in response to H_2O_2, compared to AMP/ADP-dependent and AMP/ADP-independent AMPK activators. (A - D) *Graphed data shows AMPK activation markers* ***(A)*** *AMPKα(T172) phosphorylation* ***(B)*** *ACC(S79) phosphorylation and* ***(C)*** *AMPK specific activity, plotted against their respective cell ATP/ADP ratios. Plotted along side the*

control compounds (respiratory chain inhibitors, selective AMPK activator (991) and inhibitor (CC)) is the H_2O_2 titration (10 and 30 min). Data is graphed as mean ± SEM of n ≥ 3 or mean ± range of n = 2 biological replicates. All values are expressed as % UT control. The graph shows AMP/ADP-dependent (red background) and AMP/ADP-independent (green background) distinct signatures of AMPK activation, as previously described.

4.2.4 Effects of mitochondrial ROS on cellular redox state, AMPK activity and ATP/ADP ratios

To test the effects of mitochondrial ROS on AMPK activity, C2C12 myotubes were treated with the mitochondria-targeted redox cycler, MitoParaquat (MPQ), which generates superoxide rapidly and selectively within mitochondria (Robb et al., 2015) **(Figure 4.16).**

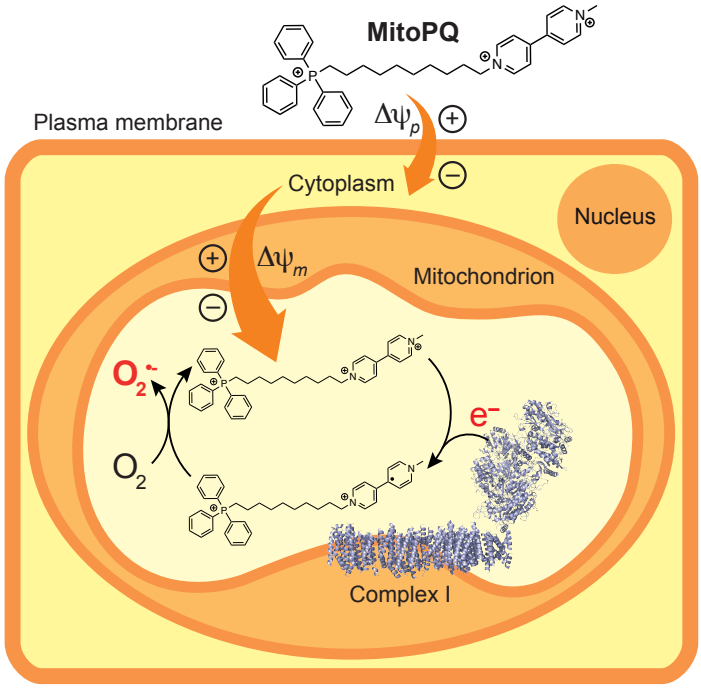

Figure 4.16. Uptake of MitoParaquat (MPQ) by the mitochondria and generation of superoxide from complex I. *MPQ is comprised of a triphenylphosphonium lipophilic cation conjugated to the redox cycler, paraquat by a carbon linker. MPQ accumulates selectively in the mitochondrial matrix, driven by the membrane potential, where MPQ produces superoxide by redox cycling at the flavin mononucleotide (FMN) site of complex I, selectively increasing superoxide production within mitochondria (Robb et al., 2015).*

To confirm that ROS was being generated in the mitochondrial matrix and not in the cytosol, I tested the effects of increasing concentrations of MPQ on Prx 3 (matrix) and Prx 2 (cytosol) dimerisation **(Figure 4.17 & 4.18)**. Again, diamide was used as a positive control for maximal Prx 2 and Prx 3 dimerisation. MPQ caused dose-dependent and cumulative increases in mitochondrial Prx 3 dimerisation from

6 h to 24 h, but had no effect on cytosolic Prx 2 dimerisation, suggesting that the ROS generated in the mitochondrial matrix was not transmitted to the cytosol.

Prx 3 dimerisation was maintained at 24 h at close to maximal levels, presumably as a result of continuous low-grade ROS production by MPQ in the matrix and not a single high-dose bolus of H_2O_2 that has rapid effects. Similarly, Prx 2 dimerisation caused by diamide was only observed at 30 min and not at later time-points, suggesting the diamide was either being metabolized and Prx 2 dimerisation reversed or Prx 2 was becoming hyper-oxidised with formation of sulfinic or sulfonic acid modifications that present as loss of dimerisation. Prx 3 dimerisation in response to diamide was only slightly diminished at 6 and 24 h, possibly for the same reasons that H_2O_2 had more observable effects on Prx 3 dimerisation than on Prx 2 dimerisation: 1) diamide-Prx oxidation may be slower in the mitochondrial matrix compared to the cytosol for equivalent [diamide]; 2) it may take longer for the diamide to transfer into the mitochondrial matrix than the cytosol, making the local [diamide] in the matrix lower than in the cytosol; 3) some diamide metabolism may have occurred in the cytosol before reaching the matrix.

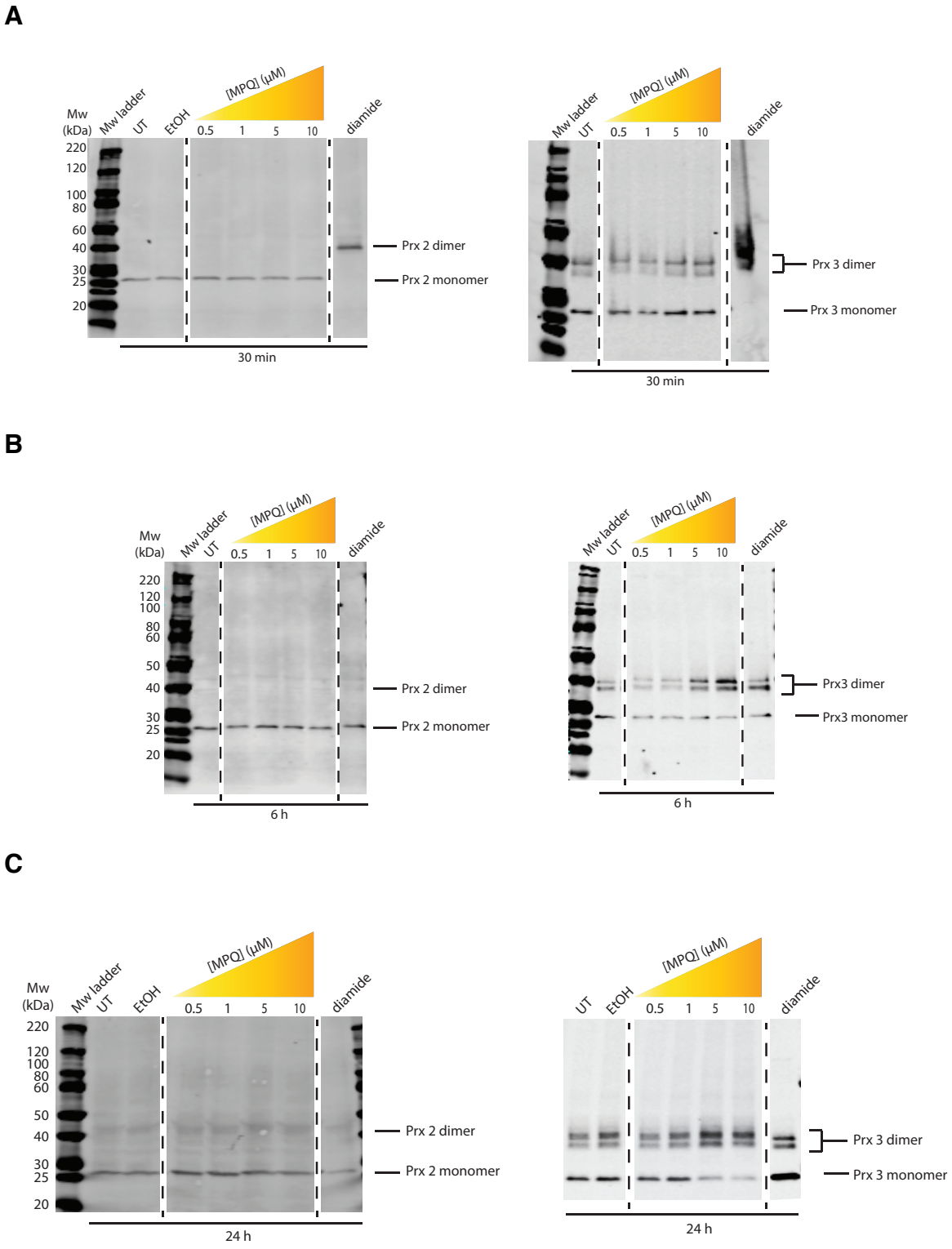

Figure 4.17 Prx 2 (cytosol) and Prx 3 (matrix) dimerisation in C2C12 myotubes in response to MPQ, assayed by Western blot. *C2C12 myotubes were treated with MPQ (500 nM, 1 μM, 5 μM or 10 μM), or EtOH as a vehicle control or diamide (500 μM) as a positive control for thiol oxidation in fresh media for* ***(A)*** *0.5 h,* ***(B)*** *6 h or* ***(C)*** *24 h to selectively increase mitochondrial ROS production. Cells were rapidly lysed in ice-cold RIPA buffer and Prx dimerisation assays were performed as described in* ***Figure 4.9****. Representative Western blots* ***(A - C)*** *were imaged*

using the Odyssey® CLx Infrared Imaging System (fluorescence emission at 680 nm (for Prx 2) or 800 nm (for Prx 3)). After imaging, the middle sections outlined above were reflected so that lanes containing MPQ treated lysates were arranged low (500 nM) to high (10 µM), from left to right for clarity.

A

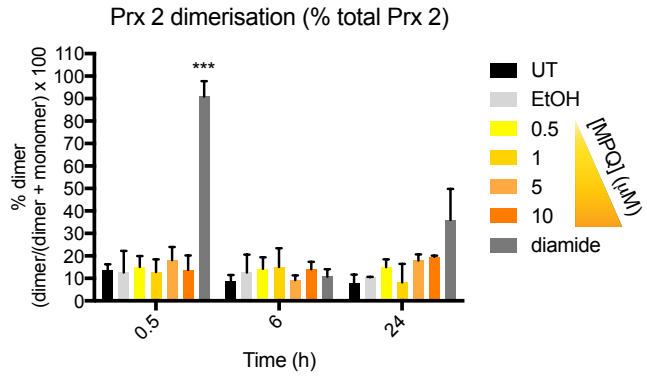

B

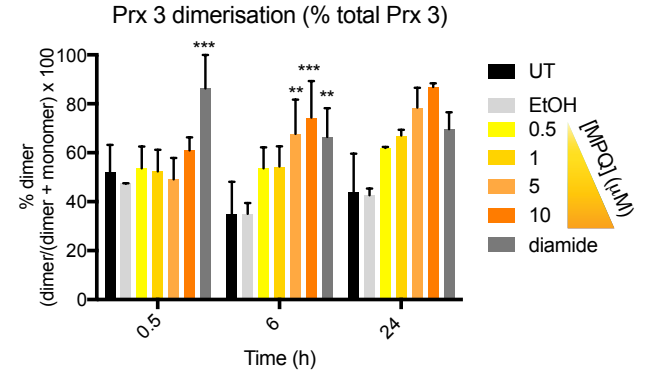

C

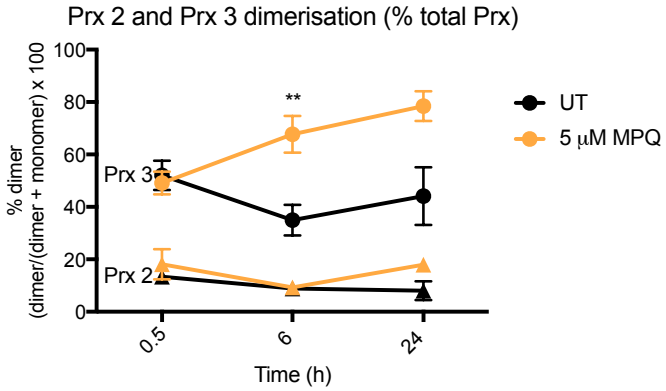

Figure 4.18 Prx 2 (cytosol) and Prx 3 (matrix) dimerisation in C2C12 myotubes in response to MPQ: Western blot quantification. (A - C) *The Western blot signal intensities (SI) of Prx 2* ***(A)*** *and Prx 3* ***(B)*** *dimers (quantified from* ***Figure 4.17****) were normalised to those of their respective monomer bands and expressed as % dimer (% dimer = (SI dimer / (SI dimer + SI monomer)) x*

*100). **(A & B)** Graphed data (0.5 h) is mean ± SEM of n ≥ 3 or mean ± range of n = 2 (EtOH) biological replicates; graphed data (6 h) is mean ± SEM of n ≥ 3 biological replicates; graphed data (24 h) is mean ± range of n = 2 biological replicates. Statistical analysis was performed by one-way ANOVA (where n ≥ 3) with Dunnett's Multiple Comparison post-test comparing MPQ treatments or EtOH to UT control, at 0.5 or 6 h time-points. Means were considered significantly different when P < 0.05. ** P < 0.01, *** P < 0.001. **(C)** Graphed data highlights the cumulative increase in Prx 3 dimerisation by MPQ. Data is presented as mean ± SEM of n ≥ 3 or mean ± range of n = 2 (24 h) biological replicates, analysed by unpaired, one-tailed t tests compared to individual UT controls. Means were considered significantly different when P < 0.05. ** P < 0.01.*

AMPK activity markers in cells were then tested in response to increasing [MPQ] **(Figure 4.19).** MPQ had low-grade effects on ACC phosphorylation at 6 h (237 ± 46 % UT control after 5 μM MPQ (mean ± SEM of n = 4)), however this was not statistically significant compared to the vehicle (EtOH) control. Prx 3 (matrix) dimerisation was first observed at this time-point. Low-grade ACC phosphorylation appeared to be sustained at 24 h, as was Prx 3 dimerisation, without any evidence of oxidation of the cytosol. The results suggest that the low-grade AMPK activation (measured as ACC phosphorylation) occurred independently of a change in the redox state of the cytosol but coinciding with a redox change in the matrix. Supporting data is currently limited: MPQ effects on AMPK phosphorylation were only observed at 24 h and were highly variable at 233 ± 144% of UT control (mean ± range of n = 2) and AMPK specific activity has not yet been measured, so future experiments will be required to expand the results.

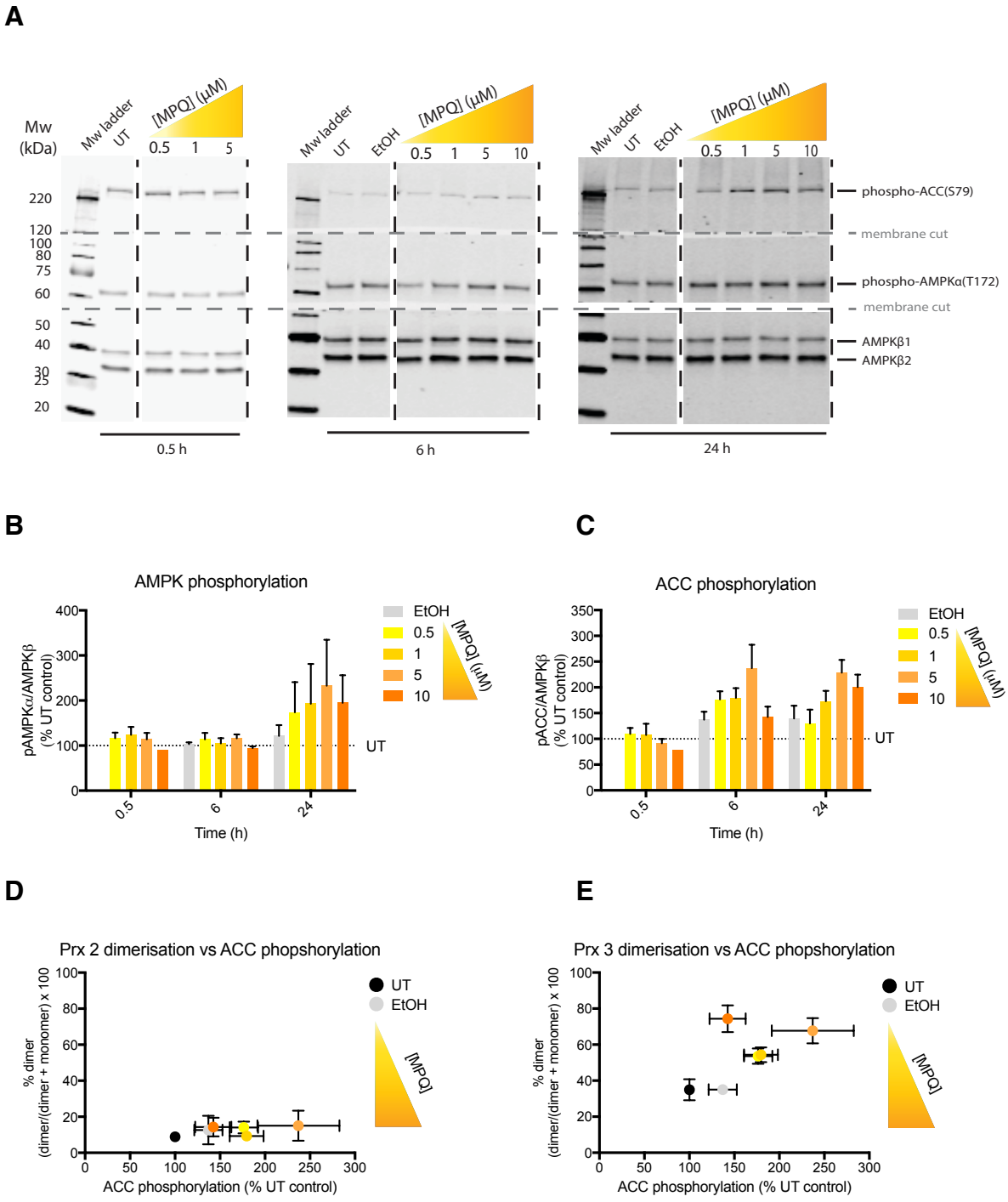

Figure 4.19 AMPK activity markers (phosphorylation) in C2C12 myotubes in response MPQ, assayed by Western blot. (A) *C2C12 myotubes were treated with MPQ (500 nM, 1 μM, 5 μM or 10 μM) or EtOH as a vehicle control, as described in* ***Figure 4.17.*** *Cells were rapidly lysed in ice-cold Hepes lysis buffer and Western blots were performed as previously described.* ***(B & C)*** *The Western blot signal intensities of* ***(B)*** *AMPKα1/2-phosphoT172 and* ***(C)*** *ACC1/2-phosphoS79 target bands (from* ***(A)****) were normalised to those of AMPKβ2 as a loading control. Graphed data is mean ± SEM of n ≥ 3 biological replicates expressed as % untreated (UT) control, except for 10 μM MPQ at 30 min (n = 1), and the 24 h treatments (mean ± range of n = 2)* ***(D & E)*** *Graphed data shows the*

relationship between Prx dimerisation and ACC phosphorylation in MPQ-treated cells at 6 h. Data is presented as mean ± SEM of n ≥ 3 biological replicates.

MPQ had no statistically significant effect on cell ATP/ADP ratios at 30 min **(Figure 5.20)**, however, a low dose of MPQ appeared to increase ATP/ADP ratios by an as yet unclear mechanism. At 6 h, ATP/ADP ratios appeared to slightly decrease with increasing [MPQ], with an ATP/ADP ratio of 86.5 ± 2.8 % UT control (mean ± SEM of n = 4 biological experiments) in cells treated with 10 µM MPQ, however this did not reach statistical significance. The ATP/ADP ratio trend appeared to correlate with increasing Prx 3 (matrix) dimerisation and occurred in the absence of Prx 2 (cytosolic) dimerisation. These results suggest that a change in the redox state of the mitochondrial matrix by ROS produced by MPQ may cause slight decreases in cell ATP/ADP ratios.

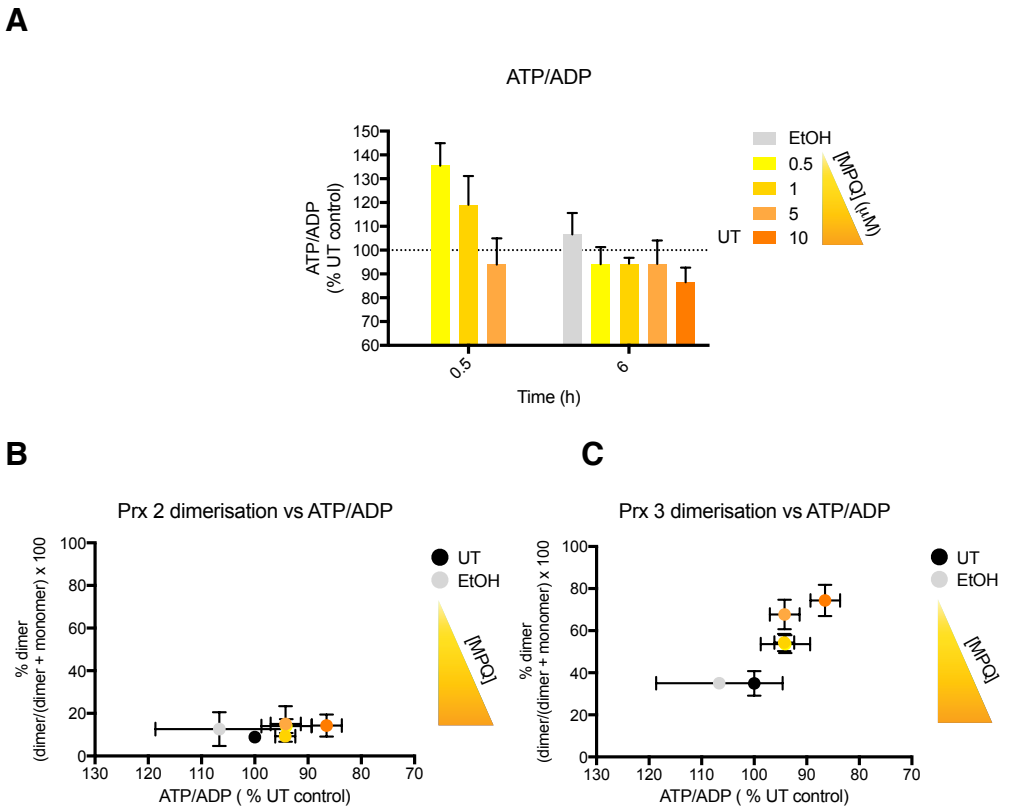

Figure 4.20 ATP/ADP ratios in C2C12 myotubes in response to MPQ, measured by a luciferase/luciferin bioluminescence assay. (A) *C2C12 myotubes were treated with MPQ (500 nM – 10 µM, or EtOH as a vehicle control) as described in* ***Figure 4.17****. Cells were rapidly lysed in ice-cold PCA and ATP/ADP assays were performed as previously described. Graphed data is mean ± SEM of n ≥ 3 biological replicates, expressed as % untreated (UT) control.* ***(B & C)*** *Graphed data*

shows the relationship between Prx dimerisation and ATP/ADP ratios in MPQ-treated cells at 6 h. Data is presented as mean ± SEM of n ≥ 3 biological replicates.

When compared to control compounds of AMP/ADP-dependent (red background) and AMP/ADP-independent (green background) AMPK activation **(Figure 4.21)**, it was apparent that both H_2O_2- and MPQ-induced activation of AMPK (low-grade with respect to MPQ) appear to follow an AMP/ADP-dependent mechanism, only occurring when the cell ATP/ADP ratios are decreased.

A

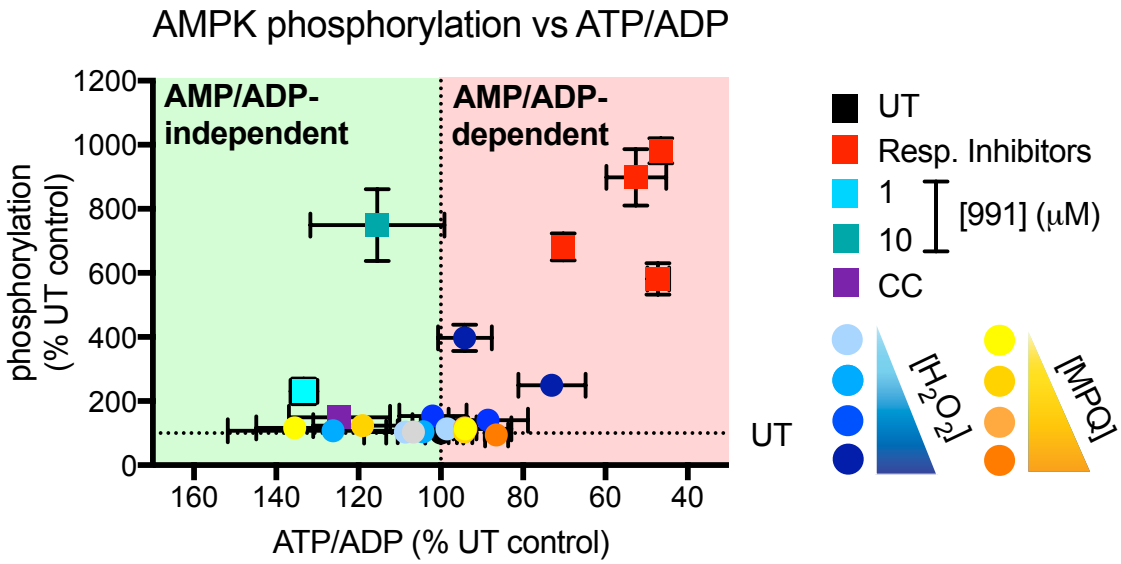

B

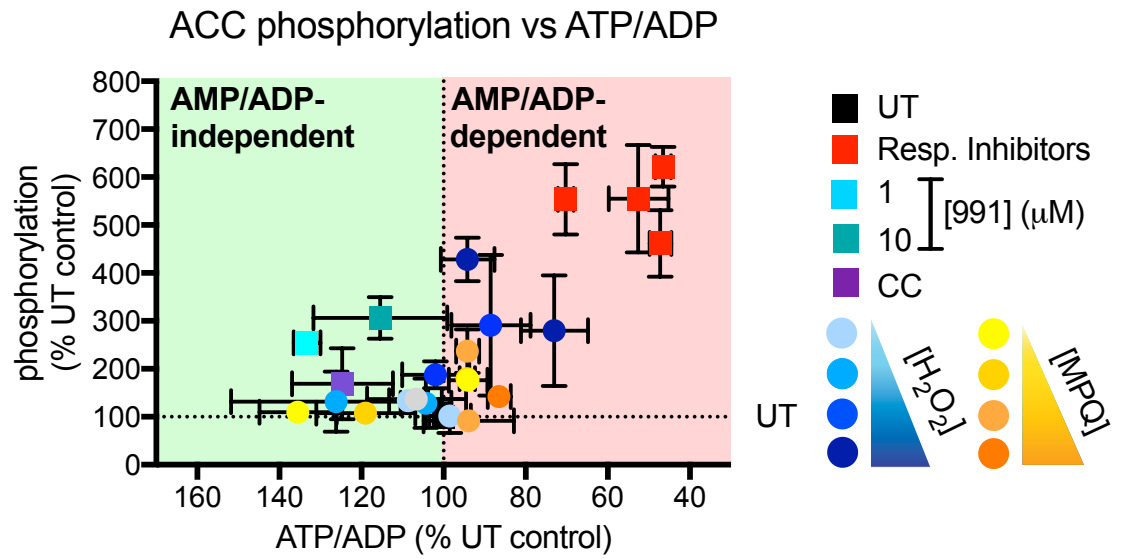

Figure 4.21 Relationship between AMPK activity markers and ATP/ADP ratios in C2C12 myotubes in response to MPQ, compared to AMP/ADP-dependent and AMP/ADP-independent AMPK activators. (A & B) *Graphed data shows AMPK activation markers* ***(A)*** *AMPKα1/2-T172 phosphorylation and* ***(B)*** *ACC1/2-S79 phosphorylation plotted against their respective cell ATP/ADP ratios. Plotted along side the control compounds (respiratory chain inhibitors, selective AMPK activator (991) and inhibitor (CC)) is the H_2O_2 titration (10 and 30 min) and the MPQ titration (0.5 & 6 h). All data points are graphed as mean ± SEM of n ≥ 3 or mean ± range of n = 2 biological replicates. All values are expressed as % UT control.*

4.3 Discussion and future work

In summary, the results from this chapter have indicated that in differentiated C2C12 mouse skeletal myotubes, exogenous H_2O_2 and selective mitochondria-generated ROS both activate AMPK in a primarily AMP/ADP-dependent way. H_2O_2 boluses greater than 7.5 µM oxidised Prx 2 in the cytosol, an important redox-regulated protein that protects against oxidative stress and can also participate in redox-relays that facilitate H_2O_2 signalling (Sobotta et al., 2015). AMPK was not significantly activated by exogenous H_2O_2 until treatment with the 750 µM bolus, at which point there was evidence of oxidative stress: loss of Prx 2 dimerisation and cell ATP/ADP ratios appeared to decrease. In response to this oxidative stress, a high level of AMPK activity was observed at 10 min post bolus addition and at a lower level at 30 min as ATP/ADP ratios appeared to recover. On the other hand, selective mitochondria-generated ROS by the redox-cycler, MPQ, increased matrix Prx 3 oxidation over time. There was no detectable Prx 2 dimerisation over time, indicating that the ROS was contained within the mitochondria and was not transmitted to the cytosol where AMPK is located. At 6 h, there appeared to be slight decreases in the cell ATP/ADP ratio and slight increases in ACC phosphorylation, a marker of AMPK activity. The effects were not statistically significant and raised important questions relating to the compartmentalization of ROS in cells, discussed further below.

The results discussed in this chapter compliment and expand previous studies into the role of ROS in AMPK activity (Auciello et al., 2014, Hawley et al., 2010, Zmijewski et al., 2010). An AMP/ADP-independent redox mechanism for AMPK activation was proposed in (Zmijewski et al., 2010), in which the authors detected redox changes to conserved cysteine residues in the AMPK catalytic subunit in response to continuous, extracellular H_2O_2 generation by glucose oxidase. Here, the H_2O_2 stimulus was sustained and not metabolized rapidly as are individual boluses of H_2O_2. The authors observed increases in AMPK activity in extracellular experiments and in HEK 293 cells without detectable decreases in cell ATP/ADP

ratios and thus credited the activation to cysteine-oxidation induced allosteric activation. Building upon this and other previous studies, (Auciello et al., 2014) also utilised the glucose oxidase method of extracellular H_2O_2 generation, using HEK 293 cells expressing the AMP/ADP-insensitive AMPK γ subunit R531G (RG) mutant, which renders AMPK unable to be allosterically activated by AMP or allosterically protected from dephosphorylation by AMP or ADP. In this study, the authors no longer observed high levels of AMPK activity even as ATP/ADP ratios were significantly decreased, however, they did observe a low-grade but statistically significant increase in AMPK activity with time. The authors also tested the effects of single high-dose H_2O_2 boluses on the RG mutant expressing cells. Again, high levels of AMPK activity were no longer observed in these cells even as ATP/ADP levels decreased. But again, small increases in AMPK activity were observed at 10 min, decreasing with time, as the H_2O_2 was metabolized from the cell. The authors excluded the action of Ca^{2+}-activated CaMKKβ as an alternative AMPK kinase in response to H_2O_2. Thus, the authors concluded that activation of AMPK by exogenous H_2O_2 is primarily an AMP/ADP-dependent event, and that different sensitivities in measuring cell ATP/ADP ratios may have played a role in the discrepancies between their study and that of (Zmijewski et al., 2010). However, (Auciello et al., 2014) did show evidence that H_2O_2 may play a minor role in AMPK regulation by inhibiting AMPK dephosphorylation, potentially by H_2O_2-induced inhibition of upstream phosphatases.

My work largely agrees with (Auciello et al., 2014), in that I only observed significant increases in AMPK activity markers in response to boluses of H_2O_2 when cell ATP/ADP ratios appeared to be decreased **(Figure 4.12 – 4.14)**. The benefit of treating cells with boluses of H_2O_2 and not glucose oxidase, which maintains steady or increasing levels of extracellular H_2O_2 with time, is that time-dependent effects of H_2O_2 and its degradation can be observed. In a change from (Auciello et al., 2014), I administered the H_2O_2 boluses in serum-free media, to eliminate catalase and other proteins in serum that may speed up the degradation of extracellular H_2O_2. I also simultaneously monitored the redox state of the H_2O_2

scavenger, Prx, in different cellular subcompartments, as a read-out of the intracellular effects of extracellular H_2O_2 boluses. I observed that immunoprecipitated AMPK kinase activity was increased at 10 min (which appeared to coincide with decreased ATP/ADP ratios). The specific activity later decreased at 30 min (as cell ATP/ADP ratios recovered) but remained significantly increased from baseline **(Figure 4.13)**. I also observed the possibility that H_2O_2 may inhibit AMPK and ACC dephosphorylation, as AMPK and ACC phosphorylation were maintained and increased at 30 min post bolus addition **(Figure 4.12)**, even as cell ATP/ADP ratios appeared to recover **(Figure 4.14)**. Protein phosphatases are reported to be sensitive to oxidative stress, although by an unclear mechanism (Jin Jung et al., 2013). Thus, one explanation for this result is that while dephosphorylation of AMPK and ACC may have been independently inhibited in cells due to H_2O_2 inhibition of phosphatases, allosteric activation of AMPK may have been decreased at 30 min due to a removal of the allosteric effects of AMP. Another possibility is that the redox-dependent mechanism reported in (Zmijewski et al., 2010) may have contributed to increased AMPK specific activity at 10 min, and decreased at 30 min as H_2O_2 was further metabolized and degraded. Although I performed the extracellular kinase assays in reducing conditions, cysteine thiol glutathionylation, reported to promote kinase activity (Zmijewski et al., 2010), may have been preserved. The authors of (Auciello et al., 2014) also did not exclude the possibility of the cysteine oxidation mechanism playing a minor role in this model of AMPK activation.

Regarding my experiments using exogenous H_2O_2 boluses, a number of experiments can be performed in future work in order to expand and clarify the results. In analyzing the Prx dimerisation data set, it is currently unclear if the H_2O_2 boluses were degraded between the 10 min and 30 min time-points or if the H_2O_2 continued to hyper-oxidise the Prx pools, presenting as loss of dimerisation (here I refer to a detailed study which investigated the metabolism of H_2O_2 boluses and Prx dynamics (Sobotta et al., 2013)). However, this study was performed in a different cell model and I note that in C2C12 myotubes, the cell

ATP/ADP ratios recovered at 30 min from an apparent decrease at 10 min, which suggests the H_2O_2 was being degraded. Although Prx-SO_3 Western blots to test for formation of hyper-oxidised Prxs were attempted, the Western blots were poor and will require optimisation in future work. Similarly, some intracellular H_2O_2-measurement experiments on live cells were attempted using cytosol or mitochondrial matrix targeted fluorescent H_2O_2 probes, visualized by confocal microscopy: cyto-roGFP-Orp1 or mito-roGFP-Orp1 (Albrecht et al., 2011), discussed in **2.7 Live cell confocal microscopy and imaging**. High sensitivity to H_2O_2 boluses (50 µM) was observed in transiently transfected undifferentiated C2C12 myoblasts in preliminary experiments (data not shown). However, as previously discussed, protein expression profiles are different in undifferentiated C2C12 myoblasts compared to differentiated C2C12 myotubes so H_2O_2 metabolism may also be different. Thus, the experiment was repeated using stable C2C12 cell lines expressing the genes so that H_2O_2 levels in differentiated C2C12 myotubes could also be analysed. As differentiated C2C12 myotubes are non-proliferating, transient transfection with the current retroviral host vector posed technical difficulties so the cells were transfected and selected in the undifferentiated, myoblast state before initiating differentiation of the stable, transgene-expressing cells. In preliminary experiments, it was observed that H_2O_2 –sensitivity was greatly decreased in stable C2C12 cell lines expressing the cyto-roGFP-Orp1 or mito-roGFP-Orp1 gene (in both the undifferentiated (myoblast) or the differentiated (myotube) state), compared to transiently transfected C2C12 myoblasts. The reasons for the decreased sensitivity are currently unclear, but it may be possible that some post-translational modifications of the probes occurred in the cells which affected the sensitivity, particularly as the stable cell lines were expressing the genes constitutively. Thus, in future work I aim to optimise this experiment because real-time data showing relative levels of intracellular H_2O_2 and its degradation will be valuable in elucidating a clear picture of how AMPK activity responds to H_2O_2.

I expanded the work of (Auciello et al., 2014, Zmijewski et al., 2010) by investigating the effects of selective mitochondrially-derived ROS on AMPK activity, as we and other labs hypothesize that mitochondria may be a key source of physiologically relevant ROS in the cell. I hope to use the roGFP-Orp1 or other probes to further analyze ROS production by MPQ and characterize the spatio-temporal characteristics of mitochondrially-derived ROS: i.e. does ROS generated in the mitochondrial matrix transfer to the cytosol at a detectable level and thus affect signalling processes there, or is mitochondrially-derived ROS compartmentalized within healthy mitochondria, only being released upon damage to the mitochondria? Although extracellular boluses of H_2O_2 were capable of oxidising the mitochondrial matrix, suggesting that H_2O_2 can transfer across the mitochondrial membranes, matrix Prx 3 dimerisation only increased at supra-physiological concentrations of H_2O_2 (≥ 75 uM bolus). As previously discussed, it is possible that cytosolic Prx 2 hyper-oxidation may have started to occur at this bolus concentration. If confirmed, this would indicate oxidative damage, not physiologically relevant redox-signalling. On the other hand, MPQ generated superoxide selectively and cumulatively within the mitochondrial matrix, inducing ~ 87% Prx 3 dimerisation at 24 h, compared to ~ 44% dimerisation in untreated cells. Even with this high level of mitochondrial ROS production, there was no detectable increase in cytosolic Prx 2 dimerisation, suggesting that the ROS was contained within the matrix. Furthermore, at 6 h, the ATP/ADP ratio was only slightly decreased, measuring at ~ 87% UT control and was not statistically significant. Combined with the supporting data showing undetectable changes in AMPK phosphorylation and only slight increases in ACC phosphorylation, the experiment suggested that the cells were not undergoing a high level of stress. It is possible that mitochondrial compartmentalization of matrix-generated ROS is dependent on the expression levels of ROS scavenging proteins, and this may be cell type specific (Shao et al., 2014, Auciello et al., 2014). Thus, in this model it would be interesting to modulate the protein expression level of Trx 2 in the mitochondrial matrix, which catalyses the reversal of inactive Prx dimers back to functional monomers, preventing oxidative damage. Furthermore, it has been reported that

the action of Trx 1 in the cytosol prevents oxidation and inactivation of AMPK in the heart (Shao et al., 2014). As this remains the only report of reversible redox-dependent AMPK inhibition, it is possible that in different cells types with different ROS scavenging protein profiles, the same levels of ROS can either part-take in reversible redox signalling, or irreversible oxidative damage.

A further point of interest that has arisen from the comparison of whole cellular oxidation versus selective mitochondrial oxidation are the relative effects on cell ATP/ADP ratios. Combined cytosolic and mitochondrial matrix oxidation had a more severe effect on ATP/ADP ratios **(Figure 4.14)** (and thus AMPK activity) than mitochondrial matrix oxidation alone **(Figure 4.20)**. Although, as previously discussed, differentiated C2C12 myotubes have relatively high mitochondrial content, glycolysis remains a key source of ATP production in this cell model, as in all commonly used cell lines. Evidence of this can be observed in **Figure 4.5**, as inhibition of mitochondrial ATP production by oligomycin, which inhibits F_OF_1ATP synthase, decreased cell ATP/ADP ratios by ~ 53%, suggesting that glycolysis was also an important source of ATP. One possible reason for the more severe effects of whole cellular oxidation on ATP/ADP ratios is ROS-induced inhibition of glycolysis, also discussed by (Auciello et al., 2014). For example, GAPDH catalyses the 6 th step in glycolysis, thereby regulating ATP production by this pathway. GAPDH is a highly redox-responsive protein and its activity is inhibited by H_2O_2 (Grant et al., 1999). Thus, it is possible that exogenous H_2O_2 effected both glycolytic and mitochondrial ATP production by several possible mechanisms, whereas MPQ may have only affected mitochondrial ATP production in a minor way.

Chapter 5

Creating stable cell lines expressing alternative respiratory enzymes to modulate mitochondrial ROS production

5.1 Introduction and aims

Mitochondrial ROS production has previously been considered a nonspecific by-product of respiratory chain dysfunction during or following oxidative damage or energy stress. However, recently it has been shown that ROS production by RET (known to be a tightly regulated process dependent on high mitochondrial membrane potential and/or a highly reduced Q pool) is a physiologically relevant signalling mechanism that drives inflammation (Mills et al., 2016), promotes lifespan (Scialo et al., 2016) and in pathology, is a key source of ROS contributing to ischaemia reperfusion injury (Chouchani et al., 2016). In order to study the downstream effects of RET in pathology or in redox signalling, it is necessary to be able to modulate the levels of ROS generated from mitochondria without the use of inhibitors (e.g. antimycin A, rotenone, oligomycin), as these will inhibit ATP production and alter the ΔP as well as increasing ROS production and so will greatly complicate the interpretation of results. One way of modulating mitochondrial ROS production without inhibiting respiratory chain function is by co-expressing alternative respiratory enzymes (from lower order organisms) alongside native respiratory complexes in a higher order model of interest (e.g. mammalian cell line, fruit fly, mouse etc.). There is now evidence that expressing these alternative respiratory enzymes alongside their native counterparts can alter the redox state of the Q pool in the IMM, which in turn can change the level of superoxide production by RET from complex I (Scialo et al., 2016, El-Khoury et al., 2013, Mills et al., 2016, Rustin and Jacobs, 2009). Co-expressing alternative respiratory enzymes with native complexes does not halt OXPHOS and in fact can bypass respiratory chain deficiencies and so is being explored as a potential therapy (Rustin and Jacobs, 2009, El-Khoury et al., 2013, Fernandez-Ayala et al., 2009, Seo et al., 1999, Kemppainen et al., 2014, El-Khoury et al., 2014, Yagi et al., 2006).

The immediate aim of this project was to create a stable mammalian cell line allowing inducible, titratable expression of the single subunit NADH dehydrogenase, NDI1, hypothesized to increase ROS production by RET (Scialo et

al., 2016). In parallel, a second stable cell line was created, expressing the single-subunit alterative oxidase, AOX (hypothesized to inhibit ROS production by RET). A second aim was to characterize the effects of each alternative respiratory enzyme on mitochondrial ROS production and on cellular bioenergetics (OXPHOS, cell ATP/ADP ratios etc.). Ultimately, we hope to create a model system for investigating down-stream effects of increased or decreased mitochondrial ROS production by RET without requiring respiratory chain inhibitors which may cause non-specific effects. The model system would also allow further investigation into the possibility of AMPK redox regulation and other potential redox crosstalk mechanisms between mitochondria and other cell compartments. Unlike the models of ROS tested in **Chapter 4**, mitochondrial ROS production by RET is hypothesized to be a natural mitochondrial redox signal that may occur under different physiological or pathophysiological stresses (Chouchani et al., 2016, Mills et al., 2016, Scialo et al., 2016, Buskiewicz et al., 2016). Thus, creating a cell system that allows us to sensitively modulate ROS production by RET will prove useful in further understanding the biological relevance of this phenomenon.

5.2 Alternative respiratory enzymes: background and hypotheses

Mitochondrial respiratory chain dysfunction plays a role in a number of human diseases. Dysfunction can be caused by inherited or somatic DNA mutations (Viscomi and Zeviani, 2017, Gorman et al., 2016), or following exposure to toxins or other environmental stresses (Exner et al., 2012). Respiratory chain dysfunction often presents as degenerative neuromuscular syndromes with often heterogeneous symptoms in multiple organs or organ systems, e.g. cardiomyopathy, deafness, diabetes and epilepsy (Viscomi and Zeviani, 2017, Gorman et al., 2016). Although progress has been made in the elucidation of the molecular mechanisms and pathogenesis of such disorders (e.g. development of metabolic acidosis, metabolic blockade, loss of ion homeostasis, increased ROS production) they remain untreatable in many cases (Viscomi and Zeviani, 2017,

Rustin and Jacobs, 2009). One treatment strategy that is being investigated by several research groups is respiratory chain bypass by expression of alternative respiratory enzymes (Rustin and Jacobs, 2009, Fernandez-Ayala et al., 2009, Barber-Singh et al., 2009, Yagi et al., 2006, Kemppainen et al., 2014). Alternative respiratory enzymes are not found naturally in mammals or other higher order animals but confer respiratory chain flexibility to lower order organisms (e.g. plants, yeast and invertebrates), including insensitivity to certain environmental toxins (e.g. rotenone and cyanide). For example, in plants, alternative respiratory enzymes play a role in maintaining mitochondrial redox balance and metabolite cycles in daylight when OXPHOS is inhibited by high rates of ATP production from photosynthesis (Rustin and Jacobs, 2009, Affourtit et al., 2001). Below, I outline in greater detail the contributions of the alternative respiratory enzymes NDI1 and AOX to respiratory chain bypass experiments and the effects of these enzymes on mitochondrial ROS production.

5.2.1 Single subunit NADH dehydrogenase - NDI1

In most eukaryotes, complex I catalyses mitochondrial NADH oxidation and electron donation to the ETC, and proton pumping from the matrix to the IMS contributing to the ΔP required for ATP production by OXPHOS. However, *S. cerevisiae* has lost complex I in evolution, instead using two simpler, single-subunit, non-proton translocating enzymes, Nde1p and Ndi1p, which oxidise cytosolic and mitochondrial NADH, respectively, and pass electrons to the Q pool in the IMM (Yagi et al., 2006). Unlike complex I, the single subunit NADH dehydrogenase (NDI1) is rotenone-insensitive, allowing growth in the presence of this environmental toxin. In mammalian cell line, fruit fly and mouse experiments, transgenic NDI1 expression has been found to successfully bypass complex I deficiencies (Seo et al., 1999, Sanz et al., 2010, Barber-Singh et al., 2009), permitting ongoing research into NDI1 delivery as a therapeutic strategy for human complex I deficiency disorders (Rustin and Jacobs, 2009). Furthermore, when co-expressed alongside complex I in *D. melanogaster*, it has been found that NDI1 increases mitochondrial ROS production (Scialo et al., 2016). As more electrons

pass into the Q pool following the enzymatic action of NDI1, without being opposed by proton pumping, the Q pool becomes hyper-reduced. This very reduced Q pool can subsequently drive the production of superoxide from complex I by RET **(Figure 5.1)**. As discussed in **1.4.1 How mitochondrial ROS can behave as a redox signal,** superoxide production by RET is emerging as a physiologically relevant redox signal in the cell.

A

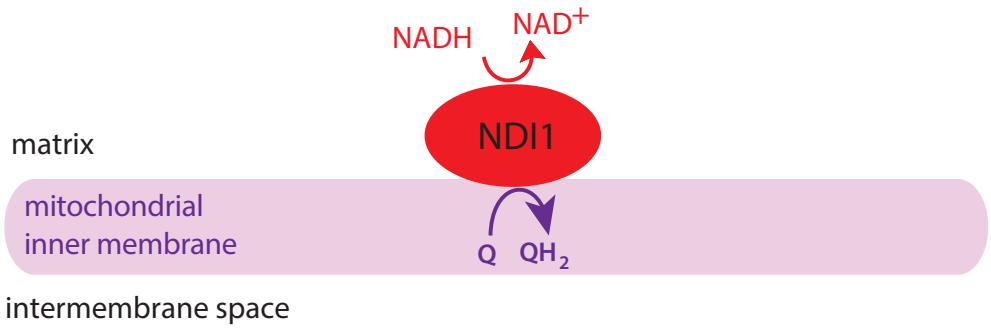

B

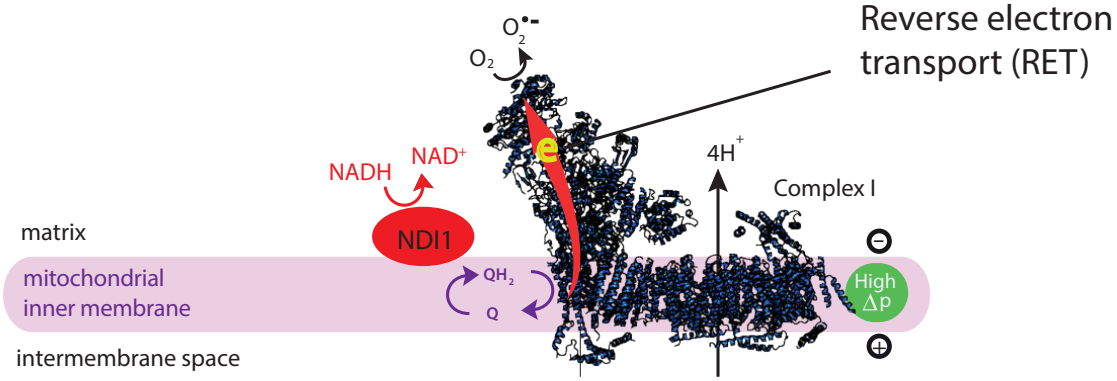

Figure 5.1. Effects of NDI1 expression on Q pool redox state and mitochondrial ROS production. ***(A)*** *NDI1 catalyses the oxidation of NADH and donates electrons to the Q pool.* ***(B)*** *When NDI1 is co-expressed with functional complex I, the Q pool becomes hyper-reduced. Combined with a high ΔP generated by the rest of the respiratory chain, this hyper-reduced Q pool can cause electrons to be driven backward from the Q pool onto the flavin mononucleotide (FMN) of complex I, reducing the FMN, which can pass one electron to oxygen to generate superoxide. The red arrow in complex I indicates RET.*

5.2.2 Alternative oxidase - AOX

Alternative oxidases (AOX) are found in many species of fungi, plants, protists and metazoans, but not in vertebrates or arthropods (Rustin and Jacobs, 2009). The AOX gene from the urochordate *Ciona intestinalis* is most commonly used in AOX-transgene experiments, including those in cell lines, fruit fly and mouse. A terminal oxidase, the cyanide-insensitive, non-proton-pumping AOX can bypass complexes III and IV of the respiratory chain by receiving electrons from reduced Q and transferring them directly to oxygen to form water. In this way, AOX can maintain electron transfer in case of a blockade of the cytochrome pathway and bypass experiments have been successfully performed in mammalian cell lines, fruit fly and mouse. It has also been observed that AOX does not negatively affect respiration when co-expressed with functional complex III and IV (Rustin and Jacobs, 2009, El-Khoury et al., 2013, Fernandez-Ayala et al., 2009, Dassa et al., 2009). As AOX uses electrons from the Q pool to reduce oxygen, AOX expression thereby prevents the hyper reduction of the Q pool and thus prevents RET. Therefore, as well as a therapeutic strategy for combatting complex III or IV deficiency in humans, AOX expression can be used to modulate mitochondrial ROS production by RET. In a mouse model, mitochondrial ROS production caused by antimycin A is inhibited by AOX expression (El-Khoury et al., 2013). Similarly, by preventing hyper-reduction of the Q pool, it has been found that when AOX is co-expressed alongside NDI1 and complex I in *D. melanogaster*, the previously observed increased superoxide production from complex I by RET is negated (Scialo et al., 2016) **(Figure 5.2).**

A

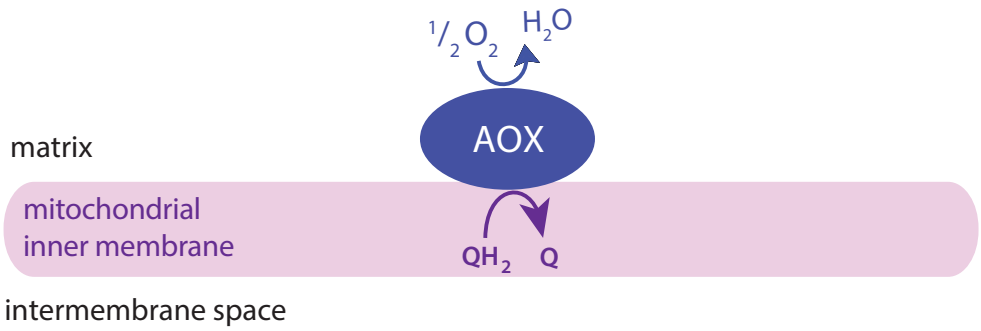

B

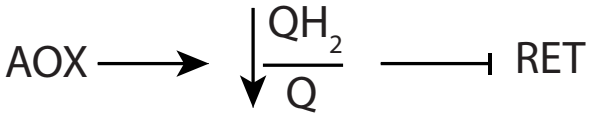

Figure 5.2. Effects of AOX expression on Q pool redox state and mitochondrial ROS production. (A) *AOX uses electrons from reduced Q to reduce oxygen to water.* ***(B)*** *AOX negates the effect of NDI1 and complex I co-expression on Q pool hyper-reduction, inhibiting ROS production by RET.*

5.2.2 Mammalian cell lines expressing NDI1 and AOX

In early studies investigating the potential therapeutic benefit of alternative respiratory enzymes in bypassing human respiratory chain deficiencies, NDI1 and AOX were expressed in human and other cell lines by various methods (Hakkaart et al., 2006, Seo et al., 1999, Seo et al., 2000, Birsoy et al., 2014). A Flp-In™T-REx™293-AOX cell line has previously been created (Hakkaart et al., 2006), which allows Doxycycline (Dox) -induced expression of the gene. This method of stable cell line creation offers control of the genome integration site and control of protein expression, preventing basal protein expression, which may lead to adaptive responses over time. NDI1 cell lines have been created in a number of ways, including: the Invitrogen pHook™ system (allows transfection of dividing cells without genome integration and allows separation of transfected and untransfected cells) (Seo et al., 1999); recombinant Adeno-Associated Virus (rAAV) transfection (achieves high frequency transfection of dividing and non-dividing cells without genome integration) (Seo et al., 2000); retroviral transfection (transfection of dividing cells only, with genome integration) (Birsoy et al., 2014). Although these methods of transfection offer several useful characteristics (e.g. the ability to transfect non-dividing or difficult to transfect cells), the level of protein expression achieved is difficult to control, can be variable between experiments, and in some cases can result in non-specific genome integration, which may cause off-target effects in the cell. While these issues may not be problematic in preliminary tests of respiratory chain bypass experiments, where enzymatic activity is easily detectable, a more controlled cell expression system is preferable for investigating the effects of NDI1 on mitochondrial ROS production by RET. Thus, the main aim of this project was to create a Flp-In™T-REx™293-NDI1 stable cell line, allowing controlled, Dox-inducible protein expression and site-specific genome integration. A Flp-In™T-REx™293-AOX cell line was also created at the same time using host cells from the same stock to minimize variation. By being able to modulate the redox state of the Q pool and mitochondrial ROS production, human cell models expressing alternative respiratory enzymes can be useful tools in elucidating

mitochondrial redox-signalling pathways and particularly the biological role of RET in cells. Below is a summary of preliminary data in the development of NDI1 and AOX cell lines.

5.3 Methods and Results

5.3.1 Flp-In™ T-REx™ cell expression system

Flp-In™ T-REx™ host cell lines allow exogenous gene insertion into a specific site in the host cell genome and also inducible expression of this gene of interest by the addition of a tetracycline (Dox) to the culture medium (**Figure 5.3**). The cDNA of a gene of interest can be cloned into the pcDNA5/FRT/TO inducible expression vector designed for use with the Flp-In™ T-REx™ System. When cotransfected with the pOG44 Flp recombinase expression plasmid into a Flp-In™ T-REx™ host cell line, the pcDNA5/FRT/TO vector containing the gene of interest is integrated in a Flp recombinase-dependent manner into a specific site in the host cell genome, creating a stable, tetracycline-inducible cell line.

A

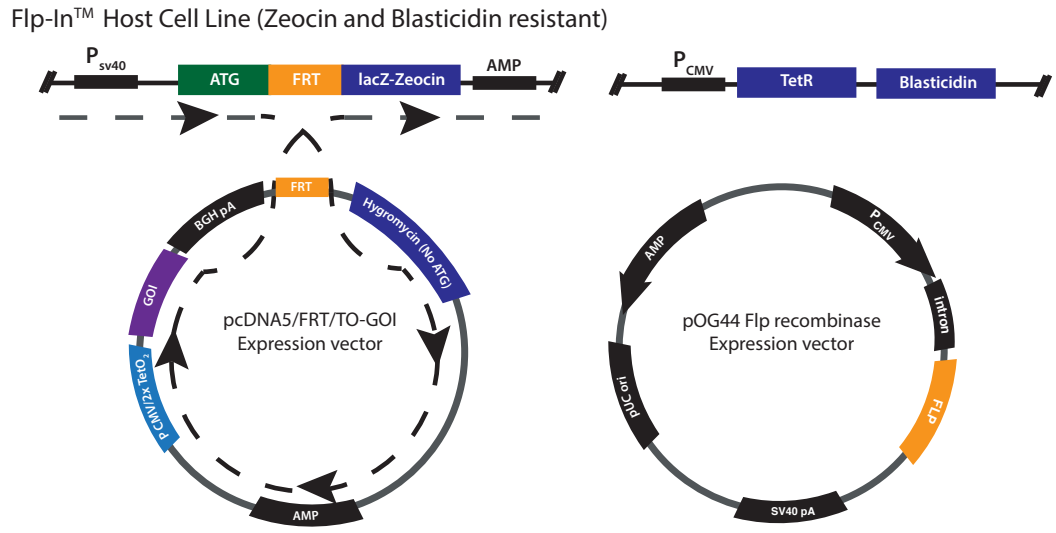

B

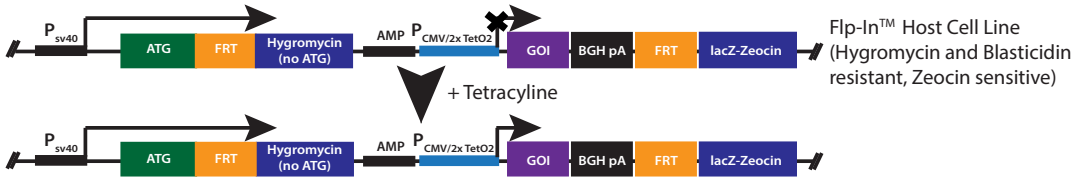

Figure 5.3. Transfection and selection of a stable Flp-In™ T-REx™cell line and induction of gene expression. (A) *The Flp-In™ T-REx™ Host Cell Line is co-transfected with the pcDNA5/FRT/TO expression vector (containing the gene of interest (GOI)) and the pOG44 Flp Recombinase expression vector;* ***(B)*** *Flp recombinase-mediated homologous recombination at FRT*

sites integrates the pcDNA5/FRT/TO expression vector into the host cell genome, bringing the SV40 promoter and start codon into proximity and frame with the hygromycin resistance gene and the GOI transcription machinery, and simultaneously inhibiting transcription of the Zeocin resistance gene. Treatment of cells with a tetracycline (Dox) then inhibits the TET repressor binding to the TET operator, allowing GOI trancription.

5.3.2 NDI1 expression vector preparation, amplification and purification

The cDNA insert coding for NDI1 (approx. 1.5 kb) was PCR amplified from the pWPI donor plasmid and subcloned into the pcDNA5/FRT/TO expression vector for use with the Flp-In™ T-REx™ stable, inducible mammalian cell expression system (see **Figure 5.4** and **2.9 Molecular Cloning** for expanded methods). pcDNA5/FRT/TO was linearised by restriction digest at the KpnI site (5') and NotI site (3') in the multiple cloning site (MCS) of the vector. The linear vector was dephosphorylated and gel purified prior to ligation with the insert. KpnI and NotI restriction sites were introduced onto the 5' and 3' ends of the NDI1 cDNA in the pWPI donor plasmid by PCR. The linear PCR product was gel purified and digested by KpnI-HF and NotI-HF enzymes to generate 5' and 3' compatible ends for ligation with the linear vector. The new insert was again gel purified prior to ligation with the linear vector. XL1-Blue electrocompetant *E. coli* were transformed with ligation mix to isolate and amplify the novel vector. Selection was performed in the presence of 100 µg/ml ampicillin. Colonies arising from transformation were selected and grown overnight at 37°C in LB broth containing 100 µg/ml ampicillin. Vector DNA was isolated using a QIAGEN® Mini-prep kit and diagnostic restriction digests were performed to assess the presence of insert DNA of the desired size (approx. 1.55 kb). Vectors with inserts of the desired size were sent for Sanger sequencing analysis (Source Bioscience) to confirm the identity of the inserts (see **Appendix A**). *E. coli* were then retransformed with the correct vector in order to amplify and isolate endotoxin-free vector for mammalian cell transfection, performed using the QIAGEN® Mini-prep kit.

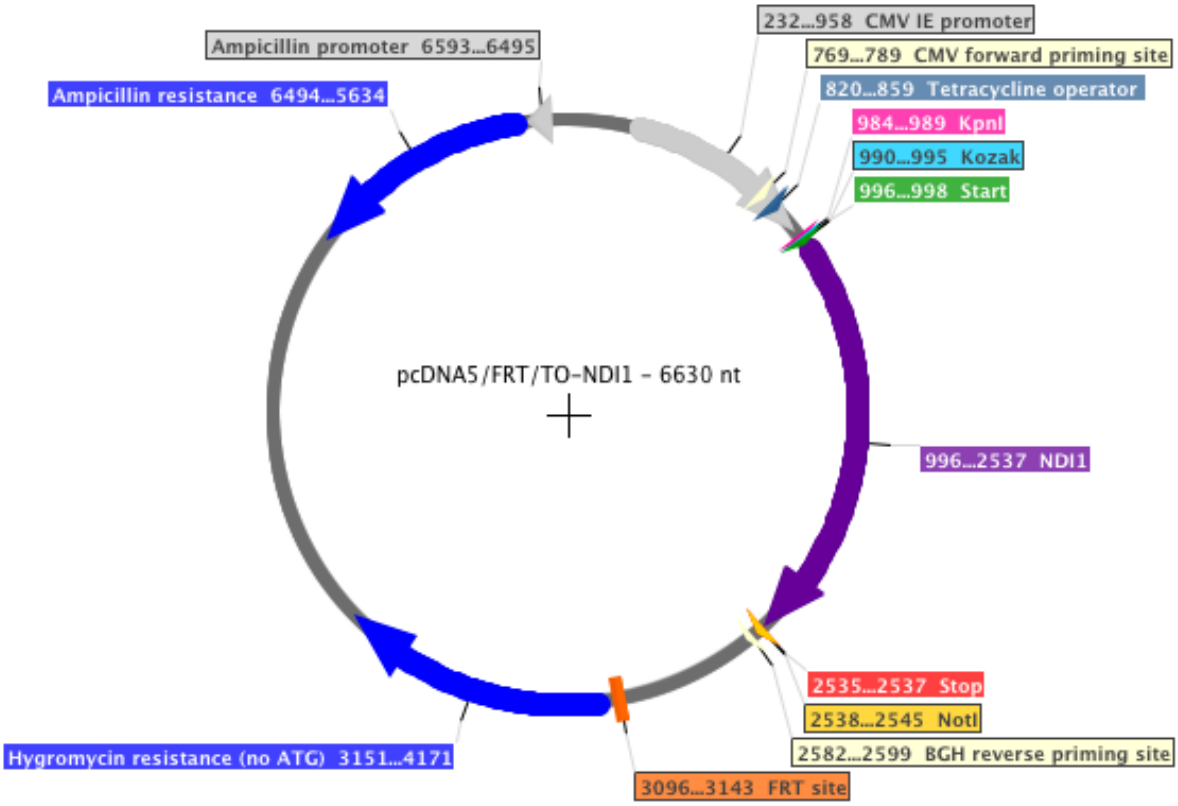

Figure 5.4. Scale map of the pcDNA5/FRT/TO-NDI1 expression vector highlighting key features. *NDI1 cDNA was subcloned into the pcDNA5/FRT/TO expression vector by restriction digest and ligation at 5' KpnI and 3'NotI restriction sites. The NDI1 sequence was engineered to contain a Kozak consensus sequence before the start codon to aid initiation of protein translation in cells (see* ***2.9 Molecular Cloning*** *and* ***Appendix B****). The expression vector contained a number of key features: the CMV promoter to enable high level expression of NDI1; the Ampicillin resistance gene and its respective promoter to enable selection of positive bacterial colonies; the Tetracycline (TET) operator, which when bound by the TET repressor protein (expressed by the host cell line) in the absence of Tetracycline in the culture media inhibits NDI1 gene expression; the FRT site which allows site-specific vector integration into the whole cell genome at a corresponding FRT site by homologous recombination; the Hygromycin resistance gene (lacking a start codon) which when integrated into the correct site of the host cell genome will confer hygromycin resistance to the cell and enable selection of positive clones. The scale map was created using SerialCloner 2-6-1. The pcDNA5/FRT/TO DNA sequence was imported from the manufacturer's online resource (https://tools.thermofisher.com/content/sfs/vectors/pcdna5frtto_seq.txt). The NDI1 vector and sequence map were a gift from Dr. Alberto Sanz (Institute for Cell and Molecular Biosciences & Newcastle University Institute for Ageing, Newcastle University, Newcastle, UK). See* ***Appendix A*** *for sequences.*

5.3.3 Inducing NDI1 protein expression in the Flp-In™ T-REx™ 293-NDI1 stable cell line

Following transfection and selection of a stable Flp-In™ T-REx™ 293-NDI1 cell line (see **2.2.6 Exogenous gene expression in mammalian cell lines**), expression of NDI1 was induced by addition of Dox to the cell culture medium. NDI1 protein expression was confirmed by performing a Western blot on cell lysates (uninduced and induced) using a primary antibody raised against NDI1 (see **2.1.2.1.1 Primary antibodies)**. A Dox titration was performed to optimise and titrate protein expression (**Figure 5.5**). NDI1 protein was first detectable after treatment (24 h) with 1 ng Dox/ml and peaked upon treatment with 10 - 100 ng Dox/ml. NDI1 protein expression was maintained at higher concentrations of Dox, but at a lower level. A consistent gradation of NDI1 protein expression in cells was achieved within the range of 1 – 100 ng/ml Dox, which was one of the aims of the experiment.

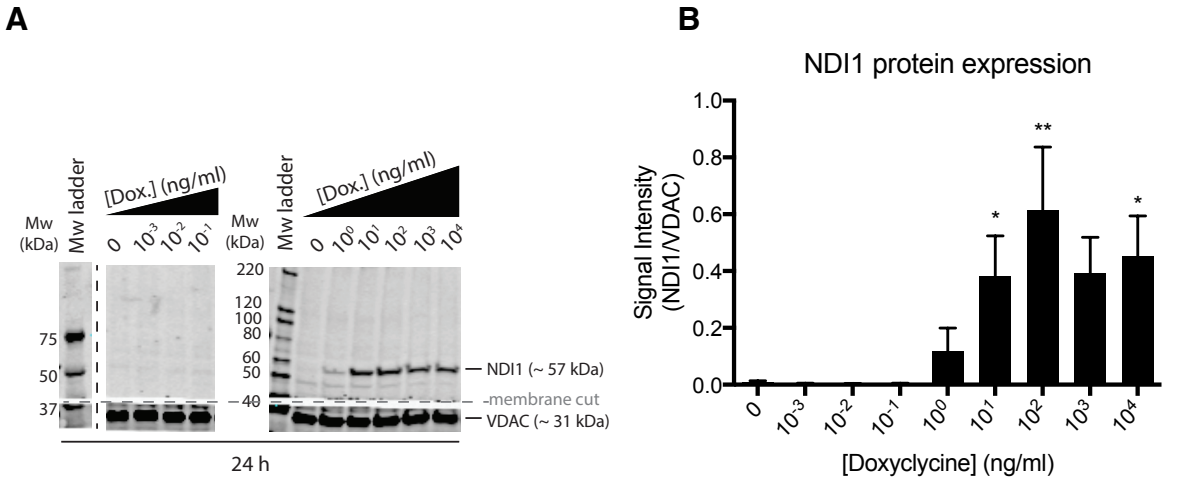

Figure 5.5. NDI1 protein expression in Flp-In™ T-REx™ 293 - NDI1 cells in response to Dox induction. (A) *Cells were plated on 6-well plates at a density of 20,000 cells/cm^2 in Tet-free medium (4.5 g/l glucose) (see **2.2. Mammalian cell culture**) supplemented with blasticidin and hygromycin. When cells reached 70 – 80% confluency, NDI1 gene expression was induced with serially diluted Dox in Tet-free medium for 24 h. Cells were then washed in ice-cold PBS and lysed in ice-cold RIPA buffer (150 mM sodium chloride, 1.0 % (v/v) Triton X-100, 0.5 % (w/v) sodium deoxycholate, 0.1 % (w/v) SDS, 50 mM Tris, pH 8.0 at 4°C, supplemented with DTT and protease inhibitors. Cells were scraped from the plate surface, transferred to 1.5 ml Eppendorf tubes on ice, sonicated and then centrifuged (17,000 X g for 10 min at 4°C). Supernatants were stored on ice for immediate use or snap-frozen on dry ice and stored at - 20°C. SDS-PAGE (25 µg protein) and Western blotting was performed as standard. Post blocking, PVDF membranes were cut horizontally with a razor blade (as indicated by the grey dotted line) and each section was*

*individually incubated with the appropriate primary antibody (rabbit) for the Mw range of that section, indicated by band descriptions (see **2.1.2.1.1 Primary antibodies**). All rabbit primary antibodies were labeled with the same fluorescent secondary antibody (see **2.1.2.1.2 Secondary antibodies**). Western blots were imaged using the Odyssey® CLx Infrared Imaging System (fluorescence emission at 800 nm); **(B**) The Western blot signal intensity of NDI1 (quantified with LI-COR Biosciences Image Studio™ Lite software) from **(A)** was normalized to that of VDAC as a loading control. Graphed data is mean ± SEM of n ≥ 3 biological replicates. Statistical analysis was performed by one-way ANOVA with Dunnett's Multiple Comparison post-test comparing all treatments to UT control. Means were considered significantly different when $P < 0.05$. *$P < 0.05$, **$P < 0.01$. UT, untreated.*

5.3.4 Preliminary characterization of the effects of NDI1 protein expression in cells

Having confirmed Dox- inducible, titratable NDI1 protein expression, I next investigated the functionality of NDI1. NDI1 is an NADH dehydrogenase, as is complex I, so the same NADH-linked substrates can be used to measure complex I- or NDI1- mediated respiration in whole cells (e.g. pyruvate or glutamate). As both complex I and NDI1 (Dox induced) are expressed in the cell model, the challenge was to differentiate between the contributions of both enzymes to NADH-linked respiration. Unlike complex I, NDI1 is insensitive to the inhibitor rotenone (Rustin and Jacobs, 2009, Seo et al., 1999). In the presence of NADH-linked substrates, cell respiration in cells containing complex I but not NDI1 will cease in the presence of rotenone. However, if both complex I and NDI1 are functionally expressed in cells, upon addition of rotenone to the system respiration should be only partially decreased, with NDI1-driven respiration remaining uninhibited. The difference between rotenone-sensitive and rotenone-insensitive respiration can thus be used as a measure of functional NDI1 expression in mammalian cells. I used the Seahorse Bioscience XF96 analyzer to measure the oxygen consumption rate (OCR) of unpermeabilised cells in the presence of pyruvate: a measure of NADH-linked respiration (see **Figure 5.6** and **2.8 Seahorse XF96 Respirometry).** Dox-induced cells exhibited 62.3 ± 8.6 % rotenone-insensitive respiration (mean ± SEM, whereas uninduced cells exhibited 8.0 ± 1.3 % rotenone-insensitive respiration, confirming the presence of functional NDI1 in the Dox-induced cells.

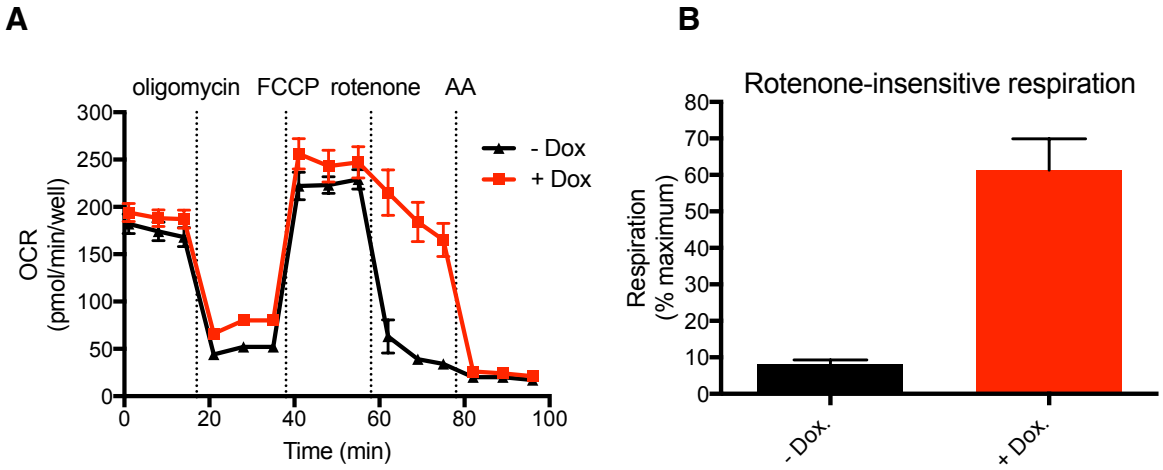

Figure 5.6. Oxygen consumption rate comparison of Dox-induced and uninduced cells, measured using the Seahorse Bioscience XF96 analyzer, showing the partial rotenone insensitivity of NDI1-expressing cells. (A) *Flp-In™ T-REx™ 293 - NDI1 cells were plated at a density of 50,000 cells/ well of a 96 well plate in low glucose (1 g/l) Tet-free medium supplemented with blasticidin and hygromycin. Cells were plated ± Dox (1 µg/ml). 24 h later, cell medium was replaced with low glucose Seahorse assay medium (180 µl/well), following a cell wash in the same medium. The cell plate was incubated in a CO_2-free incubator for 1 h prior to assay. Compound injections (final concentrations) were the following: oligomycin (1 µM), FCCP (1 µM), rotenone (2 µM), antimycin A (AA) (50 µM). Graphed data represents mean ± SEM of n ≥ 6 technical replicates;* ***(B)*** *quantification of rotenone-insensitive mitochondrial respiration in Dox-induced versus uninduced cells, expressed as % max. mitochondrial respiration (mean ± SEM of n ≥ 6 technical replicates).*

Having confirmed functional NDI1 expression in the cell model, another question to be addressed was the effect of NDI1 expression on mitochondrial ROS production. Mitochondrial ROS production in whole cells can be measured in a number of ways, e.g. using mitochondria-targeted redox-responsive probes for analysis by mass-spectrometry or fluorescent probes for visualization by confocal microscopy (Dikalov and Harrison, 2014, Cocheme et al., 2012). These approaches can be time-consuming, particularly when applied to a new and untested system, and sensitivity can also be a limiting factor. In order to gain a preliminary insight into the effects of NDI1 on mitochondrial ROS production, I investigated the protein expression of a biological marker, manganese superoxide dismutase (MnSOD), which is located in the mitochondrial matrix and is involved in the detoxification of superoxide in cells (Murphy, 2009). MnSOD catalyses the rapid dismutation of superoxide to H_2O_2, which can then be metabolized to H_2O by peroxidases, GSH and catalase. There is evidence that increased mitochondrial superoxide levels

induce upregulation of MnSOD protein expression in cells (Hart et al., 2015, Kim et al., 2005). Thus, I investigated the expression of MnSOD in uninduced and induced cell lysates, 24 h post-Dox addition (**Figure 5.7**). There was no significant increase in MnSOD protein expression, although the trend appeared to follow that of NDI1 protein expression between the titratable [Dox] range (1 – 100 ng/ml Dox). However, this should be considered cautiously as levels then appeared to decrease. A Dox-induction time-course has not yet been performed. If NDI1 protein expression is not detectable before the 24 h time-point, it is conceivable that an adaptive response to increased mitochondrial ROS production (if occurring) may take longer to occur.

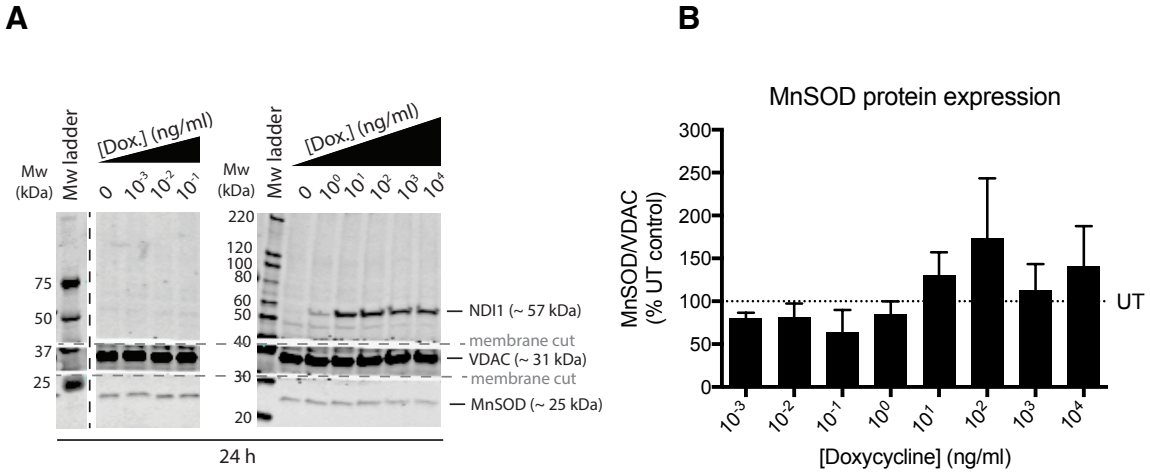

Figure 5.7. MnSOD protein expression in Dox-induced NDI1 cells, measured by Western blotting. (A) *Cell lysates were prepared and SDS-PAGE and Western blot performed as described in* ***Figure 5.5.*** *PVDF membranes sections were individually incubated with the appropriate primary antibody (rabbit) for the Mw range of that section (indicated by band descriptions). Western blots were imaged using the Odyssey® CLx Infrared Imaging System (fluorescence emission at 800 nm);* ***(B****) The Western blot signal intensity of MnSOD from* ***(A)*** *was normalized to that of VDAC as a loading control. Graphed data is mean ± SEM of n ≥ 3 biological replicates. UT, untreated.*

To investigate longer-term effects of NDI1 protein expression on MnSOD protein expression as a marker of increased mitochondrial ROS production, cells were treated with Dox for 72 h. However, it appears that Dox is unstable in cell culture media for that time duration as NDI1 protein expression was greatly decreased (**Figure 5.8**). There is anecdotal evidence to suggest that Dox is unstable after 48

h in cell culture media, so future experiments will require Dox replacement every 24 – 48 h to maintain stable NDI1 expression for longer time-points. To summarise, the effects of NDI1 protein expression on mitochondrial ROS production in this cell line are currently unknown and will require future experiments.

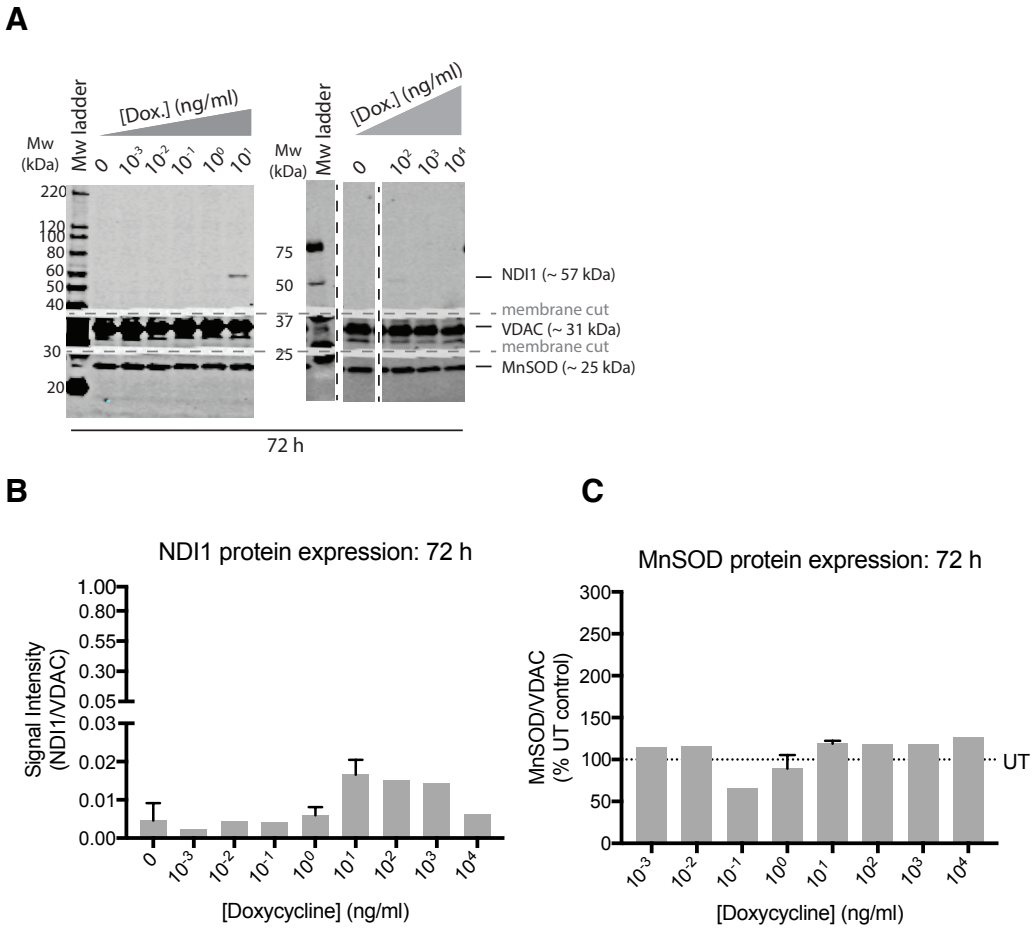

Figure 5.8. NDI1 and MnSOD protein expression in Dox-induced NDI1 cells 72 h post Dox addition, measured by Western blotting. (A) *Cells were plated on 6-well plates at a density of 10,000 cells/cm^2 in Tet-free medium (4.5 g/l glucose) supplemented with blasticidin and hygromycin. When cells reached approx. 30% confluency, NDI1 gene expression was induced with serially diluted Dox in Tet-free medium for 72 h. Cell lysis, SDS-PAGE and Western blotting were all performed as previously described. Western blots were imaged using the Odyssey® CLx Infrared Imaging System (fluorescence emission at 800 nm);* ***(B)*** *The Western blot signal intensities of NDI1 or MnSOD from* ***(A)*** *were normalized to that of VDAC as a loading control. Graphed data is n = 1 or mean ± range of n = 2 biological replicates. UT, untreated.*

In parallel, I investigated the effects of NDI1 protein expression on AMPK activity. As discussed in **Chapter 4**, AMPK redox-regulation independent of changes to the

cell ATP/ADP ratio has been reported by a number of groups (Emerling et al., 2009, Hart et al., 2015, Mungai et al., 2011, Shao et al., 2014, Zmijewski et al., 2010). However, I did not observe conclusive evidence of redox-regulation of AMPK in a previous cell line (terminally differentiated C2C12 mouse myotubes) in response to either cytosolic or mitochondrially-derived ROS, instead showing that AMPK activity was only increased when ATP/ADP ratios were decreased. Working with the hypothesis that co-expression of NDI1 and complex I in a mammalian cell line (in this case by using a human, HEK 293 background) might increase mitochondrial ROS production by RET, I investigated if any changes occurred to AMPK activity upon expression of NDI1 **(Figure 5.9 & 5.10)**.

AMPK phosphorylation was increased in Dox-induced cells (24 h post-induction) at concentrations previously shown to induce NDI1 protein expression (≥ 1 ng Dox/ml) and not at lower concentrations. ACC phosphorylation also appeared to increase dose-dependently between 0.1 and 10 ng Dox/ml, but this did not reach statistical significance. Levels decreased at higher concentrations of Dox. In cells lysed 72 h post-induction (previously shown to have greatly decreased or undetectable NDI1 protein expression levels), AMPK phosphorylation followed a dose-dependent trend but to a lesser extent (preliminary data, n = 1). ACC phosphorylation appeared to be unchanged from untreated cells. AMPK is primarily activated by decreases in the cell ATP/ADP or ATP/AMP ratios. Thus, using the respirometry data presented in **Figure 5.6,** I also calculated ADP-linked respiration (basal – oligomycin-treated OCR) to test if NDI1 expression (or Dox treatment) was affecting ATP synthesis by F_OF_1 - ATP synthase (**Figure 5.9)**. Dox-induced cells exhibited 60.3 ± 3.4 % ADP-linked respiration, and uninduced cells exhibited 71.8 ± 4.3 % ADP-linked respiration, suggesting that the NDI1 protein expression or Dox treatment may affect ATP synthesis by F_OF_1 - ATP synthase. This data is preliminary, as it was from technical replicates from one biological experiment, and so further experiments will be required to expand the result. ATP/ADP assays will be also be required to test for any small changes in ATP/ADP ratios caused by protein expression or Dox treatment that could affect AMPK activity. Similarly, the

effects of Dox on AMPK activity in WT cells will need to be tested. As observed in **Figure 5.10**, it is currently difficult to confirm or exclude any off-target effects of Dox on AMPK activity in NDI1 stable cells. Although I have not observed any published reports that suggest Dox treatment basally induces AMPK activation, Dox has been reported to alter cell metabolism in different cell lines (Ahler et al., 2013). Thus, the effects of Dox on AMPK activity in untransfected cells will need to be investigated in future work.

The preliminary data confirms that this cell line expresses a gradation of Dox-induced, functional, NDI1, within a range of 1 – 100 ng/ml Dox. NDI1 expression coincides with increased AMPK phosphorylation within this range. Dox-induced cells exhibit a potential decrease in ADP-linked respiration (although it should be noted that the cells in the Seahorse experiment were induced with 1 µg/ml Dox, a 10-fold higher concentration than the [Dox] that induced peak NDI1 expression). Increased ROS production in the cells remains undetermined. The preliminary data suggests that NDI1 protein expression may be having a biological effect in the cells. However, the mechanism behind the AMPK activation is currently unclear and the preliminary data should be interpreted cautiously with the above points in mind. In future experiments (if off-target effects of NDI1 protein expression and Dox treatment are ruled out), NDI1-dependent hypotheses can be investigated, e.g. does NDI1 protein expression increase ROS production in cells by RET? And if so, is this ROS production capable of altering the redox-state of the cytosol and also of AMPK?

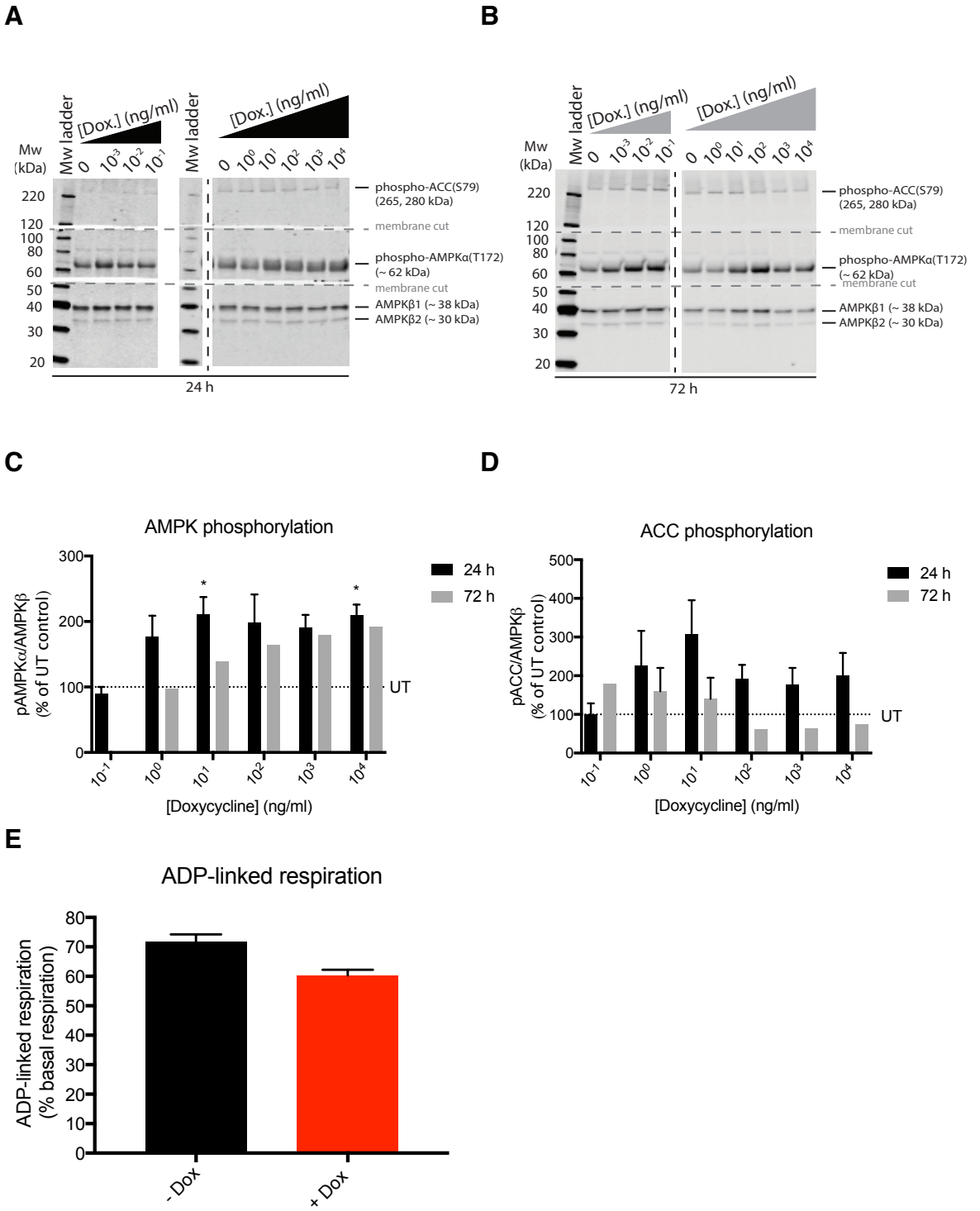

Figure 5.9. AMPK and ACC phosphorylation in Dox-induced NDI1 cells 24 h or 72 h post Dox addition (measured by Western blotting) and a comparison of ADP-linked respiration in 24h-Dox-induced and uninduced cells (measured by Seahorse XF96 respirometry). (A – D) *Cells were plated and induced for 24 h **(A)** or 72 h **(B)** as described in **Figures 5.5** and **5.8**, respectively. Cells were lysed in Hepes lysis buffer, supplemented with DTT and protease inhibitors, and SDS-PAGE and Western blotting was performed as described in **2.4 AMPK assays.** Western blots were imaged using the Odyssey® CLx Infrared Imaging System (fluorescence emission at 800 nm); **(C)***

*The Western blot signal intensities of AMPKα1/2-phosphoT172 bands from **(A & B)** were normalized to the signal intensity of AMPKβ1 a loading control. **(D)** The Western blot signal intensities of ACC1/2-phosphoS79 bands from **(A & B)** were also normalized to the signal intensity of AMPKβ1 a loading control. **(C & D)** Graphed data is mean ± SEM of n ≥ 3 biological replicates from **(A)** or n = 1 from **(B)**; Statistical analysis was performed by one-way ANOVA with Dunnett's Multiple Comparison post-test comparing all treatments to UT control. Means were considered significantly different when P < 0.05. *P < 0.05. **(E)** Quantification of ADP-linked mitochondrial respiration in Dox-induced versus uninduced cells (from **Figure 5.6**), expressed as % basal respiration (mean ± SEM of n ≥ 6 technical replicates). UT, untreated.*

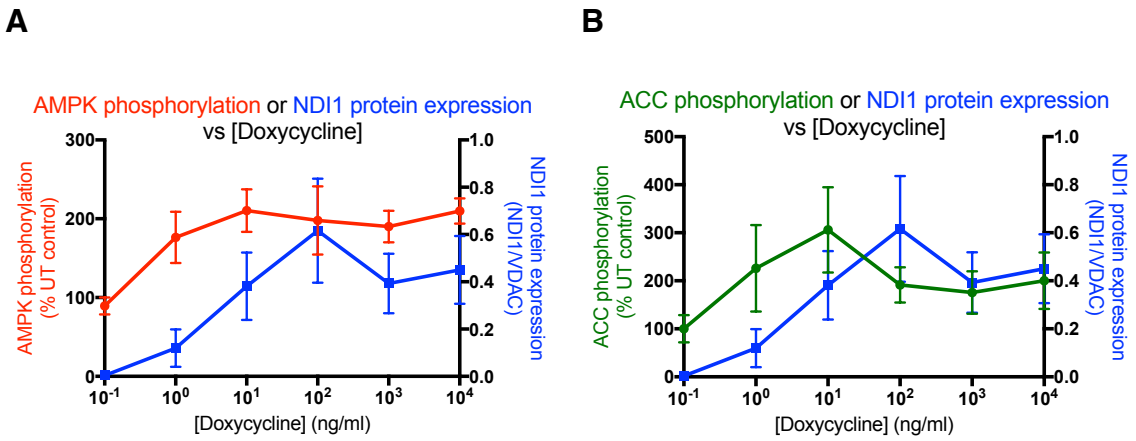

***Figure 5.10. Comparison of the effects of Dox on NDI1 protein expression and AMPK or ACC phosphorylation.** **(A)** AMPK phosphorylation and **(B)** ACC phosphorylation versus NDI1 protein expression.*

5.3.5 AOX expression vector preparation, amplification and purification

An AOX stable cell line was created in parallel to the NDI1 stable cell line, using host cells from the same stock. Molecular cloning of AOX was perfomed by Aonghus McCarthy (MRC Mitochondrial Biology Unit, University of Cambridge, Wellcome Trust/MRC Building, Cambridge Biomedical Campus, Hills Road, Cambridge CB2 0XY, UK) in the course of a summer studentship sponsored by the Amgen Scholars programme, Cambridge 2016. The cDNA insert coding for AOX (~ 1.1 kb) was PCR amplified from the pWPI donor plasmid and subcloned into the pcDNA5/FRT/TO expression vector for use with the Flp-In™ T-REx™ stable, inducible mammalian cell expression system, as previously described (see **Figure 5.11).** The pcDNA5/FRT/TO was linearised by restriction digest at the BamHI site (5') and XhoI site (3') in the MCS. The linear vector was dephosphorylated and gel purified prior to ligation with the insert. BamHI and XhoI restriction sites were introduced onto the 5' and 3' ends of the NDI1 cDNA in the pWPI donor plasmid by PCR. The linear PCR product was gel purified and digested by BamHI-HF and XhoI enzymes to generate 5' and 3' compatible ends. The new insert was again gel purified prior to ligation with the linear vector. XL1-Blue electrocompetant *E.coli* were transformed, selected and grown as previously described. Vector DNA was isolated (QIAGEN® Mini-prep kit) and diagnostic restriction digests were performed to assess the presence of insert DNA of the desired size (~ 1.1 kb). Vectors with inserts of the desired size were sent for Sanger sequencing analysis (Source Bioscience) to confirm the identity of the inserts (see **Appendix A**). The correct vector was then amplified for mammalian cell transfection as previously described.

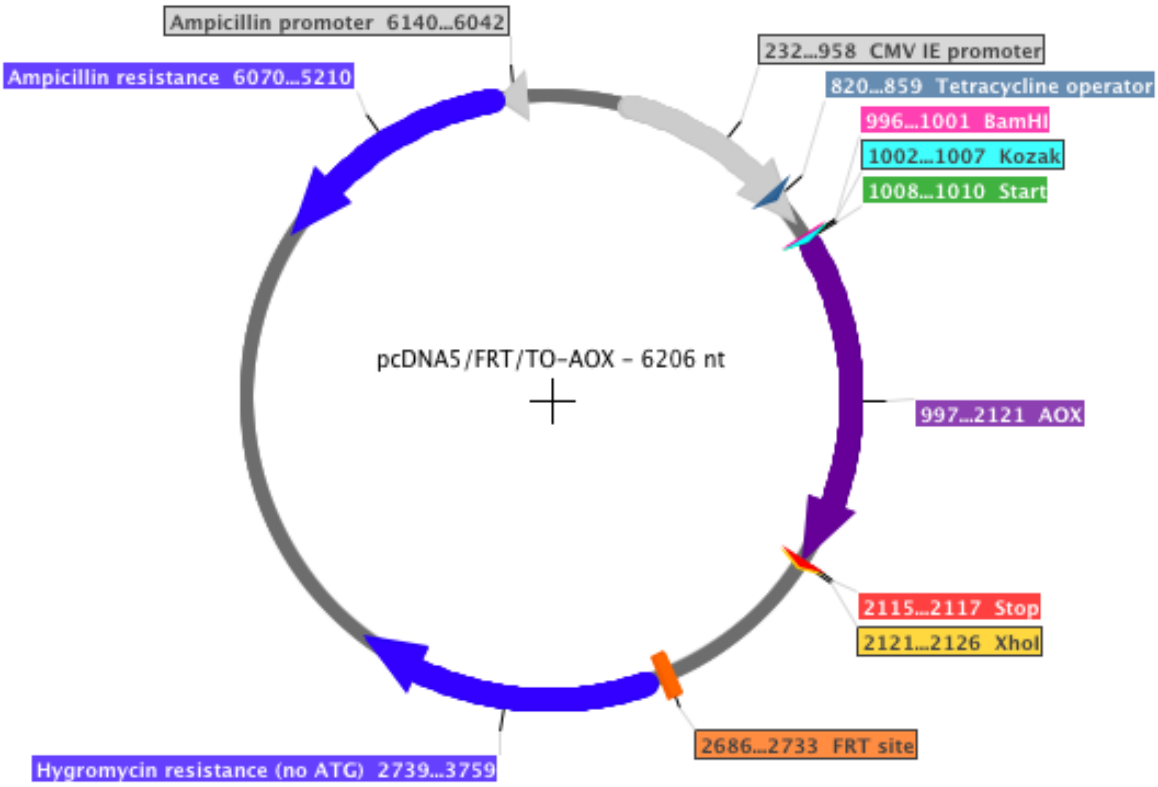

Figure 5.11. Scale map of the pcDNA5/FRT/TO-AOX expression vector highlighting key features. *AOX cDNA was subcloned into the pcDNA5/FRT/TO expression vector by restriction digest and ligation at 5' BamHI and 3'XhoI restriction sites. Key features highlighted are as described above. The scale map was created using SerialCloner 2-6-1, using the pcDNA5/FRT/TO DNA backbone sequence as previously described. The AOX vector and sequence map were a gift from Dr. Alberto Sanz (Institute for Cell and Molecular Biosciences & Newcastle University Institute for Ageing, Newcastle University, Newcastle, UK).*

5.3.6 Inducing AOX protein expression in the Flp-In™ T-REx™ 293-AOX stable cell line

Following transfection and selection of a stable Flp-In™ T-REx™ 293-AOX cell line (as described for NDI1), expression of AOX was induced by addition of Dox to the cell culture medium. AOX protein expression was confirmed by performing a Western blot on cell lysates (uninduced and induced) using a primary antibody raised against AOX (see **2.1.2.1.1 Primary antibodies)**. A Dox titration was performed to optimise and titrate protein expression (**Figure 5.12**). AOX protein was first detectable after treatment (24 h) with 10 ng Dox/ml and peaked upon treatment with 100 ng Dox/ml, with a high level of AOX protein expression maintained at higher concentrations of Dox. Dox concentrations between 1 – 10 ng/ml will be investigated in future experiments to see if lower but still detectable levels of NDI1 protein can be observed.

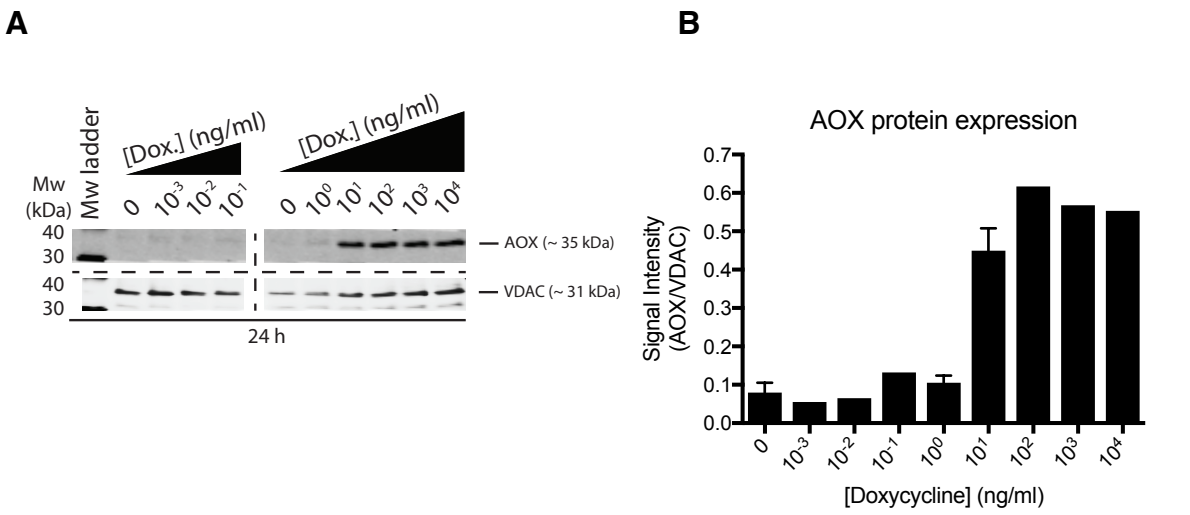

Figure 5.12. AOX protein expression in Flp-In™ T-REx™ 293 - AOX cells in response to Dox induction. (A) *Cell lysates were prepared and SDS-PAGE and Western blotting performed as described in* ***Figure 5.5****. PVDF membranes were dual incubated with primary antibodies: rabbit-α-AOX and mouse-α-VDAC. Rabbit and mouse primary antibodies were differentially labeled with fluorescent secondary antibodies (****see 2.1.2.1.2 Secondary antibodies****). Western blots were imaged using the Odyssey® CLx Infrared Imaging System (fluorescence emission at 800 nm for AOX and 680 nm for VDAC);* ***(B****) The Western blot signal intensity of AOX from* ***(A)*** *was normalized to that of VDAC as a loading control. Graphed data is n = 1 or mean ± range of n = 2 biological replicates.*

5.3.7 Preliminary characterization of the effects of AOX protein expression in cells

Although respirometry analysis of AOX protein expression in cells has not yet been tested, I did have opportunity to begin to characterize AMPK activation in the cells (**Figure 5.13 and 5.14**) and compare the results to those of NDI1 expressing cells. I found that AMPK phosphorylation in AOX cells increased dose-dependently in response to Dox treatment (n = 1 or 2). ACC phosphorylation was less clear. The preliminary results show that it is currently impossible to distinguish between the effects of individual protein expression and [Dox] on AMPK activity in these NDI1 and AOX stable cell lines and control experiments on untransfected cells are required before investigating any potential protein-specific effects.

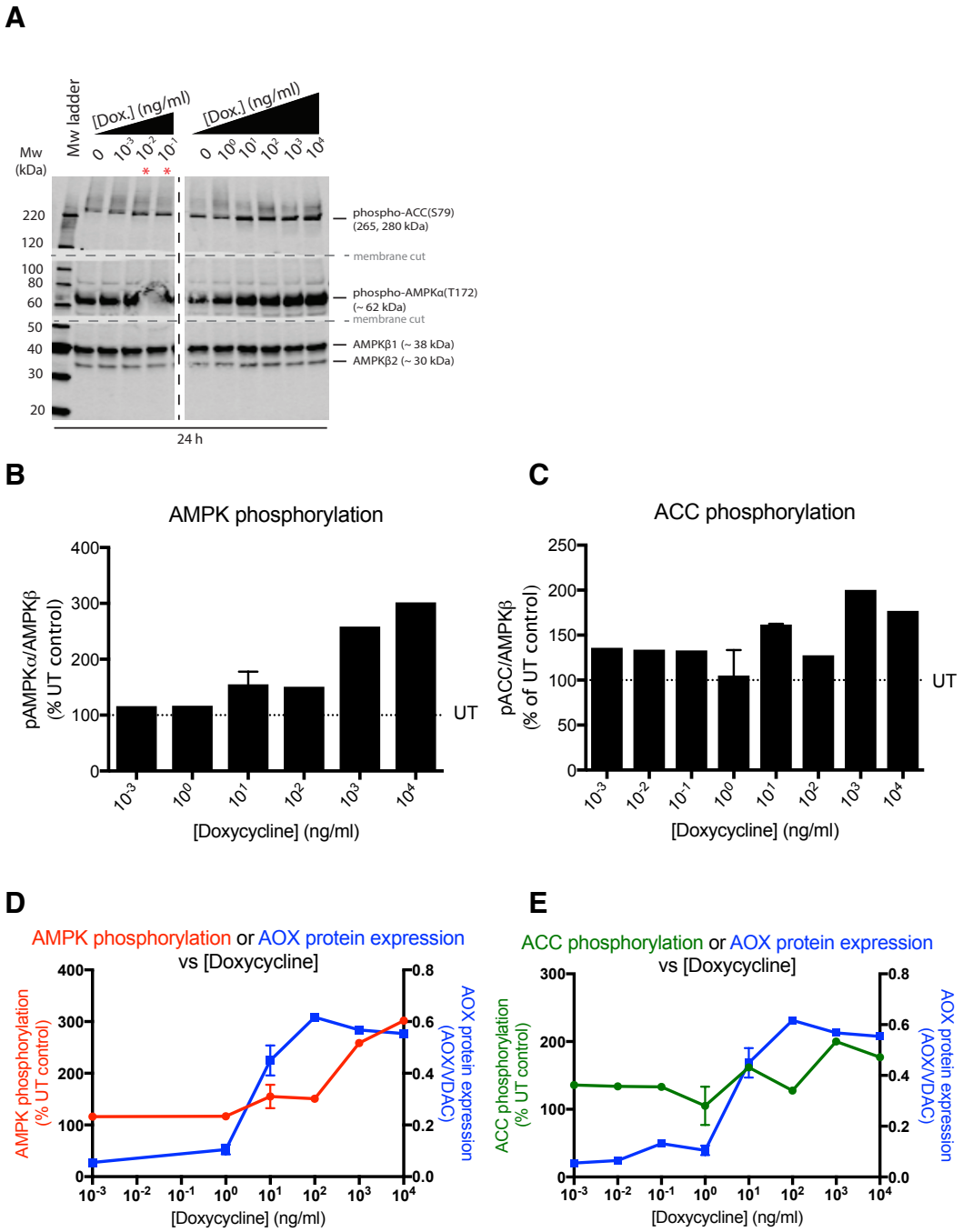

Figure 5.13. AMPK and ACC phosphorylation in Dox-induced AOX cells 24 h post Dox addition, measured by Western blotting. ***(A)*** *Cell lysates were prepared and SDS-PAGE and Western blotting performed as described in* ***Figure 5.9****;* ***(B)*** *The Western blot signal intensity of AMPKα1/2-phosphoT172 from* ***(A)*** *was normalized to the signal intensity of AMPKβ1 a loading control. The lanes marked by the red asterisks were excluded from the quantification due to transfer flaws;* ***(C)*** *The Western blot signal intensity of ACC1/2-phosphoS79 from* ***(A)*** *was also normalized to the signal intensity of AMPKβ1 a loading control;* ***(D)*** *AMPK phosphorylation increases as AOX protein expression increases, however, the effects on* ***(E)*** *ACC phosphorylation are less clear. Graphed data is n = 1 or mean ± range of n = 2 biological replicates. UT, untreated.*

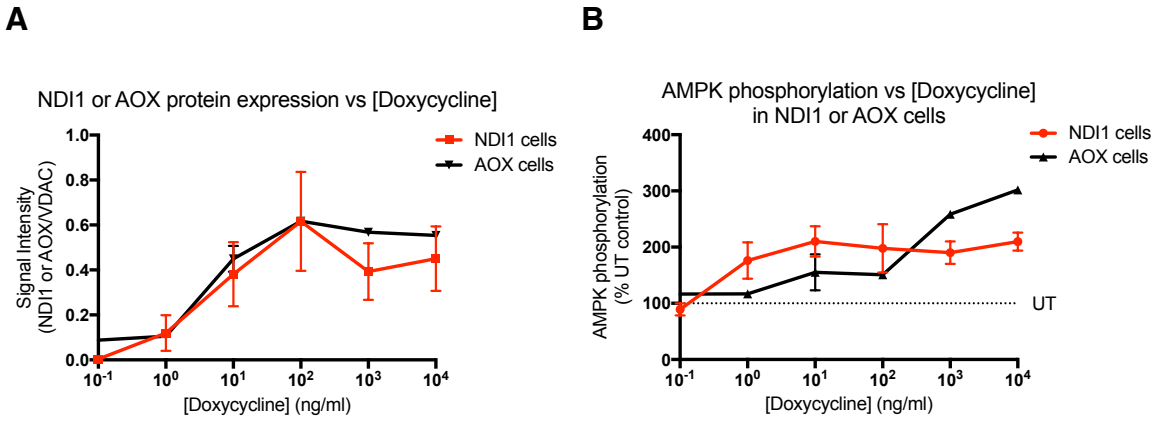

Figure 5.14. Comparison of the effects of Dox on NDI1 or AOX protein expression and on AMPK phosphorylation. (A) *[Dox] has similar effects on NDI1 or AOX expression in the respective stable cell lines;* ***(B)*** *Preliminary data shows that [Dox] increases AMPK phosphorylation in both NDI1 and AOX stable cell lines;* ***(A & B)*** *Graphed NDI1 data is mean ± SEM of n ≥ 3 biological replicates, graphed AOX data is n = 1 or mean ± range of n = 2 biological replicates. UT, untreated.*

5.4 Discussion and future work

This chapter describes the preliminary data on this project obtained to date. The goal of this project is to create stable cell lines expressing the alternative respiratory enzymes, NDI1 and AOX, so that the biological effects of RET in cells can be investigated. NDI1 and AOX have previously been shown to increase or decrease mitochondrial ROS production by RET by reducing or oxidizing the Q pool, respectively. Stable cell lines in which expression of the alternative respiratory enzymes can be acutely controlled is favourable, as it should enable ROS production by RET to be turned on or off, or increased gradually. Although progress has been made in characterising the cell lines, a number of questions remain unaddressed and will require future experiments.

I have confirmed that both the NDI1 and AOX cell lines express proteins under the control of Dox. A gradation of NDI1 protein expression can be achieved between 1 – 100 ng Dox/ml and AOX between 10 – 100 ng Dox/ml. High protein expression levels are beneficial for characterising enzymatic activity, however, high levels of expression of matrix or IMM associated proteins may have a negative effect on the ΔP. For testing the effects of NDI1 and AOX on ROS production (which is also dependent on the magnitude of the ΔP) it is favourable to be able to titrate the protein expression, from low to high. While functional NDI1 protein expression was confirmed by Seahorse XF96 respirometry (measured as rotenone-insensitive mitochondrial respiration), the functionality of AOX has not yet been confirmed. AOX is cyanide-resistant (unlike complex IV, which is cyanide sensitive) but is inhibited by propyl gallate (Fernandez-Ayala et al., 2009). My aim is to perform a similar respiration experiment as in NDI1 cells, utilising sensitivity to propyl gallate as a measure of functional AOX expression.

In response to induction with a high [Dox] (1 µg/ml), ADP-linked respiration in NDI1 cells appeared to be slightly decreased (preliminary data, n = 1). Similarly, it is currently unclear if Dox is having off-target effects on the cell, as AMPK

phosphorylation may be increased in both NDI1 and AOX cell lines in response to Dox. While there may be biological reasons for the increased AMPK phosphorylation (relating to the activities of the alternative respiratory enzymes or their effects on ROS production) an important control that needs to be performed is to test the effects of Dox on untransfected host cells. This experiment will quickly confirm or exclude any effects of the Dox treatment on AMPK activity. Furthermore, ATP/ADP assays on Dox-treated untransfected host cells will identify if Dox has mild cytotoxic effects that may induce mild AMPK activation. If these results are negative, then ATP/ADP assays on Dox-induced NDI1 and AOX cell lines will tell us if the AMPK phosphorylation is caused by the NDI1 or AOX enzymes affecting ATP levels in the cell, or if there are other potential ways in which the enzymes are signalling to AMPK, e.g. via ROS production.

ROS production in Dox-induced NDI1 cells has not yet been confirmed. This will be tested in a number of ways. My aim is utilise the redox-sensitive mito-roGFP-ORP1 and cyto-roGFP-ORP1 probes (Gutscher et al., 2009, Albrecht et al., 2011) previously discussed (**2.7 Live cell confocal microscopy and imaging**). The probes are targeted to the mitochondrial matrix and the cytosol, respectively, so can detect H_2O_2 in both compartments. This approach will be particularly useful in determining the source of ROS production (if it occurs) and if the ROS can cross the mitochondrial membranes to the cytosol and affect processes there. Similarly, Prx 3 (mitochondrial) and Prx2 (cytosolic) dimerisation assays (**2.6 Peroxiredoxin dimerisation assays**) can be performed as a biologically relevant readout of increased ROS production. Prior to the ROS measurements, it will be necessary to perform a Dox induction time-course to identify the minimum incubation time required to detect NDI1 protein expression. ROS measurements can then be performed at regular intervals after NDI1 expression, as detection of increased ROS production may be time-sensitive. The same induction time-course and ROS measurements can also be performed on the AOX cell line.

Finally, when characterisation of the cell lines has been completed, the goal of this project is to investigate ROS production by RET in greater detail. RET is emerging as a physiologically relevant phenomenon that may play a role in cell signalling pathways, as a way in which mitochondria communicate with the rest of the cell. The cell models may be useful in investigating potential redox-regulated proteins, e.g. AMPK, as well as the response of known ROS scavenging proteins to a form of ROS production that can be technically difficult to induce in cell lines without mitochondrial inhibitors. Although the AOX cell line may (as was the case in the AOX mouse (El-Khoury et al., 2013)) require a blockade of electron transfer in order for activation, the evidence in the literature to date suggests that expression of functional NDI1 is sufficient to promote hyper-reduction of the Q pool and increase ROS production. Thus, creating a cell system that allows us to recreate RET conditions will be useful for further investigations by our lab and others in the field.

Chapter 6

General discussion and future aims

The focus of this thesis has been to work towards characterising the effects of primarily mitochondrially-derived ROS on AMPK activity in cells. In **Chapter 4**, I described the effects of both exogenous H_2O_2 (delivered as external boluses) and mitochondrially-derived ROS (produced by MPQ) on AMPK activity, cell ATP/ADP ratios and cellular redox state. Following these experiments, I arrived at the conclusion that, at least in this cell model, ROS primarily activates AMPK indirectly, by an AMP/ADP-dependent mechanism. However, regarding the H_2O_2 experiments, the magnitude of the AMPK activity markers (AMPK specific activity, and AMPK and ACC phosphorylation) were time-dependent, and did not correlate perfectly with changes in the cell's ATP/ADP ratio in response to H_2O_2. These results somewhat mirror other published results in the field (Auciello et al., 2014), which have been attributed to possible upstream effects of ROS, such as the response of phosphatases to H_2O_2, or to a direct mechanism possibly playing a minor role in the extent of AMPK activation in response to ROS (Zmijewski et al., 2010). Although this remains an intriguing possibility, AMPK activation in response to H_2O_2 in my experiments was only observed in response to supra-physiological concentrations of H_2O_2 (750 μM). At these concentrations, the evidence of Prx 2 hyperoxidation suggests that there is extensive oxidative damage, so any minor effects on AMPK activity at this concentration are unlikely to be physiologically relevant.

The results of selective, mitochondrially-derived ROS on AMPK activity were clearer. The first conclusion that can be made from these experiments is that although MPQ generated ROS rapidly and cumulatively within the mitochondrial matrix, there was no evidence that this ROS was transferring to the cytosol (undetectable Prx 2 dimerisation). This itself raises important questions in the redox-signalling field, relating to the threshold of mitochondrial matrix oxidation that needs to be reached before H_2O_2 can potentially diffuse from the matrix to the rest of the cell. As previously described, the mitochondrial matrix contains many antioxidant defence systems, including Prx, Trx and GSH systems. While it is conceivable that cell lines may have greater expression levels of these systems

than primary cells and tissues, going forward, it will be important to monitor the flux of ROS from mitochondria before implicating mitochondrial ROS in cytosolic, nuclear or other cellular signalling pathways that occur outside of the mitochondria. Of course, it may be that redox signals originate as elevated H_2O_2 within mitochondria, but that these signals are converted to a thiol redox relay in the IMS that passes on the signal to the rest of the cell . In this scenario, H_2O_2 may not be detected leaving the organelle. A second conclusion that can be made is that there was no significant change in AMPK activity in response to high levels of oxidation to the matrix caused by mitochondrially-derived ROS. Thirdly, any slight (not statistically significant) change in AMPK activity only occurred when the cell ATP/ADP ratios appeared to decrease slightly, indicating that any effects were due to mitochondrial ROS affecting ATP/ADP ratios, possibly by inhibiting mitochondrial ATP production. However, as neither the AMPK activation nor the decrease in ATP/ADP ratios was statistically significant, this conclusion is a tentative one at the moment.

Regarding the concept of compartmentalisation of mitochondrial ROS, a number of experiments could be performed in the future to confirm and build on my results. The conclusion would benefit from real-time data in live cells, possibly by utilising the cyto-roGFP-ORP1 or mito-roGFP-ORP1 probes, which allow visualisation of cytosolic or mitochondrial H_2O_2 (Gutscher et al., 2009, Sobotta et al., 2013). If a threshold of mitochondrial oxidation needs to be reached before H_2O_2 can diffuse from mitochondria, then it is likely that this threshold can be modulated by factors that affect the redox state of the mitochondrial matrix or H_2O_2 metabolism. An obvious candidate is Trx 2, which recharges Prx 3 in the mitochondrial matrix using the NADPH pool. Modulating the protein expression of Trx 2 (by overexpression or by knock-down/knock-out experiments) may help to clarify the spatiotemporal dynamics of ROS generation in the matrix. Furthermore, AMPK was identified as a target of Trx 1 in the cytosol (Shao et al., 2014), suggesting that cytosolic expression levels of antioxidant defence proteins play a role in how AMPK responds to ROS. Thus, modulating the expression of Trx 1 may also alter the

results of both the H_2O_2 and MPQ experiments, and thus clarify the biological mechanisms. Overexpressing the AMP/ADP-insensitive RG AMPK mutant (Hawley et al., 2010) in these cells would also offer further clarification of whether AMPK is directly in response to mitochondrial ROS.

The results from **Chapter 4** were observed in parallel with the development of an approach to analyse the redox state of candidate proteins in cells, Click-PEGylation **(Chapter 3)**. The goal was to adapt this method to analysing the redox state of AMPK in cell lysates in response to ROS, specifically mitochondrially-derived ROS. As the results from **Chapter 4** indicated that direct redox-regulation of AMPK was unlikely to be a main mechanism of activation in this cell model, the Click-PEGylation experiments on AMPK were halted after a few preliminary investigations of purified AMPK and AMPK in cell lysates. Prior to this, however, collaborator Lucie A.G. van Leeuwen and I performed a series of proof of principle experiments on the redox exemplar, GAPDH, and established the method as a useful alternative tool in the redox biology field (van Leeuwen et al., 2017). In Click-PEGylation, cysteine residues are differentially labelled according to thiol redox state, which is then assessed by mobility shift electrophoresis. The thiol-labelling step by maleimide derivatisation is separated from the PEG labelling (which confers mobility shifts), and linked using Click chemistry. This approach offers greater flexibility compared to existing single-step strategies. While broad redox-dependent mobility shifts were observable in purified AMPK α in response to differential pre-treatments with reductant (TCEP) or oxidant (diamide), detecting AMPK α in cell lysates proved more challenging. The reasons for the poor detection in cell lysates were likely technical issues which can be optimized in future experiments on AMPK or other proteins of interest, including: 1) the starting protein concentration of the cell lysate can be increased from 500 µg protein/ml. The various steps in the Click-PEGylation protocol, including spin column and protein purification steps, can lead to sample loss. While this is not a problem for highly expressed metabolic proteins, such as GAPDH, AMPK is less highly expressed in cells and so sample loss greatly dimished AMPK protein detection by

Western blotting. Thus, increasing the starting protein concentration should minimise this problem; 2) some protein degradation may have occurred during the catalyst incubation. This may have occurred if any of the reagents had become oxidised during preparation, with the formation of small amounts of H_2O_2. This can lead to Fenton-like chemistry (due to the presence of Cu^{1+}) and the formation of hydroxyl radical, which can lead to protein degradation (Finney and O'Halloran, 2003). Thus, adding antioxidants to the catalyst incubation (e.g. butylated hydroxyanisole (Verhagen et al., 1991)) may inhibit protein degradation if it remains an issue.

Although the AMPK α catalytic subunit has previously been the focus of experiments searching for redox-sensitive cysteine residues that may play a role in AMPK regulation (Zmijewski et al., 2010, Shao et al., 2014), the β subunit also plays a vital role in AMPK regulation, particularly by AMP/ADP-independent activation by small molecules that bind the ADaM site. This mode of activation appears to be affected by post-translational modifications to the β subunit (Hardie, 2016). It is also reported that the β1 and β2 isoforms have different affinities for glycogen (Koay et al., 2010), differential expression in different cell types (Birk and Wojtaszewski, 2006, Hardie, 2017), and are differentially activated by ADaM-site activators (Hardie, 2017). The human β1 isoform contains three cysteine residues and the β2 isoform contains two. Thus, the response of the β subunit to oxidation could in principle confer differential effects on AMPK activity in an isoform-dependent manner. As no published paper to date (nor this body of work) have explicitly excluded ROS from having a minor role in AMPK regulation, focusing on the β subunit may help to clarify some of the interesting differences observed in the magnitude of AMPK activation in response to different stimuli. Due to the relatively low molecular weights of the AMPK β subunit isoforms (30 or 38 kDa), the small number of cysteine residues and the availability of sensitive primary antibodies, it should be possible to assess the redox state of the β subunit isoforms by Click-PEGylation.

Chapter 5 described the preliminary data of a project that is of interest to other work in the lab as well as my own. The goal of this project is to create stable cell lines expressing the alternative respiratory enzymes, NDI1 and AOX, so that the biological effects of RET in cells can be investigated. NDI1 and AOX have previously been shown to increase or decrease mitochondrial ROS production by RET by reducing or oxidizing the Q pool, respectively. Stable cell lines in which expression of the alternative respiratory enzymes can be controlled and preferably titrated is favourable, as it should enable ROS production by RET to be turned on or off, or increased gradually. The results presented are very much preliminary but I confirmed that both the NDI1 and AOX cell lines express proteins under the control of Dox. A gradation of NDI1 protein expression was achieved between 1 – 100 ng Dox/ml and AOX between 10 – 100 ng Dox/ml. Functional NDI1 protein expression was confirmed by Seahorse XF96 respirometry (measured as rotenone-insensitive mitochondrial respiration). However, the functionality of AOX has not yet been confirmed. AOX is cyanide-resistant (unlike complex IV, which is cyanide sensitive) but is inhibited by propyl gallate (Fernandez-Ayala et al., 2009). Thus, sensitivity to propyl gallate can be used as a measure of functional AOX expression. ROS production in Dox-induced NDI1 or AOX cells has not yet been measured and will be a key focus of experiments in the immediate future, tested by previously described or other methods. If NDI1 and AOX have opposing effects on ROS production, then the nature of the ROS production will need to be confirmed, i.e. is it the result of forward or reverse electron transfer. RET is characterised by a hyper-reduced Q pool, high ΔP, and superoxide production from complex I that is inhibited by rotenone (which binds the Q-binding site, blocking electron flow to the complex I FMN) and FCCP (which dissipates the ΔP). Q redox state, likely to be the key determinant of RET in these cell lines, can be assessed by HPLC separation followed by identification by differential UV/Vis absorption spectra (Scialo et al., 2016). If the results from the single-gene expressing cell lines are promising, a future experiment may involve co-expressing AOX and NDI1 in the same cell model. Previous papers have found that AOX is most functional when there is a blockade of the ETC (El-Khoury et al., 2013) or when there is increased

electron donation to the Q pool, such as from NDI1 co-expression (Scialo et al., 2016).

Finally, as discussed in **Chapter 5**, the effects of NDI1 or AOX expression on AMPK activity are currently complicated by possible off-target effects of Dox on AMPK activity. This can be easily addressed with appropriate control experiments. However, whether AMPK will still be seen as a potential target of mitochondrial ROS signalling by RET is debatable, although the expansion of the results discussed in **Chapter 4** would be vital to completely address this hypothesis. Even so, a cell model of RET will be a valuable tool for our and other labs in studying the downstream targets of ROS production by RET, be that AMPK or other proteins.

Together, the work in this thesis offers further understanding into the role of ROS and mitochondrial ROS in AMPK activity, has resulted in the generation of a new method for easily assessing the redox state of candidate proteins and will potentially result in a cell model of mitochondrial ROS production of RET, with a wide scope for future work that can follow. However, at this stage my view is that the redox regulation of AMPK activity seems unlikely to be a significant aspect of its natural regulation, a conclusion that is in agreement with other published results that have emerged during the course of this project (Auciello et al., 2014).

7. References

AFFOURTIT, C., KRAB, K. & MOORE, A. L. 2001. Control of plant mitochondrial respiration. *Biochim Biophys Acta,* 1504**,** 58-69.

AHLER, E., SULLIVAN, W. J., CASS, A., BRAAS, D., YORK, A. G., BENSINGER, S. J., GRAEBER, T. G. & CHRISTOFK, H. R. 2013. Doxycycline alters metabolism and proliferation of human cell lines. *PLoS One,* 8**,** e64561.

AKRAM, M. 2014. Citric acid cycle and role of its intermediates in metabolism. *Cell Biochem Biophys,* 68**,** 475-8.

ALBRECHT, S. C., BARATA, A. G., GROSSHANS, J., TELEMAN, A. A. & DICK, T. P. 2011. In vivo mapping of hydrogen peroxide and oxidized glutathione reveals chemical and regional specificity of redox homeostasis. *Cell Metab,* 14**,** 819-29.

ANDRES, V. & WALSH, K. 1996. Myogenin expression, cell cycle withdrawal, and phenotypic differentiation are temporally separable events that precede cell fusion upon myogenesis. *J Cell Biol,* 132**,** 657-66.

ARNOULT, D., SOARES, F., TATTOLI, I. & GIRARDIN, S. E. 2011. Mitochondria in innate immunity. *EMBO Rep,* 12**,** 901-10.

AUCIELLO, F. R., ROSS, F. A., IKEMATSU, N. & HARDIE, D. G. 2014. Oxidative stress activates AMPK in cultured cells primarily by increasing cellular AMP and/or ADP. *FEBS Lett,* 588**,** 3361-6.

AZEVEDO, D., TACNET, F., DELAUNAY, A., RODRIGUES-POUSADA, C. & TOLEDANO, M. B. 2003. Two redox centers within Yap1 for H2O2 and thiol-reactive chemicals signaling. *Free Radic Biol Med,* 35**,** 889-900.

BARBER-SINGH, J., SEO, B. B., NAKAMARU-OGISO, E., LAU, Y. S., MATSUNO-YAGI, A. & YAGI, T. 2009. Neuroprotective effect of long-term NDI1 gene expression in a chronic mouse model of Parkinson disorder. *Rejuvenation Res,* 12**,** 259-67.

BARRANCO-MEDINA, S., LAZARO, J. J. & DIETZ, K. J. 2009. The oligomeric conformation of peroxiredoxins links redox state to function. *FEBS Lett,* 583**,** 1809-16.

BELL, E. L. & CHANDEL, N. S. 2007. Mitochondrial oxygen sensing: regulation of hypoxia-inducible factor by mitochondrial generated reactive oxygen species. *Essays Biochem,* 43**,** 17-27.

BENITEZ, L. V. & ALLISON, W. S. 1974. The inactivation of the acyl phosphatase activity catalyzed by the sulfenic acid form of glyceraldehyde 3-phosphate dehydrogenase by dimedone and olefins. *J Biol Chem,* 249**,** 6234-43.

BIENERT, G. P., MOLLER, A. L., KRISTIANSEN, K. A., SCHULZ, A., MOLLER, I. M., SCHJOERRING, J. K. & JAHN, T. P. 2007. Specific aquaporins facilitate the diffusion of hydrogen peroxide across membranes. *J Biol Chem,* 282**,** 1183-92.

BIRK, J. B. & WOJTASZEWSKI, J. F. 2006. Predominant alpha2/beta2/gamma3 AMPK activation during exercise in human skeletal muscle. *J Physiol,* 577**,** 1021-32.

BIRSOY, K., POSSEMATO, R., LORBEER, F. K., BAYRAKTAR, E. C., THIRU, P., YUCEL, B., WANG, T., CHEN, W. W., CLISH, C. B. & SABATINI, D. M. 2014. Metabolic determinants of cancer cell sensitivity to glucose limitation and biguanides. *Nature,* 508**,** 108-12.

BLAZA, J. N., SERRELI, R., JONES, A. J., MOHAMMED, K. & HIRST, J. 2014. Kinetic evidence against partitioning of the ubiquinone pool and the catalytic relevance of respiratory-chain supercomplexes. *Proc Natl Acad Sci U S A,* 111**,** 15735-40.

BRAND, M. D. & MURPHY, M. P. 1987. Control of electron flux through the respiratory chain in mitochondria and cells. *Biol Rev Camb Philos Soc,* 62**,** 141-93.

BRANDES, N., SCHMITT, S. & JAKOB, U. 2009. Thiol-based redox switches in eukaryotic proteins. *Antioxid Redox Signal,* 11**,** 997-1014.

BRIDGES, H. R., JONES, A. J., POLLAK, M. N. & HIRST, J. 2014. Effects of metformin and other biguanides on oxidative phosphorylation in mitochondria. *Biochem J,* 462**,** 475-87.

BROWN, G. C. 1992. Control of respiration and ATP synthesis in mammalian mitochondria and cells. *Biochem J,* 284 (Pt 1)**,** 1-13.

BROWN, G. C., LAKIN-THOMAS, P. L. & BRAND, M. D. 1990. Control of respiration and oxidative phosphorylation in isolated rat liver cells. *Eur J Biochem,* 192**,** 355-62.

BURGOYNE, J. R., OVIOSU, O. & EATON, P. 2013. The PEG-switch assay: a fast semi-quantitative method to determine protein reversible cysteine oxidation. *J Pharmacol Toxicol Methods,* 68**,** 297-301.

BUSKIEWICZ, I. A., MONTGOMERY, T., YASEWICZ, E. C., HUBER, S. A., MURPHY, M. P., HARTLEY, R. C., KELLY, R., CROW, M. K., PERL, A., BUDD, R. C. & KOENIG, A. 2016. Reactive oxygen species induce virus-independent MAVS oligomerization in systemic lupus erythematosus. *Sci Signal,* 9**,** ra115.

CALAMITA, G., FERRI, D., GENA, P., LIQUORI, G. E., CAVALIER, A., THOMAS, D. & SVELTO, M. 2005. The inner mitochondrial membrane has aquaporin-8 water channels and is highly permeable to water. *J Biol Chem,* 280**,** 17149-53.

CARLING, D., MAYER, F. V., SANDERS, M. J. & GAMBLIN, S. J. 2011. AMP-activated protein kinase: nature's energy sensor. *Nat Chem Biol,* 7**,** 512-8.

CAVALIER-SMITH, T. 2006. Origin of mitochondria by intracellular enslavement of a photosynthetic purple bacterium. *Proc Biol Sci,* 273**,** 1943-52.

CHAE, H. Z., ROBISON, K., POOLE, L. B., CHURCH, G., STORZ, G. & RHEE, S. G. 1994. Cloning and sequencing of thiol-specific antioxidant from mammalian brain: alkyl hydroperoxide reductase and thiol-specific antioxidant define a large family of antioxidant enzymes. *Proc Natl Acad Sci U S A,* 91**,** 7017-21.

CHANCE, B. & WILLIAMS, G. R. 1956. Respiratory enzymes in oxidative phosphorylation. VI. The effects of adenosine diphosphate on azide-treated mitochondria. *J Biol Chem,* 221**,** 477-89.

CHANDEL, N. S., MALTEPE, E., GOLDWASSER, E., MATHIEU, C. E., SIMON, M. C. & SCHUMACKER, P. T. 1998. Mitochondrial reactive oxygen species trigger hypoxia-induced transcription. *Proc Natl Acad Sci U S A,* 95**,** 11715-20.

CHEUNG, P. C., SALT, I. P., DAVIES, S. P., HARDIE, D. G. & CARLING, D. 2000. Characterization of AMP-activated protein kinase gamma-subunit isoforms and their role in AMP binding. *Biochem J,* 346 Pt 3**,** 659-69.

CHOUCHANI, E. T., PELL, V. R., GAUDE, E., AKSENTIJEVIC, D., SUNDIER, S. Y., ROBB, E. L., LOGAN, A., NADTOCHIY, S. M., ORD, E. N., SMITH, A. C., EYASSU, F., SHIRLEY, R., HU, C. H., DARE, A. J., JAMES, A. M., ROGATTI, S., HARTLEY, R. C., EATON, S., COSTA, A. S., BROOKES, P. S., DAVIDSON, S. M., DUCHEN, M. R., SAEB-PARSY, K., SHATTOCK, M. J., ROBINSON, A. J., WORK, L. M., FREZZA, C., KRIEG, T. & MURPHY, M. P. 2014. Ischaemic accumulation of succinate controls reperfusion injury through mitochondrial ROS. *Nature,* 515**,** 431-5.

CHOUCHANI, E. T., PELL, V. R., JAMES, A. M., WORK, L. M., SAEB-PARSY, K., FREZZA, C., KRIEG, T. & MURPHY, M. P. 2016. A Unifying Mechanism for Mitochondrial Superoxide Production during Ischemia-Reperfusion Injury. *Cell Metab,* 23**,** 254-63.

CIVITARESE, A. E., CARLING, S., HEILBRONN, L. K., HULVER, M. H., UKROPCOVA, B., DEUTSCH, W. A., SMITH, S. R., RAVUSSIN, E. & TEAM, C. P. 2007. Calorie restriction increases muscle mitochondrial biogenesis in healthy humans. *PLoS Med,* 4**,** e76.

COCHEME, H. M., LOGAN, A., PRIME, T. A., ABAKUMOVA, I., QUIN, C., MCQUAKER, S. J., PATEL, J. V., FEARNLEY, I. M., JAMES, A. M., PORTEOUS, C. M., SMITH, R. A., HARTLEY, R. C., PARTRIDGE, L. & MURPHY, M. P. 2012. Using the mitochondria-targeted ratiometric mass spectrometry probe MitoB to measure H2O2 in living Drosophila. *Nat Protoc,* 7**,** 946-58.

COLLINS, Y., CHOUCHANI, E. T., JAMES, A. M., MENGER, K. E., COCHEME, H. M. & MURPHY, M. P. 2012. Mitochondrial redox signalling at a glance. *J Cell Sci,* 125**,** 801-6.

COOL, B., ZINKER, B., CHIOU, W., KIFLE, L., CAO, N., PERHAM, M., DICKINSON, R., ADLER, A., GAGNE, G., IYENGAR, R., ZHAO, G., MARSH, K., KYM, P., JUNG, P., CAMP, H. S. & FREVERT, E. 2006. Identification and characterization of a small molecule AMPK activator that treats key components of type 2 diabetes and the metabolic syndrome. *Cell Metab,* 3**,** 403-16.

COUGHLAN, K. A., VALENTINE, R. J., RUDERMAN, N. B. & SAHA, A. K. 2014. AMPK activation: a therapeutic target for type 2 diabetes? *Diabetes Metab Syndr Obes,* 7**,** 241-53.

COVIAN, R. & BALABAN, R. S. 2012. Cardiac mitochondrial matrix and respiratory complex protein phosphorylation. *Am J Physiol Heart Circ Physiol,* 303**,** H940-66.

COX, A. G., PULLAR, J. M., HUGHES, G., LEDGERWOOD, E. C. & HAMPTON, M. B. 2008. Oxidation of mitochondrial peroxiredoxin 3 during the initiation of receptor-mediated apoptosis. *Free Radic Biol Med,* 44**,** 1001-9.

COX, A. G., WINTERBOURN, C. C. & HAMPTON, M. B. 2009. Mitochondrial peroxiredoxin involvement in antioxidant defence and redox signalling. *Biochem J,* 425**,** 313-25.

DASSA, E. P., DUFOUR, E., GONCALVES, S., PAUPE, V., HAKKAART, G. A., JACOBS, H. T. & RUSTIN, P. 2009. Expression of the alternative oxidase complements cytochrome c oxidase deficiency in human cells. *EMBO Mol Med,* 1**,** 30-6.

DAVIES, S. P., HELPS, N. R., COHEN, P. T. & HARDIE, D. G. 1995. 5'-AMP inhibits dephosphorylation, as well as promoting phosphorylation, of the AMP-activated protein kinase.

Studies using bacterially expressed human protein phosphatase-2C alpha and native bovine protein phosphatase-2AC. *FEBS Lett,* 377**,** 421-5.

DIETZ, K. J., HORLING, F., KONIG, J. & BAIER, M. 2002. The function of the chloroplast 2-cysteine peroxiredoxin in peroxide detoxification and its regulation. *J Exp Bot,* 53**,** 1321-9.

DIKALOV, S. I. & HARRISON, D. G. 2014. Methods for detection of mitochondrial and cellular reactive oxygen species. *Antioxid Redox Signal,* 20**,** 372-82.

DRISDEL, R. C. & GREEN, W. N. 2004. Labeling and quantifying sites of protein palmitoylation. *Biotechniques,* 36**,** 276-85.

DROSE, S., STEPANOVA, A. & GALKIN, A. 2016. Ischemic A/D transition of mitochondrial complex I and its role in ROS generation. *Biochim Biophys Acta,* 1857**,** 946-57.

DUCHEN, M. R. & SZABADKAI, G. 2010. Roles of mitochondria in human disease. *Essays Biochem,* 47**,** 115-37.

EL-KHOURY, R., DUFOUR, E., RAK, M., RAMANANTSOA, N., GRANDCHAMP, N., CSABA, Z., DUVILLIE, B., BENIT, P., GALLEGO, J., GRESSENS, P., SARKIS, C., JACOBS, H. T. & RUSTIN, P. 2013. Alternative oxidase expression in the mouse enables bypassing cytochrome c oxidase blockade and limits mitochondrial ROS overproduction. *PLoS Genet,* 9**,** e1003182.

EL-KHOURY, R., KEMPPAINEN, K. K., DUFOUR, E., SZIBOR, M., JACOBS, H. T. & RUSTIN, P. 2014. Engineering the alternative oxidase gene to better understand and counteract mitochondrial defects: state of the art and perspectives. *Br J Pharmacol,* 171**,** 2243-9.

ELKALAF, M., ANDEL, M. & TRNKA, J. 2013. Low glucose but not galactose enhances oxidative mitochondrial metabolism in C2C12 myoblasts and myotubes. *PLoS One,* 8**,** e70772.

EMERLING, B. M., WEINBERG, F., SNYDER, C., BURGESS, Z., MUTLU, G. M., VIOLLET, B., BUDINGER, G. R. & CHANDEL, N. S. 2009. Hypoxic activation of AMPK is dependent on mitochondrial ROS but independent of an increase in AMP/ATP ratio. *Free Radic Biol Med,* 46**,** 1386-91.

EXNER, N., LUTZ, A. K., HAASS, C. & WINKLHOFER, K. F. 2012. Mitochondrial dysfunction in Parkinson's disease: molecular mechanisms and pathophysiological consequences. *EMBO J,* 31**,** 3038-62.

FERNANDEZ-AYALA, D. J., SANZ, A., VARTIAINEN, S., KEMPPAINEN, K. K., BABUSIAK, M., MUSTALAHTI, E., COSTA, R., TUOMELA, T., ZEVIANI, M., CHUNG, J., O'DELL, K. M., RUSTIN, P. & JACOBS, H. T. 2009. Expression of the Ciona intestinalis alternative oxidase (AOX) in Drosophila complements defects in mitochondrial oxidative phosphorylation. *Cell Metab,* 9**,** 449-60.

FINKEL, T. 2012. Signal transduction by mitochondrial oxidants. *J Biol Chem,* 287**,** 4434-40.

FINNEY, L. A. & O'HALLORAN, T. V. 2003. Transition metal speciation in the cell: insights from the chemistry of metal ion receptors. *Science,* 300**,** 931-6.

FREY, T. G. & MANNELLA, C. A. 2000. The internal structure of mitochondria. *Trends Biochem Sci,* 25**,** 319-24.

FRIEDMAN, J. R. & NUNNARI, J. 2014. Mitochondrial form and function. *Nature,* 505**,** 335-43.

FULLERTON, M. D., GALIC, S., MARCINKO, K., SIKKEMA, S., PULINILKUNNIL, T., CHEN, Z. P., O'NEILL, H. M., FORD, R. J., PALANIVEL, R., O'BRIEN, M., HARDIE, D. G., MACAULAY, S. L., SCHERTZER, J. D., DYCK, J. R., VAN DENDEREN, B. J., KEMP, B. E. & STEINBERG, G. R. 2013. Single phosphorylation sites in Acc1 and Acc2 regulate lipid homeostasis and the insulin-sensitizing effects of metformin. *Nat Med,* 19**,** 1649-54.

GARCIA, D. & SHAW, R. J. 2017. AMPK: Mechanisms of Cellular Energy Sensing and Restoration of Metabolic Balance. *Mol Cell,* 66**,** 789-800.

GARDNER, P. R. 2002. Aconitase: sensitive target and measure of superoxide. *Methods Enzymol,* 349**,** 9-23.

GORENKOVA, N., ROBINSON, E., GRIEVE, D. J. & GALKIN, A. 2013. Conformational change of mitochondrial complex I increases ROS sensitivity during ischemia. *Antioxid Redox Signal,* 19**,** 1459-68.

GORMAN, G. S., CHINNERY, P. F., DIMAURO, S., HIRANO, M., KOGA, Y., MCFARLAND, R., SUOMALAINEN, A., THORBURN, D. R., ZEVIANI, M. & TURNBULL, D. M. 2016. Mitochondrial diseases. *Nat Rev Dis Primers,* 2**,** 16080.

GOUGH, D. R. & COTTER, T. G. 2011. Hydrogen peroxide: a Jekyll and Hyde signalling molecule. *Cell Death Dis,* 2**,** e213.

GOWANS, G. J., HAWLEY, S. A., ROSS, F. A. & HARDIE, D. G. 2013. AMP is a true physiological regulator of AMP-activated protein kinase by both allosteric activation and enhancing net phosphorylation. *Cell Metab,* 18**,** 556-66.

GRANT, C. M., QUINN, K. A. & DAWES, I. W. 1999. Differential protein S-thiolation of glyceraldehyde-3-phosphate dehydrogenase isoenzymes influences sensitivity to oxidative stress. *Mol Cell Biol,* 19**,** 2650-6.

GRAY, M. W. 2012. Mitochondrial evolution. *Cold Spring Harb Perspect Biol,* 4**,** a011403.

GREEN, D. R., GALLUZZI, L. & KROEMER, G. 2011. Mitochondria and the autophagy-inflammation-cell death axis in organismal aging. *Science,* 333**,** 1109-12.

GREER, E. L., OSKOUI, P. R., BANKO, M. R., MANIAR, J. M., GYGI, M. P., GYGI, S. P. & BRUNET, A. 2007. The energy sensor AMP-activated protein kinase directly regulates the mammalian FOXO3 transcription factor. *J Biol Chem,* 282**,** 30107-19.

GUSTAFSSON, C. M., FALKENBERG, M. & LARSSON, N. G. 2016. Maintenance and Expression of Mammalian Mitochondrial DNA. *Annu Rev Biochem,* 85**,** 133-60.

GUTSCHER, M., SOBOTTA, M. C., WABNITZ, G. H., BALLIKAYA, S., MEYER, A. J., SAMSTAG, Y. & DICK, T. P. 2009. Proximity-based protein thiol oxidation by H2O2-scavenging peroxidases. *J Biol Chem,* 284**,** 31532-40.

HAKKAART, G. A., DASSA, E. P., JACOBS, H. T. & RUSTIN, P. 2006. Allotopic expression of a mitochondrial alternative oxidase confers cyanide resistance to human cell respiration. *EMBO Rep,* 7**,** 341-5.

HALESTRAP, A. 2005. Biochemistry: a pore way to die. *Nature,* 434**,** 578-9.

HALL, A., KARPLUS, P. A. & POOLE, L. B. 2009. Typical 2-Cys peroxiredoxins--structures, mechanisms and functions. *FEBS J,* 276**,** 2469-77.

HAMANAKA, R. B. & CHANDEL, N. S. 2012. Targeting glucose metabolism for cancer therapy. *J Exp Med,* 209**,** 211-5.

HARDIE, D. G. 2011. AMP-activated protein kinase: an energy sensor that regulates all aspects of cell function. *Genes Dev,* 25**,** 1895-908.

HARDIE, D. G. 2016. Regulation of AMP-activated protein kinase by natural and synthetic activators. *Acta Pharm Sin B,* 6**,** 1-19.

HARDIE, D. G. 2017. Targeting an energy sensor to treat diabetes. *Science,* 357**,** 455-456.

HARDIE, D. G. & ALESSI, D. R. 2013. LKB1 and AMPK and the cancer-metabolism link - ten years after. *BMC Biol,* 11**,** 36.

HARDIE, D. G., CARLING, D. & GAMBLIN, S. J. 2011. AMP-activated protein kinase: also regulated by ADP? *Trends Biochem Sci,* 36**,** 470-7.

HARDIE, D. G. & HAWLEY, S. A. 2001. AMP-activated protein kinase: the energy charge hypothesis revisited. *Bioessays,* 2**3,** 1112-1119.

HARDIE, D. G., ROSS, F. A. & HAWLEY, S. A. 2012. AMPK: a nutrient and energy sensor that maintains energy homeostasis. *Nat Rev Mol Cell Biol,* 13**,** 251-62.

HARDIE, D. G., SALT, I. P. & DAVIES, S. P. 2000. Analysis of the role of the AMP-activated protein kinase in the response to cellular stress. *Methods Mol Biol,* 99**,** 63-74.

HARDIE, D. G., SCHAFFER, B. E. & BRUNET, A. 2016. AMPK: An Energy-Sensing Pathway with Multiple Inputs and Outputs. *Trends Cell Biol,* 26**,** 190-201.

HART, P. C., MAO, M., DE ABREU, A. L., ANSENBERGER-FRICANO, K., EKOUE, D. N., GANINI, D., KAJDACSY-BALLA, A., DIAMOND, A. M., MINSHALL, R. D., CONSOLARO, M. E., SANTOS, J. H. & BONINI, M. G. 2015. MnSOD upregulation sustains the Warburg effect via mitochondrial ROS and AMPK-dependent signalling in cancer. *Nat Commun,* 6**,** 6053.

HAWLEY, S. A., BOUDEAU, J., REID, J. L., MUSTARD, K. J., UDD, L., MAKELA, T. P., ALESSI, D. R. & HARDIE, D. G. 2003. Complexes between the LKB1 tumor suppressor, STRAD alpha/beta and MO25 alpha/beta are upstream kinases in the AMP-activated protein kinase cascade. *J Biol,* 2**,** 28.

HAWLEY, S. A., DAVISON, M., WOODS, A., DAVIES, S. P., BERI, R. K., CARLING, D. & HARDIE, D. G. 1996. Characterization of the AMP-activated protein kinase kinase from rat liver and identification of threonine 172 as the major site at which it phosphorylates AMP-activated protein kinase. *J Biol Chem,* 271**,** 27879-87.

HAWLEY, S. A., FULLERTON, M. D., ROSS, F. A., SCHERTZER, J. D., CHEVTZOFF, C., WALKER, K. J., PEGGIE, M. W., ZIBROVA, D., GREEN, K. A., MUSTARD, K. J., KEMP, B. E., SAKAMOTO, K., STEINBERG, G. R. & HARDIE, D. G. 2012. The ancient drug salicylate directly activates AMP-activated protein kinase. *Science,* 336**,** 918-22.

HAWLEY, S. A., PAN, D. A., MUSTARD, K. J., ROSS, L., BAIN, J., EDELMAN, A. M., FRENGUELLI, B. G. & HARDIE, D. G. 2005. Calmodulin-dependent protein kinase kinase-beta is an alternative upstream kinase for AMP-activated protein kinase. *Cell Metab,* 2**,** 9-19.

HAWLEY, S. A., ROSS, F. A., CHEVTZOFF, C., GREEN, K. A., EVANS, A., FOGARTY, S., TOWLER, M. C., BROWN, L. J., OGUNBAYO, O. A., EVANS, A. M. & HARDIE, D. G. 2010. Use of Cells Expressing gamma Subunit Variants to Identify Diverse Mechanisms of AMPK Activation. *Cell Metabolism,* 11**,** 554-565.

HELD, J. M., DANIELSON, S. R., BEHRING, J. B., ATSRIKU, C., BRITTON, D. J., PUCKETT, R. L., SCHILLING, B., CAMPISI, J., BENZ, C. C. & GIBSON, B. W. 2010. Targeted quantitation of site-specific cysteine oxidation in endogenous proteins using a differential alkylation and multiple reaction monitoring mass spectrometry approach. *Mol Cell Proteomics,* 9**,** 1400-10.

HELD, J. M. & GIBSON, B. W. 2012. Regulatory control or oxidative damage? Proteomic approaches to interrogate the role of cysteine oxidation status in biological processes. *Mol Cell Proteomics,* 11**,** R111 013037.

HERRMANN, J. M. & RIEMER, J. 2010. The intermembrane space of mitochondria. *Antioxid Redox Signal,* 13**,** 1341-58.

HERRMANN, J. M. & RIEMER, J. 2012. Mitochondrial disulfide relay: redox-regulated protein import into the intermembrane space. *J Biol Chem,* 287**,** 4426-33.

HILL, B. G., REILY, C., OH, J. Y., JOHNSON, M. S. & LANDAR, A. 2009. Methods for the determination and quantification of the reactive thiol proteome. *Free Radic Biol Med,* 47**,** 675-83.

HIRST, J. & ROESSLER, M. M. 2016. Energy conversion, redox catalysis and generation of reactive oxygen species by respiratory complex I. *Biochim Biophys Acta,* 1857**,** 872-83.

HOLLOSZY, J. O. 1967. Biochemical adaptations in muscle. Effects of exercise on mitochondrial oxygen uptake and respiratory enzyme activity in skeletal muscle. *J Biol Chem,* 242**,** 2278-82.

HOLMSTROM, K. M. & FINKEL, T. 2014. Cellular mechanisms and physiological consequences of redox-dependent signalling. *Nat Rev Mol Cell Biol,* 15**,** 411-21.

HONG, S. P., LEIPER, F. C., WOODS, A., CARLING, D. & CARLSON, M. 2003. Activation of yeast Snf1 and mammalian AMP-activated protein kinase by upstream kinases. *Proc Natl Acad Sci U S A,* 100**,** 8839-43.

HOUDE, V. P., RITORTO, M. S., GOURLAY, R., VARGHESE, J., DAVIES, P., SHPIRO, N., SAKAMOTO, K. & ALESSI, D. R. 2014. Investigation of LKB1 Ser431 phosphorylation and Cys433 farnesylation using mouse knockin analysis reveals an unexpected role of prenylation in regulating AMPK activity. *Biochem J,* 458**,** 41-56.

HURD, T. R., COLLINS, Y., ABAKUMOVA, I., CHOUCHANI, E. T., BARANOWSKI, B., FEARNLEY, I. M., PRIME, T. A., MURPHY, M. P. & JAMES, A. M. 2012. Inactivation of pyruvate dehydrogenase kinase 2 by mitochondrial reactive oxygen species. *J Biol Chem,* 287**,** 35153-60.

JAFFREY, S. R., ERDJUMENT-BROMAGE, H., FERRIS, C. D., TEMPST, P. & SNYDER, S. H. 2001. Protein S-nitrosylation: a physiological signal for neuronal nitric oxide. *Nat Cell Biol,* 3**,** 193-7.

JAGER, S., HANDSCHIN, C., ST-PIERRE, J. & SPIEGELMAN, B. M. 2007. AMP-activated protein kinase (AMPK) action in skeletal muscle via direct phosphorylation of PGC-1alpha. *Proc Natl Acad Sci U S A,* 104**,** 12017-22.

JANSSEN-HEININGER, Y. M., MOSSMAN, B. T., HEINTZ, N. H., FORMAN, H. J., KALYANARAMAN, B., FINKEL, T., STAMLER, J. S., RHEE, S. G. & VAN DER VLIET, A. 2008. Redox-based regulation of signal transduction: principles, pitfalls, and promises. *Free Radic Biol Med,* 45**,** 1-17.

JIN JUNG, K., HYUN KIM, D., KYEONG LEE, E., WOO SONG, C., PAL YU, B. & YOUNG CHUNG, H. 2013. Oxidative stress induces inactivation of protein phosphatase 2A, promoting proinflammatory NF-kappaB in aged rat kidney. *Free Radic Biol Med,* 61**,** 206-17.

JORNAYVAZ, F. R. & SHULMAN, G. I. 2010. Regulation of mitochondrial biogenesis. *Essays Biochem,* 47**,** 69-84.

KEMPPAINEN, K. K., RINNE, J., SRIRAM, A., LAKANMAA, M., ZEB, A., TUOMELA, T., POPPLESTONE, A., SINGH, S., SANZ, A., RUSTIN, P. & JACOBS, H. T. 2014. Expression of alternative oxidase in Drosophila ameliorates diverse phenotypes due to cytochrome oxidase deficiency. *Hum Mol Genet,* 23**,** 2078-93.

KIM, A., MURPHY, M. P. & OBERLEY, T. D. 2005. Mitochondrial redox state regulates transcription of the nuclear-encoded mitochondrial protein manganese superoxide dismutase: a proposed adaptive response to mitochondrial redox imbalance. *Free Radic Biol Med,* 38**,** 644-54.

KIM, A. S., MILLER, E. J., WRIGHT, T. M., LI, J., QI, D., ATSINA, K., ZAHA, V., SAKAMOTO, K. & YOUNG, L. H. 2011. A small molecule AMPK activator protects the heart against ischemia-reperfusion injury. *J Mol Cell Cardiol,* 51**,** 24-32.

KOAY, A., WOODCROFT, B., PETRIE, E. J., YUE, H., EMANUELLE, S., BIERI, M., BAILEY, M. F., HARGREAVES, M., PARK, J. T., PARK, K. H., RALPH, S., NEUMANN, D., STAPLETON, D. & GOOLEY, P. R. 2010. AMPK beta subunits display isoform specific affinities for carbohydrates. *FEBS Lett,* 584**,** 3499-503.

KOBAYASHI, M. & YAMAMOTO, M. 2006. Nrf2-Keap1 regulation of cellular defense mechanisms against electrophiles and reactive oxygen species. *Adv Enzyme Regul,* 46**,** 113-40.

KOLB, H. C., FINN, M. G. & SHARPLESS, K. B. 2001. Click Chemistry: Diverse Chemical Function from a Few Good Reactions. *Angew Chem Int Ed Engl,* 40**,** 2004-2021.

KOSOWER, N. S. & KOSOWER, E. M. 1995. Diamide: an oxidant probe for thiols. *Methods Enzymol,* 251**,** 123-33.

KUMAR, V., KLEFFMANN, T., HAMPTON, M. B., CANNELL, M. B. & WINTERBOURN, C. C. 2013. Redox proteomics of thiol proteins in mouse heart during ischemia/reperfusion using ICAT reagents and mass spectrometry. *Free Radic Biol Med,* 58**,** 109-17.

LANE, N. & MARTIN, W. 2010. The energetics of genome complexity. *Nature,* 467**,** 929-34.

LANGENDORF, C. G. & KEMP, B. E. 2015. Choreography of AMPK activation. *Cell Res,* 25**,** 5-6.

LEARY, S. C., BATTERSBY, B. J., HANSFORD, R. G. & MOYES, C. D. 1998. Interactions between bioenergetics and mitochondrial biogenesis. *Biochim Biophys Acta,* 1365**,** 522-30.

LEE, H. & YOON, Y. 2016. Mitochondrial fission and fusion. *Biochem Soc Trans,* 44**,** 1725-1735.

LEICHERT, L. I., GEHRKE, F., GUDISEVA, H. V., BLACKWELL, T., ILBERT, M., WALKER, A. K., STRAHLER, J. R., ANDREWS, P. C. & JAKOB, U. 2008. Quantifying changes in the thiol redox proteome upon oxidative stress in vivo. *Proc Natl Acad Sci U S A,* 105**,** 8197-202.

LEICHERT, L. I. & JAKOB, U. 2004. Protein thiol modifications visualized in vivo. *PLoS Biol,* 2**,** e333.

LIANG, J., XU, Z. X., DING, Z., LU, Y., YU, Q., WERLE, K. D., ZHOU, G., PARK, Y. Y., PENG, G., GAMBELLO, M. J. & MILLS, G. B. 2015. Myristoylation confers noncanonical AMPK functions in autophagy selectivity and mitochondrial surveillance. *Nat Commun,* 6**,** 7926.

LIU, X., CHHIPA, R. R., NAKANO, I. & DASGUPTA, B. 2014. The AMPK inhibitor compound C is a potent AMPK-independent antiglioma agent. *Mol Cancer Ther,* 13**,** 596-605.

LODISH, H. F. & DARNELL, J. E. 1995. *Molecular cell biology,* New York, Scientific American Books : Distributed by W.H. Freeman and Co.

LOPEZ-FABUEL, I., LE DOUCE, J., LOGAN, A., JAMES, A. M., BONVENTO, G., MURPHY, M. P., ALMEIDA, A. & BOLANOS, J. P. 2016. Complex I assembly into supercomplexes determines differential mitochondrial ROS production in neurons and astrocytes. *Proc Natl Acad Sci U S A,* 113**,** 13063-13068.

MACHOVIC, M. & JANECEK, S. 2006. The evolution of putative starch-binding domains. *FEBS Lett,* 580**,** 6349-56.

MAMMUCARI, C., PATRON, M., GRANATIERO, V. & RIZZUTO, R. 2011. Molecules and roles of mitochondrial calcium signaling. *Biofactors,* 37**,** 219-27.

MANNELLA, C. A. 1992. The 'ins' and 'outs' of mitochondrial membrane channels. *Trends Biochem Sci,* 17**,** 315-20.

MARCHISSIO, M. J., FRANCES, D. E., CARNOVALE, C. E. & MARINELLI, R. A. 2012. Mitochondrial aquaporin-8 knockdown in human hepatoma HepG2 cells causes ROS-induced mitochondrial depolarization and loss of viability. *Toxicol Appl Pharmacol,* 264**,** 246-54.

MARINO, S. M. & GLADYSHEV, V. N. 2010. Cysteine function governs its conservation and degeneration and restricts its utilization on protein surfaces. *J Mol Biol,* 404**,** 902-16.

MARSIN, A. S., BERTRAND, L., RIDER, M. H., DEPREZ, J., BEAULOYE, C., VINCENT, M. F., VAN DEN BERGHE, G., CARLING, D. & HUE, L. 2000. Phosphorylation and activation of heart PFK-2 by AMPK has a role in the stimulation of glycolysis during ischaemia. *Curr Biol,* 10**,** 1247-55.

MCBRIDE, A., GHILAGABER, S., NIKOLAEV, A. & HARDIE, D. G. 2009. The glycogen-binding domain on the AMPK beta subunit allows the kinase to act as a glycogen sensor. *Cell Metab,* 9**,** 23-34.

MCCORMACK, J. G., HALESTRAP, A. P. & DENTON, R. M. 1990. Role of calcium ions in regulation of mammalian intramitochondrial metabolism. *Physiol Rev,* 70**,** 391-425.

MENG, T. C., FUKADA, T. & TONKS, N. K. 2002. Reversible oxidation and inactivation of protein tyrosine phosphatases in vivo. *Mol Cell,* 9**,** 387-99.

MENGER, K. E., JAMES, A. M., COCHEME, H. M., HARBOUR, M. E., CHOUCHANI, E. T., DING, S., FEARNLEY, I. M., PARTRIDGE, L. & MURPHY, M. P. 2015. Fasting, but Not Aging,

Dramatically Alters the Redox Status of Cysteine Residues on Proteins in Drosophila melanogaster. *Cell Rep,* 11**,** 1856-65.

MILLER, E. W., DICKINSON, B. C. & CHANG, C. J. 2010. Aquaporin-3 mediates hydrogen peroxide uptake to regulate downstream intracellular signaling. *Proc Natl Acad Sci U S A,* 107**,** 15681-6.

MILLS, E. L., KELLY, B., LOGAN, A., COSTA, A. S., VARMA, M., BRYANT, C. E., TOURLOMOUSIS, P., DABRITZ, J. H., GOTTLIEB, E., LATORRE, I., CORR, S. C., MCMANUS, G., RYAN, D., JACOBS, H. T., SZIBOR, M., XAVIER, R. J., BRAUN, T., FREZZA, C., MURPHY, M. P. & O'NEILL, L. A. 2016. Succinate Dehydrogenase Supports Metabolic Repurposing of Mitochondria to Drive Inflammatory Macrophages. *Cell,* 167**,** 457-470 e13.

MIRANDA-SAAVEDRA, D., STARK, M. J., PACKER, J. C., VIVARES, C. P., DOERIG, C. & BARTON, G. J. 2007. The complement of protein kinases of the microsporidium Encephalitozoon cuniculi in relation to those of Saccharomyces cerevisiae and Schizosaccharomyces pombe. *BMC Genomics,* 8**,** 309.

MITCHELL, P. 1961. Coupling of phosphorylation to electron and hydrogen transfer by a chemi-osmotic type of mechanism. *Nature,* 191**,** 144-8.

MORENO-LOSHUERTOS, R. & ENRIQUEZ, J. A. 2016. Respiratory supercomplexes and the functional segmentation of the CoQ pool. *Free Radic Biol Med,* 100**,** 5-13.

MUELLER, S. & ARNHOLD, J. 1995. Fast and sensitive chemiluminescence determination of H2O2 concentration in stimulated human neutrophils. *J Biolumin Chemilumin,* 10**,** 229-37.

MUNGAI, P. T., WAYPA, G. B., JAIRAMAN, A., PRAKRIYA, M., DOKIC, D., BALL, M. K. & SCHUMACKER, P. T. 2011. Hypoxia triggers AMPK activation through reactive oxygen species-mediated activation of calcium release-activated calcium channels. *Mol Cell Biol,* 31**,** 3531-45.

MURLEY, A. & NUNNARI, J. 2016. The Emerging Network of Mitochondria-Organelle Contacts. *Mol Cell,* 61**,** 648-53.

MURPHY, M. P. 2009. How mitochondria produce reactive oxygen species. *Biochem J,* 417**,** 1-13.

MURPHY, M. P. 2012. Mitochondrial thiols in antioxidant protection and redox signaling: distinct roles for glutathionylation and other thiol modifications. *Antioxid Redox Signal,* 16**,** 476-95.

MURPHY, M. P. 2015. Redox Modulation by Reversal of the Mitochondrial Nicotinamide Nucleotide Transhydrogenase. *Cell Metab,* 22**,** 363-5.

MURPHY, M. P. & BRAND, M. D. 1987. The control of electron flux through cytochrome oxidase. *Biochem J,* 243**,** 499-505.

NAKAMURA, J., FUJIKAWA, M. & YOSHIDA, M. 2013. IF1, a natural inhibitor of mitochondrial ATP synthase, is not essential for the normal growth and breeding of mice. *Biosci Rep,* 33.

NICKEL, A. G., VON HARDENBERG, A., HOHL, M., LOFFLER, J. R., KOHLHAAS, M., BECKER, J., REIL, J. C., KAZAKOV, A., BONNEKOH, J., STADELMAIER, M., PUHL, S. L., WAGNER, M., BOGESKI, I., CORTASSA, S., KAPPL, R., PASIEKA, B., LAFONTAINE, M., LANCASTER, C. R., BLACKER, T. S., HALL, A. R., DUCHEN, M. R., KASTNER, L., LIPP, P., ZELLER, T., MULLER, C., KNOPP, A., LAUFS, U., BOHM, M., HOTH, M. & MAACK, C. 2015. Reversal of Mitochondrial Transhydrogenase Causes Oxidative Stress in Heart Failure. *Cell Metab,* 22**,** 472-84.

NIESLER, C. U., MYBURGH, K. H. & MOORE, F. 2007. The changing AMPK expression profile in differentiating mouse skeletal muscle myoblast cells helps confer increasing resistance to apoptosis. *Exp Physiol,* 92**,** 207-17.

NOH, Y. H., BAEK, J. Y., JEONG, W., RHEE, S. G. & CHANG, T. S. 2009. Sulfiredoxin Translocation into Mitochondria Plays a Crucial Role in Reducing Hyperoxidized Peroxiredoxin III. *J Biol Chem,* 284**,** 8470-7.

O'NEILL, H. M., MAARBJERG, S. J., CRANE, J. D., JEPPESEN, J., JORGENSEN, S. B., SCHERTZER, J. D., SHYROKA, O., KIENS, B., VAN DENDEREN, B. J., TARNOPOLSKY, M. A., KEMP, B. E., RICHTER, E. A. & STEINBERG, G. R. 2011. AMP-activated protein kinase (AMPK) beta1beta2 muscle null mice reveal an essential role for AMPK in maintaining mitochondrial content and glucose uptake during exercise. *Proc Natl Acad Sci U S A,* 108**,** 16092-7.

O'NEILL, L. A. & HARDIE, D. G. 2013. Metabolism of inflammation limited by AMPK and pseudo-starvation. *Nature,* 493**,** 346-55.

OAKHILL, J. S., CHEN, Z. P., SCOTT, J. W., STEEL, R., CASTELLI, L. A., LING, N., MACAULAY, S. L. & KEMP, B. E. 2010. beta-Subunit myristoylation is the gatekeeper for initiating metabolic stress sensing by AMP-activated protein kinase (AMPK). *Proc Natl Acad Sci U S A,* 107**,** 19237-41.

OAKHILL, J. S., STEEL, R., CHEN, Z. P., SCOTT, J. W., LING, N., TAM, S. & KEMP, B. E. 2011. AMPK is a direct adenylate charge-regulated protein kinase. *Science,* 332**,** 1433-5.

OWEN, M. R., DORAN, E. & HALESTRAP, A. P. 2000. Evidence that metformin exerts its anti-diabetic effects through inhibition of complex 1 of the mitochondrial respiratory chain. *Biochem J,* 348 Pt 3**,** 607-14.

PAUL, M. H. & SPERLING, E. 1952. Cyclophorase system. XXIII. Correlation of cyclophorase activity and mitochondrial density in striated muscle. *Proc Soc Exp Biol Med,* 79**,** 352-4.

PAUL, V. D. & LILL, R. 2015. Biogenesis of cytosolic and nuclear iron-sulfur proteins and their role in genome stability. *Biochim Biophys Acta,* 1853**,** 1528-39.

PAULSEN, C. E. & CARROLL, K. S. 2013. Cysteine-mediated redox signaling: chemistry, biology, and tools for discovery. *Chem Rev,* 113**,** 4633-79.

PRETZER, E. & WIKTOROWICZ, J. E. 2008. Saturation fluorescence labeling of proteins for proteomic analyses. *Anal Biochem,* 374**,** 250-62.

PRYDE, K. R. & HIRST, J. 2011. Superoxide is produced by the reduced flavin in mitochondrial complex I: a single, unified mechanism that applies during both forward and reverse electron transfer. *J Biol Chem,* 286**,** 18056-65.

PUIGSERVER, P., WU, Z., PARK, C. W., GRAVES, R., WRIGHT, M. & SPIEGELMAN, B. M. 1998. A cold-inducible coactivator of nuclear receptors linked to adaptive thermogenesis. *Cell,* 92**,** 829-39.

QI, D. & YOUNG, L. H. 2015. AMPK: energy sensor and survival mechanism in the ischemic heart. *Trends Endocrinol Metab,* 26**,** 422-9.

RASOLA, A. & BERNARDI, P. 2011. Mitochondrial permeability transition in Ca(2+)-dependent apoptosis and necrosis. *Cell Calcium,* 50**,** 222-33.

REQUEJO, R., CHOUCHANI, E. T., HURD, T. R., MENGER, K. E., HAMPTON, M. B. & MURPHY, M. P. 2010. Measuring mitochondrial protein thiol redox state. *Methods Enzymol,* 474**,** 123-47.

RICH, P. R. & MARECHAL, A. 2010. The mitochondrial respiratory chain. *Essays Biochem,* 47**,** 1-23.

RINALDUCCI, S., MURGIANO, L. & ZOLLA, L. 2008. Redox proteomics: basic principles and future perspectives for the detection of protein oxidation in plants. *J Exp Bot,* 59**,** 3781-801.

RIQUIER, S., BRETON, J., ABBAS, K., CORNU, D., BOUTON, C. & DRAPIER, J. C. 2014. Peroxiredoxin post-translational modifications by redox messengers. *Redox Biol,* 2**,** 777-85.

ROBB, E. L., GAWEL, J. M., AKSENTIJEVIC, D., COCHEME, H. M., STEWART, T. S., SHCHEPINOVA, M. M., QIANG, H., PRIME, T. A., BRIGHT, T. P., JAMES, A. M., SHATTOCK, M. J., SENN, H. M., HARTLEY, R. C. & MURPHY, M. P. 2015. Selective superoxide generation within mitochondria by the targeted redox cycler MitoParaquat. *Free Radic Biol Med,* 89**,** 883-94.

ROHRIG, F. & SCHULZE, A. 2016. The multifaceted roles of fatty acid synthesis in cancer. *Nat Rev Cancer,* 16**,** 732-749.

ROSS, F. A., MACKINTOSH, C. & HARDIE, D. G. 2016. AMP-activated protein kinase: a cellular energy sensor that comes in 12 flavours. *FEBS J,* 283**,** 2987-3001.

ROSTOVTSEV, V. V., GREEN, L. G., FOKIN, V. V. & SHARPLESS, K. B. 2002. A stepwise huisgen cycloaddition process: copper(I)-catalyzed regioselective "ligation" of azides and terminal alkynes. *Angew Chem Int Ed Engl,* 41**,** 2596-9.

RUSTIN, P. & JACOBS, H. T. 2009. Respiratory chain alternative enzymes as tools to better understand and counteract respiratory chain deficiencies in human cells and animals. *Physiol Plant,* 137**,** 362-70.

SALT, I. P., JOHNSON, G., ASHCROFT, S. J. & HARDIE, D. G. 1998. AMP-activated protein kinase is activated by low glucose in cell lines derived from pancreatic beta cells, and may regulate insulin release. *Biochem J,* 335 (Pt 3)**,** 533-9.

SANJUAN-PLA, A., CERVERA, A. M., APOSTOLOVA, N., GARCIA-BOU, R., VICTOR, V. M., MURPHY, M. P. & MCCREATH, K. J. 2005. A targeted antioxidant reveals the importance of mitochondrial reactive oxygen species in the hypoxic signaling of HIF-1alpha. *FEBS Lett,* 579**,** 2669-74.

SANZ, A., SOIKKELI, M., PORTERO-OTIN, M., WILSON, A., KEMPPAINEN, E., MCILROY, G., ELLILA, S., KEMPPAINEN, K. K., TUOMELA, T., LAKANMAA, M., KIVIRANTA, E., STEFANATOS, R., DUFOUR, E., HUTZ, B., NAUDI, A., JOVE, M., ZEB, A., VARTIAINEN, S., MATSUNO-YAGI, A., YAGI, T., RUSTIN, P., PAMPLONA, R. & JACOBS, H. T. 2010. Expression of the yeast NADH dehydrogenase Ndi1 in Drosophila confers increased lifespan independently of dietary restriction. *Proc Natl Acad Sci U S A,* 107**,** 9105-10.

SAZANOV, L. A. 2015. A giant molecular proton pump: structure and mechanism of respiratory complex I. *Nat Rev Mol Cell Biol,* 16**,** 375-88.

SCHREURS, M., KUIPERS, F. & VAN DER LEIJ, F. R. 2010. Regulatory enzymes of mitochondrial beta-oxidation as targets for treatment of the metabolic syndrome. *Obes Rev,* 11**,** 380-8.

SCIALO, F., SRIRAM, A., FERNANDEZ-AYALA, D., GUBINA, N., LOHMUS, M., NELSON, G., LOGAN, A., COOPER, H. M., NAVAS, P., ENRIQUEZ, J. A., MURPHY, M. P. & SANZ, A. 2016. Mitochondrial ROS Produced via Reverse Electron Transport Extend Animal Lifespan. *Cell Metab,* 23**,** 725-34.

SEO, B. B., KITAJIMA-IHARA, T., CHAN, E. K., SCHEFFLER, I. E., MATSUNO-YAGI, A. & YAGI, T. 1998. Molecular remedy of complex I defects: rotenone-insensitive internal NADH-quinone oxidoreductase of Saccharomyces cerevisiae mitochondria restores the NADH oxidase activity of complex I-deficient mammalian cells. *Proc Natl Acad Sci U S A,* 95**,** 9167-71.

SEO, B. B., MATSUNO-YAGI, A. & YAGI, T. 1999. Modulation of oxidative phosphorylation of human kidney 293 cells by transfection with the internal rotenone-insensitive NADH-quinone oxidoreductase (NDI1) gene of Saccharomyces cerevisiae. *Biochim Biophys Acta,* 1412**,** 56-65.

SEO, B. B., WANG, J., FLOTTE, T. R., YAGI, T. & MATSUNO-YAGI, A. 2000. Use of the NADH-quinone oxidoreductase (NDI1) gene of Saccharomyces cerevisiae as a possible cure for complex I defects in human cells. *J Biol Chem,* 275**,** 37774-8.

SEVINC, M. S., ENS, W. & LOEWEN, P. C. 1995. The cysteines of catalase HPII of Escherichia coli, including Cys438 which is blocked, do not have a catalytic role. *Eur J Biochem,* 230**,** 127-32.

SHAO, D., OKA, S., LIU, T., ZHAI, P., AGO, T., SCIARRETTA, S., LI, H. & SADOSHIMA, J. 2014. A redox-dependent mechanism for regulation of AMPK activation by Thioredoxin1 during energy starvation. *Cell Metab,* 19**,** 232-45.

SHAW, R. J., KOSMATKA, M., BARDEESY, N., HURLEY, R. L., WITTERS, L. A., DEPINHO, R. A. & CANTLEY, L. C. 2004. The tumor suppressor LKB1 kinase directly activates AMP-activated kinase and regulates apoptosis in response to energy stress. *Proc Natl Acad Sci U S A,* 101**,** 3329-35.

SHENTON, D., PERRONE, G., QUINN, K. A., DAWES, I. W. & GRANT, C. M. 2002. Regulation of protein S-thiolation by glutaredoxin 5 in the yeast Saccharomyces cerevisiae. *J Biol Chem,* 277**,** 16853-9.

SIN, J., ANDRES, A. M., TAYLOR, D. J., WESTON, T., HIRAUMI, Y., STOTLAND, A., KIM, B. J., HUANG, C., DORAN, K. S. & GOTTLIEB, R. A. 2016. Mitophagy is required for mitochondrial biogenesis and myogenic differentiation of C2C12 myoblasts. *Autophagy,* 12**,** 369-80.

SMITH, R. A., HARTLEY, R. C., COCHEME, H. M. & MURPHY, M. P. 2012. Mitochondrial pharmacology. *Trends Pharmacol Sci,* 33**,** 341-52.

SMITH, R. A., HARTLEY, R. C. & MURPHY, M. P. 2011. Mitochondria-targeted small molecule therapeutics and probes. *Antioxid Redox Signal,* 15**,** 3021-38.

SOBOTTA, M. C., BARATA, A. G., SCHMIDT, U., MUELLER, S., MILLONIG, G. & DICK, T. P. 2013. Exposing cells to H2O2: a quantitative comparison between continuous low-dose and one-time high-dose treatments. *Free Radic Biol Med,* 60**,** 325-35.

SOBOTTA, M. C., LIOU, W., STOCKER, S., TALWAR, D., OEHLER, M., RUPPERT, T., SCHARF, A. N. & DICK, T. P. 2015. Peroxiredoxin-2 and STAT3 form a redox relay for H2O2 signaling. *Nat Chem Biol,* 11**,** 64-70.

STREHLER, B. L. 1974. *Adenosine-5′ -triphosphate and Creatine Phosphate: Determination with Luciferase,* New York, NY, Academic Press.

TAIT, S. W. & GREEN, D. R. 2010. Mitochondria and cell death: outer membrane permeabilization and beyond. *Nat Rev Mol Cell Biol,* 11**,** 621-32.

TORMOS, K. V., ANSO, E., HAMANAKA, R. B., EISENBART, J., JOSEPH, J., KALYANARAMAN, B. & CHANDEL, N. S. 2011. Mitochondrial complex III ROS regulate adipocyte differentiation. *Cell Metab,* 14**,** 537-44.

TORMOS, K. V. & CHANDEL, N. S. 2010. Inter-connection between mitochondria and HIFs. *J Cell Mol Med,* 14**,** 795-804.

TORNOE, C. W., CHRISTENSEN, C. & MELDAL, M. 2002. Peptidotriazoles on solid phase: [1,2,3]-triazoles by regiospecific copper(i)-catalyzed 1,3-dipolar cycloadditions of terminal alkynes to azides. *J Org Chem,* 67**,** 3057-64.

TORTORELLA, D., STORY, C. M., HUPPA, J. B., WIERTZ, E. J., JONES, T. R., BACIK, I., BENNINK, J. R., YEWDELL, J. W. & PLOEGH, H. L. 1998. Dislocation of type I membrane proteins from the ER to the cytosol is sensitive to changes in redox potential. *J Cell Biol,* 142**,** 365-76.

TYAGARAJAN, K., PRETZER, E. & WIKTOROWICZ, J. E. 2003. Thiol-reactive dyes for fluorescence labeling of proteomic samples. *Electrophoresis,* 24**,** 2348-58.

VAN LEEUWEN, L. A. G., HINCHY, E. C., MURPHY, M. P., ROBB, E. L. & COCHEME, H. M. 2017. Click-PEGylation - A mobility shift approach to assess the redox state of cysteines in candidate proteins. *Free Radic Biol Med,* 108**,** 374-382.

VERHAGEN, H., SCHILDERMAN, P. A. & KLEINJANS, J. C. 1991. Butylated hydroxyanisole in perspective. *Chem Biol Interact,* 80**,** 109-34.

VERRASTRO, I., PASHA, S., JENSEN, K. T., PITT, A. R. & SPICKETT, C. M. 2015. Mass spectrometry-based methods for identifying oxidized proteins in disease: advances and challenges. *Biomolecules,* 5**,** 378-411.

VISCOMI, C. & ZEVIANI, M. 2017. MtDNA-maintenance defects: syndromes and genes. *J Inherit Metab Dis,* 40**,** 587-599.

VISSERS, M. C. M., HAMPTON, M. & KETTLE, A. J. 2018. *Hydrogen peroxide metabolism in health and disease,* Boca Raton, Taylor & Francis/CRC Press.

WAGATSUMA, A. & SAKUMA, K. 2013. Mitochondria as a potential regulator of myogenesis. *ScientificWorldJournal,* 2013**,** 593267.

WALLACE, D. C., FAN, W. & PROCACCIO, V. 2010. Mitochondrial energetics and therapeutics. *Annu Rev Pathol,* 5**,** 297-348.

WATT, I. N., MONTGOMERY, M. G., RUNSWICK, M. J., LESLIE, A. G. & WALKER, J. E. 2010. Bioenergetic cost of making an adenosine triphosphate molecule in animal mitochondria. *Proc Natl Acad Sci U S A,* 107**,** 16823-7.

WIEDEMANN, N. & PFANNER, N. 2017. Mitochondrial Machineries for Protein Import and Assembly. *Annu Rev Biochem,* 86**,** 685-714.

WILLOWS, R., SANDERS, M. J., XIAO, B., PATEL, B. R., MARTIN, S. R., READ, J., WILSON, J. R., HUBBARD, J., GAMBLIN, S. J. & CARLING, D. 2017. Phosphorylation of AMPK by upstream kinases is required for activity in mammalian cells. *Biochem J,* 474**,** 3059-3073.

WINDER, W. W. & HARDIE, D. G. 1996. Inactivation of acetyl-CoA carboxylase and activation of AMP-activated protein kinase in muscle during exercise. *Am J Physiol,* 270**,** E299-304.

WINTERBOURN, C. C. 2013. The biological chemistry of hydrogen peroxide. *Methods Enzymol,* 528**,** 3-25.

WINTERBOURN, C. C. & HAMPTON, M. B. 2008. Thiol chemistry and specificity in redox signaling. *Free Radic Biol Med,* 45**,** 549-61.

WOODS, A., CHEUNG, P. C., SMITH, F. C., DAVISON, M. D., SCOTT, J., BERI, R. K. & CARLING, D. 1996. Characterization of AMP-activated protein kinase beta and gamma subunits. Assembly of the heterotrimeric complex in vitro. *J Biol Chem,* 271**,** 10282-90.

WOODS, A., DICKERSON, K., HEATH, R., HONG, S. P., MOMCILOVIC, M., JOHNSTONE, S. R., CARLSON, M. & CARLING, D. 2005. Ca2+/calmodulin-dependent protein kinase kinase-beta acts upstream of AMP-activated protein kinase in mammalian cells. *Cell Metab,* 2**,** 21-33.

XIAO, B., HEATH, R., SAIU, P., LEIPER, F. C., LEONE, P., JING, C., WALKER, P. A., HAIRE, L., ECCLESTON, J. F., DAVIS, C. T., MARTIN, S. R., CARLING, D. & GAMBLIN, S. J. 2007. Structural basis for AMP binding to mammalian AMP-activated protein kinase. *Nature,* 449**,** 496-500.

XIAO, B., SANDERS, M. J., CARMENA, D., BRIGHT, N. J., HAIRE, L. F., UNDERWOOD, E., PATEL, B. R., HEATH, R. B., WALKER, P. A., HALLEN, S., GIORDANETTO, F., MARTIN, S. R., CARLING, D. & GAMBLIN, S. J. 2013. Structural basis of AMPK regulation by small molecule activators. *Nat Commun,* 4**,** 3017.

XIAO, B., SANDERS, M. J., UNDERWOOD, E., HEATH, R., MAYER, F. V., CARMENA, D., JING, C., WALKER, P. A., ECCLESTON, J. F., HAIRE, L. F., SAIU, P., HOWELL, S. A., AASLAND, R., MARTIN, S. R., CARLING, D. & GAMBLIN, S. J. 2011. Structure of mammalian AMPK and its regulation by ADP. *Nature,* 472**,** 230-3.

YAGI, T., SEO, B. B., NAKAMARU-OGISO, E., MARELLA, M., BARBER-SINGH, J., YAMASHITA, T., KAO, M. C. & MATSUNO-YAGI, A. 2006. Can a single subunit yeast NADH dehydrogenase (Ndi1) remedy diseases caused by respiratory complex I defects? *Rejuvenation Res,* 9**,** 191-7.

YANG, B., ZHAO, D. & VERKMAN, A. S. 2006. Evidence against functionally significant aquaporin expression in mitochondria. *J Biol Chem,* 281**,** 16202-6.

YANG, J., GUPTA, V., TALLMAN, K. A., PORTER, N. A., CARROLL, K. S. & LIEBLER, D. C. 2015. Global, in situ, site-specific analysis of protein S-sulfenylation. *Nat Protoc,* 10**,** 1022-37.

YE, H. & ROUAULT, T. A. 2010. Human iron-sulfur cluster assembly, cellular iron homeostasis, and disease. *Biochemistry,* 49**,** 4945-56.

YOSHIKO, Y., HIRAO, K. & MAEDA, N. 2002. Differentiation in C(2)C(12) myoblasts depends on the expression of endogenous IGFs and not serum depletion. *Am J Physiol Cell Physiol,* 283**,** C1278-86.

ZAHA, V. G., QI, D., SU, K. N., PALMERI, M., LEE, H. Y., HU, X., WU, X., SHULMAN, G. I., RABINOVITCH, P. S., RUSSELL, R. R., 3RD & YOUNG, L. H. 2016. AMPK is critical for mitochondrial function during reperfusion after myocardial ischemia. *J Mol Cell Cardiol,* 91**,** 104-13.

ZHANG, C. S., HAWLEY, S. A., ZONG, Y., LI, M., WANG, Z., GRAY, A., MA, T., CUI, J., FENG, J. W., ZHU, M., WU, Y. Q., LI, T. Y., YE, Z., LIN, S. Y., YIN, H., PIAO, H. L., HARDIE, D. G. & LIN, S. C. 2017. Fructose-1,6-bisphosphate and aldolase mediate glucose sensing by AMPK. *Nature,* 548**,** 112-116.

ZHANG, C. S., JIANG, B., LI, M., ZHU, M., PENG, Y., ZHANG, Y. L., WU, Y. Q., LI, T. Y., LIANG, Y., LU, Z., LIAN, G., LIU, Q., GUO, H., YIN, Z., YE, Z., HAN, J., WU, J. W., YIN, H., LIN, S. Y. & LIN, S. C. 2014. The lysosomal v-ATPase-Ragulator complex is a common activator for AMPK and mTORC1, acting as a switch between catabolism and anabolism. *Cell Metab,* 20**,** 526-40.

ZHANG, Y. L., GUO, H., ZHANG, C. S., LIN, S. Y., YIN, Z., PENG, Y., LUO, H., SHI, Y., LIAN, G., ZHANG, C., LI, M., YE, Z., YE, J., HAN, J., LI, P., WU, J. W. & LIN, S. C. 2013. AMP as a low-energy charge signal autonomously initiates assembly of AXIN-AMPK-LKB1 complex for AMPK activation. *Cell Metab,* 18**,** 546-55.

ZHAO, X., LI, G. & LIANG, S. 2013. Several affinity tags commonly used in chromatographic purification. *J Anal Methods Chem,* 2013**,** 581093.

ZHOU, G., MYERS, R., LI, Y., CHEN, Y., SHEN, X., FENYK-MELODY, J., WU, M., VENTRE, J., DOEBBER, T., FUJII, N., MUSI, N., HIRSHMAN, M. F., GOODYEAR, L. J. & MOLLER, D. E. 2001. Role of AMP-activated protein kinase in mechanism of metformin action. *J Clin Invest,* 108**,** 1167-74.

ZMIJEWSKI, J. W., BANERJEE, S., BAE, H., FRIGGERI, A., LAZAROWSKI, E. R. & ABRAHAM, E. 2010. Exposure to hydrogen peroxide induces oxidation and activation of AMP-activated protein kinase. *J Biol Chem,* 285**,** 33154-64.

ZONG, H., REN, J. M., YOUNG, L. H., PYPAERT, M., MU, J., BIRNBAUM, M. J. & SHULMAN, G. I. 2002. AMP kinase is required for mitochondrial biogenesis in skeletal muscle in response to chronic energy deprivation. *Proc Natl Acad Sci U S A,* 99**,** 15983-7.

8. Appendices

Appendix A. Gene and plasmid sequences

AMPKα2-CT-FLAG (pcDNA3 vector backbone)

Gifted by Professor David Carling (MRC Clinical Sciences Centre, Hammersmith Hospital Campus, London, UK).

> [AMPKα2-CT-FLAG (*rattus norvegicus*) 1689 bp]

ATGGCTGAGAAGCAGAAGCACGACGGGCGTGTGAAGATCGGACACTACGTGCTGGGGGACAC
CCTGGGCGTCGGCACCTTCGGCAAAGTGAAGATTGGAGAACATCAATTGACAGGCCATAAAGT
GGCAGTTAAGATCTTAAATAGACAGAAGATTCGCAGTTTAGATGTTGTTGGAAAAATAAAACGA
GAAATTCAAAATCTTAAACTCTTTCGTCATCCTCATATTATCAAACTCTACCAAGTGATCAGCACT
CCAACAGACTTTTTTATGGTAATGGAATATGTGTCTGGAGGTGAATTGTTCGACTACATCTGTAA
ACACGGGAGGGTTGAAGAGGTGGAAGCTCGCCGGCTCTTCCAGCAGATTCTGTCTGCCGTGG
ACTACTGTCACAGGCACATGGTTGTCCACAGGGACCTGAAGCCAGAGAACGTGTTGCTGGACG
CCCAGATGAATGCTAAGATAGCTGACTTCGGACTCTCTAATATGATGTCAGATGGTGAATTTCT
ACGAACTAGCTGTGGATCGCCAAATTATGCAGCACCGGAGGTCATCTCAGGAAGGCTGTATGC
GGGTCCTGAGGTTGATATCTGGAGCTGTGGTGTTATCCTGTATGCCCTTCTCTGTGGCACCCTC
CCGTTCGACGATGAGCACGTGCCTACGCTCTTTAAGAAGATCCGAGGGGGTGTGTTCTACATC
CCGGAGTATCTCAACCGTTCTATTGCCACTCTGCTGATGCACATGCTGCAGGTGGACCCCTTG
AAGCGAGCAACTATCAAAGACATACGAGAGCATGAATGGTTTAAACAGGATTTGCCCAGTTACC
TCTTTCCTGAAGACCCCTCCTATGATGCTAACGTCATTGATGATGAGGCTGTGAAAGAAGTATG
TGAAAAATTTGAGTGTACAGAATCAGAAGTGATGAACAGTTTATACAGTGGTGACCCTCAAGAC
CAGCTCGCAGTGGCTTATCATCTCATCATTGACAATCGGAGAATAATGAACCAAGCCAGTGAGT
TCTACCTCGCCTCCAGTCCTCCAACGGGTTCCTTCATGGACGATATGGCCATGCACATTCCCCC
CGGCCTGAAACCACATCCTGAAAGGATGCCACCTCTCATAGCAGACAGCCCCAAAGCACGCTG
TCCACTGGATGCACTCAACACAACTAAGCCCAAATCTTTAGCTGTGAAAAAAGCCAAGTGGCAC
CTTGGGATCCGAAGCCAGAGCAAACCATACGACATTATGGCGGAGGTGTACCGAGCTATGAAG
CAGCTGGACTTTGAATGGAAGGTAGTGAATGCATACCATCTTCGAGTAAGAAGAAAAAACCCAG
TGACTGGCAATTACGTGAAAATGAGCTTACAGCTTTACCTGGTTGACAATCGGAGCTATCTTCT
AGACTTTAAAAGCATCGATGATGAGGTGGTGGAGCAGAGGTCTGGTTCTTCAACACCTCAGCG
CTCCTGTTCTGCTGCCGGCCTCCACAGACCTCGGTCAAGTGTCGATTCCAGCACAGCCGAGAA
CCATTCACTGTCTGGCTCTCTCACTGGTTCTTTGACTGGCAGCACTTTGTCCTCCGCTTCCCCG
CGCCTGGGCAGTCATACCATGGATTTTTTTGAAATGTGCGCCAGTCTTATCACTGCTTTAGCCC
GTGGCGGCGATTATAAAGACGACGACGACAAGTGA

Features :
Start: [1 : 3]
Linker: [1657 : 1662]
FLAG: [1663 : 1686]
Stop: [1687 : 1689]

Translation: [562 aa]

MAEKQKHDGRVKIGHYVLGDTLGVGTFGKVKIGEHQLTGHKVAVKILNRQKIRSLDVVGKIKREIQN
LKLFRHPHIIKLYQVISTPTDFFMVMEYVSGGELFDYICKHGRVEEVEARRLFQQILSAVDYCHRHMV
VHRDLKPENVLLDAQMNAKIADFGLSNMMSDGEFLRTSCGSPNYAAPEVISGRLYAGPEVDIWSCG
VILYALLCGTLPFDDEHVPTLFKKIRGGVFYIPEYLNRSIATLLMHMLQVDPLKRATIKDIREHEWFKQ

DLPSYLFPEDPSYDANVIDDEAVKEVCEKFECTESEVMNSLYSGDPQDQLAVAYHLIIDNRRIMNQA
SEFYLASSPPTGSFMDDMAMHIPPGLKPHPERMPPLIADSPKARCPLDALNTTKPKSLAVKKAKWH
LGIRSQSKPYDIMAEVYRAMKQLDFEWKVVNAYHLRVRRKNPVTGNYVKMSLQLYLVDNRSYLLDF
KSIDDEVVEQRSGSSTPQRSCSAAGLHRPRSSVDSSTAENHSLSGSLTGSLTGSTLSSASPRLGSH
TMDFFEMCASLITALARGGDYKDDDDK*

AMPKβ1 (from pcDNA3 vector backbone)

Gifted by Professor David Carling (MRC Clinical Sciences Centre, Hammersmith Hospital Campus, London, UK).

> [AMPKβ1 (*rattus norvegicus*) 813 bp]
ATGGGCAATACGAGCAGCGAGCGCGCCGCGCTGGAGCGGCAGGCTGGCCATAAGACGCCGC
GGAGGGACAGCTCGGAGGGCACCAAGGATGGGGACAGGCCCAAGATCCTGATGGACAGCCC
CGAAGACGCCGACATCTTCCACACCGAGGAAATGAAGGCTCCAGAGAAGGAGGAGTTCCTGG
CGTGGCAGCACGACCTCGAGGTGAATGAGAAAGCCCCCGCCCAGGCTCGGCCCACCGTATTT
CGATGGACAGGGGGTGGAAAGGAGGTCTACTTGTCTGGATCCTTCAACAACTGGAGCAAATTG
CCCCTCACTAGAAGCCAAAACAACTTCGTAGCCATCCTGGACCTACCGGAAGGAGAGCATCAG
TACAAGTTCTTTGTGGATGGCCAGTGGACCCACGATCCTTCCGAGCCAATAGTAACCAGCCAG
CTTGGCACAGTTAACAACATCATTCAAGTGAAGAAAACTGACTTTGAAGTATTTGATGCTTTAAT
GGTGGATTCCCAAAAGTGCTCCGATGTATCTGAGCTGTCCAGTTCCCCCCCAGGACCCTACCA
CCAGGAGCCTTACATCTCTAAACCAGAGGAGCGGTTCAAGGCCCCGCCCATCCTCCCGCCTCA
CCTGCTGCAGGTCATCTTGAACAAGGACACGGGCATCTCTTGTGATCCAGCGCTGCTTCCGGA
GCCCAACCACGTCATGCTGAACCACCTCTATGCACTCTCTATCAAGGATGGAGTGATGGTGCT
CAGTGCGACCCATCGGTACAAGAAAAAGTACGTCACCACCCTCCTCTACAAGCCCATATGA

Features:
Start: [1 : 3]
Stop: [811 : 813]

Translation: [270 aa]
MGNTSSERAALERQAGHKTPRRDSSEGTKDGDRPKILMDSPEDADIFHTEEMKAPEKEEFLAWQH
DLEVNEKAPAQARPTVFRWTGGGKEVYLSGSFNNWSKLPLTRSQNNFVAILDLPEGEHQYKFFVD
GQWTHDPSEPIVTSQLGTVNNIIQVKKTDFEVFDALMVDSQKCSDVSELSSSPPGPYHQEPYISKPE
ERFKAPPILPPHLLQVILNKDTGISCDPALLPEPNHVMLNHLYALSIKDGVMVLSATHRYKKKYVTTLL
YKPI*

AMPKγ1-NT-Myc (pcDNA3 vector backbone)

Gifted by Professor David Carling (MRC Clinical Sciences Centre, Hammersmith Hospital Campus, London, UK).

> [AMPKγ1-NT-Myc (*rattus norvegicus*) 1029 bp]
ATGGAGCAGAAGCTTATCTCCGAGGAGGACCTCGGTGGCGAGTCGGTTGCTGCAGAGAGCGC
TCCAGCTCCGGAGAATGAACACTCTCAAGAGACCCCGGAATCGAACAGTAGTGTGTACACCAC
CTTCATGAAGTCTCATCGCTGCTATGACCTGATCCCCACAAGCTCCAAGCTGGTGGTATTTGAT
ACTTCGCTGCAGGTAAAGAAAGCCTTCTTTGCCCTGGTGACTAACGGTGTTCGTGCTGCCCCTT
TGTGGGATAGTAAGAAGCAGAGCTTTGTGGGCATGCTGACCATCACTGACTTCATCAATATTCT
GCACCGATACTACAAGTCAGCCCTGGTGCAGATCTATGAACTGGAGGAGCACAAGATAGAGAC
TTGGAGAGAGGTCTACCTGCAAGACTCCTTTAAGCCACTTGTCTGCATTTCTCCAAATGCCAGC
TTGTTCGATGCTGTCTCTTCATTAATTCGAAATAAGATCCACAGGCTTCCAGTTATTGACCCGGA

GTCAGGCAACACCTTGTACATTCTTACTCACAAGCGGATCCTCAAGTTCCTCAAGTTGTTTATCA
CTGAGTTCCCCAAGCCGGAATTCATGTCTAAGTCTCTGGAAGAGCTACAGATTGGCACCTACG
CCAATATTGCCATGGTCCGTACCACTACACCTGTCTATGTGGCTCTGGGCATCTTTGTACAGCA
CCGAGTCTCCGCCTTGCCTGTGGTGGATGAGAAAGGGCGTGTGGTGGACATCTACTCCAAGTT
TGATGTGATTAATTTGGCAGCAGAAAAGACATACAACAACCTAGATGTGTCTGTGACAAAAGCC
CTACAGCACCGGTCACACTACTTCGAGGGTGTTCTCAAGTGCTACCTACATGAGACTCTAGAAG
CAATCATCAATAGACTGGTGGAAGCAGAGGTTCACCGTCTGGTGGTGGTGGATGAACATGACG
TGGTCAAGGGCATTGTATCGCTGTCTGACATCTTACAGGCTCTGGTGCTCACAGGTGGAGAGA
AGAAGCCCTGA

Features:
Start: [1 : 3]
Myc: [4 : 33]
Linker: [34 : 39]
Stop: [1027 : 1029]

Translation: [342 aa]
MEQKLISEEDLGGESVAAESAPAPENEHSQETPESNSSVYTTFMKSHRCYDLIPSSKLVVFDTSLQV
KKAFFALVTNGVRAAPLWDSKKQSFVGMLTITDFINILHRYYKSALVQIYELEEHKIETWREVYLQDS
FKPLVCISPNASLFDAVSSLIRNKIHRLPVIDPESGNTLYILTHKRILKFLKLFITEFPKPEFMSKSLEEL
QIGTYANIAMVRTTTPVYVALGIFVQHRVSALPVVDEKGRVVDIYSKFDVINLAAEKTYNNLDVSVTK
ALQHRSHYFEGVLKCYLHETLEAIINRLVEAEVHRLVVVDEHDVVKGIVSLSDILQALVLTGGEKKP*

NDI1 (pcDNA5/FRT/T0 vector backbone)

pWPI-NDI1 vector gifted by Dr. Alberto Sanz (Institute for Cell and Molecular Biosciences & Newcastle University Institute for Ageing, Newcastle University, Newcastle, UK) (Scialo et al., 2016).

> [NDI1 (*Saccharomyces cerevisiae S288C*) 1541 bp]
ATGCTATCGAAGAATTTGTATAGTAACAAGAGGTTGCTCACCTCGACGAATACGCTAGTCAGAT
TCGCTTCCACCAGATCCACAGGGGTGGAAAACTCCGGAGCAGGTCCTACATCTTTTAAGACCA
TGAAAGTCATTGACCCTCAGCACAGCGACAAACCAAACGTGCTGATACTGGGTTCGGGGTGGG
GAGCTATTTCGTTTTTAAAGCACATTGACACCAAGAAGTACAACGTTTCCATCATCTCTCCTAGA
AGCTATTTCTTATTTACGCCTTTGTTACCTTCTGCACCAGTTGGGACAGTAGACGAAAAGTCAAT
TATTGAGCCCATCGTTAATTTTGCTCTCAAGAAAAAGGGGAACGTTACCTACTATGAGGCAGAA
GCCACCTCTATCAATCCCGACAGGAATACCGTTACCATAAAATCATTATCTGCCGTTAGCCAGC
TATACCAACCTGAAAACCATCTAGGGCTGCATCAAGCAGAACCTGCTGAAATTAAGTACGATTA
TTTAATCAGTGCTGTAGGTGCGGAACCTAACACATTTGGTATTCCTGGGGTCACTGATTACGGT
CATTTCCTGAAGGAAATTCCCAACTCTTTGGAAATAAGAAGAACTTTTGCCGCCAATCTAGAGA
AGGCTAACTTATTGCCAAAGGGTGATCCCGAAAGAAGAAGACTACTGTCCATTGTCGTGGTTG
GTGGTGGGCCTACTGGTGTAGAGGCCGCTGGTGAACTACAGGATTATGTTCACCAGGACCTGA
GAAAGTTTCTCCCTGCATTGGCCGAAGAAGTCCAAATTCACTTGGTCGAAGCTCTGCCCATCGT
TTTGAATATGTTTGAGAAAAAGCTTTCATCATACGCGCAATCACATTTAGAAAACACTTCGATCA
AAGTACATCTGAGAACGGCTGTCGCCAAAGTTGAAGAAAAGCAATTGTTGGCAAAGACCAAACA
CGAAGACGGTAAAATAACCGAAGAAACTATTCCATACGGTACTTTGATTTGGGCCACGGGTAAC
AAGGCAAGACCGGTAATCACTGACCTTTTCAAGAAAATTCCTGAGCAAAACTCGTCCAAGAGAG
GATTGGCAGTGAATGACTTTTTGCAGGTGAAAGGCAGCAACAACATTTTCGCCATTGGTGACAA
TGCATTTGCTGGGTTGCCACCAACCGCCCAAGTAGCGCACCAAGAGGCCGAATATTTGGCCAA
GAATTTTGATAAAATGGCTCAAATACCAAATTTCCAAAAGAATCTATCTTCAAGAAAGGATAAAA
TTGATCTCTTGTTCGAGGAGAACAACTTTAAACCTTTCAAATACAACGATTTAGGTGCCTTAGCA
TACCTGGGATCCGAAAGGGCCATTGCAACCATACGTTCCGGTAAGAGAACATTTTACACCGGT
GGTGGCTTAATGACCTTCTACTTATGGAGAATTTTGTACTTGTCCATGATTCTATCTGCAAGATC

GAGATTAAAGGTCTTTTTCGACTGGATTAAATTAGCATTTTTCAA**AAGAGACTTTTTTAAAGGATTATAG**

Features:
Start: [1 : 3]
Stop: [1539 : 1541]
Primer annealing sites (extension/amplification): [1 : 21] [1541 : 1516]

Translation: [513 aa]
MLSKNLYSNKRLLTSTNTLVRFASTRSTGVENSGAGPTSFKTMKVIDPQHSDKPNVLILGSGWGAIS
FLKHIDTKKYNVSIISPRSYFLFTPLLPSAPVGTVDEKSIIEPIVNFALKKKGNVTYYEAEATSINPDRN
TVTIKSLSAVSQLYQPENHLGLHQAEPAEIKYDYLISAVGAEPNTFGIPGVTDYGHFLKEIPNSLEIRR
TFAANLEKANLLPKGDPERRRLLSIVVVGGGPTGVEAAGELQDYVHQDLRKFLPALAEEVQIHLVEA
LPIVLNMFEKKLSSYAQSHLENTSIKVHLRTAVAKVEEKQLLAKTKHEDGKITEETIPYGTLIWATGNK
ARPVITDLFKKIPEQNSSKRGLAVNDFLQVKGSNNIFAIGDNAFAGLPPTAQVAHQEAEYLAKNFDK
MAQIPNFQKNLSSRKDKIDLLFEENNFKPFKYNDLGALAYLGSERAIATIRSGKRTFYTGGGLMTFYL
WRILYLSMILSARSRLKVFFDWIKLAFFKRDFFKGL*

AOX (from pcDNA5/FRT/T0 vector)

pWPI-AOX vector gifted by Dr. Alberto Sanz (Institute for Cell and Molecular Biosciences & Newcastle University Institute for Ageing, Newcastle University, Newcastle, UK) (Scialo et al., 2016).

> [AOX (*Ciona intestinalis*) 1110 bp]
ATGTTGTCTACCGGAAGTAAAACTTTCCTATTTCGACCGTTCCTGGGCTCATGCCATGCACTAC
AAAGTGGAAAACTACCATGTTCAAATCTTCATACAACTCCCACGAAAATCACAGTGAAAAGATAT
TTGGTTGGATATAGTTGGTCAACTCAGCCACATTCCAGATTACTTCATTCATGTCAACAATTAAA
GATAGATGACAAAAATAAATCCGAGCATTTTAAAATTGAAACAAACGATTCAACCGATGAACCCA
ATATAGAAGTGGAAAACTTCCCTCACTTTAGAGAAGCAAAAAAAGCAAAAGAGACACAAAAAGG
AAGCTCTCTTGCTGAAGCTGAGGAGCATCCGGATGTAGAAGAAGGAAGAGCGATGCAAGATGG
AGGGTATAGACTTCCTCATCCTATCTGGCACAAACAAGAATTAGAATCAGTGCGGATATCACAT
AGACCTCCTGTTGGGAAAGTAGACAAATTGGCTTATTACAGTGTACAGTTACTTCGGACTGGCT
TTGATGTTTTTTCTGGTTATACTCTCGGTACCTACACTGGACGGCTAGATGAGAAACAGTGGGT
CAAGAGAATTATATTTTTAGAAACCATTGCTGGTGTACCAGGAATGGTCGGTGCCATGGTTCGT
CACCTGGTTTCCTTACGTAGATTAAAGCGAGACCACGGTTGGATTCACACATTGCTTGAGGAAG
CTGAAAATGAGAGAATGCACTTAATGACTGCGATGAGAATTGCTAACCCTGGTATTATCATGAG
GACGAGTATTGTGGTTGCACAAGGAATCTTTGTGTCTGGATTTTCTTTGGCTTACTTAATCTCAC
CACGATTTTGTCATCGTTTTGTCGGCTATCTGGAAGAGGAAGCAGTTAAGACTTACACGCATTG
TTTAGAAGAACTTGACAGTGGAAACCTAAAAATGTGGTGcCGAATGAAAGCGCCAGAAATTGCT
GTTGAATATTGGAAACTCCCTGACGATGCAATGATGCGAGACGTTATCCTGGCAATCCGAGCT
GATGAAGCACATCACAGATCAGTCAACCATGACTTGGGATCGAGAAAACCAGACGAGCAGAAT
CCTTATCCACCTGGACAATAG

Features :
Start: [1 : 3]
Sequencing error in AOX: [939 : 939] (from previous gifted vector)
Stop: [1108 : 1110]
Primer annealing sites (extension/amplification): [1 : 21] [1110 : 1089]

Translation: [369 aa]
MLSTGSKTFLFRPFLGSCHALQSGKLPCSNLHTTPTKITVKRYLVGYSWSTQPHSRLLHSCQQLKID
DKNKSEHFKIETNDSTDEPNIEVENFPHFREAKKAKETQKGSSLAEAEEHPDVEEGRAMQDGGYR
LPHPIWHKQELESVRISHRPPVGKVDKLAYYSVQLLRTGFDVFSGYTLGTYTGRLDEKQWVKRIIFL
ETIAGVPGMVGAMVRHLVSLRRLKRDHGWIHTLLEEAENERMHLMTAMRIANPGIIMRTSIVVAQGI
FVSGFSLAYLISPRFCHRFVGYLEEEAVKTYTHCLEELDSGNLKMWCRMKAPEIAVEYWKLPDDAM
MRDVILAIRADEAHHRSVNHDLGSRKPDEQNPYPPGQ*

pcDNA3 vector backbone

Thermo Fisher Scientific (Invitrogen): V79020

> [5446 bp]
GACGGATCGGGAGATCTCCCGATCCCCTATGGTCGACTCTCAGTACAATCTGCTCTG
ATGCCGCATAGTTAAGCCAGTATCTGCTCCCTGCTTGTGTGTTGGAGGTCGCTGAGTAGTGCG
CGAGCAAAATTTAAGCTACAACAAGGCAAGGCTTGACCGACAATTGCATGAAGAATCTGCTTAG
GGTTAGGCGTTTTGCGCTGCTTCGCGATGTACGGGCCAGATATCGCGTTGACATTGATTATTGA
CTAGTTATTAATAGTAATCAATTACGGGGTCATTAGTTCATAGCCCATATATGGAGTTCCGCGTT
ACATAACTTACGGTAAATGGCCCGCCTGGCTGACCGCCCAACGACCCCCGCCCATTGACGTCA
ATAATGACGTATGTTCCCATAGTAACGCCAATAGGGACTTTCCATTGACGTCAATGGGTGGACT
ATTTACGGTAAACTGCCCACTTGGCAGTACATCAAGTGTATCATATGCCAAGTACGCCCCCTAT
TGACGTCAATGACGGTAAATGGCCCGCCTGGCATTATGCCCAGTACATGACCTTATGGGACTTT
CCTACTTGGCAGTACATCTACGTATTAGTCATCGCTATTACCATGGTGATGCGGTTTTGGCAGT
ACATCAATGGGCGTGGATAGCGGTTTGACTCACGGGGATTTCCAAGTCTCCACCCCATTGACG
TCAATGGGAGTTTGTTTTGGCACCAAAATCAACGGGACTTTCCAAAATGTCGTAACAACTCCGC
CCCATTGA**CGCAAATGGGCGGTAGGCGTGT**ACGGTGGGAGGTCTATATAAGCAGAGCTCTCT
GGCTAACTAGAGAACCCACTGCTTACTGGCTTATCGAAATTAATACGACTCACTATAGGGAGAC
CCAAGCTTGGTACCGAGCTCGGATCCACTAGTAACGGCCGCCAGTGTGCTGGAATTCTGCAGA
TATCCATCACACTGGCGGCCGCTCGAGCATGCATCTAGAGGGCCCTATTCTATAGTGTCACCTA
AATGCTAGAGCTCGCTGATCAG**CCTCGACTGTGCCTTCTA**GTTGCCAGCCATCTGTTGTTTGCC
CCTCCCCCGTGCCTTCCTTGACCCTGGAAGGTGCCACTCCCACTGTCCTTTCCTAATAAAATGA
GGAAATTGCATCGCATTGTCTGAGTAGGTGTCATTCTATTCTGGGGGGTGGGGTGGGGCAGGA
CAGCAAGGGGGAGGATTGGGAAGACAATAGCAGGCATGCTGGGGATGCGGTGGGCTCTATGG
CTTCTGAGGCGGAAAGAACCAGCTGGGGCTCTAGGGGGTATCCCCACGCGCCCTGTAGCGGC
GCATTAAGCGCGGCGGGTGTGGTGGTTACGCGCAGCGTGACCGCTACACTTGCCAGCGCCCT
AGCGCCCGCTCCTTTCGCTTTCTTCCCTTCCTTTCTCGCCACGTTCGCCGGCTTTCCCCGTCAA
GCTCTAAATCGGGGCATCCCTTTAGGGTTCCGATTTAGTGCTTTACGGCACCTCGACCCCAAAA
AACTTGATTAGGGTGATGGTTCACGTAGTGGGCCATCGCCCTGATAGACGGTTTTTCGCCCTTT
GACGTTGGAGTCCACGTTCTTTAATAGTGGACTCTTGTTCCAAACTGGAACAACACTCAACCCT
ATCTCGGTCTATTCTTTTGATTTATAAGGGATTTTGGGGATTTCGGCCTATTGGTTAAAAAATGA
GCTGATTTAACAAAAATTTAACGCGAATTAATTCTGTGGAATGTGTGTCAGTTAGGGTGTGGAA
AGTCCCCAGGCTCCCCAGGCAGGCAGAAGTATGCAAAGCATGCATCTCAATTAGTCAGCAACC
AGGTGTGGAAAGTCCCCAGGCTCCCCAGCAGGCAGAAGTATGCAAAGCATGCATCTCAATTAG
TCAGCAACCATAGTCCCGCCCCTAACTCCGCCCATCCCGCCCCTAACTCCGCCCAGTTCCGCC
CATTCTCCGCCCCATGGCTGACTAATTTTTTTTATTTATGCAGAGGCCGAGGCCGCCTCTGCCT
CTGAGCTATTCCAGAAGTAGTGAGGAGGCTTTTTTGGAGGCCTAGGCTTTTGCAAAAAGCTCCC
GGGAGCTTGTATATCCATTTTCGGATCTGATCAAGAGACAGGATGAGGATCGTTTCGCATGATT
GAACAAGATGGATTGCACGCAGGTTCTCCGGCCGCTTGGGTGGAGAGGCTATTCGGCTATGAC
TGGGCACAACAGACAATCGGCTGCTCTGATGCCGCCGTGTTCCGGCTGTCAGCGCAGGGGCG
CCCGGTTCTTTTTGTCAAGACCGACCTGTCCGGTGCCCTGAATGAACTGCAGGACGAGGCAGC
GCGGCTATCGTGGCTGGCCACGACGGGCGTTCCTTGCGCAGCTGTGCTCGACGTTGTCACTG
AAGCGGGAAGGGACTGGCTGCTATTGGGCGAAGTGCCGGGGCAGGATCTCCTGTCATCTCAC
CTTGCTCCTGCCGAGAAAGTATCCATCATGGCTGATGCAATGCGGCGGCTGCATACGCTTGAT
CCGGCTACCTGCCCATTCGACCACCAAGCGAAACATCGCATCGAGCGAGCACGTACTCGGATG
GAAGCCGGTCTTGTCGATCAGGATGATCTGGACGAAGAGCATCAGGGGCTCGCGCCAGCCGA

ACTGTTCGCCAGGCTCAAGGCGCGCATGCCCGACGGCGAGGATCTCGTCGTGACCCATGGCG
ATGCCTGCTTGCCGAATATCATGGTGGAAAATGGCCGCTTTTCTGGATTCATCGACTGTGGCCG
GCTGGGTGTGGCGGACCGCTATCAGGACATAGCGTTGGCTACCCGTGATATTGCTGAAGAGCT
TGGCGGCGAATGGGCTGACCGCTTCCTCGTGCTTTACGGTATCGCCGCTCCCGATTCGCAGC
GCATCGCCTTCTATCGCCTTCTTGACGAGTTCTTCTGAGCGGGACTCTGGGGTTCGAAATGAC
CGACCAAGCGACGCCCAACCTGCCATCACGAGATTTCGATTCCACCGCCGCCTTCTATGAAAG
GTTGGGCTTCGGAATCGTTTTCCGGGACGCCGGCTGGATGATCCTCCAGCGCGGGGATCTCAT
GCTGGAGTTCTTCGCCCACCCCAACTTGTTTATTGCAGCTTATAATGGTTACAAATAAAGCAATA
GCATCACAAATTTCACAAATAAAGCATTTTTTTCACTGCATTCTAGTTGTGGTTTGTCCAAACTCA
TCAATGTATCTTATCATGTCTGTATACCGTCGACCTCTAGCTAGAGCTTGGCGTAATCATGGTCA
TAGCTGTTTCCTGTGTGAAATTGTTATCCGCTCACAATTCCACACAACATACGAGCCGGAAGCA
TAAAGTGTAAAGCCTGGGGTGCCTAATGAGTGAGCTAACTCACATTAATTGCGTTGCGCTCACT
GCCCGCTTTCCAGTCGGGAAACCTGTCGTGCCAGCTGCATTAATGAATCGGCCAACGCGCGG
GGAGAGGCGGTTTGCGTATTGGGCGCTCTTCCGCTTCCTCGCTCACTGACTCGCTGCGCTCGG
TCGTTCGGCTGCGGCGAGCGGTATCAGCTCACTCAAAGGCGGTAATACGGTTATCCACAGAAT
CAGGGGATAACGCAGGAAAGAACATGTGAGCAAAAGGCCAGCAAAAGGCCAGGAACCGTAAA
AAGGCCGCGTTGCTGGCGTTTTTCCATAGGCTCCGCCCCCCTGACGAGCATCACAAAAATCGA
CGCTCAAGTCAGAGGTGGCGAAACCCGACAGGACTATAAAGATACCAGGCGTTTCCCCCTGGA
AGCTCCCTCGTGCGCTCTCCTGTTCCGACCCTGCCGCTTACCGGATACCTGTCCGCCTTTCTC
CCTTCGGGAAGCGTGGCGCTTTCTCAATGCTCACGCTGTAGGTATCTCAGTTCGGTGTAGGTC
GTTCGCTCCAAGCTGGGCTGTGTGCACGAACCCCCCGTTCAGCCCGACCGCTGCGCCTTATCC
GGTAACTATCGTCTTGAGTCCAACCCGGTAAGACACGACTTATCGCCACTGGCAGCAGCCACT
GGTAACAGGATTAGCAGAGCGAGGTATGTAGGCGGTGCTACAGAGTTCTTGAAGTGGTGGCCT
AACTACGGCTACACTAGAAGGACAGTATTTGGTATCTGCGCTCTGCTGAAGCCAGTTACCTTCG
GAAAAAGAGTTGGTAGCTCTTGATCCGGCAAACAAACCACCGCTGGTAGCGGTGGTTTTTTTGT
TTGCAAGCAGCAGATTACGCGCAGAAAAAAAGGATCTCAAGAAGATCCTTTGATCTTTTCTACG
GGGTCTGACGCTCAGTGGAACGAAAACTCACGTTAAGGGATTTTGGTCATGAGATTATCAAAAA
GGATCTTCACCTAGATCCTTTTAAATTAAAAATGAAGTTTTAAATCAATCTAAAGTATATATGAGT
AAACTTGGTCTGACAGTTACCAATGCTTAATCAGTGAGGCACCTATCTCAGCGATCTGTCTATTT
CGTTCATCCATAGTTGCCTGACTCCCCGTCGTGTAGATAACTACGATACGGGAGGGCTTACCAT
CTGGCCCCAGTGCTGCAATGATACCGCGAGACCCACGCTCACCGGCTCCAGATTTATCAGCAA
TAAACCAGCCAGCCGGAAGGGCCGAGCGCAGAAGTGGTCCTGCAACTTTATCCGCCTCCATCC
AGTCTATTAATTGTTGCCGGGAAGCTAGAGTAAGTAGTTCGCCAGTTAATAGTTTGCGCAACGT
TGTTGCCATTGCTACAGGCATCGTGGTGTCACGCTCGTCGTTTGGTATGGCTTCATTCAGCTCC
GGTTCCCAACGATCAAGGCGAGTTACATGATCCCCCATGTTGTGCAAAAAAGCGGTTAGCTCC
TTCGGTCCTCCGATCGTTGTCAGAAGTAAGTTGGCCGCAGTGTTATCACTCATGGTTATGGCAG
CACTGCATAATTCTCTTACTGTCATGCCATCCGTAAGATGCTTTTCTGTGACTGGTGAGTACTCA
ACCAAGTCATTCTGAGAATAGTGTATGCGGCGACCGAGTTGCTCTTGCCCGGCGTCAATACGG
GATAATACCGCGCCACATAGCAGAACTTTAAAAGTGCTCATCATTGGAAAACGTTCTTCGGGGC
GAAAACTCTCAAGGATCTTACCGCTGTTGAGATCCAGTTCGATGTAACCCACTCGTGCACCCAA
CTGATCTTCAGCATCTTTTACTTTCACCAGCGTTTCTGGGTGAGCAAAAACAGGAAGGCAAAAT
GCCGCAAAAAAGGGAATAAGGGCGACACGGAAATGTTGAATACTCATACTCTTCCTTTTTCAAT
ATTATTGAAGCATTTATCAGGGTTATTGTCTCATGAGCGGATACATATTTGAATGTATTTAGAAA
AATAAACAAATAGGGGTTCCGCGCACATTTCCCCGAAAAGTGCCACCTGACGTC

Features:
Primer annealing sites (sequencing): [769 : 789] [1053 : 1036]

pcDNA5/FRT/T0 vector backbone

Thermo Fisher Scientific (Invitrogen): V652020

> [5137 bp]

GACGGATCGGGAGATCTCCCGATCCCCTATGGTGCACTCTCAGTACAATCTGCTCTGATGCCG
CATAGTTAAGCCAGTATCTGCTCCCTGCTTGTGTGTTGGAGGTCGCTGAGTAGTGCGCGAGCA
AAATTTAAGCTACAACAAGGCAAGGCTTGACCGACAATTGCATGAAGAATCTGCTTAGGGTTAG
GCGTTTTGCGCTGCTTCGCGATGTACGGGCCAGATATACGCGTTGACATTGATTATTGACTAGT
TATTAATAGTAATCAATTACGGGGTCATTAGTTCATAGCCCATATATGGAGTTCCGCGTTACATA
ACTTACGGTAAATGGCCCGCCTGGCTGACCGCCCAACGACCCCCGCCCATTGACGTCAATAAT
GACGTATGTTCCCATAGTAACGCCAATAGGGACTTTCCATTGACGTCAATGGGTGGAGTATTTA
CGGTAAACTGCCCACTTGGCAGTACATCAAGTGTATCATATGCCAAGTACGCCCCCTATTGACG
TCAATGACGGTAAATGGCCCGCCTGGCATTATGCCCAGTACATGACCTTATGGGACTTTCCTAC
TTGGCAGTACATCTACGTATTAGTCATCGCTATTACCATGGTGATGCGGTTTTGGCAGTACATC
AATGGGCGTGGATAGCGGTTTGACTCACGGGGATTTCCAAGTCTCCACCCCATTGACGTCAAT
GGGAGTTTGTTTTGGCACCAAAATCAACGGGACTTTCCAAAATGTCGTAACAACTCCGCCCCAT
TGA**CGCAAATGGGCGGTAGGCGT**GTACGGTGGGAGGTCTATATAAGCAGAGCTCTCCCTATC
AGTGATAGAGATCTCCCTATCAGTGATAGAGATCGTCGACGAGCTCGTTTAGTGAACCGTCAGA
TCGCCTGGAGACGCCATCCACGCTGTTTTGACCTCCATAGAAGACACCGGGACCGATCCAGCC
TCCGGACTCTAGCGTTTAAACTTAAGCTTGGTACCGAGCTCGGATCCACTAGTCCAGTGTGGTG
GAATTCTGCAGATATCCAGCACAGTGGCGGCCGCTCGAGTCTAGAGGGCCCGTTTAAACCCGC
TGATCAG**CCTCGACTGTGCCTTCTA**GTTGCCAGCCATCTGTTGTTTGCCCCTCCCCCGTGCCTT
CCTTGACCCTGGAAGGTGCCACTCCCACTGTCCTTTCCTAATAAAATGAGGAAATTGCATCGCA
TTGTCTGAGTAGGTGTCATTCTATTCTGGGGGGTGGGGTGGGGCAGGACAGCAAGGGGGAGG
ATTGGGAAGACAATAGCAGGCATGCTGGGGATGCGGTGGGCTCTATGGCTTCTGAGGCGGAA
AGAACCAGCTGGGGCTCTAGGGGGTATCCCCACGCGCCCTGTAGCGGCGCATTAAGCGCGGC
GGGTGTGGTGGTTACGCGCAGCGTGACCGCTACACTTGCCAGCGCCCTAGCGCCCGCTCCTT
TCGCTTTCTTCCCTTCCTTTCTCGCCACGTTCGCCGGCTTTCCCCGTCAAGCTCTAAATCGGGG
GCTCCCTTTAGGGTTCCGATTTAGTGCTTTACGGCACCTCGACCCCAAAAAACTTGATTAGGGT
GATGGTTCACGTACCTAGAAGTTCCTATTCCGAAGTTCCTATTCTCTAGAAAGTATAGGAACTTC
CTTGGCCAAAAAGCCTGAACTCACCGCGACGTCTGTCGAGAAGTTTCTGATCGAAAAGTTCGA
CAGCGTCTCCGACCTGATGCAGCTCTCGGAGGGCGAAGAATCTCGTGCTTTCAGCTTCGATGT
AGGAGGGCGTGGATATGTCCTGCGGGTAAATAGCTGCGCCGATGGTTTCTACAAAGATCGTTA
TGTTTATCGGCACTTTGCATCGGCCGCGCTCCCGATTCCGGAAGTGCTTGACATTGGGGAATT
CAGCGAGAGCCTGACCTATTGCATCTCCCGCCGTGCACAGGGTGTCACGTTGCAAGACCTGCC
TGAAACCGAACTGCCCGCTGTTCTGCAGCCGGTCGCGGAGGCCATGGATGCGATCGCTGCGG
CCGATCTTAGCCAGACGAGCGGGTTCGGCCCATTCGGACCGCAAGGAATCGGTCAATACACTA
CATGGCGTGATTTCATATGCGCGATTGCTGATCCCCATGTGTATCACTGGCAAACTGTGATGGA
CGACACCGTCAGTGCGTCCGTCGCGCAGGCTCTCGATGAGCTGATGCTTTGGGCCGAGGACT
GCCCCGAAGTCCGGCACCTCGTGCACGCGGATTTCGGCTCCAACAATGTCCTGACGGACAATG
GCCGCATAACAGCGGTCATTGACTGGAGCGAGGCGATGTTCGGGGATTCCCAATACGAGGTC
GCCAACATCTTCTTCTGGAGGCCGTGGTTGGCTTGTATGGAGCAGCAGACGCGCTACTTCGAG
CGGAGGCATCCGGAGCTTGCAGGATCGCCGCGGCTCCGGGCGTATATGCTCCGCATTGGTCT
TGACCAACTCTATCAGAGCTTGGTTGACGGCAATTTCGATGATGCAGCTTGGGCGCAGGGTCG
ATGCGACGCAATCGTCCGATCCGGAGCCGGGACTGTCGGGCGTACACAAATCGCCCGCAGAA
GCGCGGCCGTCTGGACCGATGGCTGTGTAGAAGTACTCGCCGATAGTGGAAACCGACGCCCC
AGCACTCGTCCGAGGGCAAAGGAATAGCACGTACTACGAGATTTCGATTCCACCGCCGCCTTC
TATGAAAGGTTGGGCTTCGGAATCGTTTTCCGGGACGCCGGCTGGATGATCCTCCAGCGCGG
GGATCTCATGCTGGAGTTCTTCGCCCACCCCAACTTGTTTATTGCAGCTTATAATGGTTACAAAT
AAAGCAATAGCATCACAAATTTCACAAATAAAGCATTTTTTTCACTGCATTCTAGTTGTGGTTTGT
CCAAACTCATCAATGTATCTTATCATGTCTGTATACCGTCGACCTCTAGCTAGAGCTTGGCGTAA
TCATGGTCATAGCTGTTTCCTGTGTGAAATTGTTATCCGCTCACAATTCCACACAACATACGAGC
CGGAAGCATAAAGTGTAAAGCCTGGGGTGCCTAATGAGTGAGCTAACTCACATTAATTGCGTTG
CGCTCACTGCCCGCTTTCCAGTCGGGAAACCTGTCGTGCCAGCTGCATTAATGAATCGGCCAA

CGCGCGGGGAGAGGCGGTTTGCGTATTGGGCGCTCTTCCGCTTCCTCGCTCACTGACTCGCT
GCGCTCGGTCGTTCGGCTGCGGCGAGCGGTATCAGCTCACTCAAAGGCGGTAATACGGTTATC
CACAGAATCAGGGGATAACGCAGGAAAGAACATGTGAGCAAAAGGCCAGCAAAAGGCCAGGA
ACCGTAAAAAGGCCGCGTTGCTGGCGTTTTTCCATAGGCTCCGCCCCCCTGACGAGCATCACA
AAAATCGACGCTCAAGTCAGAGGTGGCGAAACCCGACAGGACTATAAAGATACCAGGCGTTTC
CCCCTGGAAGCTCCCTCGTGCGCTCTCCTGTTCCGACCCTGCCGCTTACCGGATACCTGTCCG
CCTTTCTCCCTTCGGGAAGCGTGGCGCTTTCTCATAGCTCACGCTGTAGGTATCTCAGTTCGGT
GTAGGTCGTTCGCTCCAAGCTGGGCTGTGTGCACGAACCCCCCGTTCAGCCCGACCGCTGCG
CCTTATCCGGTAACTATCGTCTTGAGTCCAACCCGGTAAGACACGACTTATCGCCACTGGCAGC
AGCCACTGGTAACAGGATTAGCAGAGCGAGGTATGTAGGCGGTGCTACAGAGTTCTTGAAGTG
GTGGCCTAACTACGGCTACACTAGAAGAACAGTATTTGGTATCTGCGCTCTGCTGAAGCCAGTT
ACCTTCGGAAAAAGAGTTGGTAGCTCTTGATCCGGCAAACAAACCACCGCTGGTAGCGGTGGT
TTTTTTGTTTGCAAGCAGCAGATTACGCGCAGAAAAAAAGGATCTCAAGAAGATCCTTTGATCTT
TTCTACGGGGTCTGACGCTCAGTGGAACGAAAACTCACGTTAAGGGATTTTGGTCATGAGATTA
TCAAAAAGGATCTTCACCTAGATCCTTTTAAATTAAAAATGAAGTTTTAAATCAATCTAAAGTATA
TATGAGTAAACTTGGTCTGACAGTTACCAATGCTTAATCAGTGAGGCACCTATCTCAGCGATCT
GTCTATTTCGTTCATCCATAGTTGCCTGACTCCCCGTCGTGTAGATAACTACGATACGGGAGGG
CTTACCATCTGGCCCCAGTGCTGCAATGATACCGCGAGACCCACGCTCACCGGCTCCAGATTT
ATCAGCAATAAACCAGCCAGCCGGAAGGGCCGAGCGCAGAAGTGGTCCTGCAACTTTATCCGC
CTCCATCCAGTCTATTAATTGTTGCCGGGAAGCTAGAGTAAGTAGTTCGCCAGTTAATAGTTTG
CGCAACGTTGTTGCCATTGCTACAGGCATCGTGGTGTCACGCTCGTCGTTTGGTATGGCTTCAT
TCAGCTCCGGTTCCCAACGATCAAGGCGAGTTACATGATCCCCCATGTTGTGCAAAAAAGCGG
TTAGCTCCTTCGGTCCTCCGATCGTTGTCAGAAGTAAGTTGGCCGCAGTGTTATCACTCATGGT
TATGGCAGCACTGCATAATTCTCTTACTGTCATGCCATCCGTAAGATGCTTTTCTGTGACTGGT
GAGTACTCAACCAAGTCATTCTGAGAATAGTGTATGCGGCGACCGAGTTGCTCTTGCCCGGCG
TCAATACGGGATAATACCGCGCCACATAGCAGAACTTTAAAAGTGCTCATCATTGGAAAACGTT
CTTCGGGGCGAAAACTCTCAAGGATCTTACCGCTGTTGAGATCCAGTTCGATGTAACCCACTCG
TGCACCCAACTGATCTTCAGCATCTTTTACTTTCACCAGCGTTTCTGGGTGAGCAAAAACAGGA
AGGCAAAATGCCGCAAAAAAGGGAATAAGGGCGACACGGAAATGTTGAATACTCATACTCTTC
CTTTTTCAATATTATTGAAGCATTTATCAGGGTTATTGTCTCATGAGCGGATACATATTTGAATGT
ATTTAGAAAAATAAACAAATAGGGGTTCCGCGCACATTTCCCCGAAAAGTGCCACCTGACGTC

Features :
Primer annealing sites (sequencing): [769 : 789] [1106 : 1089]

pWPI vector backbone

Dr. Alberto Sanz (Institute for Cell and Molecular Biosciences & Newcastle University Institute for Ageing, Newcastle University, Newcastle, UK).

> [11101 bp]

TTGGAAGGGCTAATTCACTCCCAAAGAAGACAAGATATCCTTGATCTGTGGATCTACCACACAC
AAGGCTACTTCCCTGATTAGCAGAACTACACACCAGGGCCAGGGGTCAGATATCCACTGACCT
TTGGATGGTGCTACAAGCTAGTACCAGTTGAGCCAGATAAGGTAGAAGAGGCCAATAAAGGAG
AGAACACCAGCTTGTTACACCCTGTGAGCCTGCATGGGATGGATGACCCGGAGAGAGAAGTGT
TAGAGTGGAGGTTTGACAGCCGCCTAGCATTTCATCACGTGGCCCGAGAGCTGCATCCGGAGT
ACTTCAAGAACTGCTGATATCGAGCTTGCTACAAGGGACTTTCCGCTGGGGACTTTCCAGGGA
GGCGTGGCCTGGGCGGGACTGGGGAGTGGCGAGCCCTCAGATCCTGCATATAAGCAGCTGCT
TTTTGCCTGTACTGGGTCTCTCTGGTTAGACCAGATCTGAGCCTGGGAGCTCTCTGGCTAACTA
GGGAACCCACTGCTTAAGCCTCAATAAAGCTTGCCTTGAGTGCTTCAAGTAGTGTGTGCCCGTC
TGTTGTGTGACTCTGGTAACTAGAGATCCCTCAGACCCTTTTAGTCAGTGTGGAAAATCTCTAG
CAGTGGCGCCCGAACAGGGACTTGAAAGCGAAAGGGAAACCAGAGGAGCTCTCTCGACGCAG
GACTCGGCTTGCTGAAGCGCGCACGGCAAGAGGCGAGGGGCGGCGACTGGTGAGTACGCCA
AAAATTTTGACTAGCGGAGGCTAGAAGGAGAGAGATGGGTGCGAGAGCGTCAGTATTAAGCGG
GGGAGAATTAGATCGCGATGGGAAAAAATTCGGTTAAGGCCAGGGGGAAAGAAAAAATATAAA
TTAAAACATATAGTATGGGCAAGCAGGGAGCTAGAACGATTCGCAGTTAATCCTGGCCTGTTAG
AAACATCAGAAGGCTGTAGACAAATACTGGGACAGCTACAACCATCCCTTCAGACAGGATCAG
AAGAACTTAGATCATTATATAATACAGTAGCAACCCTCTATTGTGTGCATCAAAGGATAGAGATA
AAAGACACCAAGGAAGCTTTAGACAAGATAGAGGAAGAGCAAAACAAAAGTAAGACCACCGCA
CAGCAAGCGGCCGCTGATCTTCAGACCTGGAGGAGGAGATATGAGGGACAATTGGAGAAGTG
AATTATATAAATATAAAGTAGTAAAAATTGAACCATTAGGAGTAGCACCCACCAAGGCAAAGAG
AAGAGTGGTGCAGAGAGAAAAAAGAGCAGTGGGAATAGGAGCTTTGTTCCTTGGGTTCTTGGG
AGCAGCAGGAAGCACTATGGGCGCAGCGTCAATGACGCTGACGGTACAGGCCAGACAATTATT
GTCTGGTATAGTGCAGCAGCAGAACAATTTGCTGAGGGCTATTGAGGCGCAACAGCATCTGTT
GCAACTCACAGTCTGGGGCATCAAGCAGCTCCAGGCAAGAATCCTGGCTGTGGAAAGATACCT
AAAGGATCAACAGCTCCTGGGGATTTGGGGTTGCTCTGGAAAACTCATTTGCACCACTGCTGT
GCCTTGGAATGCTAGTTGGAGTAATAAATCTCTGGAACAGATTTGGAATCACACGACCTGGATG
GAGTGGGACAGAGAAATTAACAATTACACAAGCTTAATACACTCCTTAATTGAAGAATCGCAAA
ACCAGCAAGAAAAGAATGAACAAGAATTATTGGAATTAGATAAATGGGCAAGTTTGTGGAATTG
GTTTAACATAACAAATTGGCTGTGGTATATAAAATTATTCATAATGATAGTAGGAGGCTTGGTAG
GTTTAAGAATAGTTTTTGCTGTACTTTCTATAGTGAATAGAGTTAGGCAGGGATATTCACCATTA
TCGTTTCAGACCCACCTCCCAACCCCGAGGGGACCCGACAGGCCCGAAGGAATAGAAGAAGA
AGGTGGAGAGAGAGACAGAGACAGATCCATTCGATTAGTGAACGGATCTCGACGGTATCGATG
TCGACGATAAGCTTTGCAAAGATGGATAAAGTTTTAAACAGAGAGGAATCTTTGCAGCTAATGG
ACCTTCTAGGTCTTGAAAGGAGTGGGAATTGGCTCCGGTGCCCGTCAGTGGGCAGAGCGCAC
ATCGCCCACAGTCCCCGAGAAGTTGGGGGGAGGGGTCGGCAATTGAACCGGTGCCTAGAGAA
GGTGGCGCGGGGTAAACTGGGAAAGTGATGTCGTGTACTGGCTCCGCCTTTTTCCCGAGGGT
GGGGGAGAACCGTATATAAGTGCAGTAGTCGCCGTGAACGTTCTTTTTCGCAACGGGTTTGCC
GCCAGAACACAGGTAAGTGCCGTGTGTGGTTCCCGCGGGCCTGGCCTCTTTACGGGTTATGG
CCCTTGCGTGCCTTGAATTACTTCCACTGGCTGCAGTACGTGATTCTTGATCCCGAGCTTCGGG
TTGGAAGTGGGTGGGAGAGTTCGAGGCCTTGCGCTTAAGGAGCCCCTTCGCCTCGTGCTTGA
GTTGAGGCCTGGCCTGGGCGCTGGGGCCGCCGCGTGCGAATCTGGTGGCACCTTCGCGCCT
GTCTCGCTGCTTTCGATAAGTCTCTAGCCATTTAAAATTTTTGATGACCTGCTGCGACGCTTTTT
TTCTGGCAAGATAGTCTTGTAAATGCGGGCCAAGATCTGCACACTGGTATTTCGGTTTTTGGGG
CCGCGGGCGGCGACGGGGCCCGTGCGTCCCAGCGCACATGTTCGGCGAGGCGGGGCCTGC
GAGCGCGGCCACCGAGAATCGGACGGGGGTAGTCTCAAGCTGGCCGGCCTGCTCTGGTGCCT
GGCCTCGCGCCGCCGTGTATCGCCCCGCCCTGGGCGGCAAGGCTGGCCCGGTCGGCACCAG
TTGCGTGAGCGGAAAGATGGCCGCTTCCCGGCCCTGCTGCAGGGAGCTCAAAATGGAGGACG

CGGCGCTCGGGAGAGCGGGCGGGTGAGTCACCCACACAAAGGAAAAGGGCCTTTCCGTCCTC
AGCCGTCGCTTCATGTGACTCCACGGAGTACCGGGCGCCGTCCAGGCACCTCGATTAGTTCTC
GAGCTTTTGGAGTACGTCGTCTTTAGGTTGGGGGGAGGGGTTTTATGCGATGGAGTTTCCCCA
CACTGAGTGGGTGGAGACTGAAGTTAGGCCAGCTTGGCACTTGATGTAATTCTCCTTGGAATTT
GCCCTTTTTGAGTTTGGATCTTGGTTCATTCTCAAGCCTCAGACAGTGGTTCAAAGTTTTTTTCT
TCCATTTCAGGTGTCGTGAGGAATTTCGACATTTAAATTTAATTAATCTCGACGGTATCGGTTAA
CTTTTAAAAGAAAAGGGGGGATTGGGGGGTACAGTGCAGGGGAAAGAATAGTAGACATAATAG
CAACAGACATACAAACTAAAGAATTACAAAAACAAATTACAAAAATTCAAAATTTTCCGATCACG
AGACTAGCCTCGAGGTTTAAACTACGGGCTGCAGGAATTCCGCCCCCCCCCCCCTAACGTTAC
TGGCCGAAGCCGCTTGGAATAAGGCCGGTGTGCGTTTGTCTATATGTTATTTTCCACCATATTG
CCGTCTTTTGGCAATGTGAGGGCCCGGAAACCTGGCCCTGTCTTCTTGACGAGCATTCCTAGG
GGTCTTTCCCCTCTCGCCAAAGGAATGCAAGGTCTGTTGAATGTCGTGAAGGAAGCAGTTCCT
CTGGAAGCTTCTTGAAGACAAACAACGTCTGTAGCGACCCTTTGCAGGCAGCGGAACCCCCCA
CCTGGCGACAGGTGCCTCTGCGGCCAAAAGCCACGTGTATAAGATACACCTGCAAAGGCGGC
ACAACCCCAGTGCCACGTTGTGAGTTGGATAGTTGTGGAAAGAGTCAAATGGCTCTCCTCAAG
CGTATTCAACAAGGGGCTGAAGGATGCCCAGAAGGTACCCCATTGTATGGGATCTGATCTGGG
GCCTCGGTGCACATGCTTTACATGTGTTTAGTCGAGGTTAAAAAACGTCTAGGCCCCCCGAACC
ACGGGGACGTGGTTTTCCTTTGAAAAACACGATGATAATACCATGGTGAGCAAGGGCGAGGAG
CTGTTCACCGGGGTGGTGCCCATCCTGGTCGAGCTGGACGGCGACGTAAACGGCCACAAGTT
CAGCGTGTCCGGCGAGGGCGAGGGCGATGCCACCTACGGCAAGCTGACCCTGAAGTTCATCT
GCACCACCGGCAAGCTGCCCGTGCCCTGGCCCACCCTCGTGACCACCCTGACCTACGGCGTG
CAGTGCTTCAGCCGCTACCCCGACCACATGAAGCAGCACGACTTCTTCAAGTCCGCCATGCCC
GAAGGCTACGTCCAGGAGCGCACCATCTTCTTCAAGGACGACGGCAACTACAAGACCCGCGC
CGAGGTGAAGTTCGAGGGCGACACCCTGGTGAACCGCATCGAGCTGAAGGGCATCGACTTCA
AGGAGGACGGCAACATCCTGGGGCACAAGCTGGAGTACAACTACAACAGCCACAACGTCTATA
TCATGGCCGACAAGCAGAAGAACGGCATCAAGGTGAACTTCAAGATCCGCCACAACATCGAGG
ACGGCAGCGTGCAGCTCGCCGACCACTACCAGCAGAACACCCCCATCGGCGACGGCCCCGTG
CTGCTGCCCGACAACCACTACCTGAGCACCCAGTCCGCCCTGAGCAAAGACCCCAACGAGAA
GCGCGATCACATGGTCCTGCTGGAGTTCGTGACCGCCGCCGGGATCACTCTCGGCATGGACG
AGCTGTACAAGTCCGGACTCAGATCTCGACTAGCTAGTAGCTAGCTAGCTAGTCGAGCTCAAC
TTCGAATTCGATATCAAGCTTATCGCGATACCGTCGACCTCGAGGGAATTCCGATAATCAACCT
CTGGATTACAAAATTTGTGAAAGATTGACTGGTATTCTTAACTATGTTGCTCCTTTTACGCTATG
TGGATACGCTGCTTTAATGCCTTTGTATCATGCTATTGCTTCCCGTATGGCTTTCATTTTCTCCT
CCTTGTATAAATCCTGGTTGCTGTCTCTTTATGAGGAGTTGTGGCCCGTTGTCAGGCAACGTGG
CGTGGTGTGCACTGTGTTTGCTGACGCAACCCCCACTGGTTGGGGCATTGCCACCACCTGTCA
GCTCCTTTCCGGGACTTTCGCTTTCCCCCTCCCTATTGCCACGGCGGAACTCATCGCCGCCTG
CCTTGCCCGCTGCTGGACAGGGGCTCGGCTGTTGGGCACTGACAATTCCGTGGTGTTGTCGG
GGAAGCTGACGTCCTTTCCATGGCTGCTCGCCTGTGTTGCCACCTGGATTCTGCGCGGGACGT
CCTTCTGCTACGTCCCTTCGGCCCTCAATCCAGCGGACCTTCCTTCCCGCGGCCTGCTGCCGG
CTCTGCGGCCTCTTCCGCGTCTTCGCCTTCGCCCTCAGACGAGTCGGATCTCCCTTTGGGCCG
CCTCCCCGCATCGGGAATTCGCTCAAGCTTCGAATTAATTCTGCAGAGCTCGGTACCTTTAAGA
CCAATGACTTACAAGGCAGCTGTAGATCTTAGCCACTTTTTAAAAGAAAAGGGGGGACTGGAAG
GGCTAATTCACTCCCAACGAAGACAAGATGGGATCAATTCACCATGGGAATAACTTCGTATAGC
ATACATTATACGAAGTTATGCTGCTTTTTGCTTGTACTGGGTCTCTCTGGTTAGACCAGATCTGA
GCCTGGGAGCTCTCTGGCTAACTAGGGAACCCACTGCTTAAGCCTCAATAAAGCTTGCCTTGA
GTGCTTCAAGTAGTGTGTGCCCGTCTGTTGTGTGACTCTGGTAACTAGAGATCCCTCAGACCCT
TTTAGTCAGTGTGGAAAATCTCTAGCAGCATCTAGAATTAATTCCGTGTATTCTATAGTGTCACC
TAAATCGTATGTGTATGATACATAAGGTTATGTATTAATTGTAGCCGCGTTCTAACGACAATATG
TACAAGCCTAATTGTGTAGCATCTGGCTTACTGAAGCAGACCCTATCATCTCTCTCGTAAACTG
CCGTCAGAGTCGGTTTGGTTGGACGAACCTTCTGAGTTTCTGGTAACGCCGTCCCGCACCCGG
AAATGGTCAGCGAACCAATCAGCAGGGTCATCGCTAGCCAGATCCTCTACGCCGGACGCATCG
TGGCCGGCATCACCGGCGCCACAGGTGCGGTTGCTGGCGCCTATATCGCCGACATCACCGAT
GGGGAAGATCGGGCTCGCCACTTCGGGCTCATGAGCGCTTGTTTCGGCGTGGGTATGGTGGC
AGGCCCCGTGGCCGGGGGACTGTTGGGCGCCATCTCCTTGCATGCACCATTCCTTGCGGCGG
CGGTGCTCAACGGCCTCAACCTACTACTGGGCTGCTTCCTAATGCAGGAGTCGCATAAGGGAG

AGCGTCGAATGGTGCACTCTCAGTACAATCTGCTCTGATGCCGCATAGTTAAGCCAGCCCCGA
CACCCGCCAACACCCGCTGACGCGCCCTGACGGGCTTGTCTGCTCCCGGCATCCGCTTACAG
ACAAGCTGTGACCGTCTCCGGGAGCTGCATGTGTCAGAGGTTTTCACCGTCATCACCGAAACG
CGCGAGACGAAAGGGCCTCGTGATACGCCTATTTTTATAGGTTAATGTCATGATAATAATGGTT
TCTTAGACGTCAGGTGGCACTTTTCGGGGAAATGTGCGCGGAACCCCTATTTGTTTATTTTTCT
AAATACATTCAAATATGTATCCGCTCATGAGACAATAACCCTGATAAATGCTTCAATAATATTGA
AAAAGGAAGAGTATGAGTATTCAACATTTCCGTGTCGCCCTTATTCCCTTTTTTGCGGCATTTTG
CCTTCCTGTTTTTGCTCACCCAGAAACGCTGGTGAAAGTAAAAGATGCTGAAGATCAGTTGGGT
GCACGAGTGGGTTACATCGAACTGGATCTCAACAGCGGTAAGATCCTTGAGAGTTTTCGCCCC
GAAGAACGTTTTCCAATGATGAGCACTTTTAAAGTTCTGCTATGTGGCGCGGTATTATCCCGTA
TTGACGCCGGGCAAGAGCAACTCGGTCGCCGCATACACTATTCTCAGAATGACTTGGTTGAGT
ACTCACCAGTCACAGAAAAGCATCTTACGGATGGCATGACAGTAAGAGAATTATGCAGTGCTGC
CATAACCATGAGTGATAACACTGCGGCCAACTTACTTCTGACAACGATCGGAGGACCGAAGGA
GCTAACCGCTTTTTTGCACAACATGGGGGATCATGTAACTCGCCTTGATCGTTGGGAACCGGA
GCTGAATGAAGCCATACCAAACGACGAGCGTGACACCACGATGCCTGTAGCAATGGCAACAAC
GTTGCGCAAACTATTAACTGGCGAACTACTTACTCTAGCTTCCCGGCAACAATTAATAGACTGG
ATGGAGGCGGATAAAGTTGCAGGACCACTTCTGCGCTCGGCCCTTCCGGCTGGCTGGTTTATT
GCTGATAAATCTGGAGCCGGTGAGCGTGGGTCTCGCGGTATCATTGCAGCACTGGGGCCAGA
TGGTAAGCCCTCCCGTATCGTAGTTATCTACACGACGGGGAGTCAGGCAACTATGGATGAACG
AAATAGACAGATCGCTGAGATAGGTGCCTCACTGATTAAGCATTGGTAACTGTCAGACCAAGTT
TACTCATATATACTTTAGATTGATTTAAAACTTCATTTTTAATTTAAAAGGATCTAGGTGAAGATC
CTTTTTGATAATCTCATGACCAAAATCCCTTAACGTGAGTTTTCGTTCCACTGAGCGTCAGACCC
CGTAGAAAAGATCAAAGGATCTTCTTGAGATCCTTTTTTTCTGCGCGTAATCTGCTGCTTGCAAA
CAAAAAAACCACCGCTACCAGCGGTGGTTTGTTTGCCGGATCAAGAGCTACCAACTCTTTTTCC
GAAGGTAACTGGCTTCAGCAGAGCGCAGATACCAAATACTGTCCTTCTAGTGTAGCCGTAGTTA
GGCCACCACTTCAAGAACTCTGTAGCACCGCCTACATACCTCGCTCTGCTAATCCTGTTACCAG
TGGCTGCTGCCAGTGGCGATAAGTCGTGTCTTACCGGGTTGGACTCAAGACGATAGTTACCGG
ATAAGGCGCAGCGGTCGGGCTGAACGGGGGGTTCGTGCACACAGCCCAGCTTGGAGCGAAC
GACCTACACCGAACTGAGATACCTACAGCGTGAGCATTGAGAAAGCGCCACGCTTCCCGAAGG
GAGAAAGGCGGACAGGTATCCGGTAAGCGGCAGGGTCGGAACAGGAGAGCGCACGAGGGAG
CTTCCAGGGGGAAACGCCTGGTATCTTTATAGTCCTGTCGGGTTTCGCCACCTCTGACTTGAG
CGTCGATTTTTGTGATGCTCGTCAGGGGGGCGGAGCCTATGGAAAAACGCCAGCAACGCGGC
CTTTTTACGGTTCCTGGCCTTTTGCTGGCCTTTTGCTCACATGTTCTTTCCTGCGTTATCCCCTG
ATTCTGTGGATAACCGTATTACCGCCTTTGAGTGAGCTGATACCGCTCGCCGCAGCCGAACGA
CCGAGCGCAGCGAGTCAGTGAGCGAGGAAGCGGAAGAGCGCCCAATACGCAAACCGCCTCTC
CCCGCGCGTTGGCCGATTCATTAATGCAGCTGTGGAATGTGTGTCAGTTAGGGTGTGGAAAGT
CCCCAGGCTCCCCAGCAGGCAGAAGTATGCAAAGCATGCATCTCAATTAGTCAGCAACCAGGT
GTGGAAAGTCCCCAGGCTCCCCAGCAGGCAGAAGTATGCAAAGCATGCATCTCAATTAGTCAG
CAACCATAGTCCCGCCCCTAACTCCGCCCATCCCGCCCCTAACTCCGCCCAGTTCCGCCCATT
CTCCGCCCCATGGCTGACTAATTTTTTTTATTTATGCAGAGGCCGAGGCCGCCTCGGCCTCTGA
GCTATTCCAGAAGTAGTGAGGAGGCTTTTTTGGAGGCCTAGGCTTTTGCAAAAAGCTTGGACAC
AAGACAGGCTTGCGAGATATGTTTGAGAATACCACTTTATCCCGCGTCAGGGAGAGGCAGTGC
GTAAAAAGACGCGGACTCATGTGAAATACTGGTTTTTAGTGCGCCAGATCTCTATAATCTCGCG
CAACCTATTTTCCCCTCGAACACTTTTTAAGCCGTAGATAAACAGGCTGGGACACTTCACATGA
GCGAAAAATACATCGTCACCTGGGACATGTTGCAGATCCATGCACGTAAACTCGCAAGCCGAC
TGATGCCTTCTGAACAATGGAAAGGCATTATTGCCGTAAGCCGTGGCGGTCTGTACCGGGTGC
GTTACTGGCGCGTGAACTGGGTATTCGTCATGTCGATACCGTTTGTATTTCCAGCTACGATCAC
GACAACCAGCGCGAGCTTAAAGTGCTGAAACGCGCAGAAGGCGATGGCGAAGGCTTCATCGT
TATTGATGACCTGGTGGATACCGGTGGTACTGCGGTTGCGATTCGTGAAATGTATCCAAAAGC
GCACTTTGTCACCATCTTCGCAAAACCGGCTGGTCGTCCGCTGGTTGATGACTATGTTGTTGAT
ATCCCGCAAGATACCTGGATTGAACAGCCGTGGGATATGGGCGTCGTATTCGTCCCGCCAATC
TCCGGTCGCTAATCTTTTCAACGCCTGGCACTGCCGGGCGTTGTTCTTTTTAACTTCAGGCGGG
TTACAATAGTTTCCAGTAAGTATTCTGGAGGCTGCATCCATGACACAGGCAAACCTGAGCGAAA
CCCTGTTCAAACCCCGCTTTAAACATCCTGAAACCTCGACGCTAGTCCGCCGCTTTAATCACGG
CGCACAACCGCCTGTGCAGTCGGCCCTTGATGGTAAAACCATCCCTCACTGGTATCGCATGAT

TAACCGTCTGATGTGGATCTGGCGCGGCATTGACCCACGCGAAATCCTCGACGTCCAGGCACG
TATTGTGATGAGCGATGCCGAACGTACCGACGATGATTTATACGATACGGTGATTGGCTACCGT
GGCGGCAACTGGATTTATGAGTGGGCCCCGGATCTTTGTGAAGGAACCTTACTTCTGTGGTGT
GACATAATTGGACAAACTACCTACAGAGATTTAAAGCTCTAAGGTAAATATAAAATTTTTAAGTG
TATAATGTGTTAAACTACTGATTCTAATTGTTTGTGTATTTTAGATTCCAACCTATGGAACTGATG
AATGGGAGCAGTGGTGGAATGCCTTTAATGAGGAAAACCTGTTTTGCTCAGAAGAAATGCCATC
TAGTGATGATGAGGCTACTGCTGACTCTCAACATTCTACTCCTCCAAAAAAGAAGAGAAAGGTA
GAAGACCCCAAGGACTTTCCTTCAGAATTGCTAAGTTTTTTGAGTCATGCTGTGTTTAGTAATAG
AACTCTTGCTTGCTTTGCTATTTACACCACAAAGGAAAAAGCTGCACTGCTATACAAGAAAATTA
TGGAAAAATATTCTGTAACCTTTATAAGTAGGCATAACAGTTATAATCATAACATACTGTTTTTTC
TTACTCCACACAGGCATAGAGTGTCTGCTATTAATAACTATGCTCAAAAATTGTGTACCTTTAGC
TTTTTAATTTGTAAAGGGGTTAATAAGGAATATTTGATGTATAGTGCCTTGACTAGAGATCATAAT
CAGCCATACCACATTTGTAGAGGTTTTACTTGCTTTAAAAAACCTCCCACACCTCCCCCTGAAC
CTGAAACATAAAATGAATGCAATTGTTGTTGTTAACTTGTTTATTGCAGCTTATAATGGTTACAAA
TAAAGCAATAGCATCACAAATTTCACAAATAAAGCATTTTTTTCACTGCATTCTAGTTGTGGTTTG
TCCAAACTCATCAATGTATCTTATCATGTCTGGATCAACTGGATAACTCAAGCTAACCAAAATCA
TCCCAAACTTCCCACCCCATACCCTATTACCACTGCCAATTACCTAGTGGTTTCATTTACTCTAA
ACCTGTGATTCCTCTGAATTATTTTCATTTTAAAGAAATTGTATTTGTTAAATATGTACTACAAAC
TTAGTAG

pOG44 vector

Thermo Fisher Scientific (Invitrogen): V600520

>[5785 bp]

CCGCGGTCTTTCGGACTTTTGAAAGTGATGGTGGTGGGGGAAGGATTCGAACCTTCGAAGTCG
ATGACGGCAGATTTAGAGTCTGCTCCCTGCTTGTGTGTTGGAGGTCGCTGAGTAGTGCGCGAG
CAAAATTTAAGCTACAACAAGGCAAGGCTTGACCGACAATTGCATGAAGAATCTGCTTAGGGTT
AGGCGTTTTGCGCTGCTTCGCGATGTACGGGCCAGATATACGCGTTGACATTGATTATTGACTA
GTTATTAATAGTAATCAATTACGGGGTCATTAGTTCATAGCCCATATATGGAGTTCCGCGTTACA
TAACTTACGGTAAATGGCCCGCCTGGCTGACCGCCCAACGACCCCCGCCCATTGACGTCAATA
ATGACGTATGTTCCCATAGTAACGCCAATAGGGACTTTCCATTGACGTCAATGGGTGGAGTATT
TACGGTAAACTGCCCACTTGGCAGTACATCAAGTGTATCATATGCCAAGTACGCCCCCTATTGA
CGTCAATGACGGTAAATGGCCCGCCTGGCATTATGCCCAGTACATGACCTTATGGGACTTTCCT
ACTTGGCAGTACATCTACGTATTAGTCATCGCTATTACCATGGTGATGCGGTTTTGGCAGTACA
TCAATGGGCGTGGATAGCGGTTTGACTCACGGGGATTTCCAAGTCTCCACCCCATTGACGTCA
ATGGGAGTTTGTTTTGGCACCAAAATCAACGGGACTTTCCAAAATGTCGTAACAACTCCGCCCC
ATTGACGCAAATGGGCGGTAGGCGTGTACGGTGGGAGGTCTATATAAGCAGAGCTCTCTGGCT
AACTAGAGAACCCACTGCTTACTGGCTTATCGAAATTAATACGACTCACTATAGGGAGACCCAA
GCTTCTAGAATTCGCTGTCTGCGAGGGCCAGCTGTTGGGGTGAGTACTCCCTCTCAAAAGCGG
GCATGACTTCTGCGCTAAGATTGTCAGTTTCCAAAAACGAGGAGGATTTGATATTCACCTGGCC
CGCGGTGATGCCTTTGAGGGTGGCCGCGTCCATCTGGTCAGAAAAGACAATCTTTTTGTTGTC
AAGCTTGAGGTGTGGCAGGCTTGAGATCTGGCCATACACTTGAGTGACAATGACATCCACTTT
GCCTTTCTCTCCACAGGTGTCCACTCCCAGGTCCAACTGCAGCCCAAGCTTCCACCATGCCAC
AATTTGATATATTATGTAAAACACCACCTAAGGTGCTTGTTCGTCAGTTTGTGGAAAGGTTTGAA
AGACCTTCAGGTGAGAAAATAGCATTATGTGCTGCTGAACTAACCTATTTATGTTGGATGATTAC
ACATAACGGAACAGCAATCAAGAGAGCCACATTCATGAGCTATAATACTATCATAAGCAATTCG
CTGAGTTTGGATATTGTCAACAAGTCACTGCAGTTTAAATACAAGACGCAAAAAGCAACAATTCT
GGAAGCCTCATTAAAGAAATTGATTCCTGCTTGGGAATTTACAATTATTCCTTACTATGGACAAA
AACATCAATCTGATATCACTGATATTGTAAGTAGTTTGCAATTACAGTTCGAATCATCGGAAGAA
GCAGATAAGGGAAATAGCCACAGTAAAAAAATGCTTAAAGCACTTCTAAGTGAGGGTGAAAGCA
TCTGGGAGATCACTGAGAAAATACTAAATTCGTTTGAGTATACTTCGAGATTTACAAAAACAAAA

ACTTTATACCAATTCCTCTTCCTAGCTACTTTCATCAATTGTGGAAGATTCAGCGATATTAAGAA
CGTTGATCCGAAATCATTTAAATTAGTCCAAAATAAGTATCTGGGAGTAATAATCCAGTGTTTAG
TGACAGAGACAAAGACAAGCGTTAGTAGGCACATATACTTCTTTAGCGCAAGGGGTAGGATCG
ATCCACTTGTATATTTGGATGAATTTTTGAGGAATTCTGAACCAGTCCTAAAACGAGTAAATAGG
ACCGGCAATTCTTCAAGCAACAAGCAGGAATACCAATTATTAAAAGATAACTTAGTCAGATCGTA
CAACAAAGCTTTGAAGAAAAATGCGCCTTATTCAATCTTTGCTATAAAAAATGGCCCAAAATCTC
ACATTGGAAGACATTTGATGACCTCATTTCTTTCAATGAAGGGCCTAACGGAGTTGACTAATGTT
GTGGGAAATTGGAGCGATAAGCGTGCTTCTGCCGTGGCCAGGACAACGTATACTCATCAGATA
ACAGCAATACCTGATCACTACTTCGCACTAGTTTCTCGGTACTATGCATATGATCCAATATCAAA
GGAAATGATAGCATTGAAGGATGAGACTAATCCAATTGAGGAGTGGCAGCATATAGAACAGCTA
AAGGGTAGTGCTGAAGGAAGCATACGATACCCCGCATGGAATGGGATAATATCACAGGAGGTA
CTAGACTACCTTTCATCCTACATAAATAGACGCATATAAGTACGCATTTAAGCATAAACACGCAC
TATGCCGTTCTTCTCATGTATATATATATACAGGCAACACGCAGATATAGGTGCGACGTGAACA
GTGAGCTGTATGTGCGGGTACCGAGCTCCTCGAGGATCAGACATGATAAGATACATTGATGAG
TTTGGACAAACCACAACTAGAATGCAGTGAAAAAAATGCTTTATTTGTGAAATTTGTGATGCTAT
TGCTTTATTTGTAACCATTATAAGCTGCAATAAACAAGTTATCCTCGAGGAGCTCATGAGCGCTT
GTTTCGGCGTGGGTATGGTGGCAGGCCCGTGGCCGGGGGACTGTTGGGCGCCATCTCCTTGC
ATGCACCATTCCTTGCGGCGGCGGTGCTCAACGGCCTCAACCTACTACTGGGCTGCTTCCTAA
TGCAGGAGTCGCATAAGGGAGAGCGTCGACCTCGAGGGGGGGCCCGGTACCCAGCTTTTGTT
CCCTTTAGTGAGGGTTAATTGCGCGCTTGGCGTAATCATGGTCATAGCTGTTTCCTGTGTGAAA
TTGTTATCCGCTCACAATTCCACACAACATACGAGCCGGGAGCATAAAGTGTAAAGCCTGGGG
TGCCTAATGAGTGAGCTAACTCACATTAATTGCGTTGCGCTCACTGCCCGCTTTCCAGTCGGGA
AACCTGTCGTGCCAGCTGCATTAATGAATCGGCCAACGCGCGGGGAGAGGCGGTTTGCGTATT
GGGCGCTCTTCCGCTTCCTCGCTCACTGACTCGCTGCGCTCGGTCGTTCGGCTGCGGCGAGC
GGTATCAGCTCACTCAAAGGCGGTAATACGGTTATCCACAGAATCAGGGGATAACGCAGGAAA
GAACATGTGAGCAAAAGGCCAGCAAAAGGCCAGGAACCGTAAAAAGGCCGCGTTGCTGGCGT
TTTTCCATAGGCTCCGCCCCCCTGACGAGCATCACAAAAATCGACGCTCAAGTCAGAGGTGGC
GAAACCCGACAGGACTATAAAGATACCAGGCGTTTCCCCCTGGAAGCTCCCTCGTGCGCTCTC
CTGTTCCGACCCTGCCGCTTACCGGATACCTGTCCGCCTTTCTCTTCGGGAAGCGTGGCGCTT
TCTCATAGCTCACGCTGTAGGTATCTCAGTTCGGTGTAGGTCGTTCGCTCCAAGCTGGGCTGT
GTGCACGAACCCCCCGTTCAGCCCGACCCTGCGCCTTATCCGGTAACTATCGTCTTGAGTCCA
ACCCGGTAAGACACGACTTATCGCCACTGGCAGCAGCCACTGGTAACAGGATTAGCAGAGCGA
GGTATGTAGGCGGTGCTACAGAGTTCTTGAAGTGGTGGCCTAACTACGGCTACACTAGAAGAA
CAGTATTTGGTATCTGCGCTCTGCTGAAGCCAGTTACTTCGGAAAAAGAGTTGGTAGCTCTTGA
TCCGGCAAACAAACCGCTGGTAGCGGTGGTTTTTTTGTTTGCAAGCAGCAGATTACGCGCAGA
AAAAAAGGATCTCAAGAAGATCCTTTGATCTTTTCTACGGGGTCTGACGCTCAGTGGAACGAAA
ACTCACGTTAAGGGATTTTGGTCATGAGATTATCAAAAAGGATCTTCACCTAGATCCTTTTAAAT
TAAAAATGAAGTTTTAAATCAATCTAAAGTATATATGAGTAAACTTGGTCTGACAGTTACCAATG
CTTAATCAGTGAGGCACCTATCTCAGCGATCTGTCTATTTCGTTCATCCATAGTTGCCTGACTCC
CCGTCGTGTAGATAACTACGATACGGGAGGGCTTACCATCTGGCCCCAGTGCTGCAATGATAC
CGCGAGACCCACGCTCACCGGCTCCAGATTTATCAGCAATAAACCAGCCAGCCGGAAGGGCC
GAGCGCAGAAGTGGTCCTGCAACTTTATCCGCCTCCATCCAGTCTATTAATTGTTGCCGGGAAG
CTAGAGTAAGTAGTTCGCCAGTTAATAGTTTGCGCAACGTTGTTGCCATTGCTACAGGCATCGT
GGTGTCACGCTCGTCGTTTGGTATGGCTTCATTCAGCTCCGGTTCCCAACGATCAAGGCGAGT
TACATGATCCCCCATGTTGTGCAAAAAAGCGGTTAGCTCCTTCGGTCCTCCGATCGTTGTCAGA
AGTAAGTTGGCCGCAGTGTTATCACTCATGGTTATGGCAGCACTGCATAATTCTCTTACTGTCA
TGCCATCCGTAAGATGCTTTTCTGTGACTGGTGAGTACTCAACCAAGTCATTCTGAGAATAGTG
TATGCGGCGACCGAGTTGCTCTTGCCCGGCGTCAATACGGGATAATACCGCGCCACATAGCAG
AACTTTAAAAGTGCTCATCATTGGAAAACGTTCTTCGGGGCGAAAACTCTCAAGGATCTTACCG
CTGTTGAGATCCAGTTCGATGTAACCCACTCGTGCACCCAACTGATCTTCAGCATCTTTTACTTT
CACCAGCGTTTCTGGGTGAGCAAAAACAGGAAGGCAAAATGCCGCAAAAAAGGGAATAAGGGC
GACACGGAAATGTTGAATACTCATACTCTTCCTTTTTCAATATTATTGAAGCATTTATCAGGGTTA
TTGTCTCATGAGCGGATACATATTTGAATGTATTTAGAAAAATAAACAAATAGGGGTTCCGCGCA
CATTTCCCCGAAAAGTGCCACTAAATTGTAAGCGTTAATATTTTGTTAAAATTCGCGTTAAATTTT
TGTTAAATCAGCTCATTTTTTAACCAATAGGCCGAAATCGGCAAAATCCCTTATAAATCAAAAGA

ATAGACCGAGATAGGGTTGAGTGTTGTTCCAGTTTGGAACAAGAGTCCACTATTAAAGAACGTG
GACTCCAACGTCAAAGGGCGAAAAACCGTCTATCAGGGCGATGGCCCACTACGTGAACCATCA
CCCTAATCAAGTTTTTTGGGGTCGAGGTGCCGTAAAGCACTAAATCGGAACCCTAAAGGGAGC
CCCCGATTTAGAGCTTGACGGGGAAAGCCGGCGAACGTGGCGAGAAAGGAAGGGAAGAAAGC
GAAAGGAGCGGGCGCTAGGGCGCTGGCAAGTGTAGCGGTCACGCTGCGCGTAACCACCACAC
CCGCCGCGCTTAATGCGCCGCTACAGGGCGCGTCCCATTCGCCATTCAGGCTGCGCAACTGTT
GGGAAGGGCGATCGGTGCGGGCCTCTTCGCTATTACGCCAGCTGGCGAAAGGGGGATGTGCT
GCAAGGCGATTAAGTTGGGTAACGCCAGGGTTTTCCCAGTCACGACGTTGTAAAACGACGGCC
AGTGAGCGCGCGTAATACGACTCACTATAGGGCGAATTGGAGCTCCA

pLPCX mito roGFP2-Orp1

Dr. Tobias P. Dick (Redox Regulation (A160), Deutsches Krebsforschungszentrum, Im Neuenheimer Feld 280, 69120 Heidelberg) via Addgene (plasmid # 64992) (Gutscher et al., 2009).

> [7728 bp]
TTTGAAAGACCCCACCCGTAGGTGGCAAGCTAGCTTAAGTAACGCCACTTTGCAAGGCATGGA
AAAATACATAACTGAGAATAGAAAAGTTCAGATCAAGGTCAGGAACAAAGAAACAGCTGAATAC
CAAACAGGATATCTGTGGTAAGCGGTTCCTGCCCCGGCTCAGGGCCAAGAACAGATGAGACAG
CTGAGTGATGGGCCAAACAGGATATCTGTGGTAAGCAGTTCCTGCCCCGGCTCGGGGCCAAG
AACAGATGGTCCCCAGATGCGGTCCAGCCCTCAGCAGTTTCTAGTGAATCATCAGATGTTTCCA
GGGTGCCCCAAGGACCTGAAAATGACCCTGTACCTTATTTGAACTAACCAATCAGTTCGCTTCT
CGCTTCTGTTCGCGCGCTTCCGCTCTCCGAGCTCAATAAAAGAGCCCACAACCCCTCACTCGG
CGCGCCAGTCTTCCGATAGACTGCGTCGCCCGGGTACCCGTATTCCCAATAAAGCCTCTTGCT
GTTTGCATCCGAATCGTGGTCTCGCTGTTCCTTGGGAGGGTCTCCTCTGAGTGATTGACTACCC
ACGACGGGGGTCTTTCATTTGGGGGCTCGTCCGGGATTTGGAGACCCCTGCCCAGGGACCAC
CGACCCACCACCGGGAGGTAAGCTGGCCAGCAACTTATCTGTGTCTGTCCGATTGTCTAGTGT
CTATGTTTGATGTTATGCGCCTGCGTCTGTACTAGTTAGCTAACTAGCTCTGTATCTGGCGGAC
CCGTGGTGGAACTGACGAGTTCTGAACACCCGGCCGCAACCCTGGGAGACGTCCCAGGGACT
TTGGGGGCCGTTTTTGTGGCCCGACCTGAGGAAGGGAGTCGATGTGGAATCCGACCCCGTCA
GGATATGTGGTTCTGGTAGGAGACGAGAACCTAAAACAGTTCCCGCCTCCGTCTGAATTTTTGC
TTTCGGTTTGGAACCGAAGCCGCGCGTCTTGTCTGCTGCAGCGCTGCAGCATCGTTCTGTGTT
GTCTCTGTCTGACTGTGTTTCTGTATTTGTCTGAAAATTAGGGCCAGACTGTTACCACTCCCTTA
AGTTTGACCTTAGGTCACTGGAAAGATGTCGAGCGGATCGCTCACAACCAGTCGGTAGATGTC
AAGAAGAGACGTTGGGTTACCTTCTGCTCTGCAGAATGGCCAACCTTTAACGTCGGATGGCCG
CGAGACGGCACCTTTAACCGAGACCTCATCACCCAGGTTAAGATCAAGGTCTTTTCACCTGGC
CCGCATGGACACCCAGACCAGGTCCCCTACATCGTGACCTGGGAAGCCTTGGCTTTTGACCCC
CCTCCCTGGGTCAAGCCCTTTGTACACCCTAAGCCTCCGCCTCCTCTTCCTCCATCCGCCCCG
TCTCTCCCCCTTGAACCTCCTCGTTCGACCCCGCCTCGATCCTCCCTTTATCCAGCCCTCACTC
CTTCTCTAGGCGCCGGAATTGATCCCCCGGGCTGCAGGTCGGCCGCCACGACCGGTGCCGCC
ACCATCCCCTGACCCACGCCCCTGACCCCTCACAAGGAGACGACCTTCCATGACCGAGTACAA
GCCCACGGTGCGCCTCGCCACCCGCGACGACGTCCCCCGGGCCGTACGCACCCTCGCCGCC
GCGTTCGCCGACTACCCCGCCACGCGCCACACCGTCGACCCGGACCGCCACATCGAGCGGGT
CACCGAGCTGCAAGAACTCTTCCTCACGCGCGTCGGGCTCGACATCGGCAAGGTGTGGGTCG
CGGACGACGGCGCCGCGGTGGCGGTCTGGACCACGCCGGAGAGCGTCGAAGCGGGGGCGG
TGTTCGCCGAGATCGGCCCGCGCATGGCCGAGTTGAGCGGTTCCCGGCTGGCCGCGCAGCAA
CAGATGGAAGGCCTCCTGGCGCCGCACCGGCCCAAGGAGCCCGCGTGGTTCCTGGCCACCG
TCGGCGTCTCGCCCGACCACCAGGGCAAGGGTCTGGGCAGCGCCGTCGTGCTCCCCGGAGT
GGAGGCGGCCGAGCGCGCCGGGGTGCCCGCCTTCCTGGAGACCTCCGCGCCCCGCAACCTC
CCCTTCTACGAGCGGCTCGGCTTCACCGTCACCGCCGACGTCGAGTGCCCGAAGGACCGCGC
GACCTGGTGCATGACCCGCAAGCCCGGTGCCTGACGCCCGCCCCACGACCCGCAGCGCCCG

ACCGAAAGGAGCGCACGACCCCATGGCTCCGACCGAAGCCGACCCGGGCGGCCCCGCCGAC
CCCGCACCCGCCCCCGAGGCCCACCGACTCTAGTAATAGTAATCAATTACGGGGTCATTAGTT
CATAGCCCATATATGGAGTTCCGCGTTACATAACTTACGGTAAATGGCCCGCCTGGCTGACCG
CCCAACGACCCCCGCCCATTGACGTCAATAATGACGTATGTTCCCATAGTAACGCCAATAGGG
ACTTTCCATTGACGTCAATGGGTGGAGTATTTACGGTAAACTGCCCACTTGGCAGTACATCAAG
TGTATCATATGCCAAGTACGCCCCCTATTGACGTCAATGACGGTAAATGGCCCGCCTGGCATTA
TGCCCAGTACATGACCTTATGGGACTTTCCTACTTGGCAGTACATCTACGTATTAGTCATCGCT
ATTACCATGGTGATGCGGTTTTGGCAGTACATCAATGGGCGTGGATAGCGGTTTGACTCACGG
GGATTTCCAAGTCTCCACCCCATTGACGTCAATGGGAGTTTGTTTTGGCACCAAAATCAACGGG
ACTTTCCAAAATGTCGTAACAACTCCGCCCCATTGACGCAAATGGGCGGTAGGCGTGTACGGT
GGGAGGTCTATATAAGCAGAGCTGGTTTAGTGAACCGTCAGATCCGCTAGCGCTACCGGACTC
AGATCTCGAGATGGCCTCCACTCGTGTCCTCGCCTCTCGCCTGGCCTCCCAGATGGCTGCTTC
CGCCAAGGTTGCCCGCCCTGCTGTCCGCGTTGCTCAGGTCAGCAAGCGCACCATCCAGACTG
GCTCCCCCCTCCAGACCCTCAAGCGCACCCAGATGACCTCCATCGTCAACGCCACCACCCGCC
AGGCTTTCCAGAAGCGCGCCTACTCTTCCGGATCCGTGAGCAAGGGCGAGGAGCTGTTCACC
GGGGTGGTGCCCATCCTGGTCGAGCTGGACGGCGACGTAAACGGCCACAAGTTCAGCGTGTC
CGGCGAGGGCGAGGGCGATGCCACCTACGGCAAGCTGACCCTGAAGTTCATCTCCACCACCG
GCAAGCTGCCCGTGCCCTGGCCCACCCTCGTGACCACCCTGACCTACGGCGTGCAGTGCTTC
AGCCGCTACCCCGACCACATGAAGCAGCACGACTTCTTCAAGTCCGCCATGCCCGAAGGCTAC
GTCCAGGAGCGCACCATCTTCTTCAAGGACGACGGCAACTACAAGACCCGCGCCGAGGTGAA
GTTCGAGGGCGACACCCTGGTGAACCGCATCGAGCTGAAGGGCATCGACTTCAAGGAGGACG
GCAACATCCTGGGGCACAAGCTGGAGTACAACTACAACTGCCACAACGTCTATATCATGGCCG
ACAAGCAGAAGAACGGCATCAAGGTGAACTTCAAGATCCGCCACAACATCGAGGACGGCAGC
GTGCAGCTCGCCGACCACTACCAGCAGAACACCCCCATCGGCGACGGCCCCGTGCTGCTGCC
CGACAACCACTACCTGAGCACCTGCTCCGCCCTGAGCAAAGACCCCAACGAGAAGCGCGATC
ACATGGTCCTGCTGGAGTTCGTGACCGCCGCCGGGATCACTCTCGGCATGGACGAGCTGTAC
AAGACTAGTGGTGGTTCAGGTGGTGGTGGTTCAGGTGGTGGTGGTTCAGGTGGAGGAGGATC
AGGAGGAGGAGGATCAGGAGGAGGAGGATCAGGAGGAGAATTCGATATCTCAGAATTCTATAA
GCTAGCACCTGTTGACAAGAAAGGCCAACCATTCCCCTTCGACCAATTAAAGGGAAAAGTGGT
GCTTATCGTTAATGTTGCCTCCAAATGTGGATTCACTCCTCAATACAAAGAACTAGAGGCCTTGT
ACAAACGTTATAAGGACGAAGGATTTACCATCATCGGGTTCCCATGCAACCAGTTTGGCCACCA
AGAACCTGGCTCTGATGAAGAAATTGCCCAGTTCTGCCAACTGAACTATGGCGTGACTTTCCCC
ATTATGAAAAAAATTGACGTTAATGGTGGCAATGAGGACCCTGTTTACAAGTTTTTGAAGAGCC
AAAAATCCGGTATGTTGGGCTTGAGAGGTATCAAATGGAATTTTGAAAAATTCTTAGTCGATAAA
AAGGGTAAAGTGTACGAAAGATACTCTTCACTAACCAAACCTTCTTCGTTGTCCGAAACCATCG
AAGAACTTTTGAAAGAGGTGGAATAGATCGATAAAATAAAAGATTTTATTTAGTCTCCAGAAAAA
GGGGGGAATGAAAGACCCCACCTGTAGGTTTGGCAAGCTAGCTTAAGTAACGCCATTTTGCAA
GGCATGGAAAAATACATAACTGAGAATAGAGAAGTTCAGATCAAGGTCAGGAACAGATGGAAC
AGCTGAATATGGGCCAAACAGGATATCTGTGGTAAGCAGTTCCTGCCCCGGCTCAGGGCCAAG
AACAGATGGAACAGCTGAATATGGGCCAAACAGGATATCTGTGGTAAGCAGTTCCTGCCCCGG
CTCAGGGCCAAGAACAGATGGTCCCCAGATGCGGTCCAGCCCTCAGCAGTTTCTAGAGAACCA
TCAGATGTTTCCAGGGTGCCCCAAGGACCTGAAATGACCCTGTGCCTTATTTGAACTAACCAAT
CAGTTCGCTTCTCGCTTCTGTTCGCGCGCTTCTGCTCCCCGAGCTCAATAAAAGAGCCCACAAC
CCCTCACTCGGGGCGCCAGTCCTCCGATTGACTGAGTCGCCCGGGTACCCGTGTATCCAATAA
ACCCTCTTGCAGTTGCATCCGACTTGTGGTCTCGCTGTTCCTTGGGAGGGTCTCCTCTGAGTG
ATTGACTACCCGTCAGCGGGGGTCTTTCATTTGGGGGCTCGTCCGGGATCGGGAGACCCCTG
CCCAGGGACCACCGACCCACCACCGGGAGGTAAGCTGGCTGCCTCGCGCGTTTCGGTGATGA
CGGTGAAAACCTCTGACACATGCAGCTCCCGGAGACGGTCACAGCTTGTCTGTAAGCGGATGC
CGGGAGCAGACAAGCCCGTCAGGGCGCGTCAGCGGGTGTTGGCGGGTGTCGGGGCGCAGCC
ATGACCCAGTCACGTAGCGATAGCGGAGTGTACTGATAACTTCGTATAATGTATGCTATACGAA
GTTATTAGGTCTGAAGAGGAGTTTACGTCCAGCCAAGCTAGGGCCGCGATCCGGAACCCTTAA
TATAACTTCGTATAATGTATGCTATACGAAGTTATCAGTACTGGCTTAACTATGCGGCATCAGAG
CAGATTGTACTGAGAGTGCACCATATGCGGTGTGAAATACCGCACAGATGCGTAAGGAGAAAA
TACCGCATCAGGCGCTCTTCCGCTTCCTCGCTCACTGACTCGCTGCGCTCGGTCGTTCGGCTG
CGGCGAGCGGTATCAGCTCACTCAAAGGCGGTAATACGGTTATCCACAGAATCAGGGGATAAC

GCAGGAAAGAACATGTGAGCAAAAGGCCAGCAAAAGGCCAGGAACCGTAAAAAGGCCGCGTT
GCTGGCGTTTTTCCATAGGCTCCGCCCCCCTGACGAGCATCACAAAAATCGACGCTCAAGTCA
GAGGTGGCGAAACCCGACAGGACTATAAAGATACCAGGCGTTTCCCCCTGGAAGCTCCCTCGT
GCGCTCTCCTGTTCCGACCCTGCCGCTTACCGGATACCTGTCCGCCTTTCTCCCTTCGGGAAG
CGTGGCGCTTTCTCATAGCTCACGCTGTAGGTATCTCAGTTCGGTGTAGGTCGTTCGCTCCAA
GCTGGGCTGTGTGCACGAACCCCCCGTTCAGCCCGACCGCTGCGCCTTATCCGGTAACTATCG
TCTTGAGTCCAACCCGGTAAGACACGACTTATCGCCACTGGCAGCAGCCACTGGTAACAGGAT
TAGCAGAGCGAGGTATGTAGGCGGTGCTACAGAGTTCTTGAAGTGGTGGCCTAACTACGGCTA
CACTAGAAGGACAGTATTTGGTATCTGCGCTCTGCTGAAGCCAGTTACCTTCGGAAAAAGAGTT
GGTAGCTCTTGATCCGGCAAACAAACCACCGCTGGTAGCGGTGGTTTTTTTGTTTGCAAGCAG
CAGATTACGCGCAGAAAAAAAGGATCTCAAGAAGATCCTTTGATCTTTTCTACGGGGTCTGACG
CTCAGTGGAACGAAAACTCACGTTAAGGGATTTTGGTCATGAGATTATCAAAAAGGATCTTCAC
CTAGATCCTTTTAAATTAAAAATGAAGTTTTAAATCAATCTAAAGTATATATGAGTAAACTTGGTC
TGACAGTTACCAATGCTTAATCAGTGAGGCACCTATCTCAGCGATCTGTCTATTTCGTTCATCCA
TAGTTGCCTGACTCCCCGTCGTGTAGATAACTACGATACGGGAGGGCTTACCATCTGGCCCCA
GTGCTGCAATGATACCGCGAGACCCACGCTCACCGGCTCCAGATTTATCAGCAATAAACCAGC
CAGCCGGAAGGGCCGAGCGCAGAAGTGGTCCTGCAACTTTATCCGCCTCCATCCAGTCTATTA
ATTGTTGCCGGGAAGCTAGAGTAAGTAGTTCGCCAGTTAATAGTTTGCGCAACGTTGTTGCCAT
TGCTGCAGGCATCGTGGTGTCACGCTCGTCGTTTGGTATGGCTTCATTCAGCTCCGGTTCCCA
ACGATCAAGGCGAGTTACATGATCCCCCATGTTGTGCAAAAAAGCGGTTAGCTCCTTCGGTCCT
CCGATCGTTGTCAGAAGTAAGTTGGCCGCAGTGTTATCACTCATGGTTATGGCAGCACTGCATA
ATTCTCTTACTGTCATGCCATCCGTAAGATGCTTTTCTGTGACTGGTGAGTACTCAACCAAGTCA
TTCTGAGAATAGTGTATGCGGCGACCGAGTTGCTCTTGCCCGGCGTCAACACGGGATAATACC
GCGCCACATAGCAGAACTTTAAAAGTGCTCATCATTGGAAAACGTTCTTCGGGGCGAAAACTCT
CAAGGATCTTACCGCTGTTGAGATCCAGTTCGATGTAACCCACTCGTGCACCCAACTGATCTTC
AGCATCTTTTACTTTCACCAGCGTTTCTGGGTGAGCAAAAACAGGAAGGCAAAATGCCGCAAAA
AAGGGAATAAGGGCGACACGGAAATGTTGAATACTCATACTCTTCCTTTTTCAATATTATTGAAG
CATTTATCAGGGTTATTGTCTCATGAGCGGATACATATTTGAATGTATTTAGAAAAATAAACAAA
TAGGGGTTCCGCGCACATTTCCCCGAAAAGTGCCACCTGACGTCTAAGAAACCATTATTATCAT
GACATTAACCTATAAAAATAGGCGTATCACGAGGCCCTTTCGTCTTCAAGAATTGCTAGCAATT
GCTAGCAATTGCTAGCAATTCATACCAGATCACCGAAAACTGTCCTCCAAATGTGTCCCCCTCA
CACTCCCAAATTCGCGGGCTTCTGCCTCTTAGACCACTCTACCCTATTCCCCACACTCACCGGA
GCCAAAGCCGCGGCCCTTCCGTTTCTTTGCT

pLPCX cyto roGFP2-Orp1

Dr. Tobias P. Dick (Redox Regulation (A160), Deutsches Krebsforschungszentrum, Im Neuenheimer Feld 280, 69120 Heidelberg) via Addgene (plasmid # 64991)(Gutscher et al., 2009).

> [7518 bp]
TTTGAAAGACCCCACCCGTAGGTGGCAAGCTAGCTTAAGTAACGCCACTTTGCAAGGCATGGA
AAAATACATAACTGAGAATAGAAAAGTTCAGATCAAGGTCAGGAACAAAGAAACAGCTGAATAC
CAAACAGGATATCTGTGGTAAGCGGTTCCTGCCCCGGCTCAGGGCCAAGAACAGATGAGACAG
CTGAGTGATGGGCCAAACAGGATATCTGTGGTAAGCAGTTCCTGCCCCGGCTCGGGGCCAAG
AACAGATGGTCCCCAGATGCGGTCCAGCCCTCAGCAGTTTCTAGTGAATCATCAGATGTTTCCA
GGGTGCCCCAAGGACCTGAAAATGACCCTGTACCTTATTTGAACTAACCAATCAGTTCGCTTCT
CGCTTCTGTTCGCGCGCTTCCGCTCTCCGAGCTCAATAAAAGAGCCCACAACCCCTCACTCGG
CGCGCCAGTCTTCCGATAGACTGCGTCGCCCGGGTACCCGTATTCCCAATAAAGCCTCTTGCT
GTTTGCATCCGAATCGTGGTCTCGCTGTTCCTTGGGAGGGTCTCCTCTGAGTGATTGACTACCC
ACGACGGGGGTCTTTCATTTGGGGGCTCGTCCGGGATTTGGAGACCCCTGCCCAGGGACCAC
CGACCCACCACCGGGAGGTAAGCTGGCCAGCAACTTATCTGTGTCTGTCCGATTGTCTAGTGT
CTATGTTTGATGTTATGCGCCTGCGTCTGTACTAGTTAGCTAACTAGCTCTGTATCTGGCGGAC
CCGTGGTGGAACTGACGAGTTCTGAACACCCGGCCGCAACCCTGGGAGACGTCCCAGGGACT

TTGGGGGCCGTTTTTGTGGCCCGACCTGAGGAAGGGAGTCGATGTGGAATCCGACCCCGTCA
GGATATGTGGTTCTGGTAGGAGACGAGAACCTAAAACAGTTCCCGCCTCCGTCTGAATTTTTGC
TTTCGGTTTGGAACCGAAGCCGCGCGTCTTGTCTGCTGCAGCGCTGCAGCATCGTTCTGTGTT
GTCTCTGTCTGACTGTGTTTCTGTATTTGTCTGAAAATTAGGGCCAGACTGTTACCACTCCCTTA
AGTTTGACCTTAGGTCACTGGAAAGATGTCGAGCGGATCGCTCACAACCAGTCGGTAGATGTC
AAGAAGAGACGTTGGGTTACCTTCTGCTCTGCAGAATGGCCAACCTTTAACGTCGGATGGCCG
CGAGACGGCACCTTTAACCGAGACCTCATCACCCAGGTTAAGATCAAGGTCTTTTCACCTGGC
CCGCATGGACACCCAGACCAGGTCCCCTACATCGTGACCTGGGAAGCCTTGGCTTTTGACCCC
CCTCCCTGGGTCAAGCCCTTTGTACACCCTAAGCCTCCGCCTCCTCTTCCTCCATCCGCCCCG
TCTCTCCCCCTTGAACCTCCTCGTTCGACCCCGCCTCGATCCTCCCTTTATCCAGCCCTCACTC
CTTCTCTAGGCGCCGGAATTGATCCCCCGGGCTGCAGGTCGGCCGCCACGACCGGTGCCGCC
ACCATCCCCTGACCCACGCCCCTGACCCCTCACAAGGAGACGACCTTCCATGACCGAGTACAA
GCCCACGGTGCGCCTCGCCACCCGCGACGACGTCCCCCGGGCCGTACGCACCCTCGCCGCC
GCGTTCGCCGACTACCCCGCCACGCGCCACACCGTCGACCCGGACCGCCACATCGAGCGGGT
CACCGAGCTGCAAGAACTCTTCCTCACGCGCGTCGGGCTCGACATCGGCAAGGTGTGGGTCG
CGGACGACGGCGCCGCGGTGGCGGTCTGGACCACGCCGGAGAGCGTCGAAGCGGGGGCGG
TGTTCGCCGAGATCGGCCCGCGCATGGCCGAGTTGAGCGGTTCCCGGCTGGCCGCGCAGCAA
CAGATGGAAGGCCTCCTGGCGCCGCACCGGCCCAAGGAGCCCGCGTGGTTCCTGGCCACCG
TCGGCGTCTCGCCCGACCACCAGGGCAAGGGTCTGGGCAGCGCCGTCGTGCTCCCCGGAGT
GGAGGCGGCCGAGCGCGCCGGGGTGCCCGCCTTCCTGGAGACCTCCGCGCCCCGCAACCTC
CCCTTCTACGAGCGGCTCGGCTTCACCGTCACCGCCGACGTCGAGTGCCCGAAGGACCGCGC
GACCTGGTGCATGACCCGCAAGCCCGGTGCCTGACGCCCGCCCCACGACCCGCAGCGCCCG
ACCGAAAGGAGCGCACGACCCCATGGCTCCGACCGAAGCCGACCCGGGCGGCCCCGCCGAC
CCCGCACCCGCCCCCGAGGCCCACCGACTCTAGTAATAGTAATCAATTACGGGGTCATTAGTT
CATAGCCCATATATGGAGTTCCGCGTTACATAACTTACGGTAAATGGCCCGCCTGGCTGACCG
CCCAACGACCCCCGCCCATTGACGTCAATAATGACGTATGTTCCCATAGTAACGCCAATAGGG
ACTTTCCATTGACGTCAATGGGTGGAGTATTTACGGTAAACTGCCCACTTGGCAGTACATCAAG
TGTATCATATGCCAAGTACGCCCCCTATTGACGTCAATGACGGTAAATGGCCCGCCTGGCATTA
TGCCCAGTACATGACCTTATGGGACTTTCCTACTTGGCAGTACATCTACGTATTAGTCATCGCT
ATTACCATGGTGATGCGGTTTTGGCAGTACATCAATGGGCGTGGATAGCGGTTTGACTCACGG
GGATTTCCAAGTCTCCACCCCATTGACGTCAATGGGAGTTTGTTTTGGCACCAAAATCAACGGG
ACTTTCCAAAATGTCGTAACAACTCCGCCCCATTGACGCAAATGGGCGGTAGGCGTGTACGGT
GGGAGGTCTATATAAGCAGAGCTGGTTTAGTGAACCGTCAGATCCGCTAGCGCTACCGGACTC
AGATCTCGAGATGGTGAGCAAGGGCGAGGAGCTGTTCACCGGGGTGGTGCCCATCCTGGTCG
AGCTGGACGGCGACGTAAACGGCCACAAGTTCAGCGTGTCCGGCGAGGGCGAGGGCGATGC
CACCTACGGCAAGCTGACCCTGAAGTTCATCTCCACCACCGGCAAGCTGCCCGTGCCCTGGCC
CACCCTCGTGACCACCCTGACCTACGGCGTGCAGTGCTTCAGCCGCTACCCCGACCACATGAA
GCAGCACGACTTCTTCAAGTCCGCCATGCCCGAAGGCTACGTCCAGGAGCGCACCATCTTCTT
CAAGGACGACGGCAACTACAAGACCCGCGCCGAGGTGAAGTTCGAGGGCGACACCCTGGTGA
ACCGCATCGAGCTGAAGGGCATCGACTTCAAGGAGGACGGCAACATCCTGGGGCACAAGCTG
GAGTACAACTACAACTGCCACAACGTCTATATCATGGCCGACAAGCAGAAGAACGGCATCAAG
GTGAACTTCAAGATCCGCCACAACATCGAGGACGGCAGCGTGCAGCTCGCCGACCACTACCA
GCAGAACACCCCCATCGGCGACGGCCCCGTGCTGCTGCCCGACAACCACTACCTGAGCACCT
GCTCCGCCCTGAGCAAAGACCCCAACGAGAAGCGCGATCACATGGTCCTGCTGGAGTTCGTG
ACCGCCGCCGGGATCACTCTCGGCATGGACGAGCTGTACAAGACTAGTGGTGGTTCAGGTGG
TGGTGGTTCAGGTGGTGGTGGTTCAGGTGGAGGAGGATCAGGAGGAGGAGGATCAGGAGGA
GGAGGATCAGGAGGAGAATTCGATATCTCAGAATTCTATAAGCTAGCACCTGTTGACAAGAAAG
GCCAACCATTCCCCTTCGACCAATTAAAGGGAAAAGTGGTGCTTATCGTTAATGTTGCCTCCAA
ATGTGGATTCACTCCTCAATACAAAGAACTAGAGGCCTTGTACAAACGTTATAAGGACGAAGGA
TTTACCATCATCGGGTTCCCATGCAACCAGTTTGGCCACCAAGAACCTGGCTCTGATGAAGAAA
TTGCCCAGTTCTGCCAACTGAACTATGGCGTGACTTTCCCCATTATGAAAAAAATTGACGTTAAT
GGTGGCAATGAGGACCCTGTTTACAAGTTTTTGAAGAGCCAAAAATCCGGTATGTTGGGCTTGA
GAGGTATCAAATGGAATTTTGAAAAATTCTTAGTCGATAAAAAGGGTAAAGTGTACGAAAGATAC
TCTTCACTAACCAAACCTTCTTCGTTGTCCGAAACCATCGAAGAACTTTTGAAAGAGGTGGAAT
AGATCGATAAAATAAAAGATTTTATTTAGTCTCCAGAAAAAGGGGGGAATGAAAGACCCCACCT

GTAGGTTTGGCAAGCTAGCTTAAGTAACGCCATTTTGCAAGGCATGGAAAAATACATAACTGAG
AATAGAGAAGTTCAGATCAAGGTCAGGAACAGATGGAACAGCTGAATATGGGCCAAACAGGAT
ATCTGTGGTAAGCAGTTCCTGCCCCGGCTCAGGGCCAAGAACAGATGGAACAGCTGAATATGG
GCCAAACAGGATATCTGTGGTAAGCAGTTCCTGCCCCGGCTCAGGGCCAAGAACAGATGGTCC
CCAGATGCGGTCCAGCCCTCAGCAGTTTCTAGAGAACCATCAGATGTTTCCAGGGTGCCCCAA
GGACCTGAAATGACCCTGTGCCTTATTTGAACTAACCAATCAGTTCGCTTCTCGCTTCTGTTCG
CGCGCTTCTGCTCCCCGAGCTCAATAAAAGAGCCCACAACCCCTCACTCGGGGCGCCAGTCCT
CCGATTGACTGAGTCGCCCGGGTACCCGTGTATCCAATAAACCCTCTTGCAGTTGCATCCGAC
TTGTGGTCTCGCTGTTCCTTGGGAGGGTCTCCTCTGAGTGATTGACTACCCGTCAGCGGGGGT
CTTTCATTTGGGGGCTCGTCCGGGATCGGGAGACCCCTGCCCAGGGACCACCGACCCACCAC
CGGGAGGTAAGCTGGCTGCCTCGCGCGTTTCGGTGATGACGGTGAAAACCTCTGACACATGC
AGCTCCCGGAGACGGTCACAGCTTGTCTGTAAGCGGATGCCGGGAGCAGACAAGCCCGTCAG
GGCGCGTCAGCGGGTGTTGGCGGGTGTCGGGGCGCAGCCATGACCCAGTCACGTAGCGATA
GCGGAGTGTACTGATAACTTCGTATAATGTATGCTATACGAAGTTATTAGGTCTGAAGAGGAGT
TTACGTCCAGCCAAGCTAGGGCCGCGATCCGGAACCCTTAATATAACTTCGTATAATGTATGCT
ATACGAAGTTATCAGTACTGGCTTAACTATGCGGCATCAGAGCAGATTGTACTGAGAGTGCACC
ATATGCGGTGTGAAATACCGCACAGATGCGTAAGGAGAAAATACCGCATCAGGCGCTCTTCCG
CTTCCTCGCTCACTGACTCGCTGCGCTCGGTCGTTCGGCTGCGGCGAGCGGTATCAGCTCACT
CAAAGGCGGTAATACGGTTATCCACAGAATCAGGGGATAACGCAGGAAAGAACATGTGAGCAA
AAGGCCAGCAAAAGGCCAGGAACCGTAAAAAGGCCGCGTTGCTGGCGTTTTTCCATAGGCTCC
GCCCCCCTGACGAGCATCACAAAAATCGACGCTCAAGTCAGAGGTGGCGAAACCCGACAGGA
CTATAAAGATACCAGGCGTTTCCCCCTGGAAGCTCCCTCGTGCGCTCTCCTGTTCCGACCCTG
CCGCTTACCGGATACCTGTCCGCCTTTCTCCCTTCGGGAAGCGTGGCGCTTTCTCATAGCTCA
CGCTGTAGGTATCTCAGTTCGGTGTAGGTCGTTCGCTCCAAGCTGGGCTGTGTGCACGAACCC
CCCGTTCAGCCCGACCGCTGCGCCTTATCCGGTAACTATCGTCTTGAGTCCAACCCGGTAAGA
CACGACTTATCGCCACTGGCAGCAGCCACTGGTAACAGGATTAGCAGAGCGAGGTATGTAGGC
GGTGCTACAGAGTTCTTGAAGTGGTGGCCTAACTACGGCTACACTAGAAGGACAGTATTTGGT
ATCTGCGCTCTGCTGAAGCCAGTTACCTTCGGAAAAAGAGTTGGTAGCTCTTGATCCGGCAAAC
AAACCACCGCTGGTAGCGGTGGTTTTTTTGTTTGCAAGCAGCAGATTACGCGCAGAAAAAAAG
GATCTCAAGAAGATCCTTTGATCTTTTCTACGGGGTCTGACGCTCAGTGGAACGAAAACTCACG
TTAAGGGATTTTGGTCATGAGATTATCAAAAAGGATCTTCACCTAGATCCTTTTAAATTAAAAAT
GAAGTTTTAAATCAATCTAAAGTATATATGAGTAAACTTGGTCTGACAGTTACCAATGCTTAATC
AGTGAGGCACCTATCTCAGCGATCTGTCTATTTCGTTCATCCATAGTTGCCTGACTCCCCGTCG
TGTAGATAACTACGATACGGGAGGGCTTACCATCTGGCCCCAGTGCTGCAATGATACCGCGAG
ACCCACGCTCACCGGCTCCAGATTTATCAGCAATAAACCAGCCAGCCGGAAGGGCCGAGCGC
AGAAGTGGTCCTGCAACTTTATCCGCCTCCATCCAGTCTATTAATTGTTGCCGGGAAGCTAGAG
TAAGTAGTTCGCCAGTTAATAGTTTGCGCAACGTTGTTGCCATTGCTGCAGGCATCGTGGTGTC
ACGCTCGTCGTTTGGTATGGCTTCATTCAGCTCCGGTTCCCAACGATCAAGGCGAGTTACATGA
TCCCCCATGTTGTGCAAAAAAGCGGTTAGCTCCTTCGGTCCTCCGATCGTTGTCAGAAGTAAGT
TGGCCGCAGTGTTATCACTCATGGTTATGGCAGCACTGCATAATTCTCTTACTGTCATGCCATC
CGTAAGATGCTTTTCTGTGACTGGTGAGTACTCAACCAAGTCATTCTGAGAATAGTGTATGCGG
CGACCGAGTTGCTCTTGCCCGGCGTCAACACGGGATAATACCGCGCCACATAGCAGAACTTTA
AAAGTGCTCATCATTGGAAAACGTTCTTCGGGGCGAAAACTCTCAAGGATCTTACCGCTGTTGA
GATCCAGTTCGATGTAACCCACTCGTGCACCCAACTGATCTTCAGCATCTTTTACTTTCACCAG
CGTTTCTGGGTGAGCAAAAACAGGAAGGCAAAATGCCGCAAAAAAGGGAATAAGGGCGACAC
GGAAATGTTGAATACTCATACTCTTCCTTTTTCAATATTATTGAAGCATTTATCAGGGTTATTGTC
TCATGAGCGGATACATATTTGAATGTATTTAGAAAAATAAACAAATAGGGGTTCCGCGCACATTT
CCCCGAAAAGTGCCACCTGACGTCTAAGAAACCATTATTATCATGACATTAACCTATAAAAATAG
GCGTATCACGAGGCCCTTTCGTCTTCAAGAATTGCTAGCAATTGCTAGCAATTGCTAGCAATTC
ATACCAGATCACCGAAAACTGTCCTCCAAATGTGTCCCCCTCACACTCCCAAATTCGCGGGCTT
CTGCCTCTTAGACCACTCTACCCTATTCCCCACACTCACCGGAGCCAAAGCCGCGGCCCTTCC
GTTTCTTTGCT

Appendix B. Primer sequences

Sequencing primers			
Gene of interest	**Plasmid**	**Forward sequencing primer (5' – 3')**	**Reverse sequencing primer (5' – 3')**
AMPKα2-CT-FLAG	pcDNA3	CMV-F: **CGCAAATGGGCGGTAGGCGTGT**	BGH-R: **TAGAAGGCACAGTCGAGG**
AMPKβ1	pcDNA3	CMV-F: **CGCAAATGGGCGGTAGGCGTGT**	BGH-R: **TAGAAGGCACAGTCGAGG**
AMPKγ1-NT-Myc	pcDNA3	CMV-F: **CGCAAATGGGCGGTAGGCGTGT**	BGH-R: **TAGAAGGCACAGTCGAGG**
NDI1	pcDNA5/FRT/T0	CMV-F: **CGCAAATGGGCGGTAGGCGTGT**	BGH-R: **TAGAAGGCACAGTCGAGG**
AOX	pcDNA5/FRT/T0	CMV-F: **CGCAAATGGGCGGTAGGCGTGT**	BGH-R: **TAGAAGGCACAGTCGAGG**

Extension/Amplification primers			
Gene of interest	**Plasmid**	**Forward primer (5' – 3')**	**Reverse primer (5' – 3')**
NDI1	pWPI	TTA ATC GGT ACC GCC ACC **ATG CTA TCG AAG AAT TTG TAT** Description: 5'-Flank-KpnI-Kozak-Start-NDI1-3'	CG GGT AGC GGC GCG **CTA TAA TCC TTT AAA AAA GTC TCT T** Description: 5'-Flank-NotI-Stop-NDI1-3'
AOX	pWPI	GTC ACC GGA TCC GCC ACC **ATG TTG TCT ACC GGA AGT AAA** Description: 5'-Flank-BamHI-Kozak-Start-AOX-3'	CG GGT CTC GAG TGT **CTA TTG TCC AGG TGG ATA AGG** Description: 5'-Flank-Xho1-linker-Stop-AOX-3'

Appendix C. Publications arising from this work

Van Leeuwen[§], A. G., **Hinchy[§], E. C**., Murphy, M. P., Robb, E. L., Cochemé, H. M. (2017). Click-PEGylation – A mobility shift approach to assess the redox state of cysteines in candidate proteins. *Free Radic Bio Med,* **108**, 374 - 382.
[§] Co-first authors.

Hinchy, E. C., Murphy, M. P. (2017). Book chapter: Mitochondrial hydrogen peroxide as a redox signal. Book Title: Hydrogen Peroxide Metabolism in Health and Disease. Editors: Vissers, M. C. M., Hampton, M., Kettle, A. J. *CRC Press, Taylor and Francis Group (Florida).*

Axell, R. G., Messer, S. J., White, P. A., McCabe C., Priest, A., Statopoulou, T., Drozdzynska, M., Viscasillas, J., **Hinchy, E. C.**, Hampton-Till, J., Alibhai, H. I., Morrell, N., Pepke-Zaba, J., Large, S.R., Hoole, S. P. (2017). Ventriculo-arterial coupling detects occult RV dysfunction in chronic thromboembolic pulmonary vascular disease. *Physiol Rep,* 5(7): e13227.